Dielectric Spectroscopy of The Hydration of Organic Anions as Models for Anionic Residues of Biomolecules

Dissertation
zur Erlangung des
Doktorgrades der Naturwissenschaften
(Dr. rer. nat.)
der Naturwissenschaftlichen Fakultät IV
Chemie und Pharmazie
der Universität Regensburg

vorgelegt von
Hafiz Muhammad Abd ur Rahman
aus Jauharabad / Pakistan

Regensburg 2012

Promotionsgesuch eingereicht am:	20.06.2012
Tag des Kolloquiums:	17.07.2012
Die Arbeit wurde angeleitet von:	Apl. Prof. Dr. R. Buchner
Prüfungsausschuss:	Apl. Prof. Dr. R. Buchner Prof. Dr. W. Kunz Prof. Dr. A. Pfitzner Prof. em. Dr. Dr. h.c. J. Barthel (Vorsitzender)

for
Saadia, Huzaifa
and
my Parents

Contents

Introduction **1**

1 Theoretical background **5**
1.1 Basics of electrodynamics 5
1.1.1 Maxwell and constitutive equations 5
1.1.2 The electric displacement field 6
1.1.3 Wave equations 7
1.2 Dielectric relaxation 9
1.2.1 Polarization 9
1.2.2 Response functions of the orientational polarization 10
1.3 Empirical description of dielectric relaxation 11
1.3.1 Debye equation 11
1.3.2 Relaxation time distributions 12
1.3.3 Damped harmonic oscillator 13
1.3.4 Combination of models 14
1.4 Microscopic models of dielectric relaxation 14
1.4.1 Onsager equation 14
1.4.2 Kirkwood-Fröhlich equation 15
1.4.3 Cavell equation 15
1.4.4 Debye model of rotational diffusion 16
1.4.5 Microscopic and macroscopic relaxation times 17
1.5 Ion association 18
1.6 Temperature dependence of relaxation times 19
1.6.1 Arrhenius equation 19
1.6.2 Eyring equation 19

2 Experimental **21**
2.1 Sample preparation 21
2.2 Measurement of dielectric properties 22
2.2.1 Frequency-domain reflectometry 22
2.2.2 Interferometry 24
2.2.3 Data processing 27
2.3 Supporting measurements 29

2.3.1 Densimetry 29
2.3.2 Conductivity 29
2.3.3 Quantum mechanical calculations 30

3 Small Alkylcarboxylates **31**
3.1 Aqueous solutions of sodium formate and sodium acetate 31
3.1.1 Choice of fit model and assignment of relaxation modes 32
3.1.2 Relaxation amplitudes 42
3.1.3 Quantitative description of ion pairing 44
3.1.4 Ion hydration 47
3.1.5 Temperature dependence of ion hydration in NaOAc(aq) 51
3.1.6 Bulk water dynamics 52
3.2 Aqueous solutions of sodium trifluoroacetate 56
3.2.1 Choice of fit model and assignment of relaxation modes 56
3.2.2 Water relaxations and ion hydration 60
3.2.3 Ion association 63

4 Amphiphilic Carboxylates **67**
4.1 Aqueous solutions of sodium propanoate, butanoate and pentanoate 67
4.1.1 Choice of fit model 68
4.1.2 Relaxation modes and relaxation times 76
4.1.3 Solute relaxation and ion association 81
4.1.4 Water-relaxation amplitudes 86
4.1.5 Ion hydration 87
4.2 Aqueous solutions of sodium benzoate 92
4.2.1 Choice of fit model 92
4.2.2 Relaxation times and assignment of relaxation modes 97
4.2.3 Solute relaxation amplitude 98
4.2.4 Water relaxations and ion hydration 100

5 Methylsulfate and Methanesulfonate **103**
5.1 Choice of fit model and assignment of relaxation modes 103
5.2 Water relaxations and ion hydration 111
5.3 Ion association 117

Summary and conclusions **121**

Appendix **125**
A.1 Dielectric data of aqueous sodium chloride 125
A.2 DRS of aqueous solutions of rubidium fluoride 129
A.3 DRS of non-aqueous electrolyte solutions 139

Bibliography **149**

Preface

This dissertation is based on research carried out between April 2008 and June 2012 at Institute of Physical and Theoretical Chemistry (Faculty of Natural Sciences IV) of the University of Regensburg.

This work would not have been possible without the help and support of many people to whom I am happy to express my honest gratitude.

First of all, I am sincerely indebted to my supervisor Prof. Dr. Richard Buchner for providing me the opportunity to work in his group, allocating this fascinating topic, his excellent guidance, encouragement and scientific support throughout the whole period of my PhD studies. While doing my work I enjoyed an extraordinary degree of academic freedom. Nevertheless, he was always prepared to help me with words and deeds; and many discussions we had were essential for the success of this thesis.

I am highly thankful to the head of the institute Prof. Dr. Werner Kunz for his generous support and for providing the laboratory facilities.

I would like to express my sincere thanks to Prof. Dr. Glenn Hefter, Murdoch University, Perth, Australia, for valuable discussions and very useful suggestions. His active interest in the progress and proofreading of the English text of the present thesis is gratefully acknowledged. I cordially thank Dr. Simon Schrödle for recording initial VNA data at Murdoch University, when the VNA instrument was not available at Regensburg Institute.

I sincerely acknowledge the Higher Education Commission of Pakistan (HEC) for a PhD grant and German Academic Exchange Service (DAAD) for guidance and support. Furthermore, financial support from the Deutsche Forschungsgemeinschaft (DFG) is highly acknowledged.

Moreover, I thank the Friends of the University of Regensburg (Verein der Freunde der Universität Regensburg e. V.), for partially sponsoring me to participate in EMLG/JMLG Annual Meeting 2011, held in Warsaw/Poland.

I would like to express my gratitude to my current and former colleagues in the microwave group, Dr. Johannes Hunger, Dr. Alexander Stoppa, Saadia Shaukat, Thomas Sonnleitner, Andreas Eiberweiser, and Bernd Muehldorf, for their steady support, friendliness, and the time we shared. I am specially thankful to Dr. Johannes Hunger and Dr. Alexander Stoppa for introducing me to the mysteries of the microwave instruments.

Thanks to all members of workshops for completing my orders reliably and quickly. Furthermore, I would like to thank all staff members of the Institute of Physical and Theoretical Chemistry for their cooperativeness.

I wish to express my deep gratitude to my family members, who have been supporting and encouraging me with their best wishes throughout my studies over the years. I specially thank my sister, Parveen Akhter, and brother, M. Atta ur Rahman, who not only motivated me for the higher studies but also helped me in all regards.

Constants, symbols and acronyms

Constants

elementary charge	e_0	$= 1.60217739 \cdot 10^{-19}\,\mathrm{C}$
permittivity of free space	ε_0	$= 8.854187816 \cdot 10^{-12}\,\mathrm{C^2(Jm)^{-1}}$
Avogadro's constant	N_A	$= 6.0221367 \cdot 10^{23}\,\mathrm{mol^{-1}}$
speed of light	c_0	$= 2.99792458 \cdot 10^{8}\,\mathrm{m\,s^{-1}}$
Boltzmann's constant	k_B	$= 1.380658 \cdot 10^{-23}\,\mathrm{J\,K^{-1}}$
permeability of free space	μ_0	$= 4\pi \cdot 10^{-7}\,\mathrm{(Js)^2(C^2m)^{-1}}$
Planck's constant	h	$= 6.6260755 \cdot 10^{-34}\,\mathrm{Js}$

Symbols

$\vec{B}$	magnetic induction [$\mathrm{Vs\,m^{-2}}$]	$\vec{D}$	electric induction [$\mathrm{C\,m^{-2}}$]
$\vec{E}$	electric field strength [$\mathrm{V\,m^{-1}}$]	$\vec{H}$	magnetic field strength [$\mathrm{A\,m^{-1}}$]
ν	frequency [$\mathrm{s^{-1}}$]	ω	angular frequency [$\mathrm{s^{-1}}$]
$\vec{P}$	polarization [$\mathrm{C\,m^{-2}}$]	μ	dipole moment [C m]
$\hat{\varepsilon}$	complex dielectric permittivity	ε'	real part of $\hat{\varepsilon}$
ε''	imaginary part of $\hat{\varepsilon}$	ε	$\lim_{\nu\to 0}(\varepsilon')$
ε_∞	$\lim_{\nu\to\infty}(\varepsilon')$	τ	relaxation time [s]
T	thermodynamic temperature [K]	c	molarity $\left[\mathrm{mol\,dm^{-3}}\right]$
κ	conductivity [$\mathrm{S\,m^{-1}}$]	ρ	density [$\mathrm{kg\,m^{-3}}$]

Acronyms

DRS	dielectric relaxation spectroscopy	NMR	nuclear magnetic resonance
IFM	interferometer	VNA	vector network analyzer
DMA	*N*,*N*-dimethylacetamide	PC	propylene carbonate
QM	quantum mechanics	MD	molecular dynamics
SED	Stokes-Einstein-Debye	HN	Havriliak-Negami
D	Debye	CC	Cole-Cole
CD	Cole-Davidson	DHO	damped harmonic oscillator

Introduction

General aspects

Solute-solvent interactions are of critical importance in physical, environmental, and surface chemistry.[1] Knowledge of the nature of ion hydration is especially important in biology because it is a prerequisite for understanding the processes occurring in living cells.[1] For example, proteins and other biomolecules have evolved to function optimally in particular aqueous environments for which specific patterns of hydrophilic and hydrophobic components at their surfaces are believed to be essential.[1] Furthermore, biomolecules are known to influence their surrounding solvent layers, and this effect is reciprocal in that the solvent modifies the structure and activity of the biomolecules. Investigation of biomolecule hydration — especially of proteins — has a long tradition.[1–4] However, quantitative interpretation of the observed behaviour is often problematic, even when using the popular NMR techniques,[5] because of the similarity of the time-scales of H_2O dynamics in the vicinity of solute species and in the bulk solvent.

A common approach to get around these difficulties is to study smaller model compounds, such as amino acids or low-molecular-mass peptides, which contain key structural and/or chemical features of the larger species. Such molecules are of a size that is within the reach of computer simulations[6,7] and scattering methods.[8,9] Dielectric relaxation spectroscopy (DRS), which probes the response of dipolar species to a time-dependent electric field in the microwave region, is a particularly powerful tool for such studies because it provides quantitative information on the cooperative dynamics of both solute and solvent species.[10,11]

As already mentioned, an important feature of the hydration of many biomolecules is the close proximity of hydrophilic and hydrophobic moieties at their surfaces. However, the interaction of these disparate entities and their surrounding water molecules is not well understood. Therefore, it appears worthwhile for a deeper understanding of hydration effects to separate the contributions coming from hydrophilic and hydrophobic moieties on a molecule by investigating appropriate model compounds.

Besides the neutral hydroxyl groups and the positively charged ammonium groups, negatively charged carboxylate and phosphate but also sulfate and sulfonate, play an important role in controlling the hydrophilicity and thus the interactions of the biomolecules with water and dissolved hydrophilic compounds. In order to investigate the role of hydrophilic groups on the hydration of biomolecules, carboxylate, sulfate and sulfonate groups are the focus of the present DRS study. Carboxylate ($-COO^-$) groups are the major anionic sites in most biomolecules, being present for example in amino acids, fatty acids, lipid bilayers and

surface-active agents.[12] In addition the active sites of enzymes often feature carboxylate groups to facilitate metal-ion binding.[13] Sulfate ($-OSO_3^-$) and sulfonate ($-SO_3^-$) are also important anionic groups in biomolecules.[14] Beside their importance in biomolecules, long chain alkylsulfates and alkylsulfonates are most commonly used in detergent and soap industry as surface-active agents.[15] As already described, phosphate is also a key hydrophilic group present in the biomolecules. A detailed DRS study of hydration and ion binding of phosphate group in aqueous solution is the part of a different PhD project in our group.
The hydrophobicity of biomolecules is mainly controlled by aliphatic and/or aromatic hydrocarbons. Alkyl chain attached to the $-COO^-$ moiety was systematically increased to study the hydrophobic hydration associated with the hydrocarbon part of biomolecules. The hydration of different types of hydrophobic moieties was investigated by studying fluorinated and aromatic carboxylates.

Systems investigated and aims

Aqueous solutions of Sodium *n*-alkylcarboxylates ($C_{m-1}H_{2m-1}COONa$, where m = 1, 2, 3, 4, 5), trifluoroacetate (CF_3COONa), benzoate(C_6H_5COONa), methylsulfate (CH_3OSO_3Na) and methanesulfonate (CH_3SO_3Na) were selected for the present study. Sodium (Na^+) was taken as a counter ion as it is an important cation present in living cells. A specific concentration of Na^+ in the cytosol is vital for proper functioning of cell.[16] Furthermore, the cationic interaction with protein's carboxylate groups is of special interest due to its effect on protein association and enzymatic activity,[17] yet the details and consequences of ion pairing on molecular level are far from being fully understood. Traditionally ion-specific effects are rationalized in terms of water structuring around ions (kosmotropes vs chaotropes).[18] Modern experiments and computer simulations indicate that direct ion-protein interactions may be more important,[19] so a lot of attention was given to the cation-specific interactions with carboxylate in aqueous environments during last few years.[20–22] In this regard, the knowledge of interaction of Na^+ with $-COO^-$, $-OSO_3^-$ and $-SO_3^-$ moieties can help in understanding the consequences of direct ion-biomolecule interactions.
Collins' "law of matching water affinities"[23,24] predicts contact ion-pair (CIP) formation between Na^+ and anionic headgroups ($-COO^-$, $-OSO_3^-$ and $-SO_3^-$).[25] This prediction is further supported by experiments[26,27] and simulations.[19,25] On the other hand, on the basis of computer simulations of aqueous alkali acetate solutions, Hess and van der Vegt[22] proposed an ion-pairing mechanism, which, in contrast to the law of matching affinities, does not involve the formation of CIPs. Instead, these authors showed that solvent shared ion pairs (SIPs) are the dominant species in aqueous alkali acetate solutions. As DRS has a unique sensitivity towards different types of ion pairs,[10,11] present study can help to understand the nature of ion pairing between Na^+ and different biologically relevant anionic headgroups ($-COO^-$, $-OSO_3^-$ and $-SO_3^-$).
In the first part of this thesis, aqueous solutions of sodium formate (HCOONa, NaOFm), sodium acetate (CH_3COONa, NaOAc) and trifluoroacetate (CF_3COONa, $NaOAcF_3$) have been investigated. As formate ($HCOO^-$, OFm^-) ion does not possess a hydrophobic part, it can be used to study the hydrophilic hydration of alkylcarboxylates. Carboxylate hydration is intensively studied with computer simulations,[7,28–30] NMR,[31] neutron scattering and

infrared spectroscopy.[32–35] In terms of experiments the main sources for structural data are the publications of Kameda and coworkers on concentrated solutions of sodium and potassium salts of formate[32,33] and acetate[34,35] based on neutron and X-ray scattering, as well as on vibrational spectroscopy. The authors conclude that the number of water molecules forming hydrogen bonds to the $-COO^-$ group decreases from ∼4.5 in dilute solution to ∼1.5 in 40 mol% HCOOK. These values are close to the results obtained by Leung and Rempe in a series of *ab initio* molecular dynamics simulations[36] but somewhat smaller than the carboxylate hydration number of 5-6.5 from NMR.[31] The published value for ionic hydration number of acetate, $N = 1$,[37] through vibrational spectroscopy appears rather low although is comparable to data from conductivity measurements for formate and acetate.[38] Keeping in mind the discrepancies in the published results of carboxylate hydration, a DRS study of this biologically important moiety is worthwhile.
Additionally, a comparison of acetate (CH_3COO^-, OAc^-) and trifluoroacetate (a fluorinated alkylcarboxylate, CF_3COO^-, $OAcF_3^-$), will help to study the effect of fluorination on the hydration and ion association of carboxylate containing molecules.
The second part of the present thesis deals with the effect of systematically increasing hydrophobicity of *n*-alkylcarboxylates on hydration by studying the aqueous solutions of sodium propanoate (C_2H_5COONa, NaOPr), sodium butanoate (C_3H_7COONa, NaOBu) and sodium pentanoate (C_4H_9COONa, NaOPe). Furthermore, aqueous solutions of sodium benzoate (C_6H_5COONa, NaOBz) have been investigated to study the hydrophobic hydration of aryl substituted carboxylates. As already described above, a large amount of literature data is available on carboxylate hydration.[7,28–35] Major focus of all these studies was either the hydration of charged $-COO^-$ group or to some extent the effect of attached alkyl chain on the hydration of $-COO^-$. Even in a number of publications, it is claimed that water molecules surrounding nonpolar groups of solute behave (spectrally) roughly as water in bulk phase.[39–43] DRS has the ability to quite successfully probe the dynamics of water molecules in vicinity of both the hydrophobic (nonpolar) and hydrophilic (polar) groups of solutes. Present DRS study, in comparison with results of hydrophilic hydration of OFm^- (a representative of the hydrophilic hydration of $-COO^-$), will help to find out the hydrophobic hydration number associated with alkyl moiety of biomolecules. A comparison of hydration and aggregation of alkylhydrotrope (pentanoate) with that of the simplest arylhydrotrope (benzoate) may provide useful information about the mechanism of hydrotrope action.
In the last part of this PhD thesis, aqueous solutions of sodium methylsulfate (CH_3OSO_3Na, NaMS) and methanesulfonate (CH_3SO_3Na, NaMSn) have been investigated. These salts have widely used practical applications and sulfate and sulfonate are common ionic groups in biomolecules. Nevertheless, only very limited information on their hydration is available.[38,44] The impact of the methyl group will be accessible from the carboxylate series so that the hydration of the $-OSO_3^-$) and $-SO_3^-$ moiety can be probed. A comparison of the hydration of organic sulfate with that of already reported inorganic sulfate[45] will be possible allowing thus to check the influence of charge density on hydration.

Chapter 1

Theoretical background

1.1 Basics of electrodynamics

1.1.1 Maxwell and constitutive equations

The theory of electromagnetic fields is based on the four Maxwell's equations.[46,47] These four equations

$$\vec{\nabla} \times \vec{H} = \vec{j} + \frac{\partial}{\partial t}\vec{D} \tag{1.1}$$

$$\vec{\nabla} \times \vec{E} = -\frac{\partial}{\partial t}\vec{B} \tag{1.2}$$

$$\vec{\nabla} \cdot \vec{D} = \rho_{\mathrm{el}} \tag{1.3}$$

$$\vec{\nabla} \cdot \vec{B} = 0 \tag{1.4}$$

describe the generation of magnetic fields, $\vec{H}$ (magnetic field strength), by currents (extended Ampère's law, Eq. 1.1), explain how changing magnetic fields produce electric fields (electric field strength, $\vec{E}$; Faraday's law of induction, Eq. 1.2) and how electric charges (electric charge density, ρ_{el}) produce electric fields (Gauss' law, Eq. 1.3), and show the absence of magnetic charges (Eq. 1.4). In the above set of equations $\vec{j}$ represents the current density and $\vec{B}$ and $\vec{D}$ account for the magnetic and electric induction, also called magnetic flux density or electric displacement field, respectively.
Together with the Newton equation

$$m\frac{\partial^2}{\partial t^2}\vec{r} = q(\vec{E} + \vec{v} \times \vec{B}) \tag{1.5}$$

where q denotes a moving charge and $\vec{v}$ its velocity, Eqs. 1.1-1.4 form a complete set of linear partial differential equations which theoretically allows the calculation of all kinds of electromagnetic phenomena.

For homogenous, nondispersive, isotropic materials at low fields $\vec{D}$ can be expressed by[48]

$$\vec{D} = \varepsilon\varepsilon_0\vec{E} \tag{1.6}$$

where ε is the relative permittivity and ε_0 is the the dielectric permittivity of vacuum. In accordance with the above equation (Eq. 1.6), also a linear relationship between $\vec{H}$ and $\vec{B}$ can be defined as

$$\vec{H} = \frac{\vec{B}}{\mu\mu_0} \tag{1.7}$$

where μ is the relative magnetic permittivity and μ_0 is the magnetic permittivity of vacuum. The relation between μ_0 and ε_0 is given by, $\mu_0 = 1/\varepsilon_0 c^2$, where c is the velocity of light in vacuum.
Similar to Eq. 1.6 Ohms law

$$\vec{j} = \kappa\vec{E} \tag{1.8}$$

gives the relationship between $\vec{j}$ and $\vec{E}$ where κ is the electric conductivity.
The constitutive equations (Eqs. 1.6 & 1.7), which relate $\vec{D}$ and $\vec{H}$ to $\vec{E}$ and $\vec{B}$ by time- and field strength-independent scalars (material properties) like ε, κ and μ, are valid only for the special case of a time-independent field response.

1.1.2 The electric displacement field

The previous section is dealing with the theory of electric polarization by static, *i.e.*, time-independent electric fields where polarization caused by the electric field is in equilibrium with the field. Now consider the dynamic case, which is described with the help of harmonic, *i.e.*, sinusoidally varying electric fields. The time dependence of electric field strength is given by[48]

$$\vec{E}(t) = \vec{E}_0 \cos(\omega t) \tag{1.9}$$

where $\vec{E}_0$ is the amplitude and $\omega = 2\pi\nu$ the angular frequency of the sinusoidal variation. When the frequency of the sinusoidal electric field is sufficiently high, typically in the region of 1 MHz to 1 GHz for the condensed phase, the motion of the microscopic particles does not follow the changes in the field due to interaction or inertia within the system. As a result a frequency-dependent phase delay, $\delta(\omega)$, is observed between the electric field and the electric displacement so that

$$\vec{D}(t) = \vec{D}_0 \cos(\omega t - \delta(\omega)) \tag{1.10}$$

where $\vec{D}_0$ is the amplitude of the sinusoidal variation. Splitting Eq. 1.10 according to the addition theorem of the cosine function into two sinusoidally varying parts, one in phase with the electric field and the other having a phase difference of $\pi/2$

$$\vec{D}(t) = \vec{D}_0 \cos(\delta(\omega)) \cos(\omega t) + \vec{D}_0 \sin(\delta(\omega)) \sin(\omega t) \tag{1.11}$$

and introducing

$$\vec{D}_0 \cos(\delta(\omega)) = \varepsilon'(\omega)\varepsilon_0\vec{E}_0 \tag{1.12}$$

$$\vec{D}_0 \sin(\delta(\omega)) = \varepsilon''(\omega)\varepsilon_0\vec{E}_0 \tag{1.13}$$

the electric displacement field can be expressed as

$$\vec{D}(t) = \varepsilon'(\omega)\varepsilon_0\vec{E}_0\cos(\omega t) + \varepsilon''(\omega)\varepsilon_0\vec{E}_0\sin(\omega t) \tag{1.14}$$

and the phase delay as

$$\tan(\delta(\omega)) = \frac{\varepsilon''(\omega)}{\varepsilon'(\omega)} \tag{1.15}$$

Now, $\vec{D}(t)$ is characterized by a dispersive part (first term in Eq. 1.14), which is in-phase with $\vec{E}(t)$, and a phase-shifted dissipative term (second term in Eq. 1.14). The frequency dependent relative permittivity, $\varepsilon'(\omega)$, and dielectric loss, $\varepsilon''(\omega)$ contributions are summarized as the complex permittivity

$$\hat{\varepsilon}(\omega) = \varepsilon'(\omega) - \mathrm{i}\varepsilon''(\omega) \tag{1.16}$$

By using complex notation, the complex field vectors $\hat{\vec{E}}(t)$ and $\hat{\vec{D}}(t)$ are introduced via

$$\hat{\vec{E}}(t) = \vec{E}_0\cos(\omega t) + \mathrm{i}\vec{E}_0\sin(\omega t) = \vec{E}_0\exp(\mathrm{i}\omega t) \tag{1.17}$$

$$\hat{\vec{D}}(t) = \vec{D}_0\cos(\omega t - \delta) + \mathrm{i}\vec{D}_0\sin(\omega t - \delta) = \vec{D}_0\exp[\mathrm{i}(\omega t - \delta)] \tag{1.18}$$

Thus, the complex form of the constitutive equations is obtained for the dynamic, *i.e.*, frequency dependent, case as[48]

$$\hat{\vec{D}}(t) = \hat{\varepsilon}(\omega)\varepsilon_0\hat{\vec{E}}(t) \tag{1.19}$$

$$\hat{\vec{j}}(t) = \hat{\kappa}(\omega)\hat{\vec{E}}(t) \tag{1.20}$$

$$\hat{\vec{B}}(t) = \hat{\mu}(\omega)\mu_0\hat{\vec{H}}(t) \tag{1.21}$$

with the complex conductivity, $\hat{\kappa}(\omega)$, and the complex relative magnetic permeability, $\hat{\mu}(\omega)$.

1.1.3 Wave equations

The Maxwell equation (1.1) for harmonic fields

$$\hat{\vec{E}}(t) = \vec{E}_0\exp(\mathrm{i}\omega t) \tag{1.22}$$

$$\hat{\vec{H}}(t) = \vec{H}_0\exp(\mathrm{i}\omega t) \tag{1.23}$$

can be transformed with the help of the complex constitutive equations (1.19) - (1.21) into

$$\vec{\mathrm{rot}}\,\vec{H}_0 = (\hat{\kappa}(\omega) + \mathrm{i}\omega\hat{\varepsilon}(\omega)\varepsilon_0)\vec{E}_0 \tag{1.24}$$

In a similar way, the equation

$$\vec{\mathrm{rot}}\,\vec{E}_0 = -\mathrm{i}\omega\hat{\mu}(\omega)\mu_0\vec{H}_0 \tag{1.25}$$

is obtained from the Maxwell equation (1.2).
By application of the rotation operator to Eq. 1.24 in combination with Eq. 1.25 and the Legendre vectorial identity

$$\vec{\mathrm{rot}}\,\vec{\mathrm{rot}}\,\vec{H}_0 = \vec{\mathrm{grad}}\,\mathrm{div}\,\vec{H}_0 - \triangle\vec{H}_0 = \vec{\mathrm{grad}}\,(0) - \triangle\vec{H}_0 = -\triangle\vec{H}_0 \tag{1.26}$$

the reduced wave equation of the magnetic field is obtained

$$\triangle\vec{H}_0 + \hat{k}^2\vec{H}_0 = 0 \tag{1.27}$$

The propagation constant, $\hat{k}$, is defined as

$$\hat{k}^2 = k_0^2\left(\hat{\mu}(\omega)\hat{\varepsilon}(\omega) + \frac{\hat{\mu}(\omega)\hat{\kappa}(\omega)}{\mathrm{i}\omega\varepsilon_0}\right) \tag{1.28}$$

The propagation constant of free space, k_0, is given by

$$k_0 = \omega\sqrt{\varepsilon_0\mu_0} = \frac{2\pi}{\lambda_0} \tag{1.29}$$

with

$$c_0 = \frac{1}{\sqrt{\varepsilon_0\mu_0}} \tag{1.30}$$

where c_0 and λ_0 are the speed of light and the wavelength of a monochromatic wave in vacuum, respectively. In the case of a solenoidal medium ($\mathrm{div}\,\vec{E} = 0$) a reduced wave equation for $\vec{E}$ can be obtained

$$\triangle\hat{\vec{E}}_0 + \hat{k}^2\hat{\vec{E}}_0 = 0 \tag{1.31}$$

For nonmagnetizable materials ($\hat{\mu} = 1$), $\hat{k}$ is written as

$$\hat{k}^2 = k_0^2\left(\hat{\varepsilon}(\omega) + \frac{\hat{\kappa}(\omega)}{\mathrm{i}\omega\varepsilon_0}\right) \equiv k_0^2\hat{\eta}(\omega) \tag{1.32}$$

and the generalized complex permittivity, $\hat{\eta}(\omega) = \eta'(\omega) - \mathrm{i}\eta''(\omega)$, is defined with its real and imaginary parts as

$$\eta'(\omega) = \varepsilon'(\omega) - \frac{\kappa''(\omega)}{\omega\varepsilon_0} \tag{1.33}$$

$$\eta''(\omega) = \varepsilon''(\omega) + \frac{\kappa'(\omega)}{\omega\varepsilon_0} \tag{1.34}$$

As only $\hat{\eta}(\omega)$ is experimentally accessible, these equations show that dielectric properties and the conductivity of a system cannot be measured separately. Using the limits of $\hat{\kappa}(\omega)$, *i.e.*, $\lim_{\nu\to 0}\kappa' = \kappa$ and $\lim_{\nu\to 0}\kappa'' = 0$, where κ is the dc conductivity, one can calculate the complex dielectric permittivity from $\hat{\eta}(\omega)$ via

$$\varepsilon'(\omega) = \eta'(\omega) \tag{1.35}$$

and

$$\varepsilon''(\omega) = \eta''(\omega) - \frac{\kappa}{\omega\varepsilon_0} \tag{1.36}$$

Using this approach $\hat{\varepsilon}(\omega)$ contains all contributions to the time dependent polarization, $\vec{P}(t)$, that depend on frequency, irrespective of their rotational, vibrational, or translational character.
The theory of Debye and Falkenhagen[49] suggests some dispersion of the complex conductivity, $\hat{\kappa}$, of electrolyte solutions due to the relaxation of the ion cloud, *i.e.*, the rearrangement of the ion cloud around an ion as a consequence of the translational movement of the ion. From an experimental point of view, this effect is usually thought to be negligible.[50] Note, however that with Eqs. 1.35 & 1.36 a possible contribution from ion-cloud relaxation should show up in $\hat{\varepsilon}(\omega)$.

1.2 Dielectric relaxation

1.2.1 Polarization

The dielectric displacement field $\hat{\vec{D}}$ can be split into two contributions

$$\hat{\vec{D}} = \hat{\varepsilon}\varepsilon_0\hat{\vec{E}} = \varepsilon_0\hat{\vec{E}} + \hat{\vec{P}} \tag{1.37}$$

with

$$\hat{\vec{P}} = (\hat{\varepsilon} - 1)\varepsilon_0\hat{\vec{E}} \tag{1.38}$$

The term $\varepsilon_0\hat{\vec{E}}$ is independent of medium, whereas $\hat{\vec{P}}$ is the polarization describing the effect of an electric field on medium. Beside this macroscopic definition $\hat{\vec{P}}$ can also be interpreted microscopically[48]

$$\hat{\vec{P}} = \hat{\vec{P}}_\mu + \hat{\vec{P}}_\alpha \tag{1.39}$$

as the sum of orientational polarization

$$\hat{\vec{P}}_\mu = \sum_k \rho_k \langle\vec{\mu}_k\rangle \tag{1.40}$$

and induced polarization

$$\hat{\vec{P}}_\alpha = \sum_k \rho_k \alpha_k (\hat{\vec{E}}_\mathrm{i})_k \tag{1.41}$$

Eq. 1.40 results from the orientation of molecular dipoles of species k with permanent dipole moment, $\vec{\mu}_k$, and number density, ρ_k, in the external field against their thermal motion. For species with molecular polarizability, α_k, Eq. 1.41 describes the induced polarization in the medium caused by the inner field, $(\hat{\vec{E}}_\mathrm{i})_k$, acting at the position of the molecule.

Orientational polarization in liquids occurs at pico- to nanosecond time scales, corresponding to an approximate frequency scale of 1 MHz to 10 THz. Due to the coupling of the reorienting dipoles with the surrounding medium rather broad bands are observed. Nevertheless, determination of the frequency dependent complex permittivity can provide valuable insight into the dynamics of liquids.

The value of $\hat{\vec{P}}_\alpha$ is rather constant in the microwave range and its frequency dependence leads to information about the intramolecular dynamics of the system. It consists of two contributions, one in the infrared (atomic polarization) and the other in the ultraviolet range (electron polarization). The absorption peaks are in most cases sharper compared to those at microwave frequencies.[51]

Due to the different time scales of $\hat{\vec{P}}_\mu$ and $\hat{\vec{P}}_\alpha$, both effects are generally well separated and can be regarded as linearly independent.[52] Thus the induced polarization can be incorporated into the infinite frequency permittivity, ε_∞, as

$$\hat{\vec{P}}_\mu = \varepsilon_0(\hat{\varepsilon} - \varepsilon_\infty)\hat{\vec{E}} \tag{1.42}$$

$$\hat{\vec{P}}_\alpha = \varepsilon_0(\varepsilon_\infty - 1)\hat{\vec{E}} \tag{1.43}$$

Situated in the far-infrared, ε_∞ denotes the permittivity after the decay of orientational polarization, whereas the contribution arising from induced polarization still remains unchanged. In practice, the limiting value of the permittivity for infinite frequencies as extrapolated from the microwave range is taken for ε_∞.[51]

1.2.2 Response functions of the orientational polarization

At sufficiently high frequencies the orientational polarization decreases, because the molecular dipoles cannot align parallel to the alternating field due to inertia and friction. In the case of a linear medium, $\hat{\vec{P}}$ is related to $\hat{\vec{E}}$ via certain response functions.[48]

For small enough $\hat{\vec{E}}$, a linear medium can be assumed, meaning that if a field $\vec{E}_1$ generates a polarization $\vec{P}_1$ and field $\vec{E}_2$ a polarization $\vec{P}_2$, then the field $\vec{E}_1 + \vec{E}_2$ results in a polarization $\vec{P}_1 + \vec{P}_2$. Consider an isotropic linear dielectric material that is polarized by an electric field. At time $t = 0$, the field is switched off and the time evolution of the polarization is recorded. The induced polarization will follow changes of the applied field without delay, whereas the orientational polarization can be written as

$$\hat{\vec{P}}_\mu(t) = \hat{\vec{P}}_\mu(0) \cdot F_P^{\mathrm{or}}(t) \tag{1.44}$$

where $F_P^{\mathrm{or}}(t)$ is called the response or decay function of the polarization. It is defined as

$$F_P^{\mathrm{or}}(t) = \frac{\langle \vec{P}_\mu(0) \cdot \vec{P}_\mu(t) \rangle}{\langle \vec{P}_\mu(0) \cdot \vec{P}_\mu(0) \rangle} \tag{1.45}$$

For $t = 0$ it follows that $F_P^{\mathrm{or}}(0) = 1$; for high values of t, $\hat{\vec{P}}$ will reach the equilibrium value and consequently $F_P^{\mathrm{or}}(\infty) = 0$.

In the case of a harmonic electric field, $\hat{\vec{E}}(t) = \hat{\vec{E}}_0 \exp(-\mathrm{i}\omega t)$, the orientational polarization at any time t can be expressed as

$$\hat{\vec{P}}(\omega, t) = \varepsilon_0(\varepsilon - \varepsilon_\infty)\hat{\vec{E}}(t)\mathcal{L}_{\mathrm{i}\omega}[f_P^{\mathrm{or}}(t')] \tag{1.46}$$

with

$$\mathcal{L}_{\mathrm{i}\omega}[f_P^{\mathrm{or}}(t')] = \int_0^\infty \exp(-\mathrm{i}\omega t') f_P^{\mathrm{or}}(t')\mathrm{d}t' \tag{1.47}$$

Where $\mathcal{L}_{iw}[f_P^{\mathrm{or}}(t')]$ is the Laplace-transformed pulse response function of the orientational polarization. This can be obtained from the negative derivative of the normalized step response function

$$f_P^{\mathrm{or}}(t') = -\frac{\partial F_P^{\mathrm{or}}(t-t')}{\partial(t-t')} \quad \text{normalized with} \quad \int_0^\infty f_P^{\mathrm{or}}(t')\mathrm{d}t' = 1 \tag{1.48}$$

The complex permittivity, $\hat{\varepsilon}(\omega)$, can then be calculated as[48]

$$\hat{\varepsilon}(\omega) = \varepsilon'(\omega) - \mathrm{i}\varepsilon''(\omega) = \varepsilon_\infty + (\varepsilon - \varepsilon_\infty) \cdot \mathcal{L}_{\mathrm{i}\omega}[f_P^{\mathrm{or}}(t')] \tag{1.49}$$

1.3 Empirical description of dielectric relaxation

Dielectric relaxation processes are usually analyzed using model functions. Several empirical and semi-empirical equations are proposed in the literature to describe dielectric relaxation phenomena. As the majority of the spectra represent a sum of various relaxation processes the best description of the spectra can be achieved by a superposition of various equations.

1.3.1 Debye equation

The Debye (D) equation[53] represents the simplest way of describing dielectric spectra of liquids. It is assumed that the decrease of the orientational polarization in the absence of an external electric field is directly proportional to the polarization itself.[54] Therefore, it can be expressed by a time law of the first order

$$\frac{\partial}{\partial t}\vec{P}_\mu(t) = -\frac{1}{\tau}\vec{P}_\mu(t) \tag{1.50}$$

where τ is the relaxation time, which describes the dynamics of the process. From the solution of Eq. 1.50

$$\vec{P}_\mu(t) = \vec{P}_\mu(0)\exp\left(-\frac{t}{\tau}\right) \tag{1.51}$$

the step response function, $F_P^{\mathrm{or}}(t) = \exp\left(-\frac{t}{\tau}\right)$, can be obtained. By application of Eq. 1.48, the pulse response function

$$f_P^{\mathrm{or}}(t) = \frac{1}{\tau}\exp\left(-\frac{t}{\tau}\right) \tag{1.52}$$

can easily be calculated.
The complex dielectric permittivity is obtained by Fourier transformation of the pulse response function according to Eq. 1.49

$$\hat{\varepsilon}(\omega) = \varepsilon_\infty + (\varepsilon - \varepsilon_\infty) \cdot \mathcal{L}_{\mathrm{i}\omega}\left[\frac{1}{\tau}\exp\left(-\frac{t}{\tau}\right)\right] \tag{1.53}$$

Finally, the Debye equation can be written as

$$\hat{\varepsilon}(\omega) = \varepsilon_\infty + \frac{\varepsilon - \varepsilon_\infty}{1 + \mathrm{i}\omega\tau} \tag{1.54}$$

which can be split into the real

$$\varepsilon'(\omega) = \varepsilon_\infty + \frac{\varepsilon - \varepsilon_\infty}{1 + \omega^2\tau^2} \tag{1.55}$$

and imaginary part

$$\varepsilon''(\omega) = \omega\tau\frac{\varepsilon - \varepsilon_\infty}{1 + \omega^2\tau^2} \tag{1.56}$$

The relative permittivity, $\varepsilon' = \varepsilon'(\ln(\omega))$, is a monotonically decreasing point-symmetric function and the absorption curve, $\varepsilon'' = \varepsilon''(\ln(\omega))$, an axis-symmetric band reaching its maximum at $\omega = 2\pi\nu = 1/\tau$.

1.3.2 Relaxation time distributions

For a large number of condensed systems the Debye equation, based on the assumption of one relaxation time, is unable to provide a satisfying description. Description of these spectra can be improved by assuming a continuous relaxation time distribution, $g(\tau)$.[48] Due to practical reasons, the logarithmic representation, $G(\ln\tau)$, is preferred. The complex permittivity can then be written as

$$\hat{\varepsilon}(\omega) = \varepsilon_\infty + (\varepsilon - \varepsilon_\infty)\int_0^\infty \frac{G(\ln\tau)}{(1 + \mathrm{i}\omega\tau)}\mathrm{d}\ln\tau \quad \text{with} \quad \int_0^\infty G(\ln\tau)\mathrm{d}\ln\tau = 1. \tag{1.57}$$

Unfortunately, $G(\ln\tau)$ can not be obtained from experimental data in a straightforward way. Therefore empirical parameters are used which account for the broadness and shape of the relaxation time distribution.

Cole-Cole equation. Introduction of empirical parameter $0 \leq \alpha < 1$ into Debye equation yields the Cole-Cole (CC) equation[55,56]

$$\hat{\varepsilon}(\omega) = \varepsilon_\infty + \frac{\varepsilon - \varepsilon_\infty}{1 + (\mathrm{i}\omega\tau_0)^{1-\alpha}} \tag{1.58}$$

It is based on a symmetric relaxation time distribution around a principal relaxation time τ_0, describing symmetric dispersion and absorption curves. This kind of distribution results in flatter dispersion curves and broadened absorption spectra. For $\alpha = 0$, Eq. 1.58 reduces to the Debye equation.

Cole-Davidson equation. The Cole-Davidson (CD) equation,[57,58] with an empirical parameter $0 < \beta \leq 1$, describes an asymmetrical relaxation time distribution around the center of gravity τ_0

$$\hat{\varepsilon}(\omega) = \varepsilon_\infty + \frac{\varepsilon - \varepsilon_\infty}{(1 + \mathrm{i}\omega\tau_0)^{\beta}} \tag{1.59}$$

The CD equation describes asymmetric dispersions and absorption curves. For $\beta = 1$ this equation turns into the Debye equation.

Havriliak-Negami equation. For the description of broad asymmetric relaxation time distribution both $0 \leq \alpha < 1$ and $0 < \beta \leq 1$ are combined in the Havriliak-Negami (HN) equation[59]

$$\hat{\varepsilon}(\omega) = \varepsilon_\infty + \frac{\varepsilon - \varepsilon_\infty}{[1 + (\mathrm{i}\omega\tau_0)^{1-\alpha}]^{\beta}} \tag{1.60}$$

Both the dispersion and absorption curves are asymmetric. For $\alpha = 0$ and $\beta = 1$, Eq. 1.60 simplifies to the Debye equation.

1.3.3 Damped harmonic oscillator

Many vibrational dielectric processes (intermolecular and intramolecular vibrations as well as librations) in the THz or far-infrared regions can be modelled as a damped harmonic oscillator (DHO). Assuming a harmonic oscillator subjected to a damping force and driven by a harmonically oscillating field $E(t) = E_0 e^{\mathrm{i}\omega t}$, the frequency dependent response function of the system can be obtained

$$\hat{\varepsilon}(\omega) = \varepsilon_\infty + \frac{(\varepsilon - \varepsilon_\infty)\,\omega_0^2}{(\omega_0^2 - \omega^2) + \mathrm{i}\omega\tau_\mathrm{D}^{-1}} = \varepsilon_\infty + \frac{(\varepsilon - \varepsilon_\infty)\,\nu_0^2}{\nu_0^2 - (\frac{\omega}{2\pi})^2 + \mathrm{i}\frac{\omega}{2\pi}\gamma} \tag{1.61}$$

from the solution of the differential equation describing the time-dependent motion, $x(t)$, of an effective charge, q.[60] In Eq. 1.61, $\omega_0 = \sqrt{k/m} = 2\pi\nu_0$ and $\gamma = 1/(2\pi\tau_\mathrm{D})$ are the angular resonance frequency and damping constant of the oscillator, respectively. For $\tau_\mathrm{D} \ll \omega_0^{-1}$, Eq. 1.61 reduces to the Debye equation.

1.3.4 Combination of models

For many real systems the complex permittivity spectrum is composed of several relaxation processes. So Eq. 1.57 can be written as a superposition of n single relaxation processes

$$\hat{\varepsilon}(\omega) = \varepsilon_\infty + \sum_{j=1}^{n}(\varepsilon_j - \varepsilon_{\infty,j}) \int_0^\infty \frac{G_j(\ln \tau_j)}{1 + \mathrm{i}\omega\tau_j} \mathrm{d} \ln \tau_j \tag{1.62}$$

Each of the processes is treated separately and is characterized by its own relaxation time, τ_j, and dispersion amplitude, S_j, defined via

$$\varepsilon - \varepsilon_\infty = \sum_{j=1}^{n}(\varepsilon_j - \varepsilon_{\infty,j}) = \sum_{j=1}^{n} S_j \tag{1.63}$$

$$\varepsilon_{\infty,j} = \varepsilon_{j+1} \tag{1.64}$$

This leads to the general expression for superpositions of HN and DHO equations

$$\begin{aligned} \hat{\varepsilon}(\omega) = \varepsilon_\infty \quad &+ \quad \sum_j \frac{S_j}{[1 + (\mathrm{i}\omega\tau_j)^{1-\alpha_j}]^{\beta_j}} \\ &+ \quad \sum_l \frac{S_l\, \omega_{0,l}^2}{(\omega_{0,l}^2 - \omega^2) + \mathrm{i}\omega\tau_{\mathrm{D},l}^{-1}} \end{aligned} \tag{1.65}$$

1.4 Microscopic models of dielectric relaxation

1.4.1 Onsager equation

The Onsager model[48,61] describes dielectric polarization of dipole mixtures. It uses a continuum description of the material which provides an environment for the dipole reorientation. Specific interactions and the anisotropy of the surrounding field are neglected.
Based on this approach, Onsager deduced following relation to connect macroscopic (ε) and microscopic (the polarizability, α_j, and the dipole moment, μ_j, of molecular-level species j) properties

$$\varepsilon_0(\varepsilon - 1)\vec{E} = \vec{E}_h \cdot \sum_j \frac{\rho_j}{1 - \alpha_j f_j} \left(\alpha_j + \frac{1}{3k_\mathrm{B}T} \cdot \frac{\mu_j^2}{1 - \alpha_j f_j} \right) \tag{1.66}$$

where ρ_j represents the dipole density and f_j the reaction field factor describing a spherical cavity of finite radius, in which the particle is embedded. Note, that the Onsager equation is only valid for systems with a single dispersion step.
For a spherical cavity in a dielectric material, the cavity field, $\vec{E}_h$, is given by[48]

$$\vec{E}_h = \frac{3\varepsilon}{2\varepsilon + 1}\vec{E} \tag{1.67}$$

and thus the general form of the Onsager equation is obtained as

$$\frac{(\varepsilon-1)(2\varepsilon+1)\varepsilon_0}{3\varepsilon} = \sum_j \frac{\rho_j}{1-\alpha_j f_j}\left(\alpha_j + \frac{1}{3k_\mathrm{B}T}\cdot\frac{\mu_j^2}{1-\alpha_j f_j}\right) \tag{1.68}$$

In the case of a pure dipole liquid with non-polarizable molecules Eq. 1.68 reduces to

$$\frac{(\varepsilon-\varepsilon_\infty)(2\varepsilon+\varepsilon_\infty)}{\varepsilon(\varepsilon_\infty+2)^2} = \frac{\rho\mu^2}{9\varepsilon_0 k_\mathrm{B}T} \tag{1.69}$$

1.4.2 Kirkwood-Fröhlich equation

Specific intermolecular interactions can be accounted with the help of statistical mechanics. The theory[62,63] is based on a model of a dipole whose orientation correlates with its neighboring dipoles resulting in the Kirkwood and Fröhlich equation

$$\frac{(\varepsilon-\varepsilon_\infty)(2\varepsilon+\varepsilon_\infty)}{\varepsilon(\varepsilon_\infty+2)^2} = \frac{\rho\mu^2}{9\varepsilon_0 k_\mathrm{B}T}\cdot g_\mathrm{K} \tag{1.70}$$

where g_K is the so-called Kirkwood factor. It is a measure of the interactions among the dipoles. That is, it represents orientational correlations, with $g_\mathrm{K} > 1$ corresponding to preferentially parallel orientations and $g_\mathrm{K} < 1$ to antiparallel orientations. The value $g_\mathrm{K} = 1$ implies a statistical (*i.e.*, fully random) alignment of dipoles.

1.4.3 Cavell equation

The Cavell equation[64] represents the extension of the Onsager equation (Eq. 1.68) to systems with more than one dispersion step due to different dipolar species. It can be written as

$$\frac{\varepsilon + A_j(1-\varepsilon)}{\varepsilon}\cdot S_j = \frac{N_\mathrm{A}c_j}{3k_\mathrm{B}T\varepsilon_0}\cdot\mu_{\mathrm{eff},j}^2 \tag{1.71}$$

This equation relates the dispersion amplitude, $S_j = \varepsilon_j - \varepsilon_{j+1}$, of relaxation process j to the molar concentration of the species, c_j, and their effective dipole moments, $\mu_{\mathrm{eff},j}$. The shape factor A_j accounts for the shape of the relaxing particle; for spheres, $A_j = 1/3$, but it can be calculated for ellipsoids of any shape (half-axes $a_j > b_j > c_j$) via the equation[48,51]

$$A_j = \frac{a_j b_j c_j}{2}\int_0^\infty \frac{\mathrm{d}s}{(s+a_j^2)^{3/2}(s+b_j^2)^{1/2}(s+c_j^2)^{1/2}} \tag{1.72}$$

An expression for prolate ellipsoids ($b_j = c_j$) was derived by Scholte,[65]

$$A_j = -\frac{1}{p_j^2-1} + \frac{p_j}{(p_j^2-1)^{1.5}}\ln\left(p_j + \sqrt{p_j^2-1}\right) \qquad \text{with} \qquad p_j = \frac{a_j}{b_j} \tag{1.73}$$

The value of $\mu_{\mathrm{eff},j}$ (which can be calculated using Eq. 1.71 if c_j is known) is related to $\mu_{\mathrm{ap},j}$, the apparent dipole moment of the species in solutions in the absence of orientational correlations, as

$$\mu_{\mathrm{eff},j} = \sqrt{g_j}\,\mu_{\mathrm{ap},j} \tag{1.74}$$

where

$$\mu_{\mathrm{ap},j} = \frac{\mu_j}{1 - f_j \alpha_j} \tag{1.75}$$

includes cavity- and reaction-field effects on μ_j, the dipole moment of the isolated (gas phase) species. The (empirical) factor g_j is a measure for the strength of the correlations whose values are interpreted as for the Kirkwood factor g_{K} (Eq. 1.70), and the reaction field factor f_j can be calculated for a spherical cavity of radius a_j via[48]

$$f_j = \frac{1}{4\pi\varepsilon_0 a_j^3} \cdot \frac{2\varepsilon - 2}{2\varepsilon + 1} \tag{1.76}$$

or, more generally, for ellipsoidal particles via[66]

$$f_j = \frac{3}{4\pi\varepsilon_0 a_j b_j c_j} \cdot \frac{A_j(1 - A_j)(\varepsilon - 1)}{\varepsilon + (1 - \varepsilon)A_j} \tag{1.77}$$

1.4.4 Debye model of rotational diffusion

Debye tried to predict the relaxation time of a simple system consisting of an aggregation of spherical inelastic dipoles which do not interact with each other. Microscopically, uncorrelated collisions of the dipolar particles cause a reorientation of the dipoles. Therefore, this mechanism is called diffusion of dipole orientation.[53]
However, Debye's theory is only valid for non-associating systems and particles that are large compared to their surrounding ones[67] because of involved assumptions: for the reorientation of spherical particles, inertial effects and dipole-dipole interactions are neglected; the hydrodynamic laws of rotation of macroscopic particles in a liquid can be applied on the microscopic level.[53]
Within these limitations and by describing the inner field with a Lorentz field, Debye obtained the dipole correlation function[48]

$$\gamma(t) = \exp\left(-\frac{t}{\tau_{\mathrm{rot}}}\right) \tag{1.78}$$

where the microscopic relaxation time, τ_{rot}, is related to the friction factor, ζ,

$$\tau_{\mathrm{rot}} = \frac{\zeta}{2k_{\mathrm{B}}T} \tag{1.79}$$

Assuming a hydrodynamically controlled rotation of the sphere in a viscous media, the Stokes-Einstein-Debye (SED) equation

$$\tau_{\mathrm{rot}} = \frac{3V_{\mathrm{m}}\eta'}{k_{\mathrm{B}}T} \tag{1.80}$$

is obtained, where, V_{m} is the molecular volume of the rotating sphere and η' represents the microscopic viscosity (*i.e.*, the dynamic viscosity of the environment of the sphere).

However, the application of this theory is limited as the relation between microscopic and macroscopic (measured), η, viscosities is not clear. To overcome this problem, Dote et al.[68] derived a more general expression for the microscopic relaxation time

$$\tau_{\mathrm{rot}} = \frac{3V_{\mathrm{eff}}\eta}{k_{\mathrm{B}}T} + \tau^0_{\mathrm{rot}} \tag{1.81}$$

where τ^0_{rot} (the empirical axis intercept) can be interpreted as the correlation time of the freely rotating particle. The effective volume of rotation, V_{eff}, is defined as

$$V_{\mathrm{eff}} = fCV_{\mathrm{m}} \tag{1.82}$$

The hydrodynamic friction factor, C, accounts for difference between microscopic and macroscopic viscosities. Generally, it is treated as an empirical parameter but its limiting values are $C = 1$ for stick and $C = 1 - f^{-2/3}$ for slip boundary conditions. However, under special conditions, for example the rotation of very small molecules, values of $C < C_{\mathrm{slip}}$ are possible.[69]
For a prolate ellipsoid with major half-axis a and minor half-axis b, the shape factor, f, that accounts for deviations of the rotating particle from that of spherical shape can be calculated from the geometry of the molecule

$$f = \frac{\frac{2}{3}[1-(\alpha^{\perp})^4]}{\frac{[2-(\alpha^{\perp})^2](\alpha^{\perp})^2}{[1-(\alpha^{\perp})^2]^{1/2}} \ln\left[\frac{1+[1-(\alpha^{\perp})^2]^{1/2}}{\alpha^{\perp}}\right] - (\alpha^{\perp})^2} \tag{1.83}$$

where $\alpha^{\perp}$ is the ratio between the volume of particle and the volume swept out as the particle rotates about an axis perpendicular to the symmetry axis through the center of hydrodynamic stress ($\alpha^{\perp} = b/a$ for a prolate ellipsoid).[70]

1.4.5 Microscopic and macroscopic relaxation times

The relation between the experimentally accessible (macroscopic) dielectric relaxation time, τ, and the microscopic relaxation time (rotational correlation time), τ_{rot}, plays an important role in the interpretation of dielectric spectra and a number of theoretical approaches address this problem. Debye suggested the expression[53]

$$\tau = \frac{\varepsilon + 2}{\varepsilon_\infty + 2} \cdot \tau_{\mathrm{rot}} \tag{1.84}$$

derived under the assumption of a Lorentz field as inner field. However, this approach is not accurate enough for polar dielectrics and applies only to non-polar systems. For the case of pure rotational diffusion, Powles and Glarum,[71,72] proposed following expression

$$\tau = \frac{3\varepsilon}{2\varepsilon + \varepsilon_\infty} \cdot \tau_{\mathrm{rot}} \tag{1.85}$$

for relating microscopic and macroscopic relaxation times. A a more generalized equation, accounting for dipole-dipole correlation, is given by Madden and Kivelson[73]

$$\tau = \frac{3\varepsilon}{2\varepsilon + \varepsilon_\infty} \cdot \frac{g_{\mathrm{K}}}{\dot{g}} \cdot \tau_{\mathrm{rot}} \tag{1.86}$$

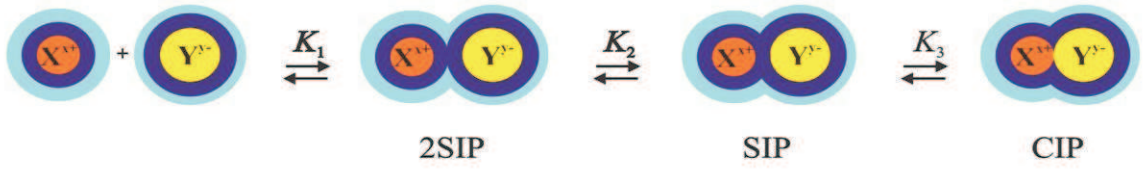

Figure 1.1: Scheme of stepwise ion association according to Eigen and Tamm.[74]

where g_K is the Kirkwood correlation factor and $\dot{g}$ is the dynamic correlation factor. For the limit $g_K/\dot{g} = 1$ Eq. 1.86 reduces to the Powles-Glarum equation (Eq. 1.85).

1.5 Ion association

Ions of opposite charge are generally considered to associate (form complexes) in aqueous solutions. Because of its great sensitivity towards ion pairs, DRS studies have been able to show that virtually all classical strong electrolytes are ion paired *to some extent*.[11] The extent of ion pairing increases with ionic charge and with decreasing solvent permittivity. A detailed three-step mechanism (Figure 1.1) for formation of ion pairs in aqueous solutions was first proposed by Eigen and Tamm in 1962.[74] This mechanism posits that ions combine initially with their solvation sheaths essentially intact, forming a double-solvent-separated ion pair (2SIP) or, in coordination chemistry terminology, an outer-outer-sphere complex

$$\underset{\text{hydrated free ions}}{M^{m+}(aq) + X^{x-}(aq)} \overset{K_1}{\rightleftharpoons} \underset{\text{2SIP}}{[M^{m+}(OH_2)(OH_2)X^{x-}](aq)} \tag{1.87}$$

This 2SIP species can then lose its intervening solvent molecules, forming successively a solvent-shared ion pair (SIP) or outer sphere complex

$$\underset{\text{2SIP}}{[M^{m+}(OH_2)(OH_2)X^{x-}](aq)} \overset{K_2}{\rightleftharpoons} \underset{\text{SIP}}{[M^{m+}(OH_2)X^{x-}](aq)} \tag{1.88}$$

and ultimately a contact ion pair (CIP) or inner-sphere complex

$$\underset{\text{SIP}}{[M^{m+}(OH_2)X^{x-}](aq)} \overset{K_3}{\rightleftharpoons} \underset{\text{CIP}}{[MX]^{(m-x)+}(aq)} \tag{1.89}$$

Each of these three steps is characterized by its equilibrium constant, $K_i, i = 1, 2, 3$, and the overall equilibrium by association constant $K_A = K_1 + K_1K_2 + K_1K_2K_3$. Obviously, not all steps of the Eigen mechanism are necessarily relevant. Depending on the salt concentration and the balance of ion-ion, ion-solvent, and solvent-solvent interactions the sequence may stop after the first or second step, or immediately yield SIP and even CIP. On the other hand, at least at high salt concentrations, larger aggregates, such as ion triples, may be formed.[75] DRS has a unique sensitivity towards the various ion-pair types in the order: 2SIP $>$ SIP $>$ CIP.[75,76]

For systems showing a distinct ion-pair dispersion, the concentration of ion pairs, c_{IP}, in solution is determined via Eqs. 1.71-1.77 (with $S_j = S_{\mathrm{IP}}$). For the calculation of A_{IP} and μ_{IP}, geometrical parameters, the polarizability and the gas phase dipole moment of the corresponding species have to be available.
The concentrations of various IP types are used to calculate the corresponding association constants, K_{A}, as

$$K_{\mathrm{A}} = c_{\mathrm{IP}}/(c - c_{\mathrm{IP}})^2 \tag{1.90}$$

To determine the standard (infinite dilution) association constant, K_{A}°, the values of K_{A} obtained via Eq. 1.90 are fitted for convenience to a Guggenheim-type function[75]

$$\log K_{\mathrm{A}} = \log K_{\mathrm{A}}^{\circ} - \frac{2A_{\mathrm{DH}}|z_+ z_-|\sqrt{I}}{1 + A_{\mathrm{K}}\sqrt{I}} + B_{\mathrm{K}} I + C_{\mathrm{K}} I^{3/2} \tag{1.91}$$

where I ($\equiv c$ for 1:1 electrolytes) is the stoichiometric ionic strength, A_{DH} is the Debye-Hückel coefficient (0.5115 $\mathrm{L}^{1/2}\mathrm{mol}^{-1/2}$ for water at 25 °C), and X_{K} ($X = A$, B, C) are adjustable parameters (A_{K} is fixed at 1.00 $\mathrm{M}^{-1/2}$ throughout for present studies).[77]

1.6 Temperature dependence of relaxation times

1.6.1 Arrhenius equation

The Arrhenius equation[78] represents one of the oldest methods for the description of the temperature dependence of rate constants. The equation is based on the assumption that particles are excited by thermal fluctuations to a transition state between two stable energetic levels which are separated by a temperature dependent energetic barrier, E_{a}, the activation energy. For relaxation times, this equation typically has the form

$$\ln \tau = \ln \tau_0 + \frac{E_{\mathrm{a}}}{RT} \tag{1.92}$$

where τ_0, the frequency factor is interpreted as the shortest possible relaxation time.

1.6.2 Eyring equation

The Eyring equation[79] is a theoretical model, based on transition state theory. It can be applied to study the temperature dependence of experimental τ

$$\ln \tau = \ln \frac{h}{k_{\mathrm{B}} T} - \frac{\Delta S^{\neq}}{R} + \frac{\Delta H^{\neq}}{RT} \tag{1.93}$$

where h is Planck's constant, R is the universal gas constant and $\Delta S^{\neq}$ and $\Delta H^{\neq}$ are respectively the activation entropy and activation enthalpy. The Gibbs energy of activation, $\Delta G^{\neq}$, can be calculated as

$$\Delta G^{\neq} = \Delta H^{\neq} - T\Delta S^{\neq} \tag{1.94}$$

Chapter 2

Experimental

2.1 Sample preparation

All salts used in the present studies were commercial analytical reagents or better. Salts were dried under vacuum ($\sim 10^{-5}$ bar) using P_2O_5 (Sicapent, Merck) as a desiccant and were subsequently stored in a nitrogen filled glove-box prior to use. Experimental details are given in Table 2.1.

Table 2.1: Substances Used and Their Purities, Drying Temperatures, T, and Minimum Drying Times, t.

substance (Abb.)	source	purity	T / K	t / h
sodium formate (NaOFm)	Merck	$\geq 99\,\%$	323	72
sodium acetate (NaOAc)	Alfa Aesar	99 %	323	72
sodium trifluoroacetate ($NaOAcF_3$)	Fluka	$\geq 98\,\%$	333	48
sodium propanoate (NaOPr)	Fluka	$\geq 99\,\%$	333	72
sodium butanoate (NaOBu)	Merck	$\geq 98\,\%$	333	72
sodium pentanoate (NaOPe)	Merck	$\geq 96\,\%$	323	48
sodium benzoate (NaOBz)	Fluka	$\geq 99\,\%$	323	48
sodium methylsulfate (NaMS)	Sigma Aldrich		333	72
sodium methanesulfonate (NaMSn)	Fluka	$\geq 98\,\%$	323	48

Solutions were prepared gravimetrically without buoyancy corrections using degassed Millipore MILLI-Q water.

2.2 Measurement of dielectric properties

2.2.1 Frequency-domain reflectometry

DR spectra of aqueous solutions of NaOFm, NaOAc, NaOPr, and NaOBz were recorded in the frequency range $\nu_{\min} \leq \nu/\mathrm{GHz} \leq 20$ at the institute of Prof. Glenn Hefter, Murdoch University (Western Australia), using a Hewlett-Packard model 85070M dielectric probe system based on an HP 8720D vector network analyzer (VNA) and an HP 85070 dielectric probe kit. The temperature was controlled by a Hetofrig (Denmark) circulator-thermostat with a precision of $\pm 0.02\,^{\circ}\mathrm{C}$ and an accuracy (NIST-traceable) of $\pm 0.05\,^{\circ}\mathrm{C}$. The value of the minimum frequency of investigation, $\nu_{\min}$, was determined by the conductivity contribution to the loss spectrum. As such, it varied with concentration and salt but was typically in the range (0.2 to 0.8) GHz.
Further, dielectric properties of aqueous solutions of $NaOAcF_3$, NaOBu, NaOPe, NaMS, and NaMSn were studied in the frequency range $0.2 \leq \nu/\mathrm{GHz} \lesssim 50$ with the new equipment at Regensburg University, consisting of a Agilent E8364B VNA connected to an electronic calibration module (Ecal, Agilent N4693A) and a dielectric probe kit (85070E). The use of Ecal module has improved the efficiency and accuracy of the new setup as it measures well known reflection standards during the measurement and thus systematic drifts, *e.g.* phase error due to thermal expansion of the coaxial lines are compensated. Two different open-ended coaxial probes, a "high temperature" probe in the frequency range $0.2 \leq \nu/\mathrm{GHz} \lesssim 20$ and a "performance" probe in the frequency range $1 \leq \nu/\mathrm{GHz} \lesssim 50$, were used at 61 and 51 different equidistant frequencies on a logarithmic scale, respectively. The data of the performance probe, however, was used only in frequency range $15 \lesssim \nu/\mathrm{GHz} \lesssim 50$ in the fitting procedure so as to have an equal density of data points throughout. Both probe heads were mounted in two different temperature controlled cells as described by Hunger.[80] The temperature was controlled with a Huber CC505 thermostat and measured with a Agilent 34970A datalogger, using a platinum resistance thermometer (PT-100) in 4-wire configuration. In order to compare the accuracy of the new setup, DRS data recorded at Murdoch University and at Regensburg University at $0.2 \leq \nu/\mathrm{GHz} \lesssim 20$ are shown in Figure 2.1, that are in excellent agreement with each other.
The VNA determines the relative complex reflection coefficient, $\hat{\Gamma}_\mathrm{a}$, at the probe head/sample interface. The relationship between $\hat{\Gamma}_\mathrm{a}$ and the normalized aperture impedance of the probe head, $\hat{Y}$, is given by

$$\hat{\Gamma}_\mathrm{a} = \frac{1-\hat{Y}}{1+\hat{Y}} \tag{2.1}$$

A simplified coaxial aperture opening model[81,82] was used to calculate the complex dielectric properties $\hat{\eta}$ from $\hat{Y}$ by solving the following equation numerically

$$\hat{Y} = \frac{\mathrm{i}\hat{k}_\mathrm{m}^2}{\pi \hat{k}_\mathrm{c} \ln(D/d)} \left[\mathrm{i} \left(I_1 - \frac{\hat{k}_\mathrm{m}^2 I_3}{2} + \frac{\hat{k}_\mathrm{m}^4 I_5}{24} - \frac{\hat{k}_\mathrm{m}^6 I_7}{720} + \ldots \right) + \left(I_2 \hat{k}_\mathrm{m} - \frac{\hat{k}_\mathrm{m}^3 I_4}{6} + \frac{\hat{k}_\mathrm{m}^5 I_6}{120} - \ldots \right) \right] \tag{2.2}$$

In Eq. 2.2, $\hat{k}_\mathrm{c} = \omega\sqrt{\hat{\eta}_\mathrm{c}\varepsilon_0\mu_0}$ is the propagation constant within the dielectric material of the coaxial probe head, $\hat{k}_\mathrm{m} = \omega\sqrt{\hat{\eta}\varepsilon_0\mu_0}$ is the propagation constant within the sample, D

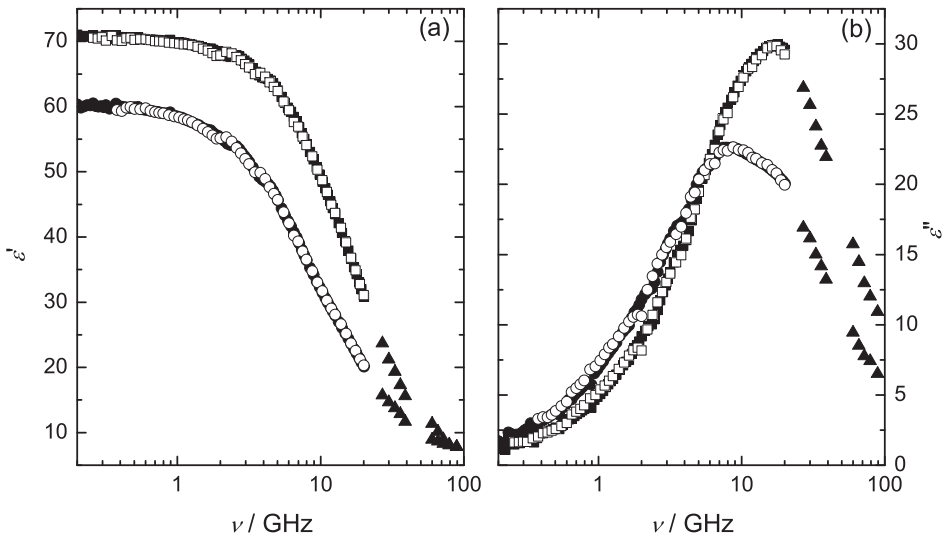

Figure 2.1: Dielectric permittivity, $\varepsilon'(\nu)$ (**a**), and loss, $\varepsilon''(\nu)$ (**b**), spectra (average of two independent calibrations) for NaOPr(aq) at 25 °C and concentrations c/M = 0.9452 (■, □) and 2.548 (●, ◯). Triangles represent data obtained with interferometer measurements; open symbols represent the data obtained at Regensburg University, using an Agilent E8364B VNA; filled symbols represent the data obtained at Murdoch University, using an HP 8720D VNA.

and d are constants representing the radii of the outer and inner conductor of the coaxial line. The first 28 probe constants, I_i, calculated from a theoretical approach and further optimized as described in Reference 82 are used for the numerical solution of Eq. 2.2.
In order to account for signal distortions between the reference planes of the probe head and that of the VNA, a standard three-point calibration (open, short and load) is performed for the measurement of $\hat{\Gamma}_\mathrm{a}$

$$\hat{\Gamma}_\mathrm{a} = \frac{\hat{\Gamma} - \hat{e}_\mathrm{d}}{\hat{e}_\mathrm{s}(\hat{\Gamma} - \hat{e}_\mathrm{d}) + \hat{e}_\mathrm{r}} \tag{2.3}$$

The complex, frequency-dependent correction constants, $\hat{e}_\mathrm{d}$, $\hat{e}_\mathrm{r}$ and $\hat{e}_\mathrm{s}$ are determined by three reference measurements of the uncorrected reflection coefficient $\hat{\Gamma}$ and application of Eq. 2.2. Air (open), mercury (short) and water (load) were used as reference standards for present studies. Mercury was purified before use according to the procedure described by Wölbl;[83] minor scum formation was removed by 'pin-hole' filtration (paper filter). Averaged data of at least two consistent independent calibrations were used for further processing.

If the dielectric properties of the sample deviate considerably from the properties of reference liquid, a complex Padé approximation,[84,85] can be applied for further correction of VNA data. This procedure was also applied in the present studies for the selected systems, using water, propylene carbonate (PC, Sigma-Aldrich, 99.7 %) and N,N-dimethylacetamide (DMA, Fluka, > 99.8 %) as secondary calibration standards. However, as the uncorrected data showed excellent agreement with the interferometer (IFM) measurements (which are thought to be very reliable as they are absolute values obtained

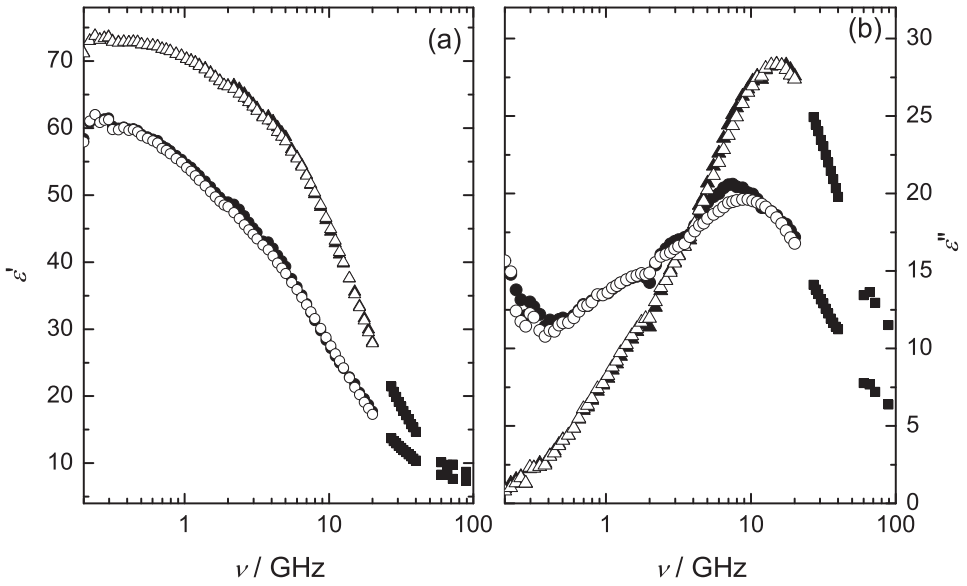

Figure 2.2: Dielectric permittivity, $\varepsilon'(\nu)$ (**a**), and loss, $\varepsilon''(\nu)$ (**b**), spectra (average of two independent calibrations) for NaOPe(aq) at 25 °C and concentrations $c/\mathrm{M} = 0.9182$ (▲, △) and 2.345 (●, ◯). Squares represent IFM (A-band and E-band) data; filled symbols correspond to raw data; open symbols represent the data corrected with a complex Padé approximation using water, PC and DMA as secondary calibration standards.

without using any reference substances for calibration) and as the Padé correction did not yield any significant improvements (Figure 2.2), it was not applied to most of the present systems.

2.2.2 Interferometry

Double-beam interferometers with a measuring cell of variable path-length in the sample beam were used for measurement of the dielectric properties at $\nu > 20\,\mathrm{GHz}$. The laboratory at Regensburg is equipped with a set of four rectangular waveguide IFMs working on the transmission principle, each with waveguides fitted to a particular microwave frequency band: X-band $8.5 \leq \nu/\mathrm{GHz} \leq 12$, Ku-band $13 \leq \nu/\mathrm{GHz} \leq 17.5$, (A-band) $27 \leq \nu/\mathrm{GHz} \leq 39$ and E-band $60 \leq \nu/\mathrm{GHz} \leq 89$. The detailed descriptions of IFMs and the measurement principle are given in Reference 86.

As VNA (Agilent E8364B) has become available for measurements at $0.2 \leq \nu/\mathrm{GHz} \leq 50$ (described in detail in previous Section), interferometric measurements are only required at $60 \leq \nu/\mathrm{GHz} \leq 89$. The setup of the E-band IFM is schematically shown in Figure 2.3. A frequency-stabilized signal is split by a directional coupler into the reference and measuring path. The reference path contains two attenuators for coarse amplitude leveling and a precision attenuator for fine tuning. The measuring path is composed of a precision phase shifter and the sample cell. The cell is composed of a piece of waveguide filled with the sample liquid and a gold-plated ceramic (waveguide) probe with variable, motor controlled,

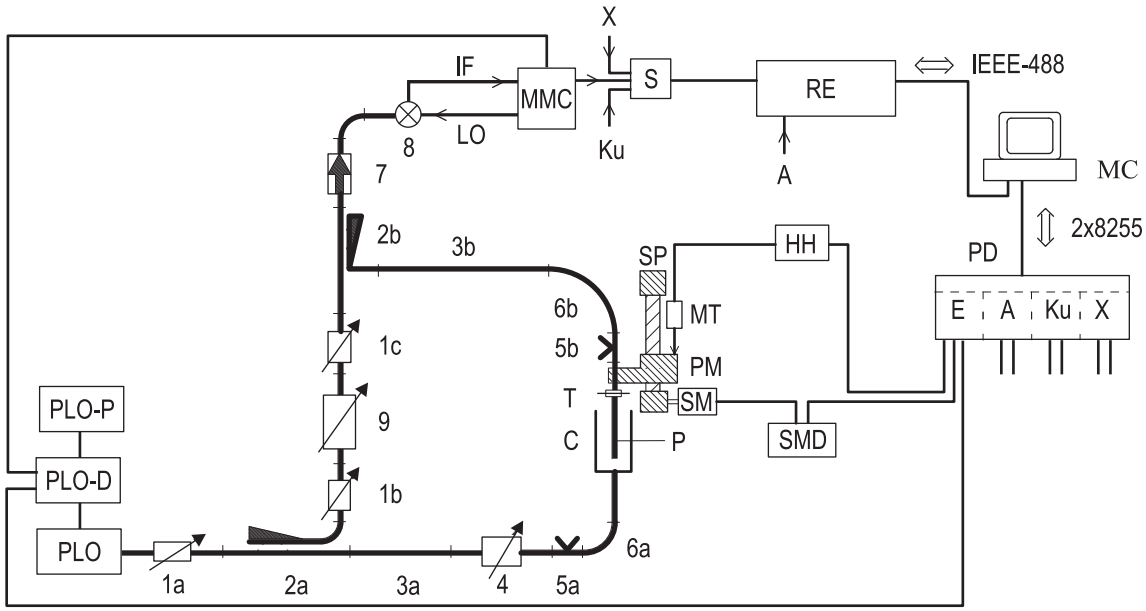

Figure 2.3: Block diagram of the E-band equipment:[86] **1a**, **b**, **c** represent variable attenuators; **2a**, **b** directional couplers; **3a**, **b** waveguide sections; **4** precision phase shifter; **5a**, **b** E/H tuners; **6a**, **b** flexible waveguides; **7** isolator; **8** harmonic mixer; **9** variable precision attenuator; **C** cell, **HH** bidirectional counter; **MC** microcomputer; **MMC** millimeter-wave to microwave converter; **MT** digital length gauge; **P** probe; **PD** parallel interface unit; **PLO** phase locked oscillators; **PLO-D** PLO-control unit; **PLO-P** PLO-power supply; **PM** probe mount; **RE** precision receiver; **S** electromechanical switch; **SM** stepping motor; **SMD** stepping motor control unit; **SP** spindle and spindle mount; **T** tapered transmission; double lines represent waveguides, thick lines semi-rigid microwave cables and normal lines symbolize data transfer connections (analog or digital).

position. Up and down movement, of the probe in the cell is made possible by flexible waveguide. The relative amplitude, A, of the recombined beams, by directional couplers, is measured by a precision attenuation receiver, equipped with proper mixers for frequency conversion, as a function of optical path length, z_0. The relative position of the probe, $(z_0 - z_0')$, is recorded with a precision gauge, where z_0' is an arbitrary probe position set at a fully destructive interference.
For each frequency, the attenuation coefficient, α, and the medium wavelength, λ_m, are obtained from a nonlinear fit of recorded interference data $A(z_0 - z_0')$ by the expression[86]

$$A(z_0 - z_0') = A_0 + 10\lg\Bigg\{1 + \exp\left[-2p\alpha(z_0 - z_0')\right] - 2\cos\left(\frac{2\pi}{\lambda_\mathrm{m}}(z_0 - z_0')\right)\cdot\exp\left[-p\alpha(z_0 - z_0')\right]\Bigg\} \tag{2.4}$$

with the conversion factor

$$p = \left(20\lg\mathrm{e}\cdot\frac{\mathrm{dB}}{\mathrm{Np}}\right)^{-1} \tag{2.5}$$

where A_0 is the relative intensity of the signal passing through the sample beam at position z_0'.
The obtained quantities α and λ_m are related to $\hat{\eta}(\nu)$ via

$$\eta'(\nu) = \left(\frac{c_0}{\nu}\right)^2\left[\left(\frac{1}{\lambda_{\mathrm{c},10}^{\mathrm{vac}}}\right)^2 + \left(\frac{1}{\lambda_\mathrm{m}(\nu)}\right)^2 - \left(\frac{\alpha(\nu)}{2\pi}\right)^2\right] \tag{2.6}$$

and

$$\eta''(\nu) = \left(\frac{c_0}{\nu}\right)^2\frac{\alpha(\nu)}{\pi\lambda_\mathrm{m}(\nu)} \tag{2.7}$$

where, $\lambda_{\mathrm{c},10}^{\mathrm{vac}}$ is the limiting vacuum frequency, characteristic for the waveguide dimensions.

When the Agilent E8364B VNA became available, the waveguide-transmission cells of the IFMs (X-, Ku-, and A-band) were connected to the VNA.[80] The temperature was controlled by a Julabo FP 50 or a Lauda RK 20 thermostat and monitored by a Pt-100 resistance with a precision of $\pm 0.02\,^\circ$C and an overall accuracy of $\pm 0.05\,^\circ$C. Dielectric data for most of the present systems, in the A-band frequency range, were recorded using this setup. This setup was preferred over the "performance" probe as data obtained (specially $\varepsilon''(\nu)$) using this probe were relatively scattered (Figure 2.4). It was observed that the scattering was more pronounced for the samples with high κ, this suggests that a suitable calibration standard with $\kappa >> 0$ is required to improve the quality and accuracy of "performance" probe for highly conducting samples.

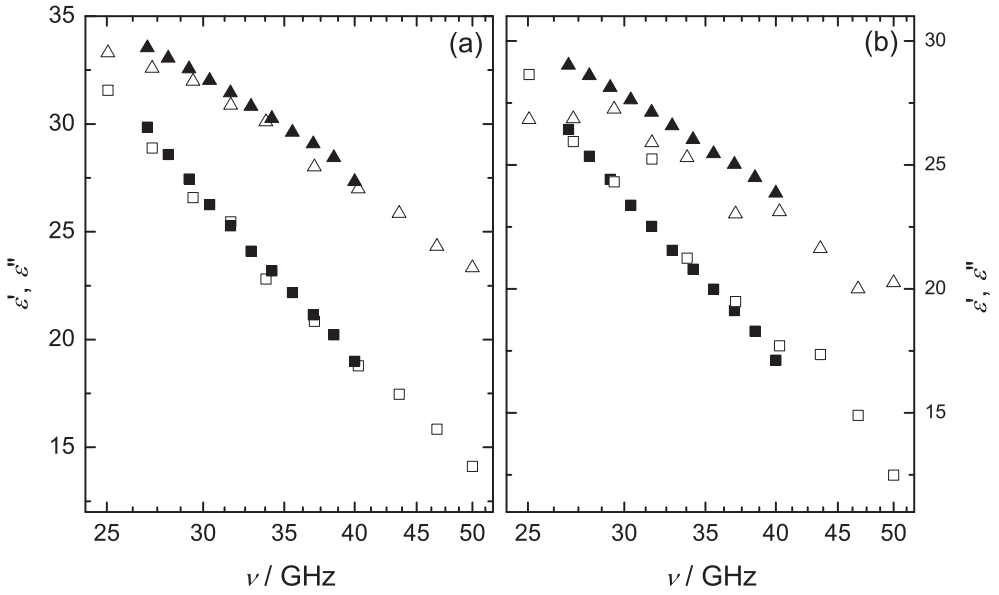

Figure 2.4: Dielectric permittivity, $\varepsilon'(\nu)$ (■, □), and loss, $\varepsilon''(\nu)$ (▲, △), spectra for $NaOAcF_3$(aq) at 25 °C and concentrations c/M = 0.09923 (**a**) and 0.7172 (**b**). Filled symbols represent the data obtained by transmission cell; open symbols represent the data obtained by the "performance" probe.

2.2.3 Data processing

To link the dielectric spectra to physical properties a frequency-continuous description has to be found. In principle the $\hat{\eta}(\nu)$ spectra can be processed, but to avoid biasing of the resulting parameters, due to large values of η'' at low ν (higher weights at low ν than at high ν), only $\hat{\varepsilon}(\nu)$ data (corrected for dc conductivity, Eq. 1.36) are analyzed. Therefore, the spectra were corrected for the measured conductivity, κ, as a starting approximation. The κ was varied slightly in order to improve the fit quality (Eq. 2.8). The difference between the experimental conductivity from low-frequency measurements in the Hz-kHz region (see Section 2.3.2) and adjusted κ values reflects errors in the measurement setup and/or in mathematical model for the equipment.[87,88]

Subsequently, the measured data triples (ν_i, ε'_i, ε''_i) have to be fitted by the relaxation models (or superpositions) described in section 1.3. Due to the broadness of relaxation modes in the condensed phase finding the right model is not trivial, and it should be kept in mind, that the successful formal description does not automatically imply that the resolved modes have a physical meaning or that they are independent of each other. Thus, the choice of the 'true' relaxation model has to follow some rules.

First of all, the parameters obtained have to be physically meaningful. Second, the normalized variance of the fit, χ^2_r, defined as

$$\chi^2_r = \frac{1}{2N-m-1}\left[\sum_{i=1}^{N} w_{\varepsilon'}(\nu_i)\delta\varepsilon'(\nu_i)^2 + \sum_{i=1}^{N} w_{\varepsilon''}(\nu_i)\delta\varepsilon''(\nu_i)^2\right] \tag{2.8}$$

should be small. In Eq. 2.8, $\delta\varepsilon'(\nu_i)$ and $\delta\varepsilon''(\nu_i)$ are the residuals, N is the number of data triples $[\nu_i, \varepsilon'(\nu_i), \varepsilon''(\nu_i)]$ and m the number of the adjustable parameters; $w_{\varepsilon'}(\nu_i)$ and $w_{\varepsilon''}(\nu_i)$ are the weights; only unweighted fits, $w_{\varepsilon'}(\nu_i) = w_{\varepsilon''}(\nu_i) = 1$, were performed in the analysis of the spectra presented here.
Additionally, the number of parameters should be as small as possible and the relaxation model should not change in a concentration series, except for specific physical reasons.
The model can depend on the measured frequency range as well as on the precision and the "density" of the data. Special care should be taken regarding the density, meaning that the number of data points should be comparable over the whole frequency range.
The different relaxation models were tested by simultaneously fitting $\varepsilon'(\nu)$ and $\varepsilon''(\nu)$ using the MWFIT program. A non-linear least-squares routine based on the method of Levenberg and Marquardt is implemented in this program.[89] Due to the nonlinear nature of the fitting process, it is not possible to assign statistically meaningful standard uncertainties to the individual fit parameters, but the square root of the diagonal elements of the covariance matrix can be used as a measure for the certainty of the resulting parameters.[89,90]
Additionally, selected dielectric spectra were fitted with an unbiased fitting procedure recently proposed by Zasetsky and Buchner.[91] The method is based on a quasi-linear procedure with constraints for least squares fitting of experimental complex dielectric permittivity spectra in the frequency domain. The solution of linear least square minimization problem with constraints[91,92] provides information on relaxation time distribution. The advantages of this procedure are that it is fast, robust, easy to use, and more importantly does not require any prior information (to be specified) on relaxation processes under study. Instead, the number of relaxation modes and their probable characteristic times and magnitudes are determined during the course of minimization runs, thus making further interpretation of fitting results much less biased.

2.3 Supporting measurements

2.3.1 Densimetry

In order to calculate molar concentrations, c, solution densities, ρ, were measured with an accuracy of $\pm 0.05\,\mathrm{kg\,m^{-3}}$ using a vibrating-tube densimeter (Anton Paar DMA 60/601 HT) according to the method of Kratky et al.[93] The instrument was calibrated with degassed Millipore MILLI-Q water and purified nitrogen at atmospheric pressure, assuming densities from standard sources.[94] The temperature was kept constant to $\pm 0.003\,^{\circ}\mathrm{C}$ with an overall accuracy of $\pm 0.02\,^{\circ}\mathrm{C}$ using a Braun Thermomix 1480 thermostat in combination with a thermostated heat sink (Lauda RK 20).

Additionally, the densities of some aqueous systems were measured with a densimeter DMA 5000 M (Anton Paar), which measures the period of oscillation, τ of a U-shaped borosilicate glass tube filled with the sample. The value of τ is related to ρ according to Eq. 2.9:

$$\rho = \mathrm{A} \times \left(\frac{\tau}{\tau_{\mathrm{ref}}}\right)^2 \times \mathrm{f}_1 - \mathrm{B} \times \mathrm{f}_2 \tag{2.9}$$

where τ_{ref} is the period of oscillation of the reference oscillator, A and B are the instrument constants, and f_1 and f_2 are the correction terms for temperature, viscosity and nonlinearity. The temperature was kept constant to $\pm 0.001\,^{\circ}\mathrm{C}$ with an overall accuracy of $\pm 0.01\,^{\circ}\mathrm{C}$ with a built-in thermoelectric temperature control. The precision of the measurements was $\pm 0.001\,\mathrm{g\,L^{-1}}$. The accuracy stated by the manufacturer is $\pm 0.005\,\mathrm{g\,L^{-1}}$. To ensure that the measuring cell was clean and properly dried, 'air check' was performed before starting measurements.

2.3.2 Conductivity

Electrical conductivities of the solutions, κ, were measured with a precision of $\pm 0.2\,\%$ and an accuracy of $\pm 0.5\,\%$ using the equipment described previously.[95–97] The temperature was controlled with a home-built precision thermostat stable to $\pm 0.001\,\mathrm{K}$ in combination with a thermostated heat sink (Lauda Kryomat K 90 SW). A set of five two-electrode capillary cells with cell constants, C, in the range $(25\text{ to }360)\,\mathrm{cm^{-1}}$ was used. The cells were calibrated with aqueous solutions of KCl.[98] The cell resistance, $R(\nu)$, was measured with a manual high-precision conductivity bridge as a function of the applied AC frequency, ν, between 120 Hz and 10 kHz. To eliminate electrode polarization, the conductivity of each sample was obtained as $\kappa = C/R_\infty$ where $R_\infty = \lim_{\nu\to\infty} R(\nu)$ was obtained by extrapolation using the empirical function $R(\nu) = R_\infty + A/\nu^a$, where A is specific to the cell and a was found to be in the range $0.5 \lesssim a \lesssim 1$.[99]

Additionally, κ of some aqueous solutions were measured with new setup, using the same (above described) conductivity cells. A computer-controlled, high precision LCR-bridge (HAMEG, HM8118) was used to measure $R(\nu)$ with an accuracy (stated by the manufacturer) of $\pm 0.05\,\%$, at different AC frequencies selected between 200 Hz and 10 kHz.* Prior

*The measuring frequency range of the LCR-bridge is from 20 Hz to 200 kHz.

to any measurement open circuit and short circuit calibration was performed in order to avoid measurement errors. The open/short circuit calibration compensates for the effects of parasitic impedances of the connections to the sample under investigation.
The cells were placed in an oil bath, whose temperature was controlled with a hydraulically sealed circulation thermostat (Huber, unistat 705). The temperature stability of the thermostat is $\pm 0.005\,\mathrm{K}$. Further, the temperature was monitored by a Pt-100 resistance thermometer with an accuracy of $\pm 0.01\,^{\circ}\mathrm{C}$. The desired quantity κ was obtained as described above.

2.3.3 Quantum mechanical calculations

Semiempirical quantum mechanical calculations for various ions and ion pairs have been performed using MOPAC2009[100] with the PM6 Hamiltonian.[101] Dipole moments were calculated assuming the geometric center (*i.e.*, the center of the longest axis of the ion/ion-pair) as pivot. The geometry of the ions was optimized using the eigenvector-following (EF) routine[102] and for the ion pairs, where it was necessary to avoid geometry reorganization, the 1SCF method was applied. Solvent effects (*e.g.*, polarization in in the condensed phase) were accounted for by applying the COSMO[103] technique using the static permittivity (78.4) of pure water. Molecular diameters, d_{max}, were obtained by taking the longest distance between two atoms and adding the van der Waals radii of the atoms.[104] WINMOSTAR[105] was used to determine the van der Waals volumes, V_{vdW}, from the optimized geometry of the ions/ion-pairs.

Chapter 3

Small Alkylcarboxylates

3.1 Aqueous solutions of sodium formate and sodium acetate

Most of the material presented in this section makes the basis of the manuscript:

Rahman, H. M. A.; Hefter, G.; Buchner, R. *'Hydration of Formate and Acetate Ions by Dielectric Relaxation Spectroscopy.' J. Phys. Chem. B*, **2012**, *116*, 314.

This section presents a detailed DRS study of the aqueous solutions of the two simplest carboxylate ions: methanoate ($HCOO^-$, formate, OFm^-) and ethanoate (CH_3COO^-, acetate, OAc^-), as their sodium salts. As OFm^- does not contain hydrophobic part, it can be considered as a model ion to investigate the hydration pattern of carboxylate ($–COO^-$) group which is the major hydrophilic anionic site in most biomolecules. The CH_3COO^- is the simplest carboxylate anion containing both hydrophilic ($–COO^-$) and hydrophobic ($–CH_3$) entities. Hydration behaviour of this model anion in comparison with that of OFm^-(aq) will help to understand the mixed hydrophilic-hydrophobic hydration phenomenon in biomolecules.
Carboxylate concentrations were investigated up to ~3.2 M (OFm^-) or ~3.7 M (OAc^-) over the frequency range $0.2 \lesssim \nu/\text{GHz} \leq 89$ (HP8720D VNA setup + A & E-band interferometer Section 2.2).* Dielectric spectra of aqueous solutions of NaOFm at 25 °C and of aqueous NaOAc solutions at (15, 25, and 35) °C were recorded. To the best of our knowledge only a few previous DRS studies of the aqueous solutions of carboxylate salts have been reported. Of particular note are those of Lyashchenko et al.,[107–109] which showed that the bulk water relaxation time decreased with increasing formate concentration whereas in propanoate solutions it increased. This difference was interpreted[108] as indicating that

*After submission of OFm^-/OAc^- manuscript[106] an additional set of measurements was performed for NaOAc(aq) at $c \lesssim 1$ M and 25 °C with improved instrumentation (Agilent E8364B VNA ($0.2 \lesssim \nu/\text{GHz} \leq 50$) and E-band interferometer ($60 \lesssim \nu/\text{GHz} \leq 89$) (Section 2.2)) focussing on the low-frequency low-amplitude Debye relaxation process observed at $c \lesssim 1$ M for NaOAc. The results of this second series of measurements are discussed in Section 3.1.3.

OFm^- is hydrophilic whereas propanoate is hydrophobic. Unfortunately, due to technological limitations (data were obtained at just seven frequencies between 7 and 25 GHz at $c \gtrsim 0.5$ M) no further significant conclusions could be drawn by the authors at that time. The present work thus represents a significant extension of the DRS database for these important ions.

3.1.1 Choice of fit model and assignment of relaxation modes

The combined $\hat{\varepsilon}(\nu)$ data were analyzed by simultaneously fitting the in-phase ($\varepsilon'(\nu)$, Figures 3.1a & 3.2a) and out-of-phase ($\varepsilon''(\nu)$, Figures 3.1b & 3.2b) components of the complex permittivity to various possible relaxation models consisting of n distinguishable relaxation processes using Equation (1.65). Simplified variants of this equation correspond to the CD, CC, and D models.[48] Other band shape functions more appropriate for intermolecular vibrations and librations, such as damped harmonic oscillators, were not considered as such modes make negligible contributions to the dielectric spectra of aqueous systems at gigahertz frequencies.[110] The quality of the fit was evaluated via χ^2_r.[89] All fitting parameters obtained from the present spectra are summarized in Tables 3.1 and 3.2. Fitting parameters obtained from the additional set of measurements for NaOAc(aq) at $c \lesssim 1$ M are summarized in Table 3.3. Additionally, selected spectra were analyzed using a recently-published procedure[91] that allows an unbiased determination of the number of relaxation processes required for formal description of $\hat{\varepsilon}(\nu)$.

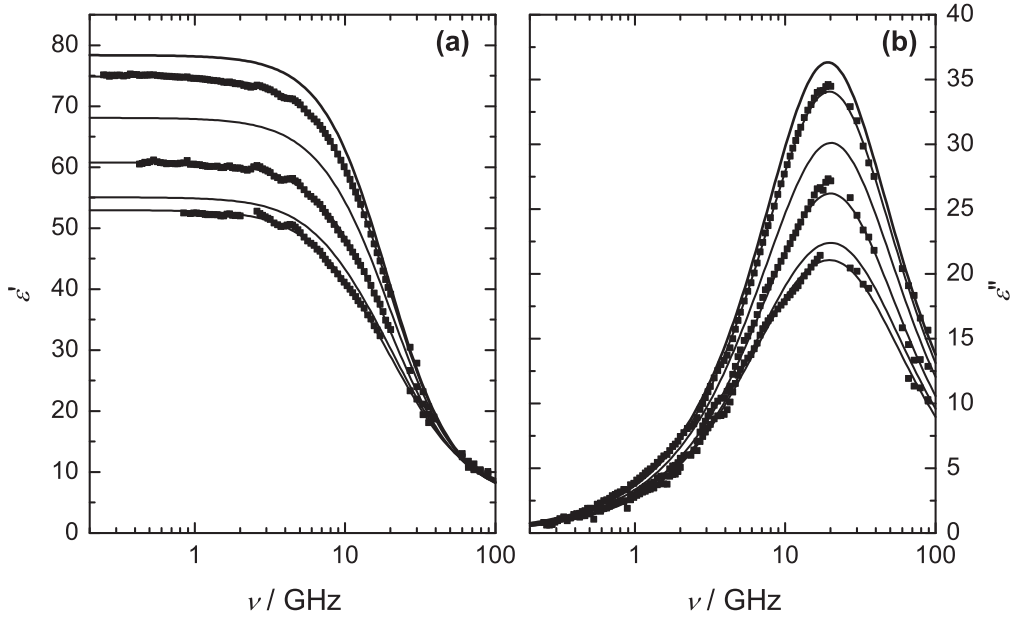

Figure 3.1: Permittivity, $\varepsilon'(\nu)$ (**a**), and dielectric loss, $\varepsilon''(\nu)$ (**b**), spectra for NaOFm(aq) at 25 °C and concentrations c/M = 0, 0.2968, 0.9617, 1.888, 2.753, and 3.171 (top to bottom). Symbols show experimental data (others are omitted for visual clarity); lines represent the D+D fit.

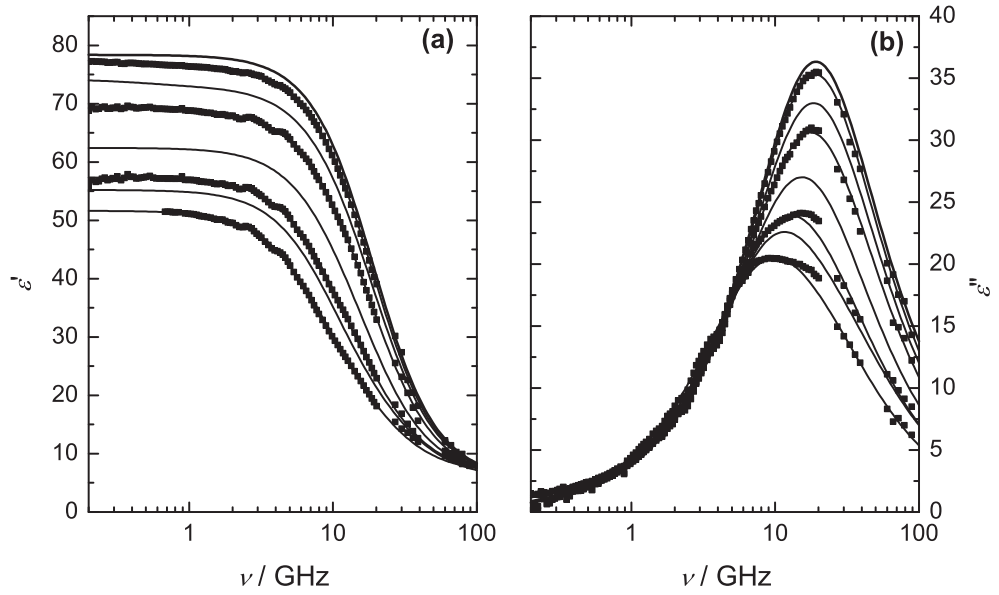

Figure 3.2: Permittivity, $\varepsilon'(\nu)$ (**a**), and dielectric loss, $\varepsilon''(\nu)$ (**b**), spectra for NaOAc(aq) at 25 °C and concentrations $c/\mathrm{M} = 0, 0.1487$, 0.4883, 0.9574, 1.838, 2.649, 3.031, and 3.717 (top to bottom). Symbols show experimental data (others are omitted for visual clarity); lines represent either the D+D+D or D+D fits.

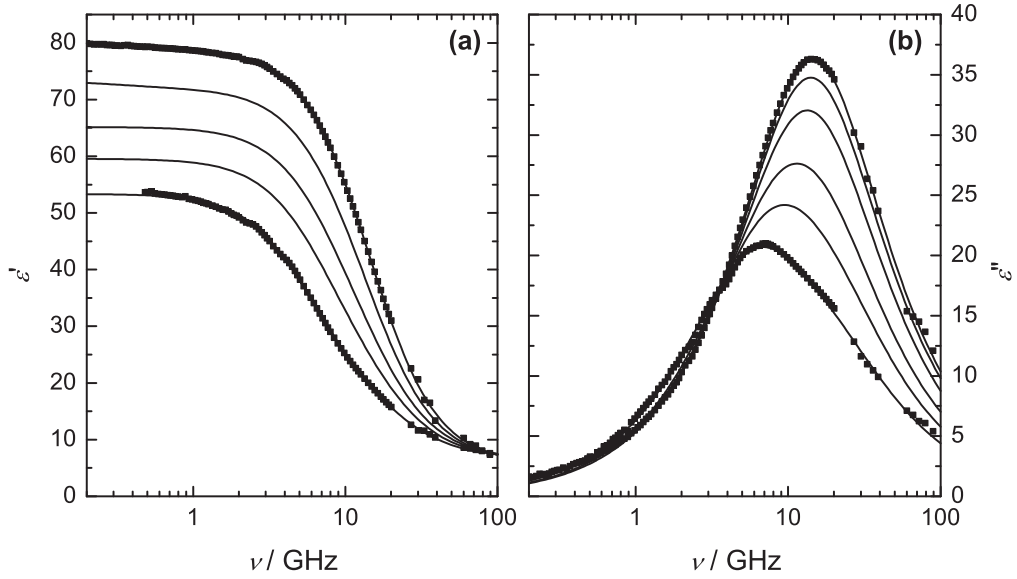

Figure 3.3: Spectra of relative permittivity, $\varepsilon'(\nu)$ **(a)**, and dielectric loss, $\varepsilon''(\nu)$ **(b)**, for NaOAc(aq) at 15 °C and concentrations, c / M = 0.2471, 0.4896, 0.9606, 1.845, 2.660, and 3.733 (top to bottom). Symbols show experimental data (others are omitted for visual clarity); lines represent either the D+D+D or D+D fits.

Representative dielectric spectra measured for NaOFm(aq) and NaOAc(aq) as a function of concentration are shown in Figures 3.1 and 3.2 respectively; those for NaOAc(aq) at 15 °C and 35 °C are given in Figures 3.3 & 3.4. Overall, the spectra were best described by a model consisting of either two (for NaOFm(aq) at all c and for NaOAc(aq) at $c > 1\,\mathrm{M}$) or three (for NaOAc(aq) at $c \lesssim 1\,\mathrm{M}$) Debye processes. Typical fits obtained with these D+D and D+D+D models are shown in Figures 3.1 to 3.6. These models were consistent with the 'bias-free' analysis of the spectra shown in Figures 3.7 & 3.8.

Table 3.1: Densities, ρ; Electrical Conductivities, κ; Limiting Permittivities, ε_j; Relaxation Times, τ_j; and Reduced Error Function Values, χ^2_r, for NaOFm(aq) at Concentrations, c; and 25 °C[a,b]

c	ρ	κ	ε	τ_1	ε_2	τ_2	ε_∞	χ^2_r
0[c]			78.37			8.32	3.48	0.048
0.07469	1.0002	0.667	77.39	15.0F	76.5	8.20	5.25	0.043
0.09944[d]	1.0012[e]	0.861[e]	77.08	15.0F	76.4	8.16F	4.77	0.024
0.1501	1.0033	1.25	76.54	15.0F	75.1	8.17	5.52	0.091
0.1984[d]	1.0053[e]	1.61[e]	76.97	15.0F	69.6	7.59	3.79	0.050
0.2968	1.0093	2.31	74.85	15.0F	68.2	7.70	5.53	0.100
0.3946[d]	1.0133[e]	2.96[e]	73.85	15.0F	71.0	7.93F	4.15	0.097
0.4894	1.0172	3.57	72.89	15.0F	68.3	7.92	5.52	0.146
0.7329[d]	1.0271[e]	4.96[e]	70.41	15.0F	65.2	7.67F	4.12	0.094
0.9617	1.0363	6.11	68.08	15.1	57.3	7.16	5.70	0.083
1.436[d]	1.0554[e]	8.20[e]	64.15	18.0	56.8	7.11F	3.95	0.090
1.888	1.0734	9.80	60.78	14.7	48.2	6.92	6.08	0.151
2.330[d]	1.0903[e]	11.0[e]	57.71	15.6	45.9	6.37F	3.22	0.172
2.753	1.1064	11.9	55.07	14.2	37.0	5.98	6.40	0.143
3.171	1.1219	12.6	53.96	14.8	35.4	5.99	6.81	0.149

[a] Parameter values followed by the letter F were held constant during the fitting procedure. [b] Units: c in M; ρ in $\mathrm{kg\,L^{-1}}$; κ in $\Omega^{-1}\,\mathrm{m}^{-1}$; τ_j in $10^{-12}\,\mathrm{s}$. [c] Reference 84. [d] VNA (0.2-20 GHz) data only. [e] Interpolated using measured values.

Table 3.2: Densities, ρ; Electrical Conductivities, κ; Limiting Permittivities, ε_j; Relaxation Times, τ_j; and Reduced Error Function Values, χ^2_r, for NaOAc(aq) at Concentrations, c; and temperatures 15 °C, 25 °C and 35 °C[a,b]

c	ρ	κ	ε	τ_1	ε_2	τ_2	ε_3	τ_3	ε_∞	χ^2_r
					At 15 °C					
0[c]			82.03					10.8	3.66	0.056
0.2471	1.0096	1.30	80.12	390	78.86	16.4F	73.56	10.7	5.80	0.040
0.4896	1.0199	2.30	77.61	342	76.30	17.0F	65.61	10.6	5.90	0.049
0.9606	1.0390	3.78	73.26	466	72.01	18.0F	53.52	10.3	6.07	0.046
1.412[d]	1.0572[e]	4.82[e]	68.52		68.52	19.0F	43.73	10.1	6.40	0.065
1.845	1.0742	5.43	65.17		65.17	19.2F	33.76	9.48	6.51	0.075
2.262[d]	1.0902[e]	5.77[e]	62.29		62.29	20.3	28.21	9.00F	6.48	0.070
2.660	1.1052	5.97	59.56		59.56	21.6F	24.32	8.50	6.66	0.056
3.044	1.1192[e]	5.95[e]	57.46		57.46	23.1	20.80	7.65	6.59	0.077
3.411	1.1325[e]	5.89[e]	55.33		55.33	24.8	19.23	7.48	6.77	0.065
3.733	1.1450	5.75	53.35		53.35	26.9	18.19	7.43	6.80	0.063
					At 25 °C					
0[c]			78.37					8.32	3.48	0.048
0.1487	1.0032	1.05	77.76	555	76.53	14.6F	74.00	8.26	5.60	0.042
0.2465	1.0073	1.63	76.55	332	75.28	14.6F	70.66	8.13	5.72	0.052
0.4883	1.0172	2.89	74.15	316	72.95	14.6F	64.96	8.11	5.92	0.038
0.7253[d]	1.0266[e]	3.98[e]	71.92	498	70.81	14.6F	57.82	8.00F	5.64	0.043
0.9574	1.0356	4.84	69.28	186	68.97	14.6	54.54	8.00	5.88	0.087
1.407[d]	1.0535[e]	6.17[e]	65.52		65.52	14.6	44.82	7.60F	4.73	0.064
1.838	1.0702	7.00	62.43		62.43	14.2	37.54	8.15	6.35	0.127
2.252[d]	1.0857[e]	7.54[e]	59.69		59.69	15.7	32.62	7.30F	4.33	0.096
2.649	1.1004	7.87	57.37		57.37	16.0F	27.14	7.82	6.56	0.138
3.031	1.1147[e]	7.94[e]	55.25		55.25	17.0	22.38	6.90	6.27	0.161
3.398	1.1283[e]	7.94[e]	53.37		53.37	18.0	20.13	6.92	6.47	0.142
3.717	1.14010	7.84	51.63		51.63	19.3	18.89	6.86	6.65	0.137
					At 35 °C					
0[c]			74.87					6.53	3.06	0.087
0.2458	1.0042	2.02	73.40	601	71.44	14.4	67.88	6.50F	5.36	0.055
0.4868	1.0142	3.55	70.46	250	69.56	12.5F	62.78	6.49	5.41	0.076
0.9548	1.0328	5.90	66.53	596	65.58	13.0F	53.06	6.35	5.56	0.183
1.403[d]	1.0504[e]	7.56[e]	62.86		62.86	13.0F	45.80	6.28F	5.68	0.141
1.833	1.0669	8.71	59.92		59.92	13.0	38.35	6.28	6.66	0.161
2.246[d]	1.0826[e]	9.47[e]	57.34		57.34	14.1	34.92	6.25F	6.99	0.245
2.641	1.0973	9.92	55.15		55.15	14.7	30.97	6.31	7.04	0.214
3.022	1.1111[e]	10.13[e]	53.09		53.09	15.9	29.35	6.25F	6.69	0.289
3.386	1.1243[e]	10.16[e]	51.37		51.37	16.2	25.87	6.25F	6.97	0.324
3.702	1.1356	10.15	49.95		49.95	16.6	22.36	6.25F	7.21	0.142

[a] Parameter values followed by the letter F were held constant during the fitting procedure. [b] Units: c in M; ρ in kg L^{-1}; κ in Ω^{-1} m^{-1}; τ_j in 10^{-12} s. [c] Reference 84. [d] VNA (0.2-20 GHz) data only. [e] Interpolated using measured values.

Table 3.3: Densities, ρ; Electrical Conductivities, κ; Limiting Permittivities, ε_j; Relaxation Times, τ_j; and Reduced Error Function Values, χ^2_r, for NaOAc(aq) (additional set of measurements) at Concentrations, c; and 25 °C[a,b]

c	ρ[c]	κ[c]	ε	τ_1	ε_2	τ_2	ε_3	τ_3	ε_∞	χ^2_r
0.0[d]			78.37					8.32	3.48	
0.1001	1.0012	0.755	77.52	334	76.89	16.4	74.58	8.26F	6.15	0.137
0.2029	1.0055	1.37	76.69	285	75.66	15.0F	71.46	8.24	6.01	0.083
0.2969	1.0094	1.91	75.68	244	74.64	15.0F	68.34	8.15	6.11	0.119
0.3919	1.0133	2.44	75.01	295	73.86	15.0F	65.45	8.04	6.08	0.090
0.4881	1.0171	2.90	74.28	310	72.85	15.0F	62.82	8.08	6.40	0.124
0.5809	1.0209	3.34	73.55	326	72.11	15.0F	60.84	7.99	6.22	0.078
0.6778	1.0246	3.76	72.78	374	71.20	15.0F	58.06	7.98	6.51	0.165
0.7721	1.0284	4.14	71.46	356	70.53	15.0F	55.10	7.89	6.56	0.107
0.8648	1.0320	4.49	70.47	328	69.77	15.0F	53.80	7.91	6.60	0.092
0.9581	1.0357	4.84	69.62	290	68.89	15.0F	52.05	7.95	6.69	0.139

[a] Parameter values followed by the letter F were held constant during the fitting procedure. [b] Units: c in M; ρ in kg L^{-1}; κ in Ω^{-1} m^{-1}; τ_j in 10^{-12} s. [c] Interpolated from Reference 106. [d] Reference 84.

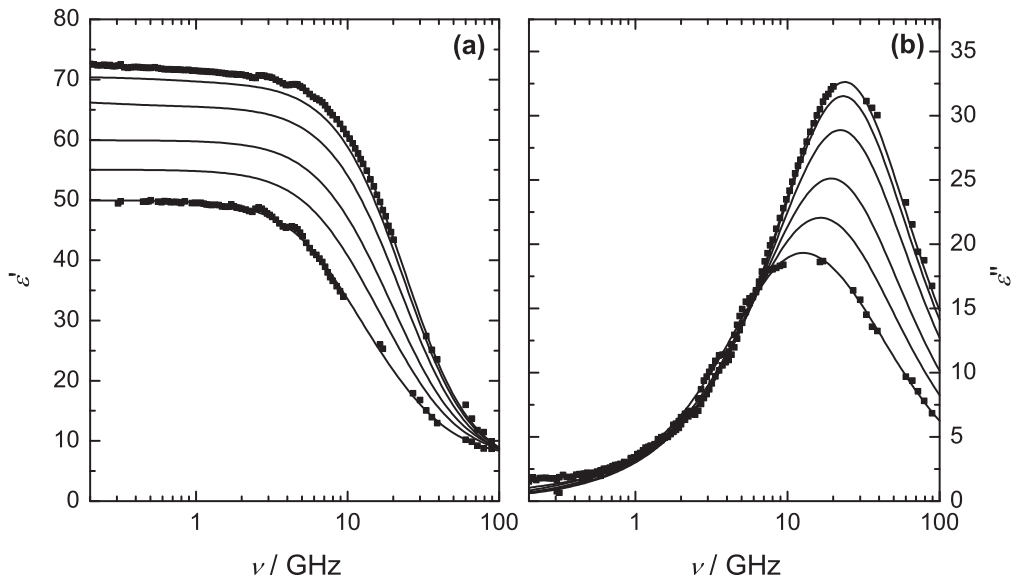

Figure 3.4: Spectra of relative permittivity, $\varepsilon'(\nu)$ **(a)**, and dielectric loss, $\varepsilon''(\nu)$ **(b)**, for NaOAc(aq) at 35 °C and concentrations, c / M = 0.2458, 0.4868, 0.9548, 1.833, 2.641, and 3.702 (top to bottom). Symbols show experimental data (others are omitted for visual clarity); lines represent either the D+D+D or D+D fits.

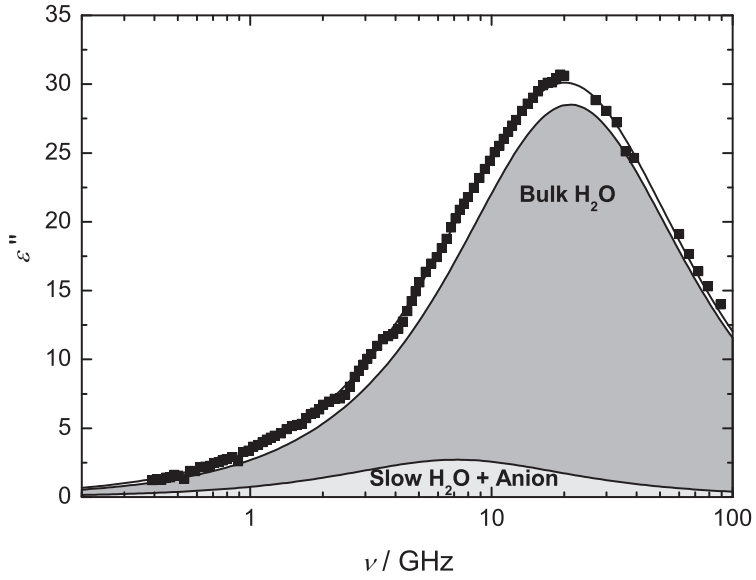

Figure 3.5: Dielectric loss spectrum, $\varepsilon''(\nu)$, of 0.9617 M NaOFm(aq) at 25 °C. Symbols represent experimental data, the line through the experimental data represents the D+D fit, and shaded areas indicate the contributions of the two relaxation modes.

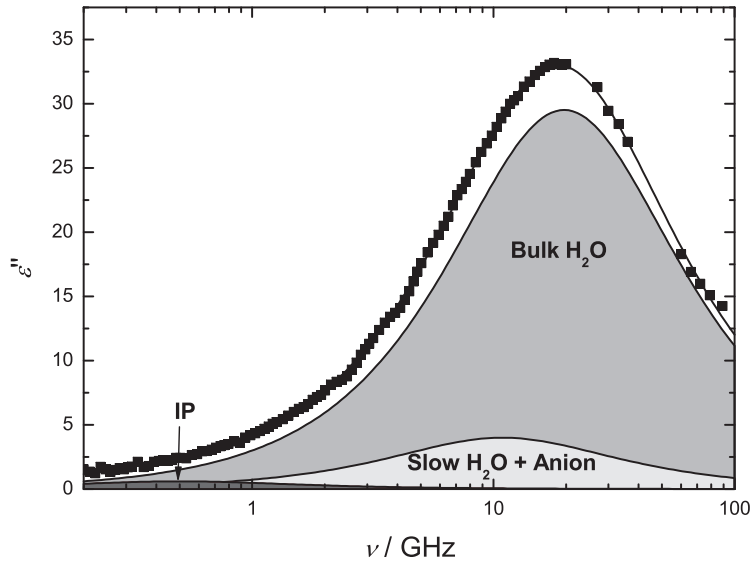

Figure 3.6: Dielectric loss spectrum, $\varepsilon''(\nu)$, of 0.4881 M NaOAc(aq) at 25 °C. Symbols represent experimental data, the line through the experimental data represents the D+D+D fit, and shaded areas indicate the contributions of the three relaxation modes.

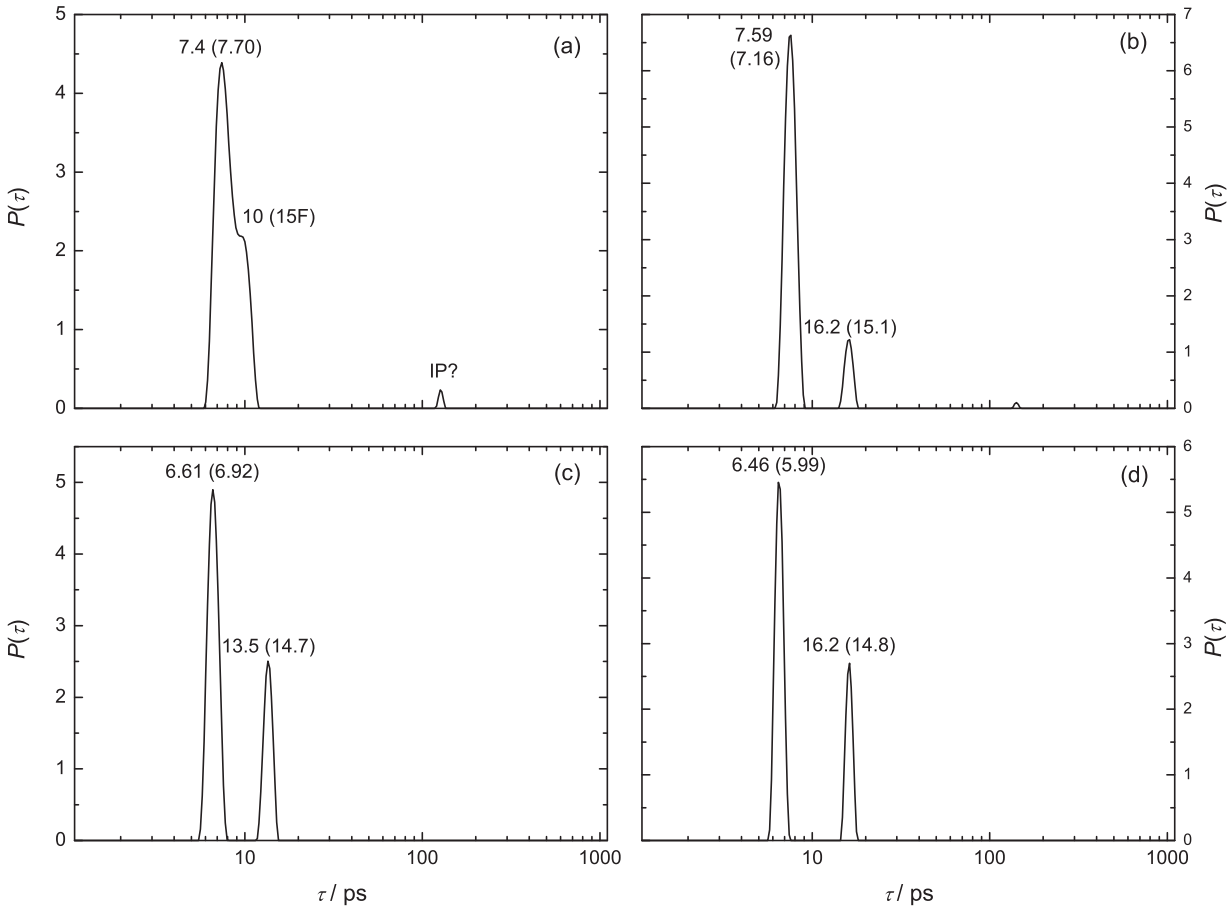

Figure 3.7: Relaxation time distribution function, $P(\tau)$, of NaOFm(aq) at 25 °C at concentrations c / M of: **(a)** 0.2968, **(b)** 0.9617, **(c)** 1.888, and **(d)** 3.171 obtained with the bias-free fitting procedure of Zasetzky and Buchner.[91] Relaxation times for the resolved modes are indicated together with the corresponding values from Table 1 (in brackets; F = fixed).

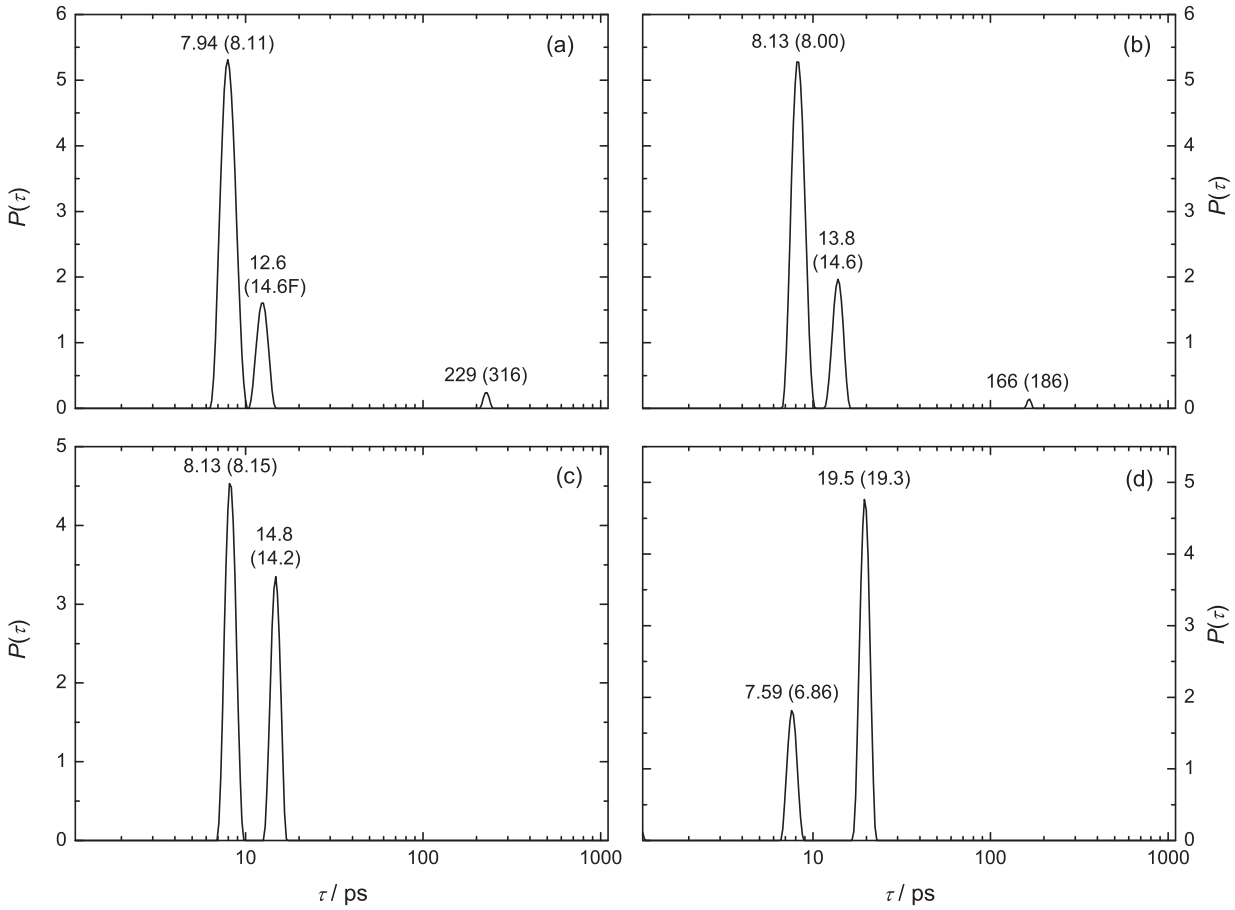

Figure 3.8: Relaxation time distribution function, $P(\tau)$, of NaOAc(aq) at 25 °C at concentrations c / M of: **(a)** 0.4883, **(b)** 0.9574, **(c)** 1.838, and **(d)** 3.717 obtained with the bias-free fitting procedure of Zasetzky and Buchner.[91] Relaxation times for the resolved modes are indicated together with the corresponding values from Table 2 (in brackets; F = fixed).

As is usual for aqueous electrolyte solutions, the spectra for the solutions of both salts were dominated by the cooperative relaxation of bulk water, readily identified by its location (∼20 GHz) and magnitude. In addition, the relaxation times for this mode, τ_b (= τ_2 for NaOFm(aq) in Table 3.1; τ_3 for NaOAc(aq) in Table 3.2), extrapolate smoothly to the pure water values, $\tau_b(0)$, of 10.8, 8.32 and 6.53 ps at 15, 25 and 35 °C, respectively (Figures 3.9 & 3.10a). There is, however, a significant difference between the two sets of salt solutions in that the position of the experimentally observed loss peak is almost invariant with c for NaOFm(aq) (Figure 3.1b) whereas for NaOAc(aq) it shifts to much lower frequencies and becomes clearly asymmetric with increasing c (Figures 3.2b, 3.3b and 3.4b).

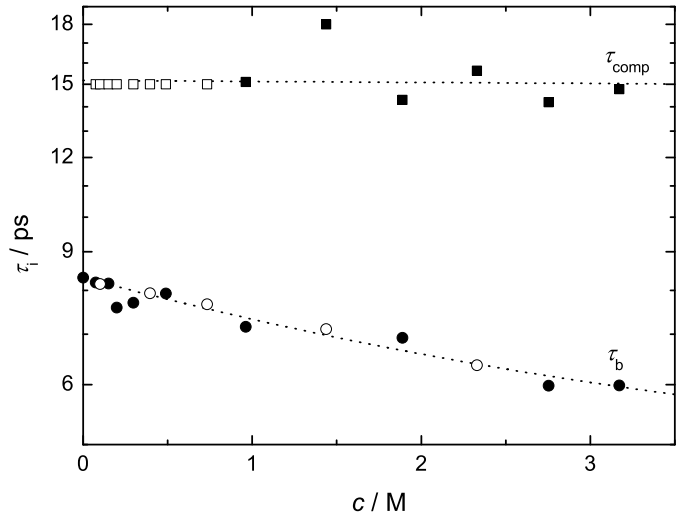

Figure 3.9: Concentration dependence for NaOFm(aq) of the "composite" mode relaxation time, τ_{comp}, and the bulk-water relaxation time, τ_b, at 25 °C. Symbols show experimental values; dotted lines are included only as a visual aid. Open symbols represent values that were held constant during the fitting procedure.

Detailed analysis indicated that this shift was due to the presence of another mode centred at ∼8 GHz whose intensity increased considerably relative to the decreasing bulk-water amplitude with increasing solute concentration. Broadly consistent with an unbiased analysis[91] of the data (Figures 3.7 & 3.8) this mode was also found to be present in the NaOFm(aq) spectra, albeit with a smaller amplitude especially at high c, which did not significantly affect the location of the maximum observed for $\varepsilon''(\nu)$. The average relaxation time[111] of this slower process at 25 °C: $\tau_1 \approx 15$ ps for NaOFm(aq) (Figure 3.9) and $\tau_2 \approx 16$ ps for NaOAc(aq) (Figure 3.10b) is almost twice that of the bulk water mode ($\tau_b \approx 8$ ps) but similar to the relaxation times observed for "slow" water molecules involved in the hydration of either hydrophobic solutes[112,113] or moderately hydrophilic anions.[114–116] Accordingly, this mode is tentatively assigned to the presence of slow water molecules. However, it must

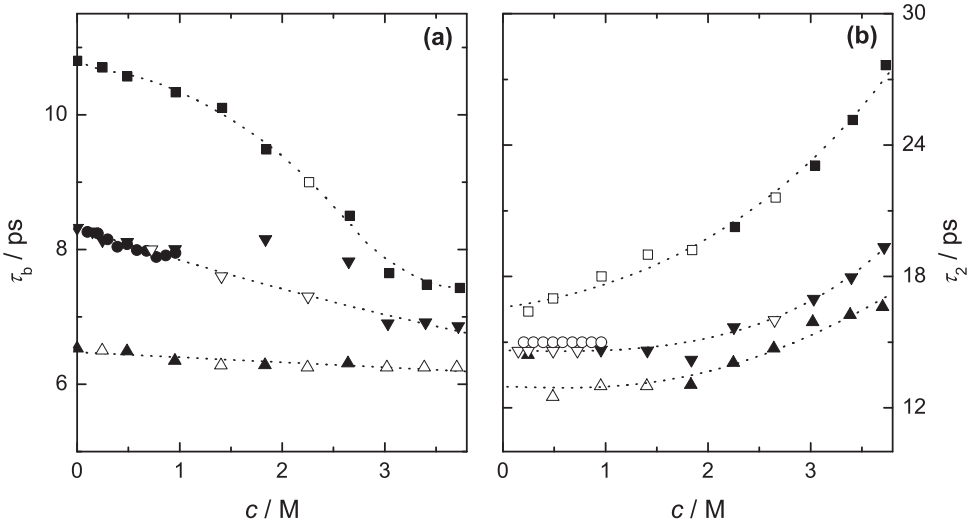

Figure 3.10: Concentration and temperature dependence for NaOAc(aq) of: (**a**) the bulk-water relaxation time, τ_b, and (**b**) the "composite" mode relaxation time, $\tau_{comp} = \tau_2$, at 15 °C (■), 25 °C (▼, for additional measurements (●)) and 35 °C (▲). Symbols show experimental values; open symbols represent values that were held constant during the fitting procedure; dotted lines are included only as a visual aid.

be remembered that both OFm^- and OAc^- have dipole moments (the gas phase values of μ_- are 1.40 D and 3.64 D respectively).[117] Since DRS is sensitive to all dipolar species,[11] both ions will contribute to the spectra. As no separate relaxation process was observed for either anion it is likely that the relaxation associated with their reorientation, which would be expected to occur at ∼5-10 GHz, is subsumed in the slow-water mode. This mode (process 1 for NaOFm(aq) (Figure 3.5) and process 2 for NaOAc(aq) (Figure 3.6)) will therefore be referred to from here on as a "composite" mode.

The detection of an additional low-frequency low-amplitude Debye relaxation, centred at ∼0.6 GHz, for NaOAc(aq) at $c \lesssim 1$ M at all temperatures (Figures 3.6 & 3.8) is consistent, from its location and amplitude, with the presence of small amounts of ion-pairs. There were slight indications (Figure 3.7a) that such species may also be present in NaOFm(aq) but the scatter in the data and the limited extent of formation precluded quantification. The presence of very weak ion pairing between Na^+(aq) and both OFm^-(aq) and OAc^-(aq) is consistent with thermodynamic data (see below), recent conductivity measurements[118] and molecular dynamics (MD) simulations.[20]

It is interesting to note that the present spectra, limited to $\nu \leq 89$ GHz, did not produce any evidence for the very fast water process centred at ∼400 GHz[110] which is sometimes[112,113] but not always[115] detected in aqueous electrolyte solutions. This absence was consistent with the bias-free simulations (Figures 3.7 & 3.8). Nevertheless, the fitted values of $\varepsilon_\infty \approx$ 5-7 (Tables 3.1 & 3.2) are considerably larger than the $\varepsilon_\infty = 3.48$ obtained for pure water,[84,110] which suggests that the fast water process is still making a minor, if unresolvable, contribution to the present spectra.

3.1.2 Relaxation amplitudes

Ion pairs. For NaOAc(aq) the ion-pair relaxation amplitude, $S_{\mathrm{IP}} = \varepsilon(c) - \varepsilon_2(c)$, and therefore the ion-pair concentration, passes through a maximum at $c \approx 0.5\,\mathrm{M}$ (Figure 3.11). The decrease in S_{IP} at $c > 0.5\,\mathrm{M}$ is consistent with the so-called "redissociation" that often occurs for weak ion pairs at high salt concentrations.[112,114] As S_{IP} is small and shows significant scatter, an additional set of data (as described earlier) was measured using new more efficient setup (Agilent E8364B VNA connected to an Ecal module, Section 2.2) for the appropriate analysis of this mode. A quantitative analysis of S_{IP} is given in Section 3.1.3.

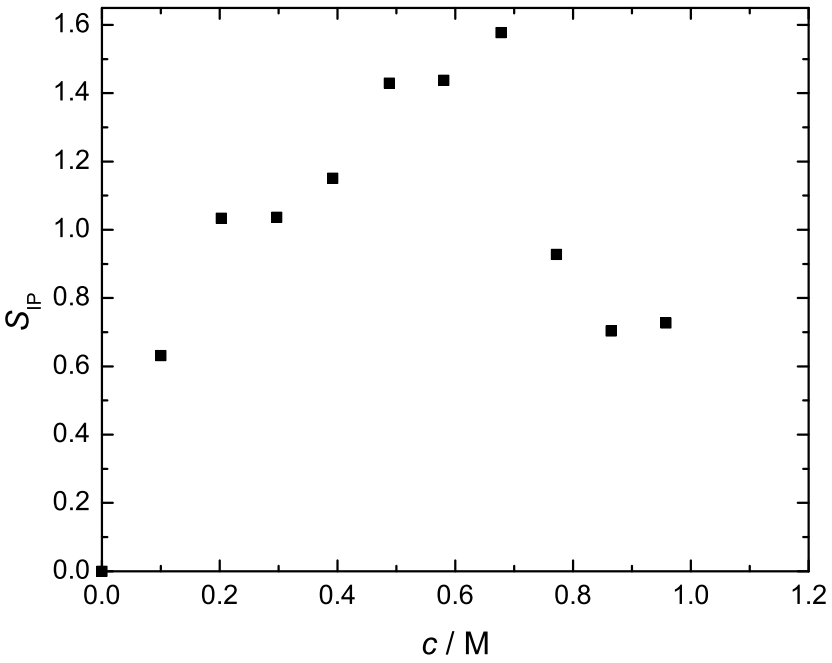

Figure 3.11: Concentration dependence of ion-pair relaxation amplitude, S_{IP}, of NaOAc(aq) (additional set of measurements) at 25 °C.

Bulk water. As shown previously,[112] the bulk and (unresolved) fast relaxations for water (at ∼20 GHz and ∼400 GHz respectively) can be treated collectively by assuming: $S_{\mathrm{b}} = \varepsilon_j(c) - \varepsilon_\infty$, where $j = 2$ for NaOFm(aq) and $j = 3$ for NaOAc(aq). For these calculations the value of ε_∞ was taken to be that obtained from ultrahigh-frequency dielectric measurements (including THz data[84]) of pure water, rather than the less accurate values derived from fitting the present spectra at $\nu \leq 89\,\mathrm{GHz}$ (Tables 3.1 & 3.2). As can be seen the magnitude of S_{b} decreases significantly with increasing c (Figure 3.12).
The dipole concentrations, c_i, corresponding to the relaxation amplitudes, S_i, can be calculated via the generalized Cavell equation (Eq. 1.71).[66] For evaluation of the bulk water

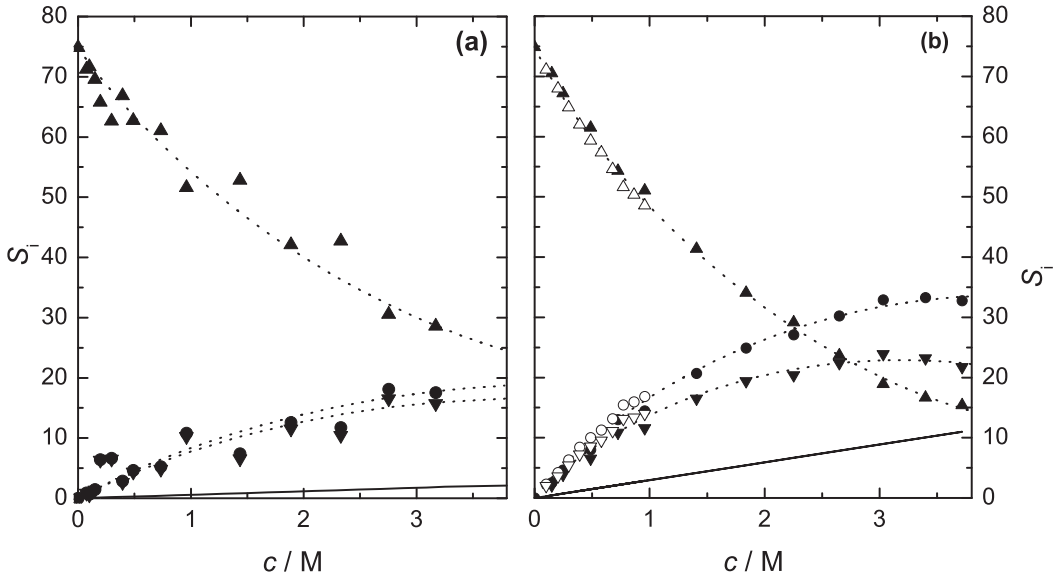

Figure 3.12: Concentration dependence for (**a**) NaOFm(aq) and (**b**) NaOAc(aq) at 25 °C of the relaxation amplitudes of: bulk water, S_b (▲), the "composite" mode, $S_\mathrm{s} + S_-$ (●), and slow water, S_s (▼). Open symbols represent the data obtained from additional set of measurements. The solid line represents S_-, calculated via Eq. 1.71; the dotted lines are included only as a visual guide.

amplitude it is advantageous to normalize Eq. 1.71 to pure water.[112,119] Additionally, for electrolyte solutions, S_b has to be corrected for the kinetic depolarization (kd) that arises from the relative motions of the ions and the surrounding solvent molecules in the external field.[120–122] Thus, the equilibrium amplitude of the overall solvent relaxation process, $S_\mathrm{b}^\mathrm{eq}(c)$, to be inserted into Eq. 1.71 is given by

$$S_\mathrm{b}^\mathrm{eq}(c) = S_\mathrm{b}(c) + \Delta_\mathrm{kd}\varepsilon(c) \tag{3.1}$$

where

$$\Delta_\mathrm{kd}\varepsilon(c) = \xi\kappa(c) \tag{3.2}$$

and

$$\xi = p \times \frac{\varepsilon(0) - \varepsilon_\infty(0)}{\varepsilon(0)} \times \frac{\tau(0)}{\varepsilon_0} \tag{3.3}$$

In Eq. 3.2, $\varepsilon(0)$ is the (relative static) permittivity of pure water and $\tau(0)$ is the relaxation time of its dominant dispersion step.[120–122] The hydrodynamic parameter p characterizes the translational motion of the ions, with $p = 1$ for *stick* and $p = 2/3$ for *slip* boundary conditions; $p = 0$ defines negligible kd. For the present systems *slip* boundary conditions were used for calculating the apparent bulk water concentrations, $c_\mathrm{b}^\mathrm{ap}(c)$, as they are considered to be the most physically realistic for the dielectric relaxation of solvated ions.[11,112,119,123]

Composite process. Figure 3.12 shows that the amplitude of the composite relaxation mode, $S_\mathrm{comp} = \varepsilon(c) - \varepsilon_j(c)$, where $j = 2$ for NaOFm(aq) and $j = 3$ for NaOAc(aq),

increases with increasing c for both sets of salt solutions, with the magnitude of the latter being somewhat larger. One reason for this is the larger contribution from the higher dipole moment of OAc^- cf. OFm^-.
The amplitude S_{comp} can be split into its constituent relaxation amplitudes as

$$S_{comp} = S_- + S_s \tag{3.4}$$

where S_- is the relaxation amplitude due to the rotation of the dipolar carboxylate anions and S_s is the relaxation amplitude of the "slow" water molecules hydrating the anion (see below). Since ion pairing is weak for the present systems, the magnitude of S_- for OFm^- and OAc^- can be calculated using Eq. 1.71. For the effective dipole moments of OFm^- and OAc^- in solution, the *ab initio* values for $\mu_{eff,-} = \mu_-/(1 - f_-\alpha_-)$, calculated by Serr and Netz,[117] 2.52 D and 5.70 D respectively, were adopted. The amplitude of the slow-water process, S_s, can then be derived via Eq. 3.4 from the observed values of S_{comp} and used to calculate the apparent concentration of slow water, $c_s^{ap}(c)$, via Eq. 1.71.
Unfortunately, a similar splitting of the composite mode relaxation time, τ_{comp} (τ_1 for NaOFm(aq) and τ_2 for NaOAc(aq)) into those for the anion, τ_-, and for slow water, τ_s, is not possible as it cannot be assumed that the relaxation rates $(\tau_-)^{-1}$ and $(\tau_s)^{-1}$ are independent of concentration and that $(\tau_{comp})^{-1}$ is their amplitude-weighted average. This is regrettable as it prevents calculation of the activation parameters for slow-water relaxation, which would be of considerable interest (see Section 3.1.6).

3.1.3 Quantitative description of ion pairing

In this section the results of the second series of measurements for NaOAc(aq) focussing on ion-pair relaxation are presented. These results are the part of the manuscript: *'Hydration and Sodium-ion Binding of Trifluoroacetate in Aqueous Solution', J. Mol. Liq., In Press.* (Section 3.2).
A detailed three-step mechanism (Figure 1.1) for formation of ion pairs in aqueous solutions proposed by Eigen and Tamm in 1962[74] is discussed in Section 1.5.
No ion-pair relaxation is resolved in aqueous NaOFm solutions in DRS time scale, whereas, weak ion pairing is observed in NaOAc(aq) at $c \lesssim 1$ M. As already noted, the presence of ion pairs in NaOAc(aq) is supported by MD simulations[20] and conductivity measurements.[118] Potentiometric studies[124] also suggest weak complexing of Na^+ with acetate ($\log K_A$ = -0.27 at $I = 0.25$ M and 25 °C) in aqueous solutions. Further support for the existence of weak-ion-pairing between Na^+(aq) and OAc^-(aq) comes from measurements of the association constant (K_A) of acetic acid in different media. Applying an equation analogous to that derived by Hefter[125] to the K_A(HOAc) values reported by Partanen in KCl and NaCl media[126] gave a value of $K_A(NaOAc) \approx 0.07\ M^{-1}$, corresponding to the equilibrium

$$Na^+(aq) + OAc^-(aq) \rightleftharpoons NaOAc^0(aq) \tag{3.5}$$

at an ionic strength $I \approx 1$ M (KCl). A similar result was obtained for K_A(NaOFm) using the analogous data for formic acid.[126]
The amplitude (S_{IP}) of the lowest frequency mode in NaOAc(aq) is used to calculate the concentrations of various possible ion-pair (IP) types, c_{IP}, using the Cavell equation

(Eq. 1.71).[66] Required polarizabilities of various IP types were calculated as $\alpha_{IP} = \alpha_+ + \alpha_- + n\alpha(H_2O)$, where n is the number of water molecules in the IP structure ($n = 0$ for CIPs; $n = 1$ for SIPs; and $n = 2$ for 2SIPs), with $\alpha/4\pi\varepsilon_o$Å$^3 = 0.211$ (Na^+),[66] 5.498 (OAc^-),[38] and 1.444 (H_2O).[66]
Dipole moments of various IP types, μ_{IP}, calculated with MOPAC[100] (Section 2.3.3) are listed in Table 3.4. Dipole moments were also calculated using procedure described by Barthel et al.[66] The moment values $\mu_{SIP} = 22.5$ D and $\mu_{2SIP} = 35.2$ D calculated using that procedure are in good agreement with the MOPAC-calculated moments listed in Table 3.4. The dipole moment for CIP ($\mu_{CIP} = 4.89$ D) is, however, smaller compared to the corresponding MOPAC value. The quantities required for evaluation of Eq. 1.71 are listed in Table 3.4 or were easily calculated using relevant equations (Eqs. 1.72 - 1.77).

Table 3.4: Ion-Pair Dipole Moments, μ_{IP}; and Resulting Parameters log K_A^o, B_K, and C_K of Eq. 1.91 for tested Ion-Pair Models of NaOAc (aq).[a]

Model	μ_{IP}	log K_A^o	B_K	C_K
CIP	7.62	2.17±0.41	-3.51±2.24	0.68±1.94
SIP	21.7	0.62±0.12	-3.17±0.77	1.18±0.72
2SIP	34.1	0.18±0.11	-2.99±0.74	1.07±0.69

[a] Units: μ_{IP} in Debye (1 D = 3.3356×10^{-30} C·m.), B_K in L·mol^{-1}, C_K in L$^{3/2}$·mol$^{-3/2}$.

The concentrations of various IP types were then used to calculate the corresponding association constant, K_A, with Equation 1.90. To determine the standard (infinite dilution) association constant, K_A^o,[†] the values of K_A so obtained were then fitted to a Guggenheim-type-equation(Eq. 1.91) (Figure 3.13).
The K_A^o, B_K, and C_K values obtained for NaOAc(aq) using Eq. 1.91, assuming the formation of CIPs, SIPs, or 2SIPs are given in Table 3.4.
For all known methods quantitative characterization of weak ion association is virtually impossible.[76] This may be the reason why, to the best of our knowledge, no independently determined K_A^o value is available in literature that would allow to infer whether CIP, SIP, or 2SIP is the predomination ion-pair species in NaOAc aqueous solutions.[11] Nevertheless, the predicted CIP association constant of 148 M^{-1} for NaOAc(aq) (Table 3.4) appears definitely too high in view of recent computer simulations[20,22] and the value of $K_A = 0.07$ M^{-1} estimated above from thermodynamic data for NaOAc in aqueous KCl at ionic strength $I \approx 1$ M.[106] Recently reported[118] $K_A^o = 12.5\pm0.7$ M^{-1} for NaOFm(aq), using dilute solutions conductivity measurements is also an argument against the possibility of CIPs. Also, the present DRS data definitely rule out CIPs for NaOAc(aq) because its

[†]Association constants reported in this section for possible IP species present in aqueous solution of NaOAc(aq) represent the **upper limit** of ion pairing between Na^+ and $-COO^-$ because of likely ion-cloud relaxation contribution to S_{IP}, see Section 3.2.3 for details.

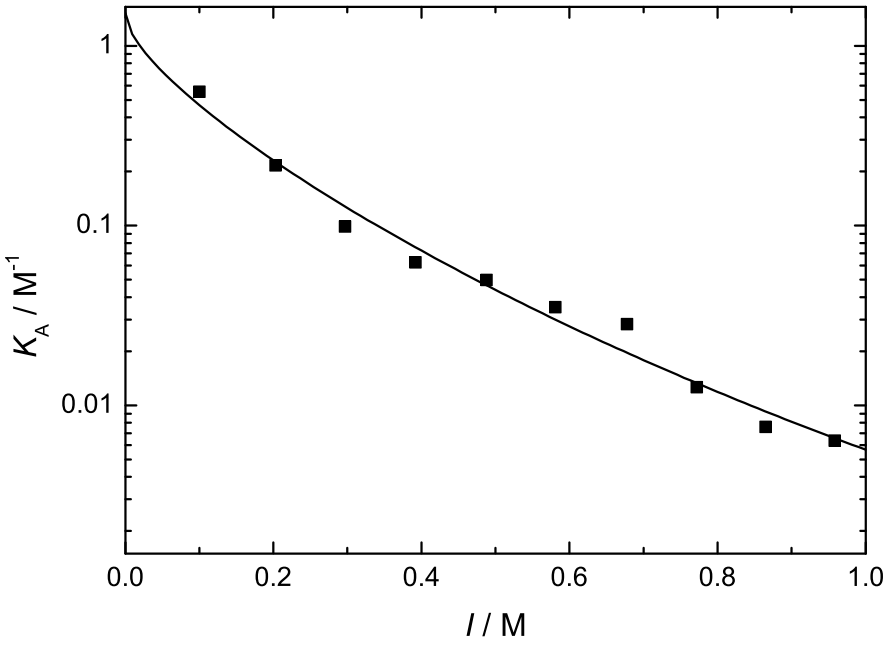

Figure 3.13: Ion association constant, K_A, as a function of nominal ionic strength, I (= c for 1:1 electrolytes), for NaOAc(aq) at 25 °C (2SIP Model). Line represents fit according to Eq. 1.91.

estimated rotational correlation time, τ', is far too short compared to the experimental value, τ'_{IP} (Table 3.5). The latter was calculated from the IP relaxation time, τ_{IP}, via the Powles-Glarum equation[71,72] (Eq. 1.85). In Table 3.5 average value of τ'_{IP} is given for NaOAc(aq).

Theoretical estimates for the rotational correlation times of CIPs, SIPs and 2SIPs, calculated for stick (τ'_{stick}) and slip (τ'_{slip}) hydrodynamic boundary conditions (Table 3.5), were obtained with the SED equation[70,127] (Eq. 1.80). For η, the value of pure water, $\eta = 0.8903$ mPa·s,[128] was used; V_{eff} was obtained applying the approach of Dote et al.[70] (Section 1.4.4) from the geometric data of the IPs provided by the MOPAC calculations.

According to the data of Table 3.5 the 2SIP is the most probable type of ion pair present in NaOAc(aq). This assignment is supported by the strong hydration of Na^+ and that of the carboxylate group (see Section 3.1.4 below), which implies that stick boundary conditions are more appropriate for ion-pair rotation as the hydrating H_2O molecules will at least partly follow this motion. Also, the simulations of Hess and van der Vegt[22] yield even at 1 mol kg^{-1} a predominance of 2SIP over SIP configurations (and few CIPs only) for NaOAc(aq). Accordingly, $K_A^\circ \lesssim 1.5\,M^{-1}$ can be estimated for association of NaOAc(aq) assuming 2SIPs as the dominating ion-pair species.

Table 3.5: Comparison of Experimental, τ'_{IP},[a] and Calculated, τ'_{slip} and τ'_{stick},[b] Rotational Correlation Times for *Stick* and *Slip* Boundary Conditions for Ion-Pair Reorientation in Aqueous Solutions of NaOAc(aq) at 25 °C.[c]

electrolyte	τ'_{IP}	IP	τ'_{slip}	τ'_{stick}
		CIP	5.3	79
NaOAc	206	SIP	27	136
		2SIP	71	223

[a] Obtained via Powles-Glarum relation (Eq. 1.85). [b] Averaged values obtained from SED relation (Eq. 1.80). [c] Unit: τ_i in ps.

3.1.4 Ion hydration

For both salts the strong decrease of S_{b} (Figure 3.12) and the emergence of the slow-water process (Figures 3.5 & 3.6) with increasing c indicate the presence of strong ion-water interactions. If such interactions are much stronger than water-water interactions, the water molecules bound to the ions effectively become immobilized ("irrotationally bound", ib) or "frozen" on the DRS time scale.
For the present systems, the sum of the DRS-detected water, $c_{\mathrm{b}}^{\mathrm{ap}} + c_{\mathrm{s}}^{\mathrm{ap}}$ (Section 3.1.2), is less than the analytical (total) water concentration, c_{w}. Water missing from the DR spectrum can be ascribed to the presence of ib water molecules and an effective hydration number, Z_{ib}, can then be defined as the number of such *immobilized* molecules per 'unit' of dissolved salt

$$Z_{\mathrm{ib}} = (c_{\mathrm{w}} - c_{\mathrm{b}}^{\mathrm{ap}} - c_{\mathrm{s}}^{\mathrm{ap}})/c \tag{3.6}$$

In contrast, the values of $c_{\mathrm{s}}^{\mathrm{ap}}(c)$ obtained from S_{s} with Eq. 1.71 can be used directly to calculate the effective number of *slow* water molecules

$$Z_{\mathrm{s}} = c_{\mathrm{s}}^{\mathrm{ap}}/c \tag{3.7}$$

The Z_{ib} values calculated in this way for NaOFm(aq) and NaOAc(aq) at 25 °C are given in Figure 3.14.[129] To partition these values into their more interesting ionic components, $Z_{\mathrm{ib}}(\mathrm{Na}^+)$ was obtained from a reanalysis of the 25 °C data for NaCl(aq)[123] with Eq. 1.71, along with the assumption of ionic additivity.[130] The Z_{ib} values so obtained for OFm^- and OAc^- are also shown in Figure 3.14. At $c \lesssim 0.75$ M, OFm^- does not appear to bind any water molecules strongly (*i.e.*, $Z_{\mathrm{ib}} \approx 0$) while $Z_{\mathrm{ib}}(\mathrm{OAc}^-) \approx 1$. At $c \gtrsim 1$ M, Z_{ib} for both anions increases slightly with increasing c. This is unusual: most ions studied to date show a decrease in Z_{ib} with increasing c,[10,131] which is thought to be due to increasing overlap of their hydration shells. A possible explanation of this unusual increase might be that some water molecules are held more tightly by bonding simultaneously to both the cation and anion, *i.e.*, as intervening solvent molecules in solvent-separated ion pairs (SIPs). Despite

fast redissociation (and thus no detectable SIP relaxation process[11]) such configurations may become frequent at $c \gtrsim 1\,\mathrm{M}$ because of steric crowding (see below).

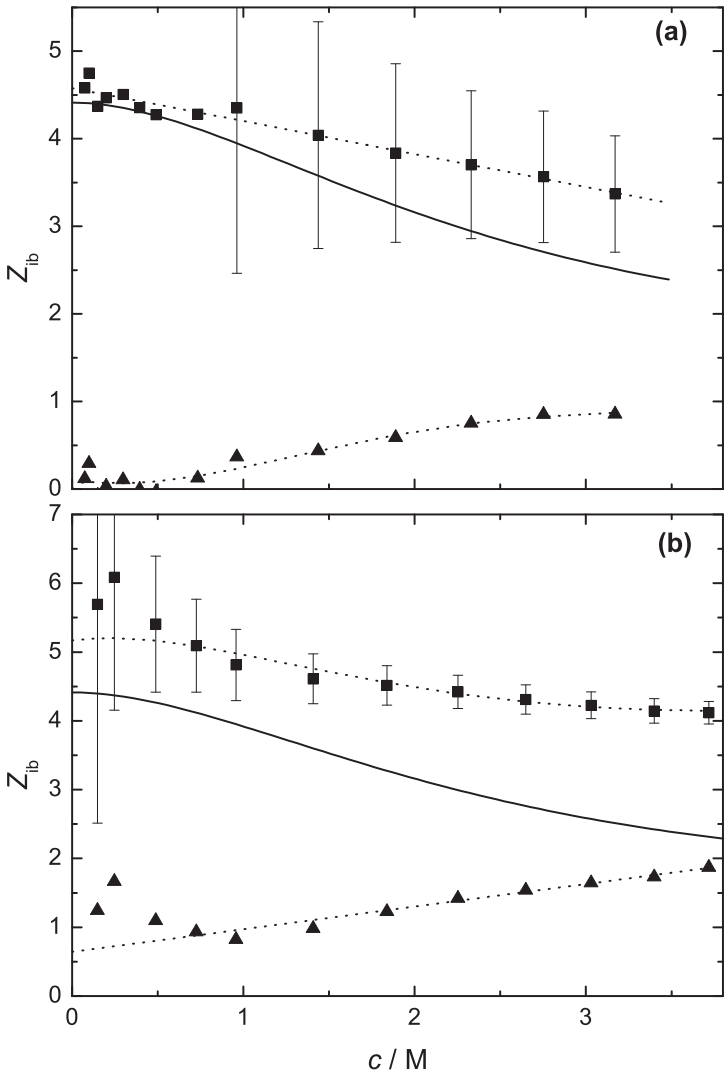

Figure 3.14: Concentration dependence of effective hydration numbers, Z_{ib}, at 25 °C for (**a**) NaOFm(aq) (■), and OFm^-(aq) (▲); and (**b**) NaOAc(aq) (■), and OAc^-(aq) (▲).[132] Solid lines represent $Z_{ib}(Na^+)$; dotted lines are included only as a visual guide.

The Z_s values calculated for NaOFm(aq) and NaOAc(aq) are shown in Figure 3.15.[129] Since aqueous solutions of common inorganic salts containing Na^+ do not show any slow water process,[45,131,133] it is reasonable to assign Z_s for both of the present systems to the anions alone. On this basis the Z_s value for OFm^-(aq) at infinite dilution is ∼5.2 and decreases linearly with increasing c (Figure 3.15). As OFm^- does not contain a hydrophobic part, these water molecules can reasonably be assumed to be H-bonded to the hydrophilic – COO^- moiety. In line with recent MD simulations[134] it is postulated that the strength of these H-bonds is greater than that of the water-water H-bonds, thereby slowing their

dynamics. This hydrophilic interaction is not strong enough to irrotationally bind these water molecules to the $-COO^-$ moiety, since $Z_{ib}(OFm^-) \approx 0$ at $c \to 0$ (Figure 3.14 a). The present assignment accords with recent theoretical investigations by Sterpone et al.[135] which suggested that the water molecules hydrating the carboxylate group in amino acids are retarded by a factor of $\sim$2.5 compared to bulk water. They also suggested that, in addition to the stronger $-COO^- \cdots H_2O$ interactions (relative to $H_2O \cdots H_2O$), excluded volume effects are important for slowing the water dynamics. Similarly, Xu and Berne[6] found that H-bond making and breaking kinetics were slower in the first solvation shell of a negatively charged polypeptide, again using MD simulations. Hydrophilically-slowed water dynamics have also been observed experimentally for several dicarboxylate ions[114] and F^-.[115,116]

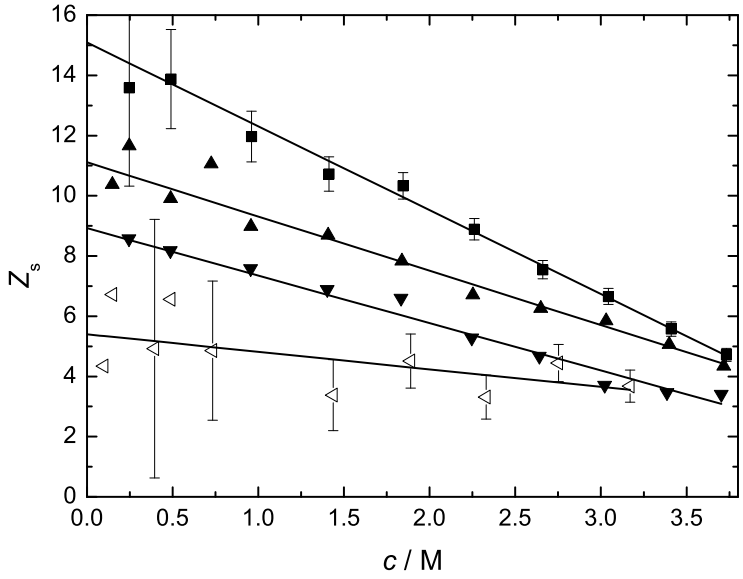

Figure 3.15: Concentration dependence of the slow-water hydration number, Z_s, for NaOFm(aq) ($\triangleleft$) at 25 °C, and for NaOAc(aq) at 15 °C ($\blacksquare$); 25 °C ($\blacktriangle$); and 35 °C ($\blacktriangledown$) (error bars[132] omitted for NaOAc(aq) at 25 °C and 35 °C for visual clarity).

Although the present Z_{ib} values are small ($\lesssim 2$) and should not be over-interpreted given the assumptions involved in obtaining them, it is interesting to note that for OFm^- the increase of Z_{ib} counterbalances a decrease in Z_s (Figure 3.15), such that their sum, the total hydration number, is approximately constant ($Z_t \equiv Z_s + Z_{ib} \approx 5$). This implies that the hydration shell of the $-COO^-$ group remains intact, with some variations in bond strength, up to fairly high concentrations. Also, the values of Z_t for the highest OAc^- concentration are roughly independent of the temperature (see below) and similar to $Z_t(OFm^-)$. The implications of this finding will be discussed in Section 3.1.5.

Most computer simulations of carboxylate hydration[7,28–30,36,134] conclude that water is highly structured around the $-COO^-$ group, with an average hydration number of 5-7. On the other hand, X-ray and neutron scattering and infrared measurements of concentrated aqueous solutions of sodium and potassium formate[32,33] and acetate[34,35] indicate that the hydration number per $-COO^-$ is < 5. NMR studies[31] have suggested there are 5.0-6.5 water molecules around each $-COO^-$ group, while statistical mechanics results suggest that the $-COO^-$ group of OAc^- forms $\sim$6 H-bonds to adjacent water molecules.[136] Except for References 32–35 which focus on very concentrated solutions, all these investigations are broadly consistent with the present study (and with each other).

The present results may be compared with those obtained for oxalate ($C_2O_4^{2-}$, ox^{2-}),[137] the simplest of the dicarboxylate anions. At infinite dilution, the total number of water molecules 'bound' to OFm^- (*i.e.*, Z_t) is $\sim$5.2, which is similar to the value of $\sim$6 found for $Z_{ib}(ox^{2-})$.[137] As already noted, Z_t remains approximately constant for OFm^- regardless of c. In contrast, the hydration shell of ox^{2-} is particularly 'fragile', decreasing rapidly with increasing solute concentration such that at 0.25 M, the highest concentration studied due to the limited solubility of $Na_2ox(s)$, $Z_{ib}(ox^{2-}) \approx 2.3$.[137] The apparent contradiction that $Z_{ib}(ox^{2-}) > Z_{ib}(OFm^-)$ at infinite dilution yet $Z_{ib}(ox^{2-})$ decreases sharply with increasing c while $Z_{ib}(OFm^-)$ increases (Figure 3.14 a) may merely reflect a failure to detect 'slow' water for $Na_2ox(aq)$ due to the limited accessible concentration range. In this context DRS measurements on aqueous solutions of the more soluble K_2ox would be of interest.

At infinite dilution $Z_s(OAc^-) \approx 11$ at 25 °C which is about double of that of formate (Figure 3.15) and although $Z_s(OAc^-)$ decreases linearly with increasing c, it always remains greater than $Z_s(OFm^-)$. Similarly, $Z_{ib}(OAc^-) > Z_{ib}(OFm^-)$ over the entire concentration range (Figure 3.14), which means that $Z_t(OAc^-) > Z_t(OFm^-)$ at all concentrations, with the difference becoming smaller at higher c. These observations are consistent with a significant contribution of the methyl group to the hydration of OAc^-. There are three plausible explanations of this contribution: (1) increased *hydrophilic* hydration of the $-COO^-$ moiety due to the electron donating effect of the $-CH_3$ group; (2) '*semihydrophilic*' hydration[138] of the $-CH_3$ moiety, as a result of the polarization of the C–H bonds by the carboxylate group; or (3) *hydrophobic* hydration of $-CH_3$.[112,139–141]

Recent QM/MM simulations of OAc^--water interactions in aqueous solution suggest[142] that semihydrophilic hydration of $-CH_3$ is unlikely; rather, a repulsive interaction seems to operate. Similarly, theoretical calculations[143] based on the partial-equalization-of-orbital-electronegativity method suggest only a slight increase of negative charge on the oxygen atoms in OAc^- compared to those in OFm^-, so the electron donating effect of $-CH_3$ also cannot explain the difference between $Z_s(OAc^-)$ and $Z_s(OFm^-)$. It follows that this difference must be due to the hydrophobicity of the $-CH_3$ group in OAc^-. This conclusion is consistent with the computer simulations and theoretical considerations of Laage et al.[141] who found that water molecules adjacent to hydrophobic moieties are retarded by a factor of $\sim$1.5 compared to bulk water.

The existence of hydrophobic hydration of the methyl group in OAc^- contrasts markedly with the behaviour observed for the methyl groups in, for example, tetramethylammonium bromide (TMAB) for which no slow water was detected.[112] This implies that the hydrophobic hydration of methyl groups is significantly affected by their structural/chemical

environment: in TMAB the $-CH_3$ groups are directly attached to a slightly hydrophilic cationic centre whereas in OAc^- the $-CH_3$ group is slightly separated from a strongly hydrophilic anionic centre. Further systematic studies will be necessary to clarify this potentially important issue.

3.1.5 Temperature dependence of ion hydration in NaOAc(aq)

Typical DR spectra obtained for NaOAc(aq) at various temperatures are given in Figures 3.2, 3.3 & 3.4. As already noted, the $\varepsilon''(\nu)$ curves show a clear shift in position towards lower frequencies with increasing c at all investigated temperatures. On the other hand, the $\varepsilon''(\nu)$ curves shift towards higher frequencies and the apparent amplitude decreases with increasing temperature (Figures 3.2, 3.3 & 3.4).

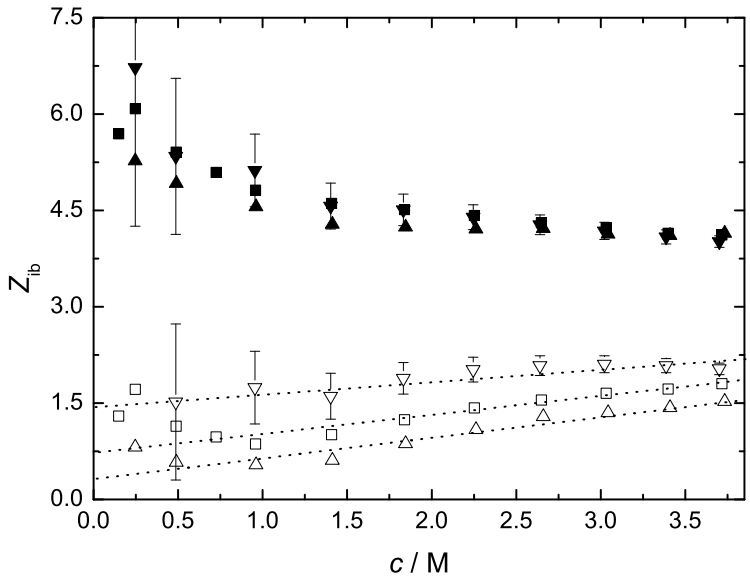

Figure 3.16: Concentration dependence of the effective hydration number, Z_{ib}, for NaOAc(aq) (filled symbols) and OAc^-(aq) (open symbols) at: 15 °C (▲, △); 25 °C (■, □); and 35 °C (▼, ▽). Error bars[69] for 15 °C and 25 °C were similar but have been omitted for visual clarity. Dotted lines are included only as a visual guide.

The amplitudes of the two water-related processes: $S_{\mathrm{b}} = \varepsilon_3(c) - \varepsilon_\infty$ and S_{s}, were used to calculate Z_{ib} and Z_{s} for NaOAc(aq) at 15 and 35 °C, following the procedure described in section 3.1.4. Figure 3.16 shows Z_{ib} for NaOAc(aq), as a function of c at different temperatures. The $Z_{\mathrm{ib}}(Na^+)$ values at 25 °C (as already noted) and 35 °C were obtained by reanalysing literature data for NaCl(aq)[123] with Eq. 1.71. Since suitable data were not available at 15 °C, the DR spectra of NaCl(aq) were recorded at this temperature

in the frequency range $0.2 \leq \nu/\mathrm{GHz} \leq 50$ (Table A.1, Figure A.1) and analysed with Eq. 1.71. The values of $Z_{\mathrm{ib}}(\mathrm{Na}^+)$ used to estimate $Z_{\mathrm{ib}}(\mathrm{OAc}^-)$ are given in Figure A.2. Note that all the ionic values are ultimately based on the assumption that $Z_{\mathrm{ib}}(\mathrm{Cl}^-) = 0$ at all temperatures.

At low concentrations the values of $Z_{\mathrm{s}}(\mathrm{OAc}^-)$ strongly decrease with increasing temperature (Figure 3.15), consistent with increased thermal motion. However, with increasing concentration this effect becomes less pronounced. Although the change is rather small, $Z_{\mathrm{ib}}(\mathrm{OAc}^-)$ seems to increase with increasing temperature (Figure 3.16), which is opposite to the usual[123] trend. The overall picture that emerges from Figures 3.15 & 3.16 is that temperature-induced dehydration of carboxylate ions becomes less effective with increasing solute concentration such that Z_{s} values become almost independent of temperature. Additionally, the already weak thermal dehydration effect at high c is partly counteracted by the increase of Z_{ib} (Figure 3.16) so that at the highest c(NaOAc) the total hydration number, $Z_{\mathrm{t}}(\mathrm{OAc}^-)$, is ∼6.3, ∼6.2 and ∼5.4 at 15, 25 and 35 °C, respectively. Since these values are also close to the concentration-independent total hydration number of formate, $Z_{\mathrm{t}}(\mathrm{OFm}^-) \approx 5.2$, it can be concluded that the data for the highest acetate concentration represents $Z_{\mathrm{t}}(-\mathrm{COO}^-)$. This also suggests that the hydrophobic hydration of the $-\mathrm{CH}_3$ moiety in OAc^- rapidly breaks down with increasing c and T. Although the present spectra provide no *direct* evidence, it may be speculated that this decrease of Z_{s} might be accompanied by some sort of aggregation of the hydrophobic methyl groups similar to what was found previously for large hydrophobic ions.[112,113]

3.1.6 Bulk water dynamics

Over the investigated concentration range of NaOFm(aq) the relaxation time of *bulk* water, τ_{b}, decreases by almost 30 % at 25 °C (Figure 3.9). For NaOAc(aq) at the same temperature (Figure 3.10a) the concentration-induced decrease is less pronounced (∼13 %) but, consistent with the exponential increase of τ_{b} in pure water, increases strongly with decreasing temperature. These two effects (Figures 3.9 & 3.10a), indicate that the solute influences not only those water molecules close to the ions (*i.e.*, in the first hydration shell), as has been claimed on the basis of time-resolved infrared studies,[144] but also the bulk water dynamics. Similar findings have been reported in dielectric[11] and neutron diffraction studies[145] of other electrolytes in aqueous solution.

The temperature dependence of τ_{b} can be analyzed in terms of the Arrhenius and Eyring equations (Eqs. 1.92 & 1.93, respectively). Application of Eqs. 1.92 & 1.93 to the bulk water relaxation time in Table 3.2 reveals that E_{a} (Figure 3.17) and $\Delta H^{\neq}$ (Figure 3.18) are nearly constant at low c but drop significantly at $c \gtrsim 1.5\,\mathrm{M}$. Over approximately the same concentration range $\Delta S^{\neq}$ (Figure 3.18) changes sign from ca. $+20\,\mathrm{J\,K^{-1}\,mol^{-1}}$ at low c to $-16\,\mathrm{J\,K^{-1}\,mol^{-1}}$.

The most interesting feature of Figure 3.18 is that, as long as the average distance between the centers of the hydrated cations and anions, $d_{\mathrm{av}}/\mathrm{nm} = 0.94 \times [c/\mathrm{M}]^{-1/3}$,[146] is relatively large, the magnitudes of $\Delta S^{\neq}$ and $\Delta H^{\neq}$ are similar to those of pure water ($20.4 \pm 0.7\,\mathrm{J\,K^{-1}\,mol^{-1}}$ and $15.9 \pm 0.2\,\mathrm{kJ\,mol^{-1}}$, respectively at 25 °C)[112]. At higher concentrations, roughly where d_{av} is less than the contact distance of the hydrated cations

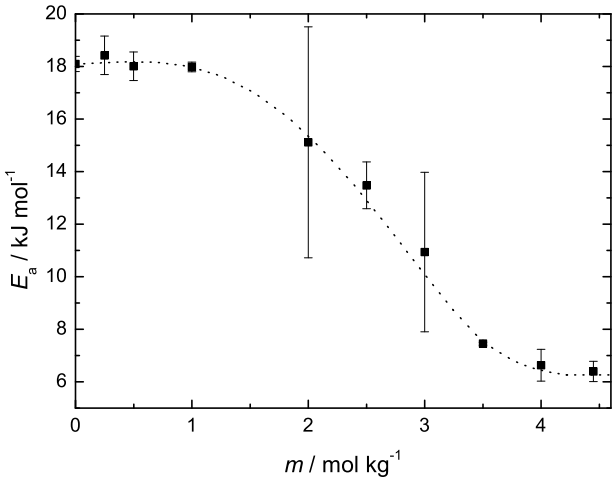

Figure 3.17: Concentration dependence of the Arrhenius activation energy, E_a, of the bulk-water relaxation time, τ_b, in NaOAc(aq). Dotted lines are included only as a visual guide.

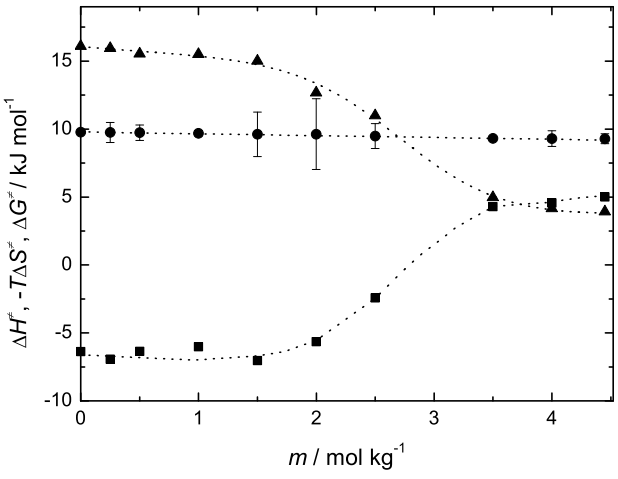

Figure 3.18: Concentration dependence of the activation parameters, $\Delta H^{\neq}$ (▲), $-T\Delta S^{\neq}$ (■, $T = 298.15\,\mathrm{K}$), and $\Delta G^{\neq}$ (●) of the bulk-water relaxation time, τ_b, in NaOAc(aq). Dotted lines are included only as a visual guide.

and anions, both $\Delta H^{\neq}$ and $\Delta S^{\neq}$ change rapidly but in opposite directions. Obviously, the structure and dynamics of whatever "bulk" water remains at these high solute concentrations differ significantly from that in dilute solutions.
The negative values for $\Delta S^{\neq}$ at $c > 3\,\mathrm{M}$ suggest that in these concentrated solutions water reorientation must be highly cooperative, possibly because of the increasing confinement and isolation of the remaining "bulk"-water pools between the hydrated ions.[147] The average number of hydrogen bonds formed by these water molecules can be calculated[112,148] as

$$\bar{n}_{\mathrm{HB}} = \frac{\Delta H^{\neq}}{\Delta_{\mathrm{HB}} H} + 1 \tag{3.8}$$

where $\Delta_{\mathrm{HB}} H = (10.9 \pm 0.4)\,\mathrm{kJ\,mol^{-1}}$ is the strength of the H_2O-H_2O hydrogen bond in the pure water.[149] As can be seen in Figure 3.19, $\bar{n}_{\mathrm{HB}}$ remains close to the bulk-water value, 2.48,[150] up to ~1.5 M but then decreases considerably, indicating a highly disrupted water structure at high solute concentrations.

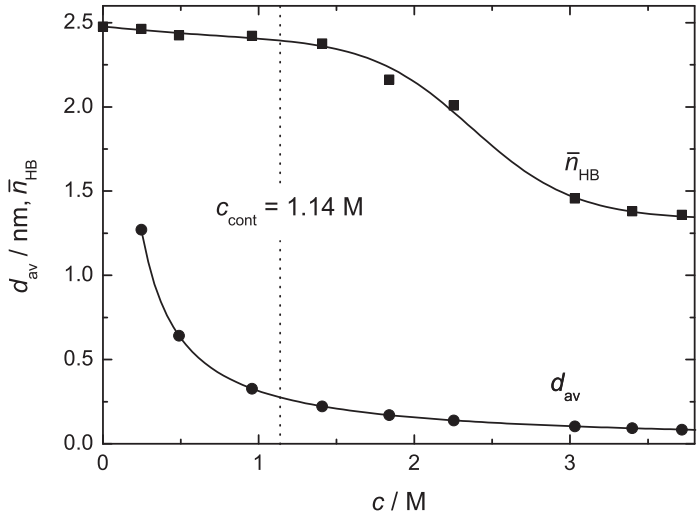

Figure 3.19: Concentration dependence of the average number of hydrogen bonds per bulk-water molecule, $\bar{n}_{\mathrm{HB}}$, and the average distance between the hydrated cations and anions, d_{av}, in NaOAc(aq). The dotted line indicates c_{cont}, the concentration at which the hydration spheres of the cations and the anions start overlapping.

Surprisingly, the Gibbs energy of activation, calculated via Eq. 1.93 shows (Figure 3.18) a pronounced enthalpy-entropy compensation (EEC) effect, which keeps $\Delta G^{\neq}$ almost constant over the entire concentration range. The plot of $\Delta H^{\neq}$ values versus $\Delta S^{\neq}$ values is linear with the slope corresponding to the compensation temperature $T_c = (309.7 \pm 0.8)\,\mathrm{K}$ (Figure 3.20). Despite of contradicting remarks about the validity of EEC effects, where Cornish-Bowden[151] called it a phantom phenomenon as a result of an artefact of statistical processing of the experimental data and on the other hand more recently Kurhe et

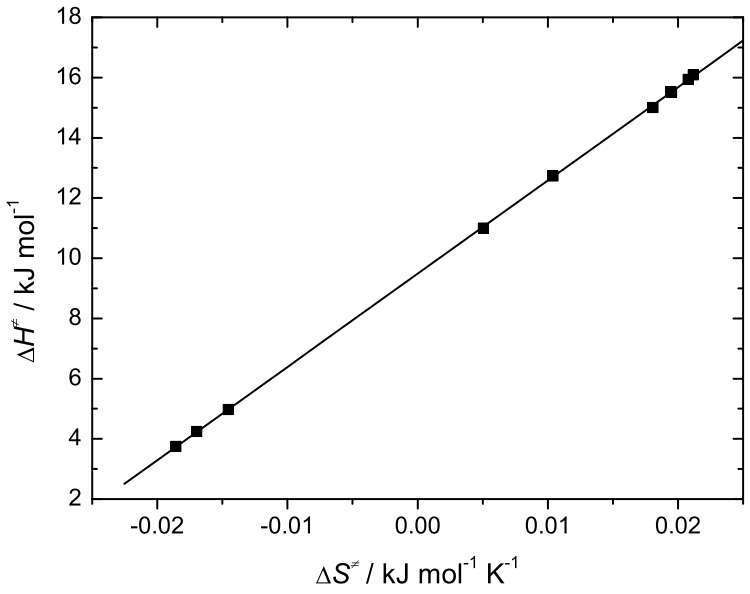

Figure 3.20: Correlation of activation enthalpy, $\Delta H^{\neq}$, and activation entropy, $\Delta S^{\neq}$ of the bulk-water relaxation time, τ_{b}, in NaOAc(aq).

al.[152] called it a real and valid phenomenon which may be useful for understanding various molecular interactions at the microscopic level, EEC effects are widely reported in the literature.[153–155]

Hefter *et al.*[156] observed that EEC is present for the transfer of small monoatomic cations like Na^+ from water to aqueous-organic solvent mixtures, whereas monoatomic anions, such as Cl^- show only little EEC. They concluded that contrary to early assertions,[157] the phenomenon of EEC is not characteristic of solutions in water nor due exclusively to its structuredness but is manifested in rather unstructured mixed aqueous-organic solvents and even in neat organic solvents.[158] They further argued[156] "that when enthalpy-entropy compensation occurs, even though the changes in $\Delta G^{\neq}$ are much smaller than those for $\Delta H^{\neq}$ and $T\Delta S^{\neq}$ they may still have significant chemical impacts." Also in the present case $\Delta G^{\neq}$ changes only marginally with salt concentration (Figure 3.18) and it is not clear what effect the observed EEC for bulk water dynamics has for the functioning of processes involving carboxylate groups but it is interesting to note that the compensation temperature, $T_c = 309.7\,\mathrm{K}$, is similar to the optimum temperature for many biological processes.

A similar analysis of the slow-water relaxation time, τ_{s}, would be of considerable interest.[85,112] Unfortunately, as explained in Section 3.1.2, this is not possible because τ_{s} cannot be easily extracted from the experimentally determined τ_{comp}.

3.2 Aqueous solutions of sodium trifluoroacetate

The material presented in this section makes the basis of the manuscript:

Rahman, H. M. A.; Buchner, R. *'Hydration and Sodium-ion Binding of Trifluoroacetate in Aqueous Solution' J. Mol. Liq. In Press.*

The use of fluorinated compounds in medicinal and biological chemistry is an active and growing field of research.[159] For example the presence of trifluoromethyl (–CF_3) groups in small bioactive molecules will often improve pharmacological profiles.[160,161] Fluorinated amphiphiles are strong surfactants in aqueous and non polar media, act as effective lubricants, and are used as fire extinguishing agents.[162] Their bio-relevant applications span from oil and fat repellents in cosmetics to oxygen carriers in artificial blood.[163,164] It is thought that the specific properties of fluorinated amphiphiles are the result of complete or partial fluorination of their hydrocarbon chains.[160,161,163,164] Consequently, there has recently been much interest in exploiting the unusual properties associated with fluorocarbons to modulate the physiochemical properties of proteins.[165,166] Several studies have concluded that introducing extensively fluorinated amino acid residues into peptides increases the stability of the peptides against unfolding[166,167] and this effect is thought to be the result of increased hydrophobicity.[166]
This section presents a detailed DRS study of the aqueous solutions of sodium trifluoroacetate (CF_3COONa, $NaOAcF_3$) over the frequency range $0.2 \lesssim \nu/\mathrm{GHz} \leq 89$ at 25 °C up to a concentration of $c = 3.647$ M. To the best of our knowledge this is the first systematic application of DRS to investigate sodium-ion binding and hydration of trifluoroacetate. Furthermore, a comparison of trifluoroacetate (a fluorinated alkylcarboxylate, CF_3COO^-, $OAcF_3^-$) and acetate (OAc^-(aq))[106] will help to understand the effect of fluorination on the hydration and ion association of carboxylate-containing molecules.
DR spectra over the frequency range $0.2 \lesssim \nu/\mathrm{GHz} \leq 50$ were measured using Agilent E8364B VNA combined with the high temperature probe ($0.2 \lesssim \nu/\mathrm{GHz} \leq 20$) and a waveguide-transmission cell ($27 \lesssim \nu/\mathrm{GHz} \leq 40$); high frequency data were obtained using the E-band interferometer (Section 2.2).

3.2.1 Choice of fit model and assignment of relaxation modes

Typical DR spectra obtained for $NaOAcF_3$(aq) at 25 °C as a function of solute concentration are given in Figure 3.21. The maximum in $\varepsilon''(\nu)$ curves shows a clear shift towards lower frequencies with increasing c. Redshift of maximum in $\varepsilon''(\nu)$ curves with increasing c is consistent with DRS studies of NaOAc(aq)[106] and is discussed in Section 3.1.
The combined $\hat{\varepsilon}(\nu)$ data were analyzed using Equation (1.65) according to the procedure described in detail in Section 2.2.3. The spectra of $NaOAcF_3$(aq) were best described by a model consisting of either three (at $c \lesssim 1.12$ M) or two (at $c > 1.12$ M) Debye processes. Typical fits obtained with these D+D+D and D+D models for $NaOAcF_3$(aq) are shown in Figures 3.21 & 3.22. These models were supported also by the bias-free analysis[91] of the spectra shown in Figure 3.23. All fitting parameters obtained from the present spectra are summarized in Table 3.6.

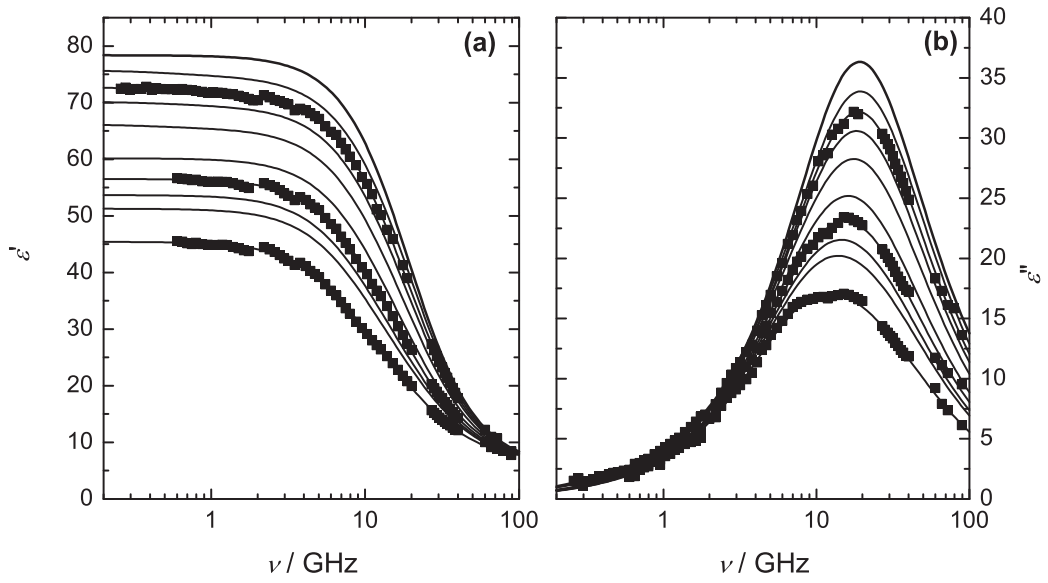

Figure 3.21: Permittivity, $\varepsilon'(\nu)$ (**a**), and dielectric loss, $\varepsilon''(\nu)$ (**b**), spectra for $NaOAcF_3$(aq) at 25 °C and concentrations c/M = 0, 0.2456, 0.4846, 0.7172, 1.120, 1.749, 2.184, 2.522, 2.810, and 3.647 (top to bottom). Symbols show experimental data (partly omitted for visual clarity); lines represent either the D+D+D or D+D fits.

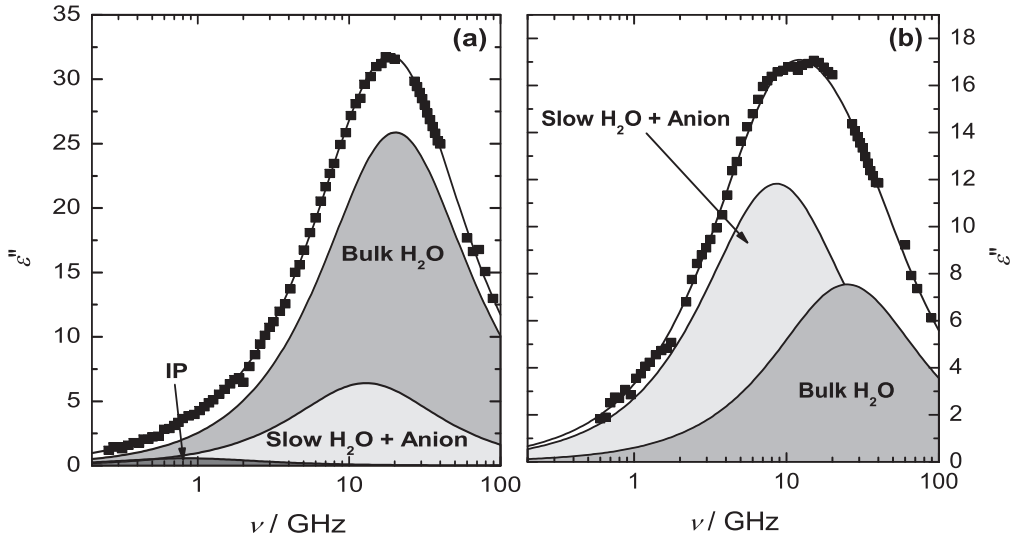

Figure 3.22: Dielectric loss spectrum, $\varepsilon''(\nu)$, of **(a)** 0.5539 M and **(b)** 3.647 M $NaOAcF_3$(aq) at 25 °C. Symbols show experimental data, the lines through the experimental data represent either a D+D+D or a D+D fit, and shaded areas indicate the contributions of different relaxation modes.

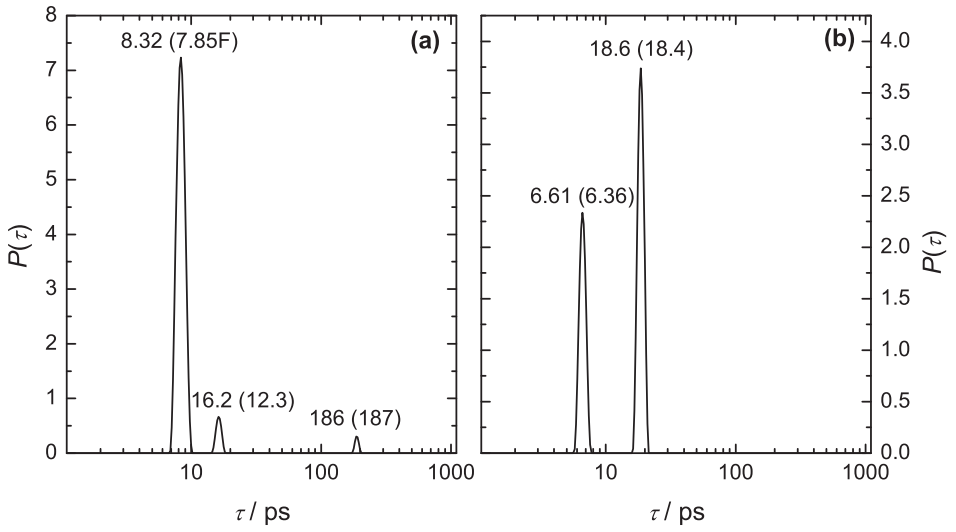

Figure 3.23: Relaxation time distribution function, $P(\tau)$, of **(a)** 0.5539 M and **(b)** 3.647 M $NaOAcF_3$(aq) at 25 °C obtained with the fitting procedure of Zasetzky and Buchner.[91] Relaxation times for the resolved modes are indicated together with the corresponding values from Table 3.6 (in brackets; F = fixed).

Table 3.6: Densities, ρ; Electrical Conductivities, κ; Limiting Permittivities, ε_j; Relaxation Times, τ_j; and Reduced Error Function Values, χ^2_r, for $NaOAcF_3$(aq) at Concentrations, c; and 25 °C [a,b]

c	ρ	κ	ε	τ_1	ε_2	τ_2	ε_3	τ_3	ε_∞	χ^2_r
0.0[c]			78.37					8.32	3.48	
0.09923	1.0049	0.754	77.18	356	76.69	22.0F	73.98	8.02	5.72	0.087
0.1484	1.0088	1.09[d]	76.70	305	75.94	19.3	71.66	7.85F	5.43	0.125
0.1972	1.0127	1.40	76.21	281	75.28	18.0F	70.10	7.82	5.47	0.101
0.2456	1.0165	1.70[d]	75.73	286	74.72	18.0F	68.53	7.81	5.43	0.110
0.4846	1.0354	3.03	72.71	238	71.76	14.5F	60.04	7.70	5.74	0.085
0.5539	1.0404[d]	3.37[d]	71.84	187	70.69	12.3	57.87	7.85F	6.12	0.068
0.7172	1.0534	4.12	70.15	257	69.41	14.6	53.16	7.50F	5.84	0.084
0.8471	1.0634[d]	4.66[d]	68.59	205	67.72	13.3	49.75	7.40F	5.93	0.068
0.9513	1.0712[d]	5.06[d]	67.59	230	66.57	13.2	46.77	7.25F	5.88	0.103
1.120	1.0838	5.64	66.17	344	65.48	14.5	44.15	7.20F	5.87	0.098
1.368	1.1027	6.48	63.67		63.67	14.2	40.73	7.35	6.38	0.106
1.749	1.1321	7.49	60.17		60.17	14.4	34.31	6.98	6.43	0.087
2.184	1.1649	8.18	56.52		56.52	15.4	30.99	6.80	6.42	0.086
2.522	1.1901	8.83	53.67		53.67	15.9	27.91	6.69	6.55	0.083
2.810	1.2117	8.89	51.27		51.27	16.2	24.94	6.31	6.48	0.084
3.647	1.2728	9.18	45.42		45.42	18.4	21.77	6.36	6.68	0.084

[a] Parameter values followed by the letter F were held constant during the fitting procedure. [b] Units: c in M; ρ in kg L^{-1}; κ in $\Omega^{-1}\,m^{-1}$; τ_j in 10^{-12} s. [c] Reference 84. [d] Interpolated using measured values.

The relaxation time, $\tau_3(c) = \tau_b$[168] (Figure 3.24), of the highest frequency mode in DR spectra of $NaOAcF_3$(aq), centered at ~20 GHz (Figure 3.22), smoothly extrapolates to the relaxation time of the dominant mode in pure water that is assigned to the cooperative relaxation of its H-bond network.[110] Therefore, this process can be unequivocally assigned to the relaxation of bulk water, *i.e.* H_2O molecules that, at least at low c, are not significantly influenced by the presence of the solute particles. However, the smooth decrease in τ_b with increasing c (Figure 3.24) indicates that there is **some** influence of the ions on the dynamics of water even beyond their hydration shells and this effect becomes more pronounced with decreasing interionic distance.

The average relaxation time[168] of the intermediate ($j = 2$) process, $\tau_2 = \tau_{comp} \approx 16$ ps (Figure 3.24), is almost twice that of the bulk water mode ($\tau_b \approx 8$ ps). As discussed in detail by Rahman et al.[106] for formate and acetate (see Section 3.1), this is a composite mode that can be assigned to the presence of slow water molecules hydrating the trifluoroacetate anion and the reorientation of $OAcF_3^-$ itself as the latter possesses a permanent dipole moment ($\mu_- = 3.93$ D according to MOPAC calculations[100]).

The slowest ($j = 1$) process centered at ~0.6 GHz, for $NaOAcF_3$(aq) detectable at $c \lesssim 1.12$ M (Figure 3.22), is consistent, from its location and amplitude, with the presence of

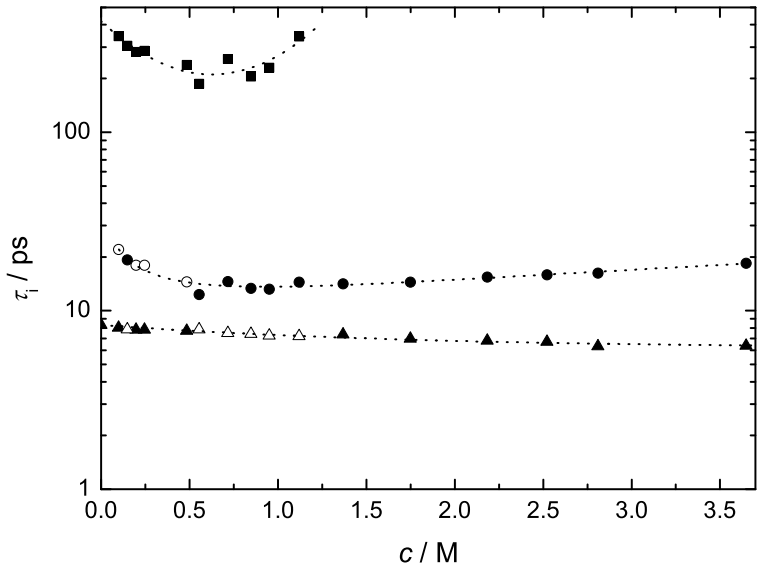

Figure 3.24: Concentration dependence of the solute relaxation time, τ_1 (■), the composite mode relaxation time, τ_{comp} (●), and the bulk-water relaxation time, τ_{b} (▲), of $NaOAcF_3$(aq) at 25 °C. Symbols show experimental data with open symbols representing values held constant during the fitting procedure; dotted lines are included only as a visual aid.

small amounts of ion pairs. A similar low-amplitude Debye relaxation at the same location was also observed for aqueous NaOAc solutions at $c \lesssim 1$ M[106] (Section 3.1), where this was assigned to ion-pair relaxation.
Interestingly, the present spectra, limited to $\nu \leq 89$ GHz, did not produce any evidence for the very fast water process centred at ∼400 GHz[110] which is sometimes[112,113] but not always[106,115] detected in aqueous electrolyte solutions. Nevertheless, the fitted values of $\varepsilon_\infty \approx$ 5-7 (Table 3.6) are considerably larger than the $\varepsilon_\infty = 3.48$ obtained for pure water,[84,110] which suggests that the fast water process is still making a minor, if unresolvable, contribution to the present spectra.

3.2.2 Water relaxations and ion hydration

As shown previously,[112] the bulk and fast relaxations for water (at ∼20 GHz and ∼400 GHz respectively) can be treated collectively by assuming: $S_{\text{b}} = \varepsilon_3(c) - \varepsilon_\infty$, where S_{b} is the amplitude of bulk-water relaxation. For these calculations the value of ε_∞ was taken to be that obtained from ultrahigh-frequency dielectric measurements (including THz data[84]) of pure water, rather than the less accurate values derived from fitting the present spectra at $\nu \leq 89$ GHz (Table 3.6). As can be seen the magnitude of S_{b} for $NaOAcF_3$ decreases

significantly with increasing c (Figure 3.25). The S_b values for $NaOAcF_3$(aq) were used to estimate c_b^{ap} with Cavell equation (Eq. 1.71), as described in Section 3.1.2.
As discussed above, the intermediate ($j = 2$) relaxation of $NaOAcF_3$(aq) is a composite mode. Its amplitude, $S_{comp} = S_2 = \varepsilon_2(c) - \varepsilon_3(c)$, which initially increases strongly with increasing c but then passes through a maximum value of ~22 at ~1.75 M (Figure 3.25), can be split into its constituent relaxation amplitudes (Eq. 3.4). Since ion pairing is weak for the present system, the magnitude of S_- for $OAcF_3^-$ can be obtained from Eq. 1.71 with the effective anion dipole moment, $\mu_-^{eff} = \mu_-/(1 - f_-\alpha_-)$, of 5.34 D for $OAcF_3^-$ from MOPAC calculations.[100] This yields the amplitude of slow water, S_s, via Eq. 3.4 and subsequently the apparent concentration of slow water, $c_s^{ap}(c)$, via Eq. 1.71.

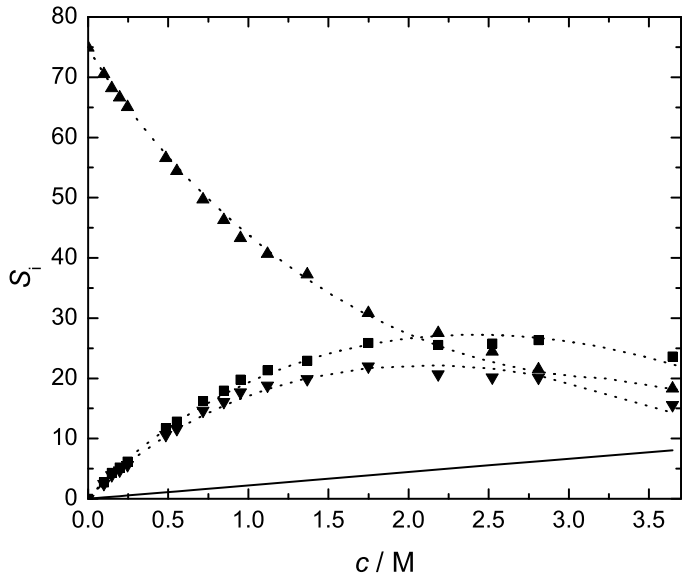

Figure 3.25: Concentration dependence of the relaxation amplitudes of bulk water, S_b (▲), the composite mode, $S_s + S_-$ (■), and slow water, S_s (▼) for $NaOAcF_3$(aq) at 25 °C. The solid line represents S_-, calculated via Eq. 1.71; the dotted lines are included only as a visual guide.

For the present system, the sum of DRS-detected water, $c_b^{ap} + c_s^{ap}$, is less than the analytical (total) water concentration, c_w. Water missing from the DR spectrum can be ascribed to the presence of ib water molecules and an effective hydration number, Z_{ib}, can then be determined via Eq. 3.6, whereas the values of $c_s^{ap}(c)$, obtained from S_s with Eq. 1.71, can be used directly to calculate the effective number of *slow* water molecules, Z_s, via Eq. 3.7. The Z_{ib} values calculated in this way for $NaOAcF_3$(aq) at 25 °C (Figure 3.26) were corrected for $Z_{ib}(Na^+)$ to yield the effective number of H_2O molecules "frozen" by the anion, $Z_{ib}(OAcF_3^-)$. For correction, recently determined more precise $Z_{ib}(Na^+)$[169] values were

used. The Z_{ib} values so obtained for $OAcF_3^-$ are also shown in Figure 3.26. Over the entire concentration range $OAcF_3^-$(aq) binds ∼1-2 water molecules strongly. The good agreement of $Z_{ib}(OAcF_3^-)$ and $Z_{ib}(OAc^-)$ (and $Z_{ib}(OFm^-)$) supports the previous assignment[106] (Section 3.1) of this quantity to water strongly bound by the carboxylate moiety.

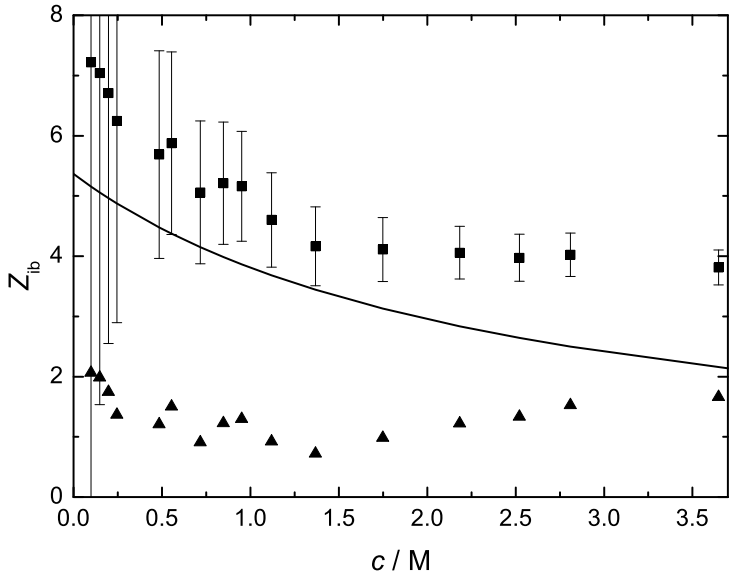

Figure 3.26: Concentration dependence of effective hydration numbers, Z_{ib}, for $NaOAcF_3$(aq) (■), and $OAcF_3^-$(aq) (▲) at 25 °C;[132] the solid line represents $Z_{ib}(Na^+)$.[169]

The effective number of *slow* water molecules, Z_s, calculated for $NaOAcF_3$(aq) with Eq. 3.7 is shown in Figure 3.27. Since aqueous solutions of typical inorganic salts containing sodium ions do not show any slow-water process[45,131,133] it is reasonable to assign Z_s for $NaOAcF_3$(aq) entirely to the $OAcF_3^-$(aq) ion. This is again similar to the situation for NaOFm(aq) and NaOAc(aq)[106] (Section 3.1). However, at low concentrations the Z_s values of the three anions differ considerably, with ∼20 water molecules weakly bound by $OAcF_3^-$ at infinite dilution, whereas OAc^- and OFm^- bind here ∼11 and ∼5 water molecules respectively (Figure 3.27). On the other hand, the Z_s values of all three electrolytes are essentially equal at $c > 3$ M.

Recent DRS studies[106] have shown that the high-concentration limit of Z_s for acetate is due to hydrophilic interactions of the $-COO^-$ group with ∼4-5 water molecules (Figure 3.27). With the additional 1-2 "frozen" H_2O, the carboxylate group is thus hydrated by ∼6 water molecules in total. The fractions of weakly and strongly interacting water molecules may vary slightly with concentration, as possibly indicated by $Z_{ib}(-COO^-, c)$ (Figure 3.26), but the total hydration number of this moiety remains essentially constant, $Z_t(-COO^-) = Z_s(-COO^-) + Z_{ib}(-COO^-) \approx 5-6$ (Section 3.1). The present data for $NaOAcF_3$(aq) fully

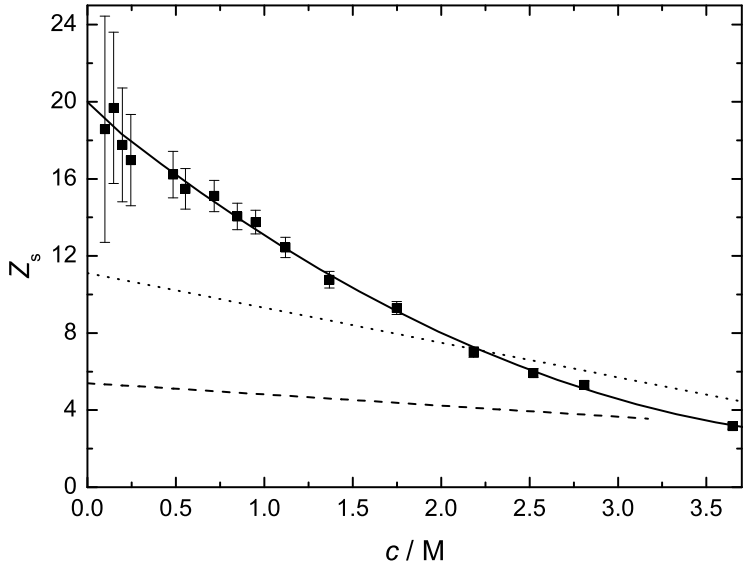

Figure 3.27: Concentration dependence of the slow-water hydration number, $Z_s(OAcF_3^-)$ (■), of trifluoroacetate anion in aqueous solutions of $NaOAcF_3$ at 25 °C.[132] The dotted and dashed lines represent $Z_s(OAc^-)(aq)$ and $Z_s(OFm^-)(aq)$,[106] respectively .

corroborate this picture.

The remaining slow water, $Z_s(-R) = Z_s - Z_s(-COO^-)$, is reasonably assigned to water molecules close to hydrophobic moiety of the anion.[106,112,139–141] The "hydrophobic" hydration number for $-CF_3$ at $c \to 0$, $Z_s(-CF_3) \approx 15$, is considerably larger than that for $-CH_3$, $Z_s(-CH_3) \approx 6$. This is consistent with the significantly larger van der Waals volume of a $-CF_3$ group, 35.4 Å^3, as compared to the value of 22.7 Å^3 for $-CH_3$.[170] However, for trifluoroacetate Z_s, and hence $Z_s(-CF_3)$, decreases much more rapidly than does Z_s for acetate (Figure 3.27). This suggests that the hydration shell of the $-CF_3$ unit is apparently even more "fragile", *i.e.*, rapidly breaks down with increasing c, than that of the methyl group. It may be speculated that this breakdown might be accompanied by some sort of aggregation of the hydrophobic $-CF_3$ groups, although the present spectra provide no direct evidence for this.

3.2.3 Ion association

Figure 3.28 shows the amplitudes, S_1, of the lowest-frequency processes of $NaOAcF_3(aq)$ and NaOAc(aq) for comparison, which are very similar to each other but also to the amplitude of a comparable mode detected for NaCl(aq).[169] In a previous publication[106] (and also in Section 3.1) this solute mode for NaOAc(aq) was assigned solely to IP reorientation as

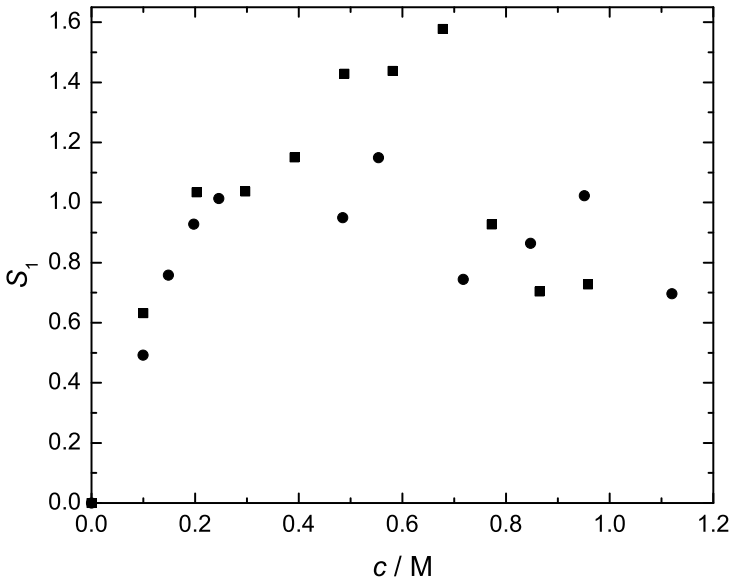

Figure 3.28: Concentration dependence of the solute amplitudes, S_1, of $NaOAcF_3$(aq) (●) and NaOAc(aq) (■) at 25 °C.

the presence of very weak ion pairing between Na^+(aq) and $-COO^-$(aq) is consistent with thermodynamic data,[106] recent conductivity measurements[118] and MD simulations.[20,22] Since recent investigations[169,171] have shown that ion-cloud relaxation, a generic feature of **all** electrolyte systems, is strong enough to notably contribute to the low-frequency mode of NaCl(aq), we have to assume that this effect is also relevant for $NaOAcF_3$(aq) and NaOAc(aq). However, ion-cloud relaxation cannot be the sole origin of the solute mode as its relaxation time should decrease strongly and monotonically with increasing concentration.[169,171] This is neither the case for $NaOAcF_3$(aq) (Figure 3.24, Table 3.6) nor for NaOAc(aq) (Table 3.3). Thus, ion pairs must also contribute to the observed solute relaxation as their relaxation time is expected to be roughly constant or slightly increasing.[11] Since only a single solute mode was observed it is also plausible that, besides predominating free ions, only one ion-pair species is present in a significant amount.

Unfortunately, independent estimation of the magnitude of ion-cloud relaxation is not possible. Hence, the subsequent analysis of $S_1 = S_{IP} = \varepsilon(c) - \varepsilon_2(c)$ was performed under the assumption that this amplitude is only due to ion-pair relaxation. As a consequence, the ion-pair concentrations, c_{IP}, calculated with Eq. 1.71, and thus the associated standard-state association constants, K_A°, derived from Eq. 1.90 with the help of the Guggenheim-type equation (Eq. 1.91) are an **upper limit** for the degree of ion pairing in $NaOAcF_3$(aq). No independent information on the nature of the ion pairs is available. Thus, S_1 was evaluated assuming that the solute relaxation arises either from CIPs, SIPs, or 2SIPs.

The polarizabilities of the different IP types required as input for Eq. 1.71 were calculated as $\alpha_{IP} = \alpha_+ + \alpha_- + n\alpha(H_2O)$, where n is the number of water molecules separating the charges in the IP structure ($n = 0$ for CIPs; $n = 1$ for SIPs; and $n = 2$ for 2SIPs), with $\alpha/(4\pi\varepsilon_0\,\text{Å}^3) = 0.211$ (Na^+),[66] 6.130 ($OAcF_3^-$),[100] and 1.444 (H_2O).[66] The dipole moments of the various ion-pair types, μ_{IP}, calculated with MOPAC[100] are listed in Table 3.7. To cross-check the results, μ_{IP} was also calculated using the procedure described by Barthel et al.[66] The results, $\mu_{CIP} = 12.2\,D$, $\mu_{SIP} = 26.7\,D$, and $\mu_{2SIP} = 39.1\,D$ for $NaOAcF_3$(aq) were generally in good agreement with MOPAC-calculated moments. From the calculated ion-pair concentrations for the CIP, SIP and 2SIP assumptions, the standard state association constants, K_A°, of Table 3.7 were derived with Eq. 1.91, together with the corresponding B_K and C_K values. Figure 3.29 shows the $K_A(I)$ values obtained with the 2SIP evaluation for $NaOAcF_3$(aq), as well as the corresponding Guggenheim fits.

Table 3.7: Ion-Pair Dipole Moments, μ_{IP}, and Resulting Parameters log K_A°, B_K, and C_K of Eq. 1.91 for the Tested Ion-Pair Models of $NaOAcF_3$(aq).[a]

Model	μ_{IP}	log K_A°	B_K	C_K
CIP	10.8	1.78±0.10	-5.35±0.69	2.96±0.62
SIP	25.6	0.58±0.07	-4.02±0.50	2.10±0.45
2SIP	37.7	0.22±0.07	-3.90±0.48	2.02±0.43

[a] Units: μ_{IP} in Debye ($1\,D = 3.3356 \times 10^{-30}$ C·m.), B_K in $L\cdot mol^{-1}$, C_K in $L^{3/2}\cdot mol^{-3/2}$.

Similar to NaOAc(aq), no independently determined K_A° value is available that would allow to infer whether CIP, SIP or 2SIP is the predomination ion-pair species in $NaOAcF_3$(aq). However, the formation of CIPs can be neglected because calculation assuming CIP model gave a value of $K_A^\circ = 60\,M^{-1}$ (Table 3.7), which is too high in light of discussion already made for NaOAc(aq) (Section 3.1). To help to establish which IP types are present in aqueous solution of $NaOAcF_3$, it was useful to compare the experimental τ'_{IP} with estimated τ', calculated according to the procedure described in detail in previous section for NaOAc(aq). Present DRS data also definitely rule out CIPs for $NaOAcF_3$(aq) because the estimated rotational correlation time, τ', is far too short compared to the experimental value, τ'_{IP} (Table 3.8).

According to the data of Table 3.8 the 2SIP is the most probable type of ion pair present in $NaOAcF_3$(aq). This assignment is supported by the strong hydration of Na^+ and of the carboxylate group, see Section 3.2.2, and is in line with the assignment of 2SIP to ion-pair relaxation process in NaOAc(aq) (Section 3.1). Accordingly, keeping in mind the likely contribution of ion-cloud relaxation to the solute amplitude, we can give upper limit of $K_A^\circ(NaOAcF_3) = 1.7\,M^{-1}$ for the association constant of aqueous sodium trifluoroacetate and postulate 2SIPs as the dominating ion-pair species at $c < 1\,M$.

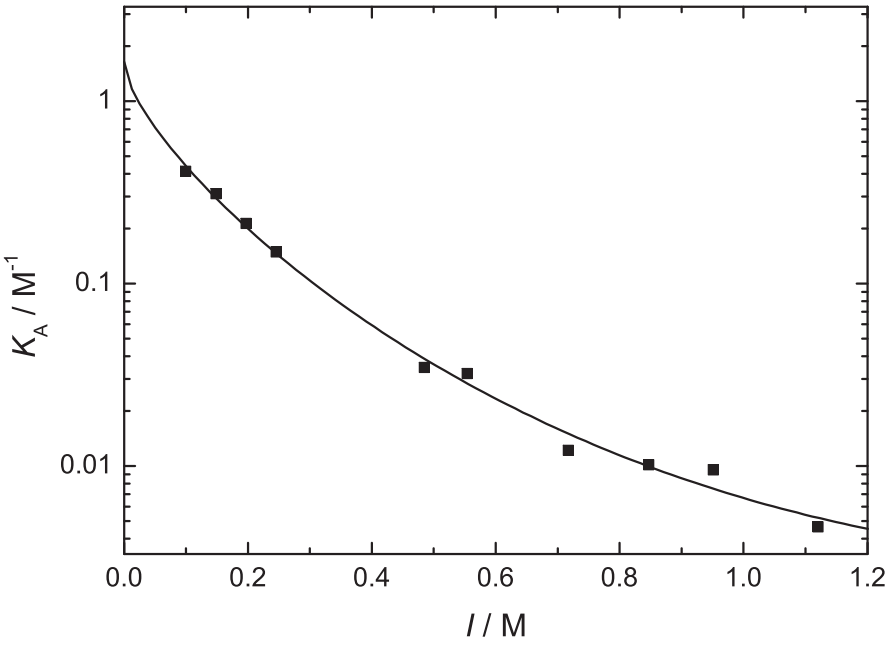

Figure 3.29: Ion association constant, K_A, for $NaOAcF_3$(aq) as a function of nominal ionic strength, I, at 25 °C. The K_A value was calculated from the solute relaxation amplitude, S_1, under the assumption that 2SIPs predominate. Also included (line) is the fit of K_A with Eq. 1.91.

Table 3.8: Comparison of Experimental, τ'_{IP},[a] and Calculated, τ'_{slip} and τ'_{stick},[b] Rotational Correlation Times for *Stick* and *Slip* Boundary Conditions for Ion-Pair Reorientation in Aqueous Solutions of $NaOAcF_3$(aq) at 25 °C.[c]

electrolyte	τ'_{IP}	IP	τ'_{slip}	τ'_{stick}
		CIP	19.0	84.0
$NaOAcF_3$	184	SIP	54.5	150
		2SIP	114	244

[a] Obtained via Powles-Glarum relation (Eq. 1.85). [b] Averaged values obtained from SED relation (Eq. 1.80). [c] Unit: τ_i in ps.

Chapter 4

Amphiphilic Carboxylates

4.1 Aqueous solutions of sodium propanoate, butanoate and pentanoate

The important constituents of biomolecules often experience mixed type of hydration, *i.e.*, hydrophobic hydration of the alkyl chains combined with electrophilic/hydrophilic hydration of the charged groups or the electron pair donor/acceptor atoms.[39–41] The cooperative effects of both types of hydration determine the overall interaction of the molecule with the surrounding aqueous medium.[40]

Propanoate ($C_2H_5COO^-$, OPr^-), butanoate (n-$C_3H_7COO^-$, OBu^-) and pentanoate (n-$C_4H_9COO^-$, OPe^-) ions possess a hydrophobic alkyl moiety attached to a hydrophilic anionic charge centre ($-COO^-$). As the carboxylate group ($-COO^-$) is one of the most important charge centres controlling the hydrophilicity of biomolecules , OPr^-(aq), OBu^-(aq) and OPe^-(aq) can be studied as model compounds of systematically increasing hydrophobicity. Study of these amphiphlilic anions by DRS help in understanding the interplay of hydrophilic and hydrophobic hydration. The counter-ion (Na^+) is also a biologically relevant cation (specific concentration of Na^+ in the cytosol is vital for proper function of cell).[16] Investigating the interaction of Na^+ with $-COO^-$ can help in understanding the consequences of direct ion-biomolecule interactions.

In order to obtain detailed information about alkylcarboxylate hydration and the interaction of Na^+ with $-COO^-$, DR spectra have been measured at 25 °C for aqueous solutions of NaOPr, NaOBu and NaOPe over a wide range of frequencies ($\sim$0.2 GHz to 89 GHz) up to high solute concentrations c / M = 3.241, 3.094, and 2.345 respectively. For NaOPr(aq), DR spectra over the frequency range $0.2 \lesssim \nu/\mathrm{GHz} \leq 20$ were measured using the HP8720D VNA setup at Murdoch University and high frequency data were measured with A & E-band interferometers. For NaOBu(aq) and NaOPe(aq) the E8364B VNA ($0.2 \lesssim \nu/\mathrm{GHz} \leq 50$)* and the E-band interferometer ($60 \lesssim \nu/\mathrm{GHz} \leq 89$) were used

*Dielectric spectra for NaOBu(aq) were recorded with two reflection probes, covering $0.2 \leq \nu/\mathrm{GHz} \leq 20$ (high-temperature probe) and $1 \leq \nu/\mathrm{GHz} \leq 50$ (performance probe) respectively, that were connected to an Agilent E8364B VNA. For NaOPe(aq), instead of the performance probe, the variable-path-length waveguide transmission cell of former A-band (26-40 GHz) interferometer was combined with a E8364B

(Section 2.2).

4.1.1 Choice of fit model

For the formal description of the spectra, various models based on the sum of n individual relaxation processes were tested, according to the procedure described in Section 2.2.3, using a nonlinear least-squares routine that simultaneously fitted the in-phase ($\varepsilon'(\nu)$, Figures 4.1a, 4.2a, & 4.3a) and out-of-phase ($\varepsilon''(\nu)$, Figures 4.1b, 4.2b, & 4.3b) components. All plausible (HN, CD, CC and D) models for various processes were investigated. After extensive testing of alternatives it was found that a sum of three Debye modes ($n = 3$; a D+D+D model) provided the best fit for the spectra of all studied concentrations of NaOPr(aq), NaOBu(aq) and NaOPe(aq). Typical fits obtained with this D+D+D model are shown in Figures 4.1 to 4.6. All fitting parameters are summarized in Tables 4.1, 4.2, and 4.3.
Additionally, selected spectra were analyzed with a recently published procedure[91] that allows an unbiased determination of the number of relaxation processes required for formal description of $\hat{\varepsilon}(\nu)$. Typical results from these analyses are shown in Figures 4.7 to 4.9. These results, for NaOPr(aq) and NaOBu(aq) at $c \gtrsim 1\,\mathrm{M}$ and for NaOPe(aq) at all c, are consistent with those obtained from our standard fitting procedure (Section 2.2.3). However for NaOPr(aq) and NaOBu(aq) at $c \lesssim 1\,\mathrm{M}$ the Buchner-Zasetzky analysis indicates there are two modes at lower frequencies (Figures 4.7a & 4.8a) whereas the standard fitting procedure resolves only one relaxation mode at $\nu < 8\,\mathrm{GHz}$ (Figures 4.4a & 4.5a). This apparent difference will be discussed in Section 4.1.2 below.

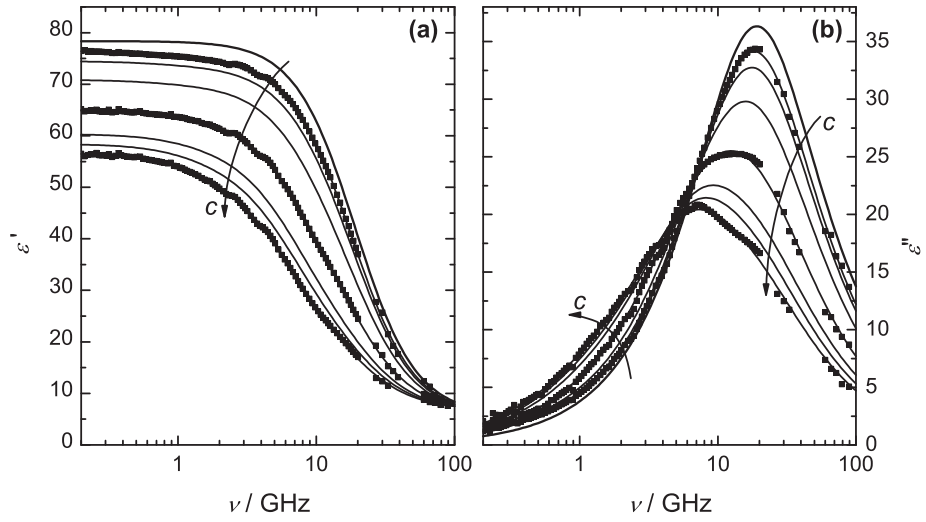

Figure 4.1: Dielectric permittivity (**a**) and loss (**b**) spectra for NaOPr(aq) at 25 °C. Arrows indicate increasing concentrations: c / M = 0, 0.2978, 0.4862, 0.9452, 1.792, 2.548, 2.906, and 3.241. Symbols are experimental data (partly omitted for visual clarity); lines represent the D+D+D fit.

VNA (Section 2.2).

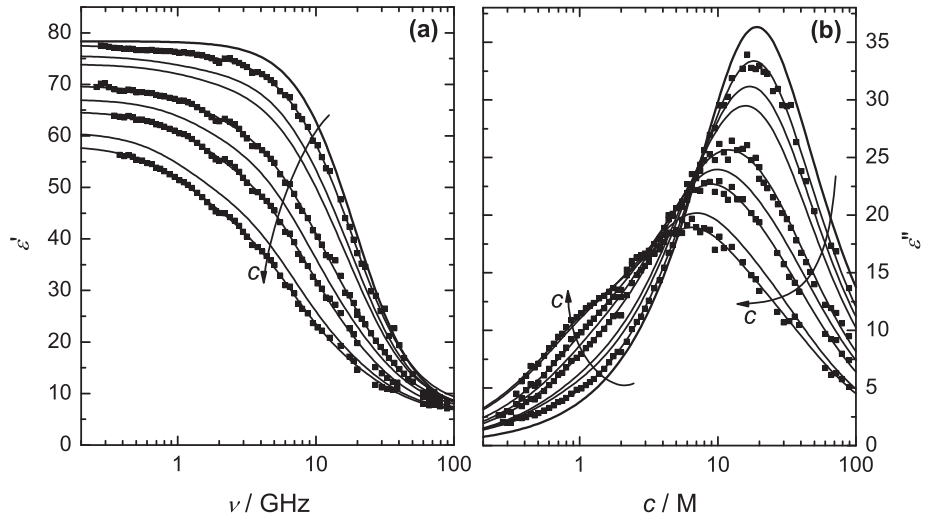

Figure 4.2: Dielectric permittivity (**a**) and loss (**b**) spectra for NaOBu(aq) at 25 °C. Arrows indicate increasing concentrations: c / M = 0, 0.1962, 0.4867, 0.7080, 1.349, 1.729, 2.104, 2.770, and 3.094. Symbols are experimental data (partly omitted for visual clarity); lines represent the D+D+D fit.

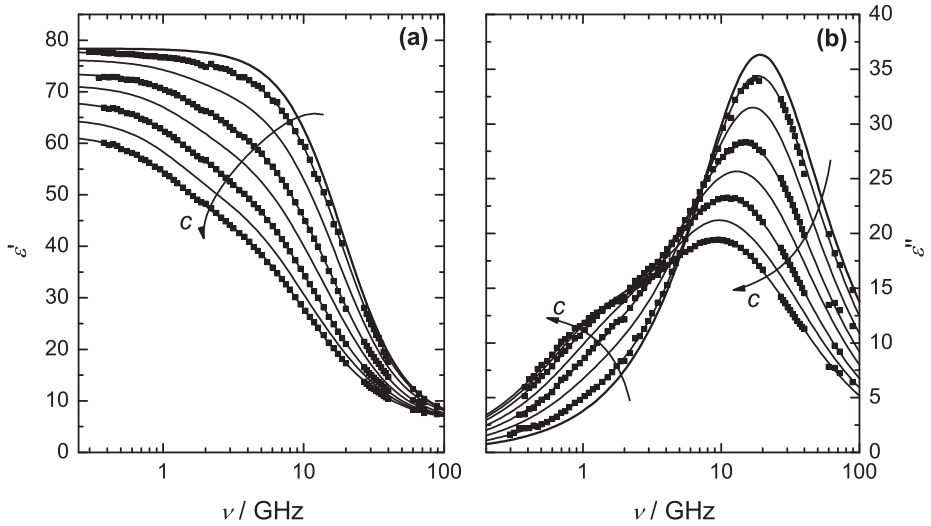

Figure 4.3: Dielectric permittivity (**a**) and loss (**b**) spectra for NaOPe(aq) at 25 °C. Arrows indicate increasing concentrations: c / M = 0, 0.1504, 0.4811, 0.9182, 1.278, 1.696, 2.045, and 2.345. Symbols are experimental data (partly omitted for visual clarity); lines represent the D+D+D fit.

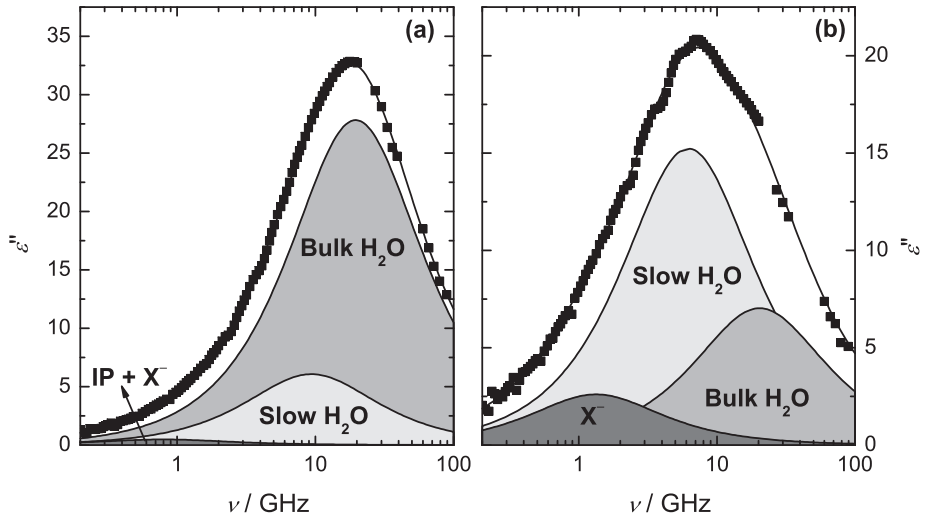

Figure 4.4: Dielectric loss curve of (**a**) 0.4862 M and (**b**) 3.241 M NaOPr(aq) at 25 °C, showing contributions of the three Debye processes. Symbols represent experimental data, lines through the experimental data represent the D+D+D fit, and shaded areas indicate the contributions of different relaxation modes.

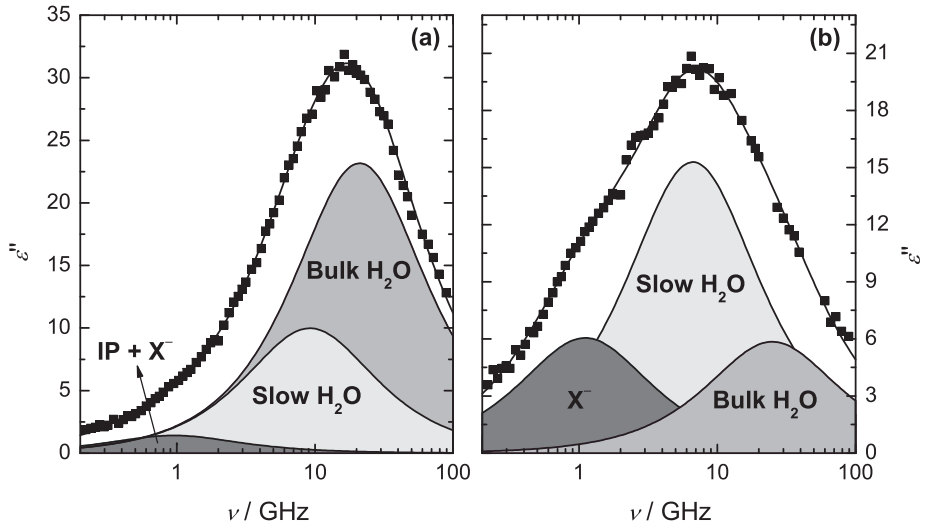

Figure 4.5: Dielectric loss curve of (**a**) 0.4867 M and (**b**) 2.770 M NaOBu(aq) at 25 °C, showing contributions of the three Debye processes. Symbols represent experimental data, lines through the experimental data represent the D+D+D fit, and shaded areas indicate the contributions of different relaxation modes.

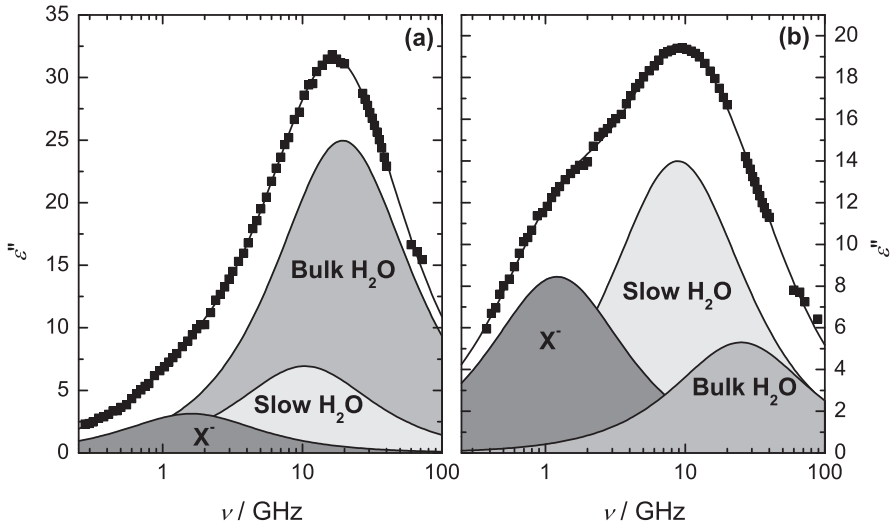

Figure 4.6: Dielectric loss curve of (**a**) 0.4811 M and (**b**) 2.345 M NaOPe(aq) at 25 °C, showing contributions of the three Debye processes. Symbols represent experimental data, lines through the experimental data represent the D+D+D fit, and shaded areas indicate the contributions of different relaxation modes.

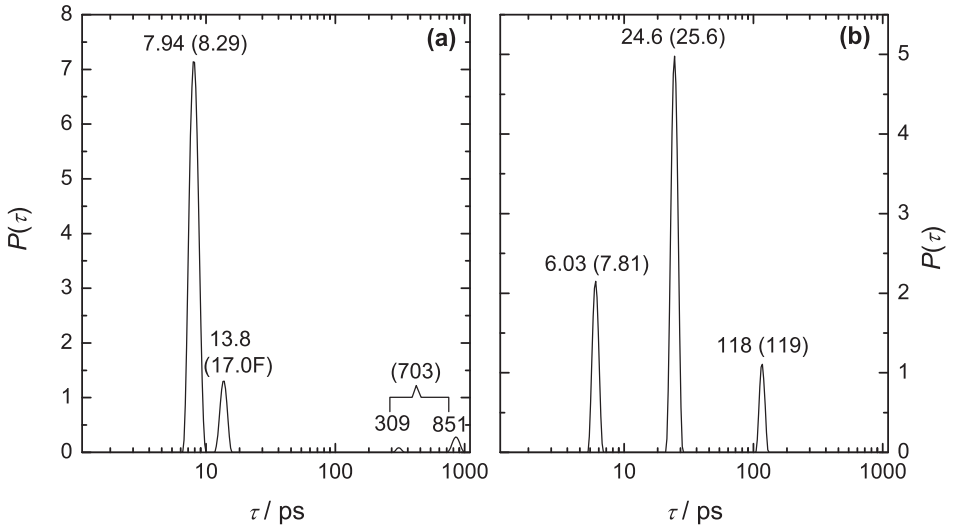

Figure 4.7: Relaxation time distribution function, $P(\tau)$, of (**a**) 0.1496 and (**b**) 3.241 M NaOPr(aq) at 25 °C obtained with the bias-free fitting procedure of Zasetzky and Buchner.[91] Relaxation times for the resolved modes are indicated together with the corresponding experimental values from Table 4.1 (in brackets; F = fixed).

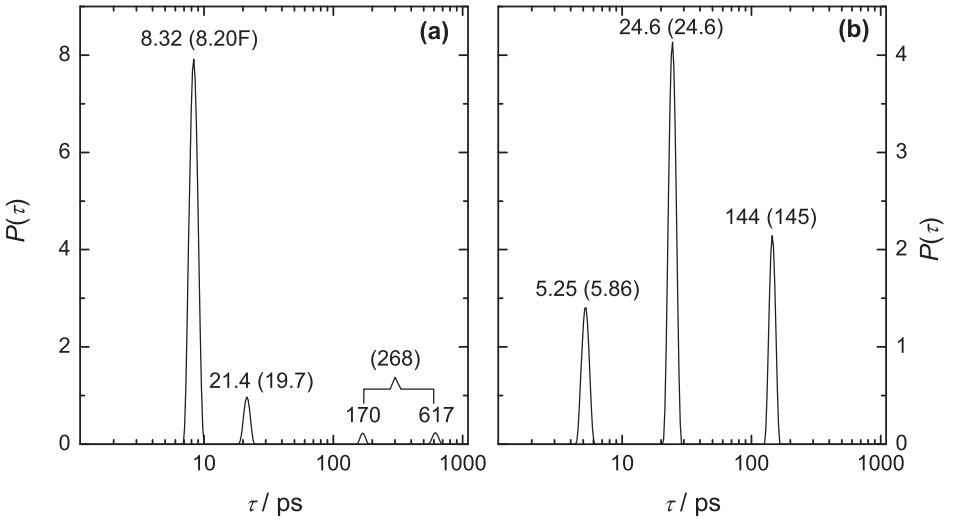

Figure 4.8: Relaxation time distribution function, $P(\tau)$, of **(a)** 0.1962 and **(b)** 3.094 M NaOBu(aq) at 25 °C obtained with the bias-free fitting procedure of Zasetzky and Buchner.[91] Relaxation times for the resolved modes are indicated together with the corresponding experimental values from Table 4.2 (in brackets; F = fixed).

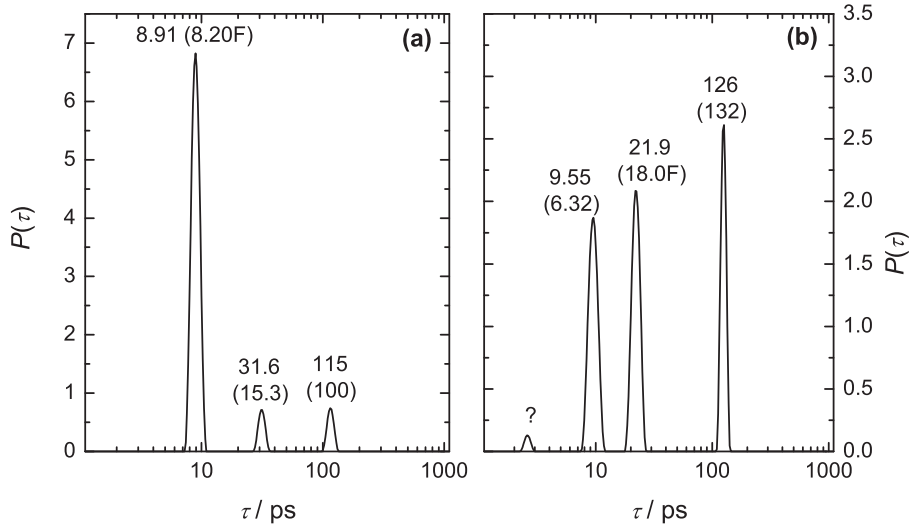

Figure 4.9: Relaxation time distribution function, $P(\tau)$, of **(a)** 0.4811 and **(b)** 2.345 M NaOPen(aq) at 25 °C obtained with the bias-free fitting procedure of Zasetzky and Buchner.[91] Relaxation times for the resolved modes are indicated together with the corresponding experimental values from Table 4.3 (in brackets; F = fixed).

Table 4.1: Densities, ρ; Electrical Conductivities, κ; Limiting Permittivities, ε_j; Relaxation Times, τ_j; and Reduced Error Function Values, χ^2_r, for NaOPr(aq) at Concentrations, c; and 25 °C [a]

c	ρ	κ	ε	τ_1	ε_2	τ_2 [b]	ε_3	τ_3 [b]	ε_∞	χ^2_r
0[c]			78.37					8.32	3.48	0.048
0.07956	1.0005	0.568	79.06	832	77.44	16.2	74.85	8.28	5.50	0.064
0.09920	1.0014	0.694	78.97	749	77.26	16.2	73.87	8.28F	5.66	0.013
0.1496	1.0034	0.997	78.88	703	76.77	17.0F	72.36	8.29	5.72	0.048
0.1973	1.0053	1.28	78.01	535	76.27	17.0	70.44	8.25F	5.77	0.017
0.2459[d]	1.0073	1.55	77.07	356	75.78	16.6	69.38	8.24F	5.57	0.012
0.2978	1.0096	1.84	76.58	301	75.31	17.2	69.22	8.38	5.84	0.041
0.4862	1.0172	2.68	74.47	200	73.51	17.0	61.37	8.13	5.73	0.062
0.9452	1.0356	4.26	70.87	212	69.85	17.9	48.36	7.89	5.98	0.050
1.380[d]	1.0527	5.24	67.71	209	66.56	20.1	41.92	7.94F	6.18	0.051
1.792	1.0685	5.87	64.96	165	63.40	21.2	35.54	7.96	6.46	0.064
2.184[d]	1.0835	6.22	62.60	157	60.48	22.7	30.59	7.70F	6.13	0.058
2.548	1.0967	6.34	60.33	124	57.14	23.2	25.71	7.53	6.54	0.059
2.906	1.1096	6.23	58.40	121	54.26	24.5	23.21	7.74	6.72	0.064
3.241	1.1216	6.21	56.59	119	51.39	25.6	20.92	7.81	6.87	0.066

[a] Units: c in M; ρ in kg L^{-1}; κ in Ω^{-1} m^{-1}; τ_j in 10^{-12} s. [b] Parameter values followed by the letter F were held constant (fixed) during the fitting procedure. [c] Reference 84. [d] VNA (0.2-20 GHz) data only.

Table 4.2: Densities, ρ; Electrical Conductivities, κ; Limiting Permittivities, ε_j; Relaxation Times, τ_j; and Reduced Error Function Values, χ^2_r, for NaOBu(aq) at Concentrations, c; and 25 °C [a]

c	ρ	κ	ε	τ_1	ε_2	τ_2	ε_3	τ_3 [b]	ε_∞	χ^2_r
0 [c]			78.37					8.32	3.48	0.048
0.02299	0.9980	0.172	79.01	1153	77.84	25.2	76.58	8.32F	6.46	0.111
0.04043	0.9986	0.302	78.84	845	77.63	24.4	75.78	8.32F	6.52	0.159
0.05948	0.9994	0.380	78.71	640	77.45	22.4	74.68	8.32F	6.82	0.208
0.08271	1.0003	0.564	78.90	644	77.24	25.0	74.18	8.32F	7.20	0.259
0.1032	1.0012	0.655	78.52	490	76.99	22.3	72.84	8.32F	7.08	0.302
0.1549	1.0032	0.976	78.04	326	76.37	20.2	70.46	8.32F	7.04	0.297
0.1962	1.0049	1.23	77.67	268	75.89	19.7	68.16	8.20F	7.13	0.321
0.2632	1.0075	1.60	77.27	249	75.23	19.2	64.39	8.00F	6.70	0.228
0.4867	1.0164	2.57	75.57	167	72.75	17.3	52.78	7.56	6.45	0.218
0.7080	1.0250	3.35	73.94	140	70.43	18.3	47.59	7.56	6.81	0.229
0.9368	1.0338	3.97	72.47	134	67.91	17.8	38.13	6.90	6.58	0.206
1.349	1.0493	4.62	69.74	121	63.32	18.7	30.94	6.76	7.01	0.209
1.729	1.0634	5.04	67.11	113	58.89	19.1	23.49	5.76	6.56	0.207
2.104	1.0768	5.20	64.75	116	54.49	20.0	20.39	5.90F	6.24	0.178
2.447	1.0884	5.22	62.69	130	51.69	22.4	19.44	5.98	6.12	0.144
2.770	1.0988	5.17	60.71	143	48.61	23.9	18.03	6.37	6.33	0.162
3.094	1.1085	5.04	58.07	145	45.12	24.6	15.99	5.86	6.09	0.174

[a] Units: c in M; ρ in $\mathrm{kg\,L^{-1}}$; κ in $\Omega^{-1}\,\mathrm{m}^{-1}$; τ_j in 10^{-12} s. [b] Parameter values followed by the letter F were held constant (fixed) during the fitting procedure. [c] Reference 84.

Table 4.3: Densities, ρ; Electrical Conductivities, κ; Limiting Permittivities, ε_j; Relaxation Times, τ_j; and Reduced Error Function Values, χ^2_r, for NaOPe(aq) at Concentrations, c; and 25 °C [a]

c	ρ	κ	ε	τ_1	ε_2	τ_2 [b]	ε_3	τ_3 [b]	ε_∞	χ^2_r
0[c]			78.37					8.32	3.48	0.048
0.02069	0.9979	0.154	78.08	139	77.54	20.2	76.34	8.17	5.70	0.093
0.04007	0.9986	0.280	78.01	125	77.38	18.3	75.32	8.13	5.72	0.076
0.05949	0.9994	0.398	78.05	178	77.26	17.5F	72.28	7.89	5.37	0.046
0.07986	1.0002	0.527	78.01	149	76.78	17.5F	72.45	8.04	5.63	0.068
0.09702	1.0008	0.616	77.96	141	76.50	17.5F	71.51	8.01	5.54	0.065
0.1504	1.0029	0.934	77.72	113	75.26	14.6	69.69	8.25F	6.10	0.084
0.1953	1.0045	1.13	77.58	116	75.02	17.5F	67.84	8.01	5.64	0.042
0.2450	1.0065	1.38	77.26	110	74.26	17.5F	65.36	8.00	6.10	0.100
0.4811	1.0154	2.36	76.25	99.7	69.97	15.3	56.10	8.20F	6.19	0.037
0.7001	1.0236	3.06	74.75	98.0	67.19	17.5F	50.30	8.04	5.95	0.066
0.9182	1.0316	3.57	73.61	103	64.13	17.5F	43.57	7.98	6.00	0.060
1.278	1.0445	4.18	71.31	109	59.03	17.5F	33.04	7.52	5.90	0.033
1.696	1.0587	4.60	68.17	118	53.21	17.3	23.57	6.89	5.96	0.016
2.045	1.0694	4.82	64.84	125	48.83	18.2	19.95	6.52	6.01	0.019
2.345	1.0777	4.97	61.64	132	44.75	18.0F	16.77	6.32	6.17	0.028

[a] Units: c in M; ρ in $\mathrm{kg\,L^{-1}}$; κ in $\Omega^{-1}\,\mathrm{m}^{-1}$; τ_j in 10^{-12} s. [b] Parameter values followed by the letter F were held constant (fixed) during the fitting procedure. [c] Reference 84.

4.1.2 Relaxation modes and relaxation times

The DR spectra obtained for NaOPr(aq), NaOBu(aq) and NaOPe(aq) as a function of solute concentration (Figures 4.1 to 4.3) are at first glance broadly similar with each other but in fact show significant differences. For example, the $\varepsilon''(\nu)$ curves for NaOBu(aq) and NaOPe(aq) show a great decrease of the dominant peak centered at ∼18 GHz and a much greater increase at frequencies around ∼1 GHz with increasing solute concentration than NaOPr(aq). All spectra are well described by a three-Debye-process (D+D+D) model. For the present spectra these modes are centered at approximately 1, 8 and 20 GHz (Figures 4.4 to 4.6). It should be kept in mind, however, that a good fit of $\hat{\varepsilon}(\nu)$ with a model based on Eq. 1.65, or any other band-shape model for that matter, does not guarantee that the chosen model is physically meaningful and it is often difficult to assign the resolved modes to specific molecular-level motions.[172] For reasons that will be discussed in detail below resolved modes are labelled "IP + X^-" (or just "X^-") for the slowest ($j = 1$) process, "slow H_2O" for intermediate frequency ($j = 2$) process and "bulk H_2O" for the highest frequency ($j = 3$) process.
As for NaOFm(aq) and NaOAc(aq) (Section 3.1), and also for $NaOAcF_3$(aq) (Section 3.2), the relaxation time, $\tau_3(c) = \tau_b$[173] (Figures 4.10 & 4.11), of the highest frequency mode cen-

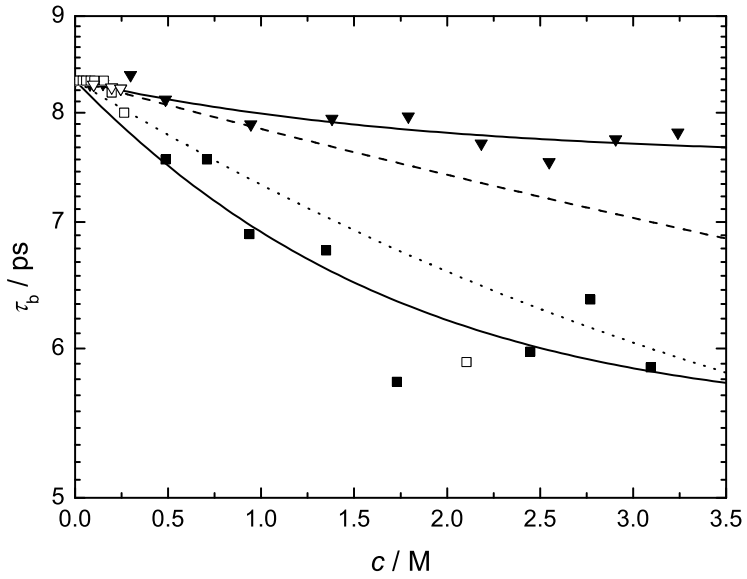

Figure 4.10: Dependence on solute concentration of the bulk-water relaxation time, τ_b, for NaOPr(aq) (▼) and NaOBu(aq) (■) at 25 °C. Open symbols represent τ_b values fixed during the fitting procedure; Solid lines represent the fit through data using Eq. 4.1; Dotted and dashed lines respectively represent τ_b for NaOFm(aq) and NaOAc(aq), fitted with Eq. 4.1.

tered at ∼18 GHz in the DR spectra of NaOPr(aq) (Figure 4.4), NaOBu(aq) (Figure 4.5), and NaOPe(aq) (Figure 4.6) smoothly extrapolates to the relaxation time of the dominant mode in pure water. This mode can therefore be assigned to the cooperative relaxation of the H-bond network of bulk water,[110] *i.e.*, H_2O molecules that are, at least at low c, not significantly influenced by the presence of the solute particles. However, the relaxation time τ_b decreases with increasing c of the studied salts. This indicates that ions influence the dynamics of water even beyond their hydration shell(s). Longinova et al.[108] reported an increase in bulk water relaxation time with increasing concentration of potassium propanoate. However, this work was done over a limited frequency range (eight frequencies between 10 and 25 GHz) and the data were fitted to a single Cole-Cole equation. The present data clearly indicates that there is more than one process in this frequency range which suggests that the increase in τ_b reported by Longinova et al. is an artefact of their limited resolution.

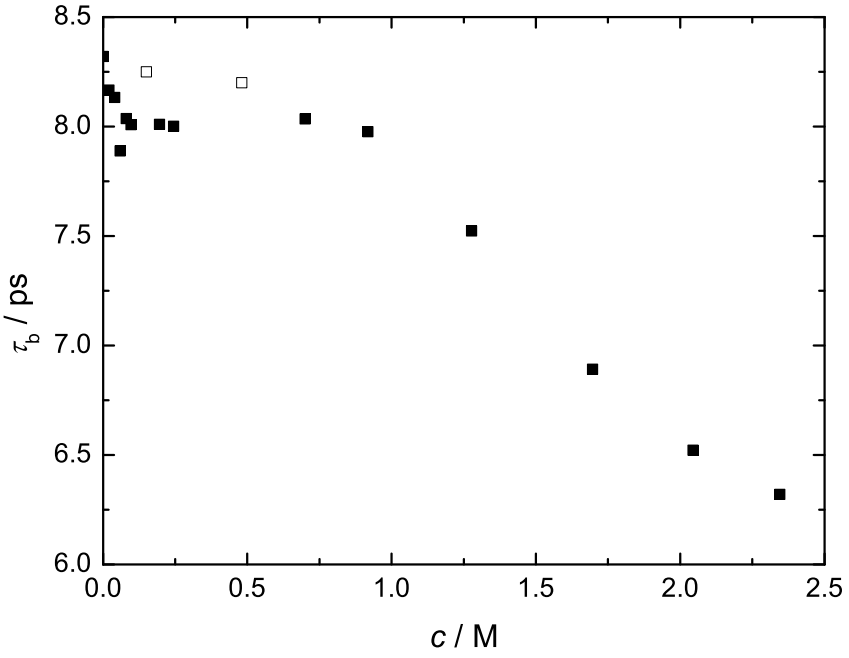

Figure 4.11: Concentration dependence of the bulk-water relaxation time, τ_b, for NaOPe(aq) at 25 °C. Open symbols represent the τ_b values fixed during the fitting procedure.

As can be seen in Figure 4.10, for NaOPr(aq) and NaOBu(aq), but also for NaOFm(aq) and NaOAc(aq) the variation in the $\tau_b(c)$ can be fitted by an exponential function

$$\tau_b(c) = a \exp(-bc) + (\tau(0) - a) \tag{4.1}$$

where the pure water value, $\tau(0) = 8.32$ ps, was taken from Reference 84.

The decrease in the $\tau_b(c)$ with increasing the solute concentration becomes less prominent from NaOFm(aq) to NaOPr(aq), *i.e.*, with increasing alkyl chain length. However there is a surprising reversal for NaOBu(aq) which decreases with c even more strongly than NaOFm(aq) (Figure 4.10).
In Table 4.4, the fitting parameters for Eq. 4.1 for the carboxylate salts from NaOFm(aq) to NaOBu(aq) is are compared with those of previously studied inorganic salts[131] (NaCl(aq), NaBr(aq) Na_2CO_3(aq) etc.), which were also fitted with Eq. 4.1.

Table 4.4: Magnitude Parameter a and Sensitivity Parameter b from Eq 4.1 for the Present and Some Previously Studied Elctrolytes[a]

electrolyte	a	b
NaOFm	3.85 ± 1.29	0.30 ± 0.14
NaOAc	4.48 ± 2.43	0.11 ± 0.07
NaOPr	0.75 ± 0.19	0.58 ± 0.29
NaOBu	2.22 ± 0.44	0.69 ± 0.23
Na_2CO_3[b]	3.50 ± 0.40	0.55 ± 0.11
NaCl[b]	1.60 ± 0.12	0.79± 0.12
NaBr[b]	1.23 ± 0.17	0.98 ± 0.21
NaSCN[b]	1.64 ± 0.25	0.99 ± 0.29
$NaClO_4$[b]	1.62 ± 0.15	1.35 ± 0.25

[a] Units: a in ps; b in L mol^{-1}. [b] Reference 131.

As argued previously,[131] the values of a, which reflect the high-concentration asymptote of the relaxation time (relative to pure water), for inorganic salts are virtually identical with the exception of Na_2CO_3. Interestingly, the a value for Na_2CO_3 is similar to that of NaOFm(aq) and to some extent NaOAc(aq) and NaOBu(aq). The very small value of a for NaOPr(aq) reflects the weak concentration dependence of $\tau_b(c)$. The values of b, which represent the sensitivity of relaxation time to concentration (the degree of curvature of the $\tau_b(c)$ plots), seems to increase with increasing the apparent size of anions with exception of NaOAc(aq). However, it is hard (because of limited number of studied organic salts) to draw a conclusion about the correlation between the size of organic anion and b values as was observed for the inorganic salts.[131] Another interesting finding is that the b values for the studied organic salts are, with the exception of NaOAc(aq), close to that of Na_2CO_3.
The bulk water relaxation time for NaOPe(aq) (Figure 4.11) cannot be fitted with Eq. 4.1 so that is not included in comparison. As can be seen in Figure 4.11, τ_b(NaOPe(aq)) shows a break point at $c \approx 0.5$ M which may indicate some form of aggregation of OPe^-(aq) at these c.
The intermediate ($j = 2$) process, centered at ∼8 GHz was resolved in the DR spectra of present electrolytes for all investigated c. The average relaxation time,[173] τ_s(NaOPr) ≈ 19 ps, τ_s(NaOBu) ≈ 21 ps, and τ_s(NaOPe) ≈ 17.5 ps, and the spectral position of this relaxation mode is similar to the "slow-water" relaxation previously observed by DRS for a number of

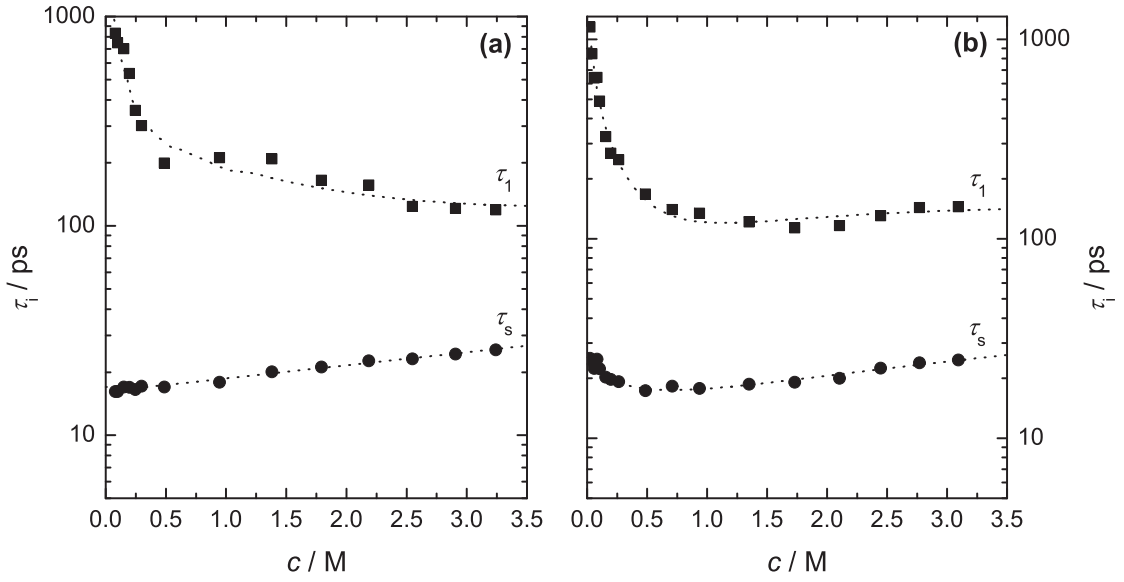

Figure 4.12: Concentration dependence of the average relaxation times for the two lower-frequency dielectric modes of: **(a)** NaOPr(aq) and **(b)** NaOBu(aq) at 25 °C. Lines are included as a visual guide only.

salts and can be so assigned.[106,112–114] This assignment is consistent with NMR[174–177] and femtosecond mid-infrared spectroscopy.[178–180] For NaOPr(aq), the relaxation time of this intermediate slow-water-relaxation process, τ_s, increases slightly with increasing c (Figure 4.12a). Whereas for NaOBu(aq), τ_s first decreases with increasing c (at $c \leq 0.5$ M) and then a steady increase (at $c > 0.5$ M), similar to that for NaOPr(aq), is observed (Figure 4.12b). For NaOPe(aq) τ_s is almost independent of c (Figure 4.13). The increase of τ_s for NaOPr(aq) and NaOBu(aq) with increasing c is consistent with previous DRS[181] study on aqueous solutions of amphiphilic tetramethylurea (TMU). For NaOBu(aq) at $c \leq 0.5$ M, slightly higher values of τ_s may possibly be due to some parametric coupling with τ_1.

The slowest ($j = 1$) process centered at ∼1 GHz for NaOPr(aq) and NaOBu(aq) appears to be a composite, suggested by the very rapid decrease in $\tau_1(c)$ as c increases from high dilution up to ∼0.5 M for both salts (Figure 4.12). In case of NaOPe(aq), however, the decrease of τ_1 at $0 \lesssim c \lesssim 0.5$ M is less pronounced (Figure 4.13) although qualitatively similar to that of τ_1 (NaOPr(aq)) and τ_1(NaOBu(aq)). A rapid decrease of $\tau_1(c)$ at $0 \lesssim c \lesssim 0.5$ M for NaOPr(aq), NaOBu(aq), and (though less pronounced) NaOPe(aq) is probably an evidence of ion-cloud relaxation[169,171] and the presence of weak ion pairing. An indication of ion association between Na^+ and carboxylate ions was found for aqueous solutions of NaOAc and $NaOAcF_3$ with DRS (see Section 3.2.3), and for NaOAc(aq) also by conductance measurements[118] and potentiometric studies.[124] However, it must be remembered that OPr^-, OBu^- and OPe^- have permanent dipole moments, with magnitudes 5.7, 8.3, and 10.7 D (MOPAC),[100] respectively. As DRS is sensitive to all the dipolar species present in solution so these carboxylate ions must contribute to the DR spectra. Consistent with the dramatic

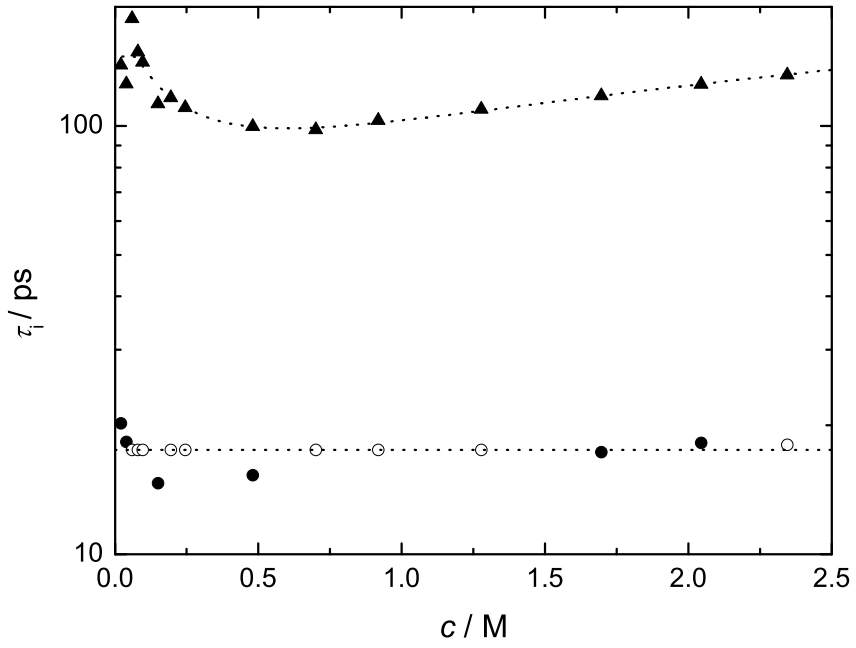

Figure 4.13: Concentration dependence of the anion relaxation time, τ_- (▲), and the slow-water relaxation time, τ_s (●), for NaOPe(aq) at 25 °C. Open symbols represent the τ_s values fixed during the fitting procedure.

changes in the effective dipole moments derived for NaOPr(aq) and NaOBu(aq) solutions (see later) it is reasonable to conclude that this mode contains concentration-dependent contributions from ion-cloud relaxation, the diffusional rotation of ion pairs and of the dipolar anions. On the other hand, the effective dipole moment calculations (see later) for NaOPe(aq) strongly suggest that this mode is essentially due to the reorientation of the dipolar OPe^- ions whereas at $c \lesssim 0.5\,M$ ion-cloud and/or ion-pair relaxations may have some small contribution. This assignment is broadly consistent with the concentration dependence of relaxation time of this mode (Figure 4.13).

Based on the above discussion, it seems quite reasonable to conclude that at $c \lesssim 1\,M$ the lowest-frequency mode for NaOPr(aq) and NaOBu(aq) is a composite mode due to the reorientation of anions and the ion-cloud and ion-pair relaxations, whereas, at $c > 1\,M$ the anion contribution predominates. Similarly, at $c \lesssim 1\,M$ the relaxation time, τ_1, of this process is some weighted average of the ion-pair relaxation time, τ_{IP}, ion-cloud relaxation time, τ_{IC}, and the anion relaxation time, τ_-, and at $c > 1\,M$ (where c_{IP} decreases due to "redissociation" and c_{IC} becomes negligible[169] (Section 3.2.3)) $\tau_1 \approx \tau_-$. For NaOPe(aq) this mode is broadly assigned to the anion (OPe^-) reorientation (small contribution coming from ion-pair and/or ion-cloud relaxations at $c \lesssim 0.5\,M$ may also be present). The presence of more than one overlapping mode at $c \lesssim 1\,M$ and predominance of only one

(anion reorientation) at $c > 1\,\mathrm{M}$ for NaOPr(aq) and NaOBu(aq), and predominant contribution of one relaxing species (OPe^- reorientation) at all c, is consistent with the bias-free simulations (Figures 4.7 to 4.9). Note that for the smaller carboxylates NaOFm(aq) and NaOAc(aq) (Section 3.1) and also for $NaOAcF_3$(aq) (Section 3.2), the anion-reorientation mode overlapped with the slow-water relaxation because of the smaller anion size.
Similar to NaOFm(aq), NaOAc(aq) and $NaOAcF_3$(aq) (Sections 3.1 & 3.2) the fast water mode centred at ~400 GHz[110], which is sometimes[112,113] but not always[106,115] detected in aqueous electrolyte solutions, could not be resolved for the present samples but the obtained values of $\varepsilon_\infty \approx 5.5\text{-}7$ (Tables 4.1, 4.2 & 4.3) suggest its presence.

4.1.3 Solute relaxation and ion association

For $c \lesssim 1\,\mathrm{M}$ of NaOPr(aq), the observed solute relaxation amplitude, $S_1 = S_{\mathrm{IP}} + S_{\mathrm{IC}} + S_-$, initially increases with increasing c before passing through a maximum at $c \approx 0.15\,\mathrm{M}$ (Figure 4.14). Whereas, at $c \geq 1\,\mathrm{M}$ for NaOPr(aq), the relaxation amplitude, $S_1 \approx S_-$, increases steadily with increasing c. For NaOBu(aq) and NaOPe(aq) S_1 increases monotonically with increasing c throughout the studied concentration range (Figure 4.14).

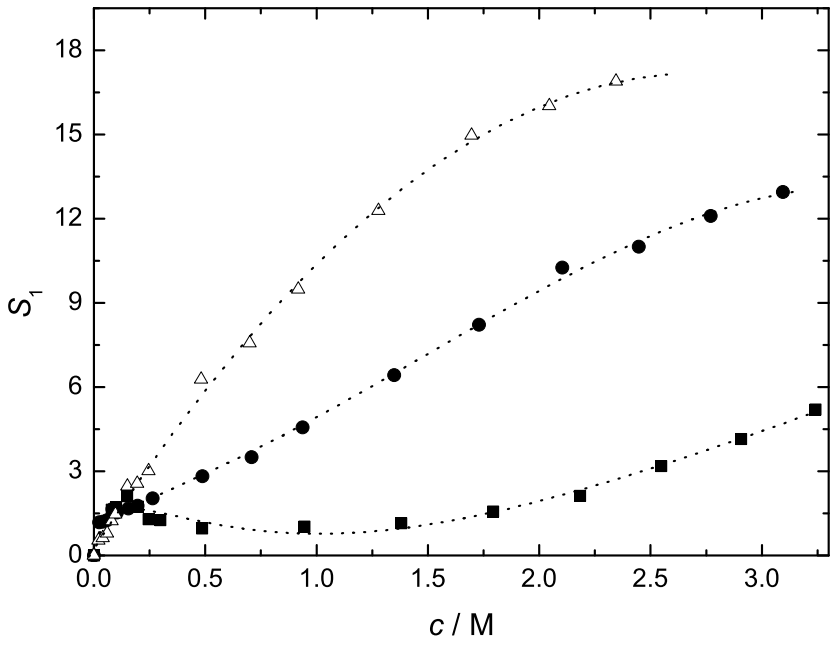

Figure 4.14: Concentration dependence of solute relaxation amplitudes, S_1, for NaOPr(aq) (■), NaOBu(aq) (●), and NaOPe(aq) (△) at 25 °C. Lines are included as a visual guide only.

Using the measured relaxation amplitude, S_1, with the assumption of negligible ion-cloud relaxation, the effective dipole moment, $\mu_{\mathrm{eff},j}$ of the relaxing species, j, can be calculated via Eq. 1.71 (Figure 4.15).
For NaOPr and NaOBu aqueous systems, the $\mu_{\mathrm{eff},j}$ values decrease strongly with increasing electrolyte concentration up to 0.5 M. Such behavior at low c has been observed for dilute solutions of ionic liquids in conventional molecular solvents and was attributed to the formation of ion-pairs.[182] The calculated effective dipole moments of ion-pairs ($[\mathrm{NaOPr}]^0$ = 20 D and $[\mathrm{NaOBu}]^0$ = 24 D) agree very well with the MOPAC-calculated moment of 21 D (assuming SIP for both NaOPr(aq) and NaOBu(aq)). The average $\mu_{\mathrm{eff},-}$ value (3.5 D) calculated via equation 1.71 for OPr^-(aq) is rather low as compared to its estimated MOPAC value of 5.9 D. However, in case of OBu^-(aq) the experimentally obtained and MOPAC value (7.5 and 7.3 D respectively) are in excellent agreement with each other. One of the possible reasons for different experimental and theoretical $\mu_{\mathrm{eff},-}$ values for NaOPr(aq) may be the improper estimation of S_1 due to overlapping of anion and ion-pair relaxation modes at low concentrations, and of anion and the slow-water relaxation modes at higher concentrations, as NaOPr is at border line of the aqueous carboxylate system where a separate relaxation is resolved for anion reorientation, *i.e.*, for formate and acetate ion the anion reorientation was merged with slow-water relaxation process. This may also be the reason for the rather large increase of $\tau_{\mathrm{s}}(c)$ for these anions.

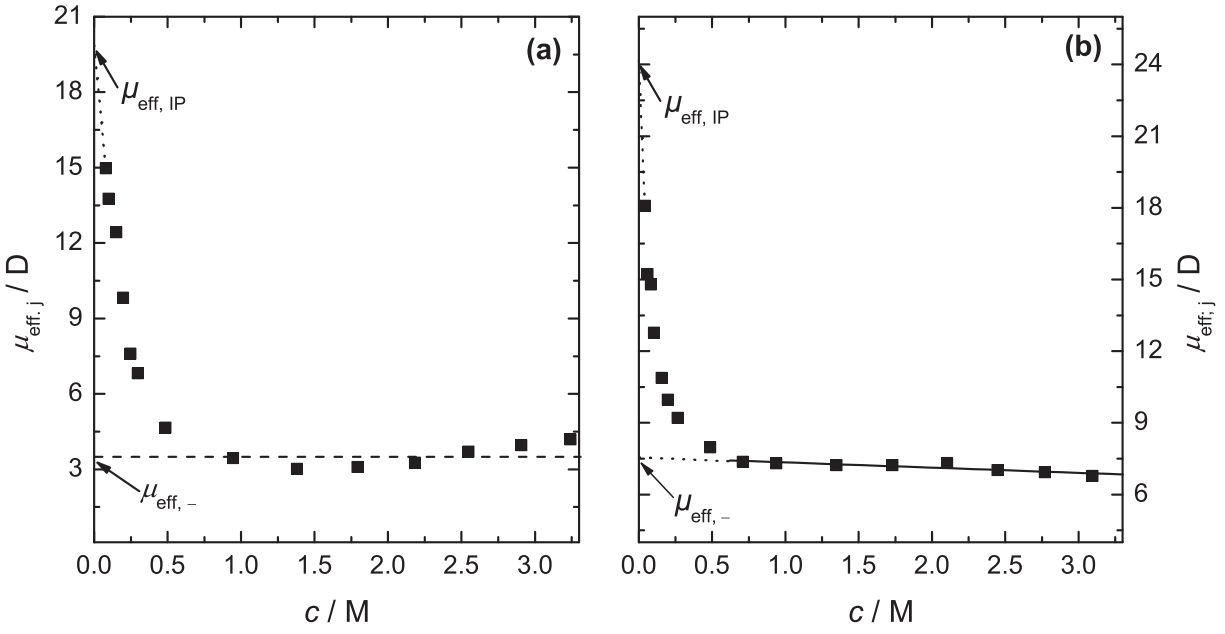

Figure 4.15: Concentration dependence of effective dipole moments, $\mu_{\mathrm{eff,\,j}}$, calculated using solute relaxation amplitude, S_1, of (**a**) NaOPr(aq) and (**b**) NaOBu(aq) at 25 °C. Dashed line represents the averaged $\mu_{\mathrm{eff,\,-}}$ of OPr^- at $c \gtrsim 1$ M; dotted lines represent the extrapolations to obtain the $\mu_{\mathrm{eff,\,j}}$ at infinite dilutions.

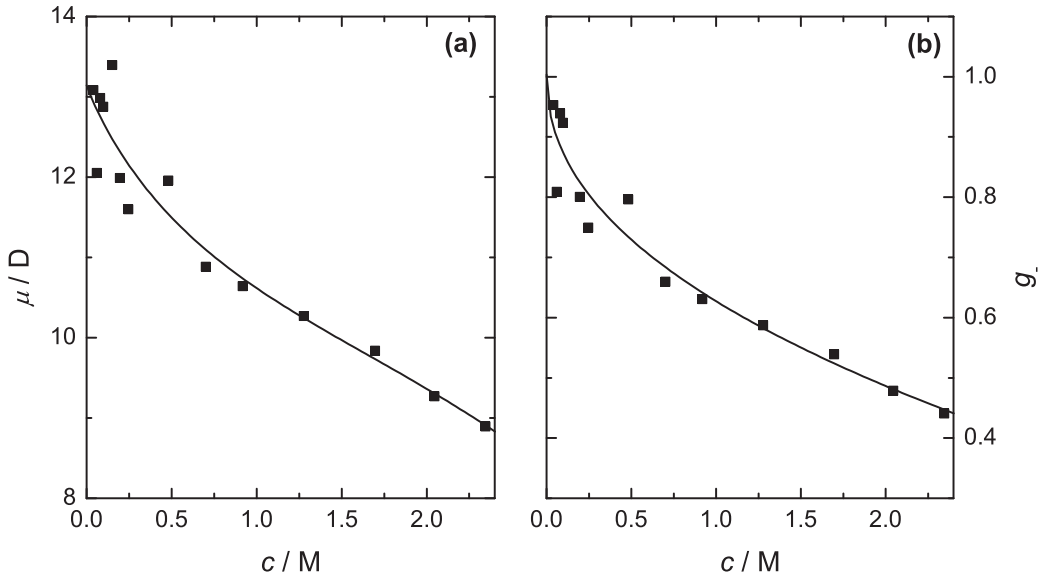

Figure 4.16: Concentration dependence in aqueous solution of NaOPe(aq) at 25 °C of: (**a**) the effective dipole moment of OPe^-(aq), $\mu_{\mathrm{eff},-}$, calculated using the anion relaxation amplitude, S_-; and (**b**) the correlation factor, g_-, of OPe^-(aq). Lines are included as a visual guide only.

Because lowest frequency process for NaOPe(aq) is associated with anion reorientation, extrapolation of calculated $\mu_{\mathrm{eff},-}$ to $c \to 0$ gives a value for the apparent dipole moment of the anion of $\mu_{\mathrm{ap},-} = 13.1\,\mathrm{D}$ (Figure 4.16). This is in very good agreement with the solvent phase dipole moment value of 13.5 D for OPe^-(aq) obtained from MOPAC. This good agreement of experimental $\mu_{\mathrm{ap},-}$ and the MOPAC-calculated moment confirms the assignment of the slowest-relaxation mode in NaOPe(aq) to OPe^- reorientation relaxation only (Section 4.1.2).

The apparent dipole moment for OPe^-, $\mu_{\mathrm{ap},-}$, can be used to estimate the orientational correlation factor, g_-, as[182]

$$g_- = \mu^2_{\mathrm{eff},-}/\mu^2_{\mathrm{ap},-} \tag{4.2}$$

The correlation factor so obtained for OPe^-(aq) is given in Figure 4.16b. Note that g_- is an empirical quantity and as such it includes possible cross correlations of all the dipolar species present in the system. Nevertheless, values of $g_- > 1$ indicate parallel and $g_- < 1$ antiparallel alignment of the dipolar species. For OPe^-(aq) the value of g_- drops remarkably with increasing c, reaching a value of $\sim$0.46 at $c = 2.34\,\mathrm{M}$. This suggests that antiparallel aggregation of the amphiphilic dipolar OPe^- in aqueous media increases with increasing solute concentration.

Quantitative description of ion pairing. As discussed earlier, the slowest process of amplitude S_1, at lower concentrations for NaOPr(aq) and NaOBu(aq) is a composite mode due to the anion, ion-cloud and ion-pair relaxations. Unfortunately, independent estimation of S_{IC} is not possible using current theories although it is generally thought that such effects while significant are not large. Hence, the analysis of S_1 was performed

assuming $S_{IC} = 0$ that S_1 is only due to the anion and ion-pair relaxations. Under this assumption a quantitative description of ion pairing requires separation of the contributions from the anion and ion pair relaxations. This can be achieved by assuming that IPs make a significant contribution to $\mu_{eff,1}$ only at $c \lesssim 0.5\,M$ (Figure 4.15a). The average value of $\mu_{eff,1} \approx 3.5\,D$ at higher c can then be assigned solely to $OPr^-(aq)$, which can then be used to calculate S_{OPr^-} via Eq. 1.71, and hence derive the ion-pair contribution S_{IP}. Note that the slight variation of $\mu_{eff,1}(c)$ at $c \gtrsim 1\,M$ will have only a minor impact on this calculation. The value of $\mu_{eff,}(OBu^-(aq))$ (7.5 D) changes only slightly but linearly with concentration at $c \gtrsim 0.5\,M$ (Figure 4.15b) and can simply be extrapolated to $c = 0$ to calculate S_{OBu^-} and subsequently S_{IP}.

To analyze the ion-pair relaxation quantitatively via Eq. 1.71, the gas phase dipole moments of various types of ion pairs are calculated with MOPAC[100] (PM6[101], 1SCF). The method described by Barthel et al.[66] gave similar values. Medium effects on gas phase dipole moment of the ion-pairs, μ_{IP}, are accounted for by estimation of the effective dipole moment, $\mu_{eff,IP}$, via Eq. 1.74. Polarizabilities of various types of ion pairs were calculated as $\alpha_{IP} = \alpha_+ + \alpha_- + n\alpha_{H_2O}$, where n is the number of intervening water molecules in the IP structure ($n = 0$ for CIPs; $n = 1$ for SIPs; $n = 2$ for 2SIPs), with $\alpha/4\pi\varepsilon_o$Å$^3 = 0.211$ (Na^+),[66] 7.333 (OPr^-),[100] 8.718 (OBu^-),[100] and 1.444 (H_2O).[66] The quantities required for the evaluation of Eq. 1.71 are listed in Table 4.5 or are easily calculated using the relevant equations in Buchner et al.[45]

Table 4.5: Ion association constants, log K_A^o, and related parameters for NaOPr(aq) and NaOBu(aq) at 25 °C[a]

Model	μ_{IP}	log K_A^o	B_K	C_K
NaOPr(aq)				
SIP	20.60	2.25±0.17	-12.03±1.34	7.79±1.25
2SIP	32.84	1.47±0.08	-9.97±0.71	6.10±0.67
NaOBu(aq)				
SIP	20.69	2.11±0.19	-14.00±2.24	11.18±2.49
2SIP	32.98	1.51±0.14	-13.03±1.80	10.40±2.04

[a] Ion-Pair Dipole Moments, μ_{IP}; and resulting parameters B_K and C_K of Eq 1.91. Units: μ_{IP} in Debye (1 D = 3.3356×10^{-30} C·m), B_K in L·mol^{-1}, C_K in L$^{3/2}$·mol$^{-3/2}$.

Insertion of the ion pair parameters into Eq. 1.71 yielded the concentrations of various possible IP types, c_{IP}. These c_{IP} values were then used to calculate the corresponding K_A values. Note that the K_A values so calculated represent **upper limits** because of the neglected contribution from ion-cloud relaxation. To determine the corresponding upper limits of the standard (infinite dilution) association constant, K_A^o, the values of K_A so obtained were then fitted for convenience to a Guggenheim-type function (Eq. 1.91).

The K_A°, B_K, and C_K values obtained in this way for NaOPr(aq) and NaOBu(aq), assuming the formation of SIPs and 2SIPs, are given in Table 4.5. The formation of CIPs can be neglected because calculations assuming CIP model give negative values for ionic strength ($I = c - c_{IP}$) and also the ions, Na^+, OPr^- and OBu^- are thought to be quite strongly hydrated (see Section 4.1.5 below). As for NaOAc(aq) and $NaOAcF_3$(aq) (Sections 3.1.3 & 3.2.3) given the likely hydration of Na^+(aq) and the hydrophilic end of OR^-(aq) it is reasonable to assume that both NaOPr(aq) and NaOBu(aq) form 2SIPs rather than SIPs in aqueous solution. On the other hand it should be noted that the calculated $\mu_{eff,IP}$ values of 20 D for NaOPr(aq) and 24 D for NaOBu(aq) (Section 4.1.3) agree better with the MOPAC-calculated values for SIPs rather than that for 2SIPs (Table 4.5). However, the approximate nature of the present calculations need to be kept in mind.

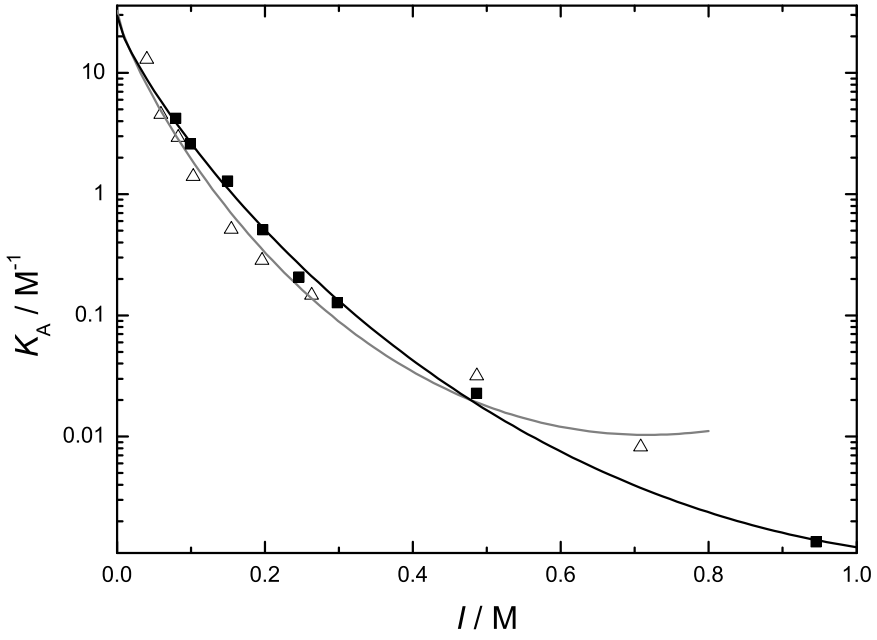

Figure 4.17: Ion association constant, K_A, as a function of nominal ionic strength, I, of NaOPr(aq) (■) and NaOBu(aq) (△) at 25 °C (2SIP Model). Lines represent fits according to Eq. 1.91 using the parameters in Table 4.5.

Figure 4.17 shows the calculated association constants, K_A, assuming only 2SIP are formed, and the respective fits with Eq. 1.91 to find K_A° for NaOPr(aq) and NaOBu(aq). The standard ion-pair association constant is the same (within the likely error limits) for both systems. This result is probably to be expected given the similar pK_a values of propanoic[183–185] and butanoic[183,185] acids (4.9 and 4.8 respectively). Accordingly, keeping in mind the likely contribution of ion-cloud relaxation to the solute amplitude, we can give upper limits of K_A°(NaOPr) $< 30\,M^{-1}$ and K_A°(NaOBu) $< 32\,M^{-1}$, respectively, for the association con-

stants. These values are more than an order of magnitude higher than those determined for NaOAc(aq) and $NaOAcF_3$(aq): $K_A^\circ \lesssim 1.5$ and $1.7\,M^{-1}$ respectively (Sections 3.1.3 & 3.2.3). This seems chemically unlikely given the similarity of their pK_a values and may indicate a much higher contribution of ion-cloud relaxation for the larger anions.

4.1.4 Water-relaxation amplitudes

Bulk water. As shown previously,[112] the bulk and fast water relaxations have to be interpreted as consecutive steps, so that the sum of their amplitudes, $S_b = \varepsilon_3(c) - \varepsilon_\infty$ for NaOR(aq), should be analyzed. For ε_∞, the value of 3.48 obtained from dielectric measurements of pure water including THz data[84] is thus used rather than the fit values shown in Tables 4.1, 4.2, & 4.3, which contain some contributions from fast water relaxation. The amplitude (relaxation strength) of the bulk-water process, S_b, decreases strongly at lower solute concentrations before starting to level off at $c \gtrsim 2\,M$ (Figure 4.18a). Furthermore at $c < 0.5\,M$ the S_b values are almost same for all the three studied electrolytes whereas at higher concentrations some differences are observed (Figure 4.18a).
The relaxation amplitudes of bulk water for NaOR(aq) were used to calculate the apparent bulk water concentration c_b^{ap} with the Cavell equation (Eq. 1.71), as described in Section 3.1.2.

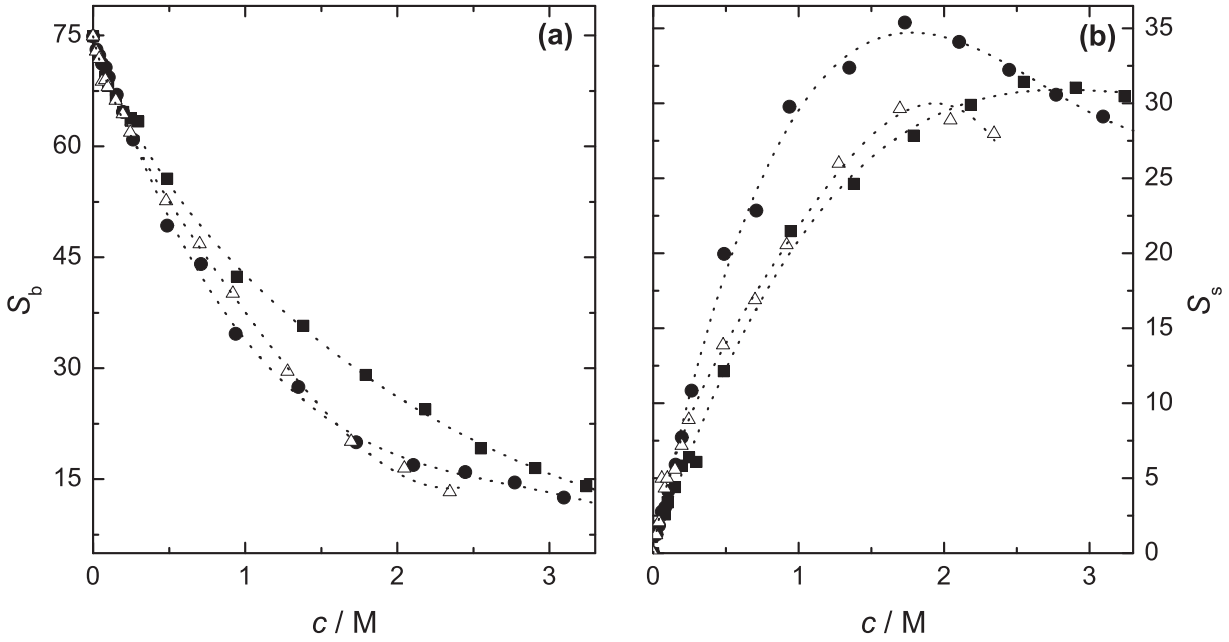

Figure 4.18: Concentration dependence for NaOPr(aq) (■), NaOBu(aq) (●), and NaOPe(aq) (△) at 25 °C of (**a**) the bulk-water relaxation amplitude, S_b, and (**b**) the slow-water relaxation amplitude, S_s. Lines are included as a visual guide only.

Slow water. The amplitude of the slow-water process, S_s, for the studied salt solutions (Figure 4.18b) initially increases strongly with increasing c, but then passes through a maximum value of 31.4 at 2.6 M for NaOPr(aq) and 35.4 and 29.6 at 1.7 M for NaOBu(aq) and NaOPe(aq), respectively. The concentration where S_s(NaOBu) and S_s(NaOPe) are maximal coincides approximately with the concentrations, ∼2 M and ∼1.7 M for NaOBu(aq) and NaOPe(aq), respectively, at which OBu^- and OPe^- anions have been reported to start aggregating in aqueous solution.[186] On the basis of similar trend of S_s of all the three aqueous systems studied, it can be assumed that aggregation of OPr^- anions, although not reported in literature so far, also occurs but at higher concentrations ($c \gtrsim 2.6$ M).
S_s can be used to calculate the apparent concentration of slow water, $c_s^{ap}(c)$, using Eq. 1.71 for the slow-water process.

4.1.5 Ion hydration

As described by Buchner and Hefter,[11] the effects of ion solvation on DR spectra manifest themselves in three major ways: (a) a generalized shift of solvent relaxation time, without a significant change of shape in the overall solvent mode; (b) a decrease of the solvent amplitude; and (c) the possible emergence of a new relaxation process arising from specific solvent molecules whose dynamics have been significantly perturbed by the presence of dissolved ions.
All the above mentioned effects can clearly be observed in the spectra of present electrolyte solutions, *i.e.*, a decrease in the bulk-water relaxation time, τ_b (Figures 4.10 & 4.11), a strong decrease of the bulk-water amplitude, S_b (Figure 4.18a), and the emergence of a slow-water relaxation process, S_s (Figures 4.4 to 4.6), as discussed in the previous section. If ion-water interactions are much stronger than the water-water interactions then the water molecules that are bonded to the ions effectively become immobilized on DR time scale. This leads to a decrease in bulk-water relaxation amplitude, S_b, beyond the effect of dilution and the experimental appearance of slow water.
For NaOPr(aq), NaOBu(aq) and NaOPe(aq), the sum of DRS-detected water, $c_b^{ap} + c_s^{ap}$, is less than the analytical (total) water concentration, c_w. Water missing from the DR spectrum can be ascribed to the presence of irrotationally bound (ib) water molecules and can be used to calculate an effective hydration number, Z_{ib}, via Eq. 3.6.
The Z_{ib} values so obtained for NaOPr(aq) and NaOBu(aq) are either smaller or almost the same as the number of irrotationally bound water molecules that would be expected to be associated with Na^+(aq),[169] indicating that $Z_{ib} \approx 0$ for both OPr^-(aq) and OBu^-(aq) (Figure 4.19). The Z_{ib} values for NaPe(aq), however, are higher than those expected to be associated with Na^+(aq) (Figure 4.20). In order to obtain the effective number of H_2O molecules "frozen" by OPe^-, $Z_{ib}(OPen^-)$, the obtained Z_{ib} values for NaOPe(aq) were corrected for $Z_{ib}(Na^+)$ using recently determined values of $Z_{ib}(Na^+)$.[169] The Z_{ib} values so obtained for OPe^- are also shown in Figure 4.20. Over the entire concentration range OPe^-(aq) binds ∼1-2 water molecules strongly. The good agreement of $Z_{ib}(OPe^-)$ and that of other carboxylate ions (*i.e.* $Z_{ib}(OFm^-)$, $Z_{ib}(OAc^-)$, and $Z_{ib}(OAcF_3^-)$ (Section 3.1)) supports the previous assignment[106] of this quantity to water strongly bound by the carboxylate moiety. This also indicates that relatively lower values of Z_{ib}(NaOPr) and Z_{ib}(NaOBu)

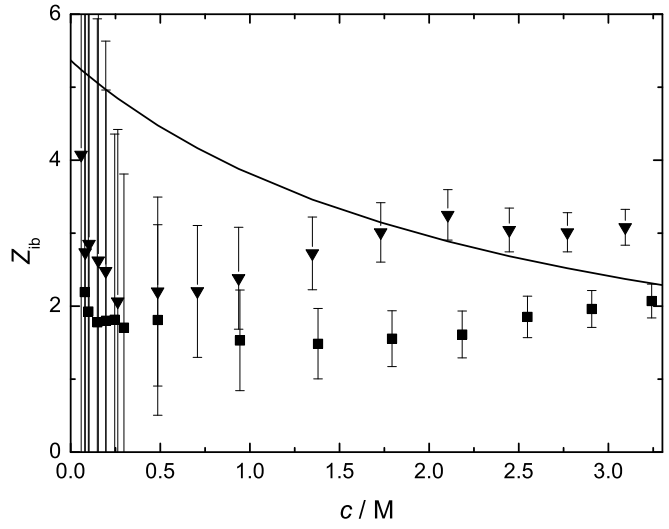

Figure 4.19: Concentration dependence of effective hydration numbers, Z_{ib}, for NaOPr(aq) (■) and NaOBu(aq) (▼) at 25 °C.[132] Solid line represents $Z_{ib}(Na^+)$.[169]

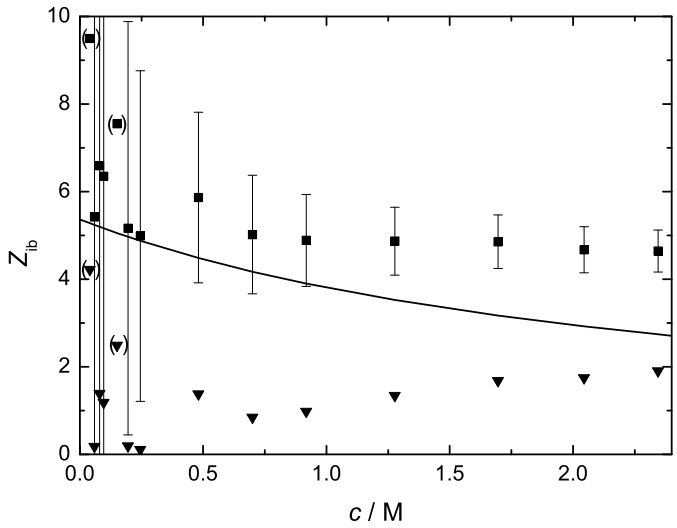

Figure 4.20: Concentration dependence of effective hydration numbers, Z_{ib}, for NaOPe(aq) (■), and $OPen^-$(aq) (▼) at 25 °C.[132] Solid line represents $Z_{ib}(Na^+)$.[169] Outliers are bracketed.

may be the result of improper estimation of S_b for aqueous solutions of both salts due to overlapping ion-cloud, ion-pair and anion relaxations.
As already described above, the intermediate process is due to the presence of slow water. The apparent concentration of slow water, $c_s^{ap}(c)$, which can be calculated from the amplitude of this process S_s, can directly be used to calculate the number of slowly-relaxing water molecules per salt 'molecule', Z_s, via Eq. 3.7. The Z_s values calculated for NaOPr(aq), NaOBu(aq), and NaOPe(aq) with Eq. 3.7 are shown in Figure 4.21. Since aqueous solutions

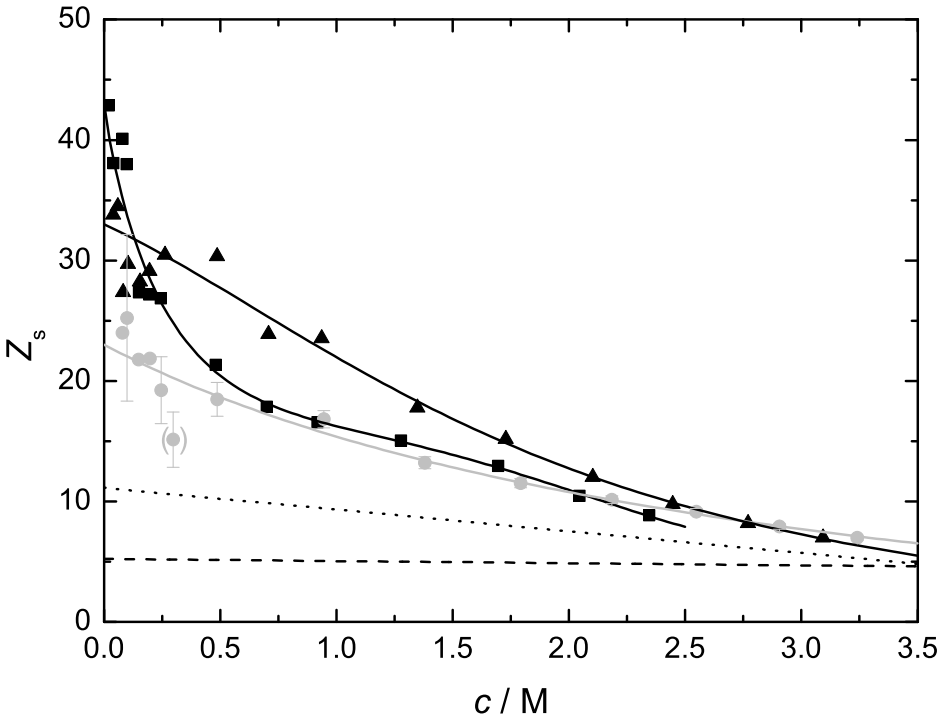

Figure 4.21: Concentration dependence of the slow-water hydration number, Z_s, for OPr^-(aq) (●), OBu^-(aq) (▲), and $OPen^-$(aq) (■) in aqueous solutions of their corresponding sodium salts at 25 °C.[132] The dotted line represents $Z_s(OAc^-)$(aq) and the dashed line represents $Z_t(OFm^-)$(aq). Outliers are bracketed.

of typical inorganic salts containing sodium ions do not show any slow water process,[131,133] it is reasonable to assign Z_s for the present salt solutions entirely to the anions. On the basis of these calculations, OPr^-, OBu^- and OPe^- appear to be associated with ∼23, ∼33, and ∼43 slow water molecules at infinite dilution, respectively.
As for OAc^-(aq) (Section 3.1.4), the value of Z_s decreases strongly with increasing c for all three of the present anions most probably because of overlapping of hydration shells. The pronounced decrease of Z_s with increasing c may also hint at the aggregation of the anions, (Section 4.1.3), and/or the breakdown of the hydration shells due to increasing

ion-ion interactions. Figure 4.21 reveals that $Z_s(OPe^-(aq))$ decreases more sharply than $Z_s(OAc^-(aq)$-$OBu^-(aq))$ at lower c. This is consistent with a greater level of aggregation for $OPe^-(aq)$ cf. $OAc^-(aq)$, $OPr^-(aq)$, and $OBu^-(aq)$.

As 5-6 *slow* water molecules are bound by the $-COO^-$ (Section 3.1.4),[106] the remaining slow water, $Z_s(-R) = Z_s - Z_s(-COO^-)$, is reasonably assigned to water molecules close to hydrophobic moiety (–R) of alkylcarboxylates.[106,112,139–141] The "hydrophobic" hydration numbers for $-C_2H_5$, $-C_3H_7$, and $-C_4H_9$ at $c \to 0$ derived from the present measurements are therefore ∼18, ∼28, and ∼38 respectively. These values of Z_s(–R) at $c \to 0$ in comparison with the values of $Z_s(OFm^-(aq)) \approx 5.2$ and $Z_s(OAc^-(aq)) \approx 11$ indicate that each $-CH_3$ or $-CH_2-$ binds ∼6-10 water molecules hydrophobically. Figure 4.21 further reveals that with increasing c the Z_s values of $OPr^-(aq)$, $OBu^-(aq)$, and OPe− tend to reach the total hydration number of the carboxylate moiety, $Z_t(-COO^-) = Z_s(-COO^-) + Z_{ib}(-COO^-) \approx 5-6$.[106] This is similar to the situation for NaOFm(aq) and NaOAc(aq) (Section 3.1.4) and $NaOAcF_3$(aq) (Section 3.2.2). As $Z_t(-COO^-)$ is almost independent of c (Section 3.1.4),[106] this suggests that it is the –R moiety of the anions that is dehydrated with increasing c.

The above discussion reveals that OPr^-, OBu^-, and OPe^- ions exhibit hydrophilic and hydrophobic hydration, the former associated with the $-COO^-$ group and the later with the non-polar alkyl chain –R. The hydrophilic hydration of the $-COO^-$ group can be explained as for $OFm^-(aq)$ (Section 3.1.4),[106] *i.e.*, the interactions between the water and the oxygens of $-COO^-$ group are stronger than the water-water interactions but not strong enough to irrotationally bind the water molecules on DRS time scale. This intermediate situation results in slowed relaxation dynamics, as compared to the bulk, of the water molecules in the vicinity of the charged $-COO^-$ group. Such hydrophilically-slowed relaxation dynamics of water, making relatively strong hydrogen bonds with anions, is also observed for F^- ion.[115] Potentiometric measurements[138] also suggest ∼7 and ∼8.5 water molecules are hydrophilically attached to OPr^- and OBu^- at infinite dilution, respectively. Recent MD simulations on formate[134] and acetate[142] ions also suggest an easy (but slower than the bulk) exchange of water molecules between the solvation shell and the bulk. Kropman and Bakker[187] investigated the dynamics of anion-water and water-water hydrogen bonds in aqueous solutions using femtosecond midinfrared spectroscopy. These authors found a significant slowing down of the relaxation of anion-water hydrogen bonds cf. the dynamics of hydrogen bonds between two water molecules in the bulk.

The hydration of the alkyl chains in OPr^-, OBu^-, and OPe^- can reasonably be assumed to be similar to that of well recognized hydrophobic ions, such as the larger R_4N^+ cations (R = *n*-Pr, *n*-Bu, *n*-Pe),[112] and Ph_4P^+ and BPh_4^-.[113] The presence of slow water around hydrophobic ions is thought[188–190] to be due to the cooperative dynamics of water being governed by the presence of "fifth neighbors", *i.e.*, by water molecules approaching, but not yet participating in a local H-bond configuration. Through their interactions with the H-bond network these "fifth neighbors" can modify the energy of a bound water molecule and initiate the breaking of its H-bonds.[191] Additionally, these fifth neighbors may act as new H-bond acceptors or donors when the released water molecule and its surroundings relax into a new equilibrium configuration.

Recently, Laage et al. argued[140,141,192,193] that slowingdown of water molecules around amphiphilic solutes in aqueous solutions can be explained through a transition-state excluded-

volume (TSEV) effect. According to them,[140] water reorientation in pure-water mainly proceeds through sudden large amplitude angular jumps.
Laage et al. argue[141,192,193] that water next to the hydrophobic groups *i.e.*, in a very different context, also reorients through such large angular jumps. The jump mechanism remains almost identical to that in bulk water but the "jump time" is elongated *i.e.*, the dynamics of water molecules near hydrophobic moieties is slowed down. This lengthening of the H-bond exchange time (jump time) is due to the fact that the approach of the new H-bonding partner water is excluded in certain geometries by presence of hydrophobic groups.

4.2 Aqueous solutions of sodium benzoate

This section deals with a DRS study of sodium benzoate (NaOBz), a salt of the simplest aromatic carboxylic acid. Benzoate ($C_6H_5COO^-$, OBz^-) ion possesses a hydrophobic phenyl-ring (–Ph) attached to a hydrophilic anionic centre ($–COO^-$). As noted earlier in this thesis (Section 3.1) the hydrophilic $–COO^-$ moiety is the most common anionic component of many biomolecules. The hydrophobic –Ph group is the key structural motif in the aminoacids phenylalanine and tyrosine. The OBz^- ion thus provides a particularly useful model compound to help to understand the hydration behaviour of biomolecules with aromatic hydrophobic entities.
It is also interesting to note that benzoates and related compounds are typical examples of hydrotropes, molecules that are able to solubilize hydrophobic molecules in water but which — in contrast to surfactants — do *not* form well-defined aggregates, such as micelles.[194] Despite their wide practical use, the mechanism behind the solubilizing power of hydrotropes is still unclear. It is believed that these molecules form loose layered aggregates enclosing solubilized molecules in their interstices but unequivocal experimental evidence is lacking. Given its ability to detect dipolar aggregates,[10,11] a DRS study of NaOBz(aq) solutions may shed some light on the functioning of hydrotropes. Comparison of such data with those of the simplest alkylcarboxylate hydrotrope (NaOPe(aq), Section 4.1) may be interesting.
DR spectra of the aqueous solutions of NaOBz(aq) were investigated over the frequency range $0.2 \lesssim \nu/\mathrm{GHz} \leq 89$ at 25 °C up to a concentration of $c = 2.473$ M. To the best of our knowledge this is the first systematic application of DRS to investigate ion-aggregation and hydration of OBz^-(aq). DR spectra at $0.2 \lesssim \nu/\mathrm{GHz} \leq 50$ were measured using an Agilent E8364B VNA in combination with a high temperature probe ($0.2 \lesssim \nu/\mathrm{GHz} \leq 20$) and a waveguide-transmission cell ($27 \lesssim \nu/\mathrm{GHz} \leq 40$); high frequency data were obtained using the E-band interferometer (Section 2.2).

4.2.1 Choice of fit model

Typical DR spectra obtained for NaOBz(aq) at 25 °C as a function of solute concentration are given in Figure 4.22. The $\varepsilon''(\nu)$ curves show a major decrease in the dominant peak centered at ∼18 GHz, with the appearance of a new peak at frequencies around ∼1 GHz, with increasing c.
The combined $\hat{\varepsilon}(\nu)$ data were analyzed by simultaneously fitting the in-phase ($\varepsilon'(\nu)$, Figure 4.22a) and out-of-phase ($\varepsilon''(\nu)$, Figure 4.22b) components of the complex permittivity to various possible relaxation models consisting of n distinguishable relaxation processes using Equation (1.65). A full description of the fitting procedure is given in Section 2.2.3 so only some salient aspects are presented here. In addition to the overall quality of the fits (Eq. 2.8), it is essential that models are physically meaningful and that the derived parameters are realistic and vary smoothly as functions of concentration. DR spectra for NaOBz(aq) were fitted well using either a three Debye (D+D+D) or a four Debye (D+D+D+D) model. Typical fits obtained with these D+D+D and D+D+D+D models for NaOBz(aq) are shown in Figures 4.22, 4.23, & 4.24. Similar to NaOPr(aq), NaOBu(aq),

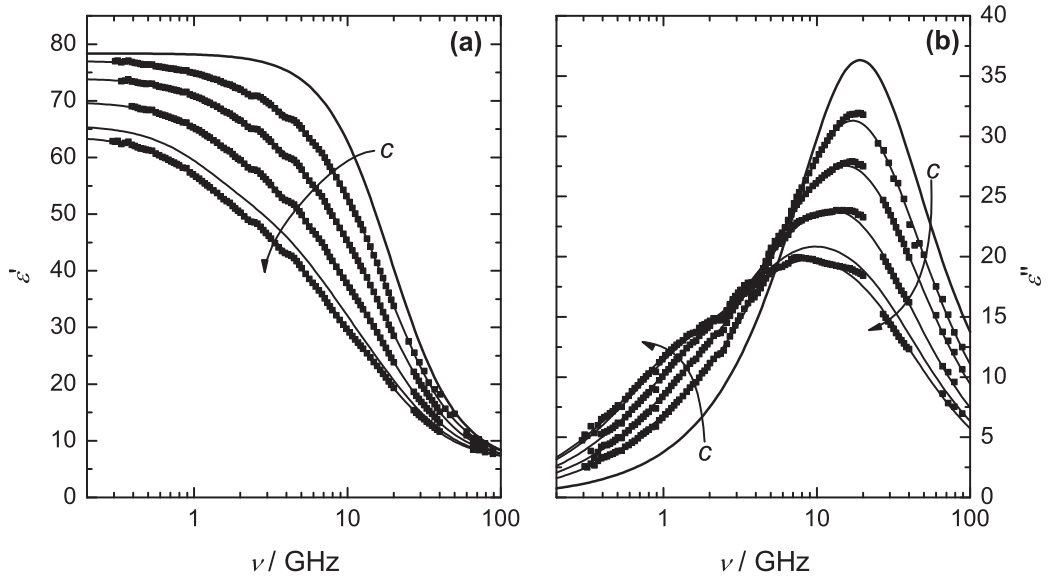

Figure 4.22: Dielectric permittivity (**a**) and loss (**b**) spectra for NaOBz(aq) at 25 °C. Arrows indicate increasing concentrations: c / M = 0, 0.5659, 1.080, 1.693, 2.225, and 2.473. Symbols are experimental data (mostly omitted for visual clarity); lines represent the D+D+D fit.

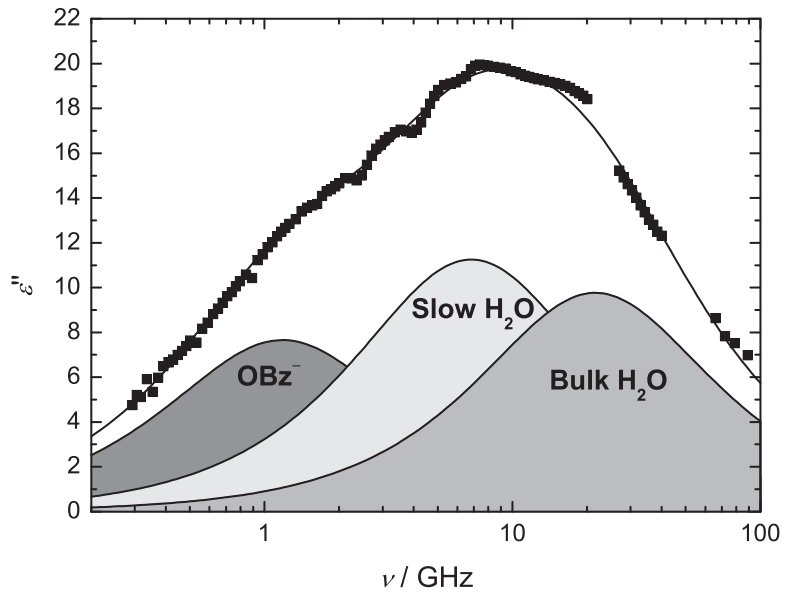

Figure 4.23: Dielectric loss curve of 2.473 M NaOBz(aq) at 25 °C, showing contributions of the three Debye processes. Symbols represent experimental data, the line through the experimental data represents the D+D+D fit, and shaded areas indicate the contributions of the various relaxation modes.

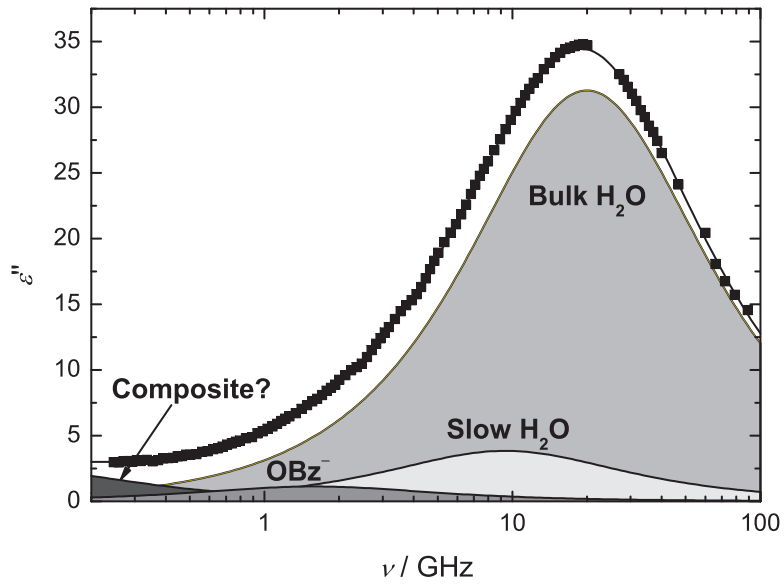

Figure 4.24: Dielectric loss curve of 0.1959 M NaOBz(aq) at 25 °C, showing contributions of the four Debye processes. Symbols represent experimental data, the line through the experimental data represents the D+D+D+D fit, and shaded areas indicate the contributions of the various relaxation modes.

and NaOPe(aq) (Section 4.1) the spectra of NaOBz(aq) show three modes centered at approximately 1, 8 and 20 GHz (Figures 4.23 & 4.24) when fitted with either the D+D+D or D+D+D+D models. As can be seen in Figure 4.24, the additional process in four Debye model is at low frequencies, partially outside our accessible frequency range. Furthermore, this mode shifted towards even lower frequencies (almost outside our frequency range) with increasing c.

The χ^2_r values, representing the overall quality of the fits, of the D+D+D+D model were slightly better than those of the D+D+D model. A physical interpretation of the resolved modes was also possible but the derived dielectric relaxation parameters obtained using that model showed significant scatter as a function of concentration. For this reason and because the χ^2_r values of the D+D+D+D model were only slightly better than those of the D+D+D model, the later was selected for further analysis. For the D+D+D model the derived DR parameters varied smoothly as a function of solute concentration. The fitting parameters so obtained are summarized in Table 4.6. Additionally, DR spectra for NaOBz(aq) at $c < 1$ M were fitted with the three Debye model by fixing the relaxation time of the lowest-frequency mode, τ_1, to the values obtained by the linear extrapolation of τ_1 at $c > 1$ M to $c \to 0$ (Table 4.7).[†] This was required as the results obtained without fixing the relaxation time of this mode showed systematic errors (Section 4.2.4). All dielectric relaxation parameters obtained from the fitting with this 'restricted 3D' model are summarized in Table 4.7.

[†]The relaxation time of the intermediate mode, τ_2, was also held constant during the fitting procedure to reduce the scatter of the corresponding amplitude (Table 4.7).

Table 4.6: Densities, ρ; Electrical Conductivities, κ; Limiting Permittivities, ε_j; Relaxation Times, τ_j; and Reduced Error Function Values, χ^2_r, for NaOBz(aq) at Concentrations, c; and 25 °C assuming a D+D+D model (see text).[a]

c	ρ	κ	ε	τ_1	ε_2	τ_2[b]	ε_3	τ_3	ε_∞	χ^2_r
0[c]			78.37					8.32	3.48	0.048
0.02485	0.9985	0.215	78.43	250	78.15	18.6F	77.46	8.30	5.70	0.051
0.04998	0.9999	0.356	78.34	138	77.77	18.6F	75.99	8.15	5.06	0.041
0.07483	1.0014	0.520	78.42	165	77.54	18.7F	74.30	8.13	5.32	0.045
0.09946	1.0027	0.669	78.48	172	77.29	18.7F	72.97	8.11	5.55	0.024
0.1477	1.0055	0.955	78.42	143	76.64	18.2	70.57	7.97	5.23	0.055
0.1959	1.0081	1.21	78.38	141	76.10	19.5	69.37	8.02	5.52	0.021
0.2916	1.0137	1.72	78.02	117	74.82	19.1F	65.91	8.05	6.02	0.072
0.3857	1.0190	2.16	77.52	113	73.84	19.3F	61.09	7.72	5.47	0.042
0.5659	1.0292	2.90	77.07	106	71.27	19.7	58.57	8.05	6.25	0.074
0.7454	1.0392	3.51	75.76	107	69.17	20.0F	51.68	7.63	5.69	0.043
1.080	1.0576	4.39	73.98	105	64.91	20.6F	45.34	7.70	6.04	0.046
1.693	1.0903	5.32	69.84	113	57.23	21.6	35.82	7.85	6.48	0.054
2.225	1.1174	5.63	65.72	130	51.21	22.8F	27.84	7.21	6.27	0.067
2.473	1.1296	5.64	63.73	134	48.42	23.3	25.90	7.37	6.37	0.063

[a] Units: c in M; ρ in $\mathrm{kg\,L^{-1}}$; κ in $\Omega^{-1}\,\mathrm{m}^{-1}$; τ_j in 10^{-12} s. [b] Parameter values followed by the letter F were held constant during the fitting procedure. [c] Reference 84.

Table 4.7: Limiting Permittivities, ε_j; Relaxation Times, τ_j; and Reduced Error Function Values, χ^2_r, of restricted 3D model for NaOBz(aq) at Low Concentrations, $c \lesssim 0.75\,\mathrm{M}$; and 25 °C [a]

c	ε	τ_1 [b]	ε_2	τ_2 [b]	ε_3	τ_3	ε_∞	χ^2_r
0 [c]	78.37					8.32	3.48	0.048
0.02485	78.34	84F	78.03	15.0F	77.53	8.31	5.71	0.051
0.04998	78.28	84F	77.58	15.0F	75.54	8.14	5.06	0.041
0.07483	78.28	86F	77.19	16.0F	74.16	8.14	5.34	0.046
0.09946	78.27	86F	76.79	16.0F	72.91	8.13	5.59	0.026
0.1477	78.21	87F	76.05	16.0F	70.47	8.00	5.27	0.058
0.1959	78.15	89F	75.36	17.0F	69.28	8.05	5.57	0.026
0.2916	77.83	89F	74.15	17.0F	65.17	8.04	6.04	0.075
0.3857	77.33	91F	73.21	17.5F	59.72	7.65	5.47	0.043
0.5659	76.95	95F	70.70	18.0F	57.30	7.99	6.25	0.074
0.7454	75.63	95F	68.49	18.5F	50.26	7.54	5.68	0.043

[a] Units: c in M; τ_j in 10^{-12} s. [b] Parameter values followed by the letter F were held constant during the fitting procedure. [c] Reference 84.

4.2.2 Relaxation times and assignment of relaxation modes

The DR spectra for NaOBz(aq) were well described by a three-Debye-process (D+D+D) model.

The relaxation time, $\tau_3(c)$ of the highest frequency mode in the DR spectra of NaOBz(aq), centered at ∼20 GHz (Figures 4.23 & 4.24), smoothly extrapolates (Figure 4.25) to the relaxation time of the dominant mode in pure water. Therefore, this process can be unequivocally assigned to the relaxation of the H-bond network[110] in bulk water, *i.e.*, the relaxation of H_2O molecules that, at least at low c, are not significantly influenced by the presence of the solute particles. However, the smooth decrease in τ_b with increasing c (Figure 4.25) indicates that there is **some** influence of the ions on the dynamics of water beyond their hydration shell(s).

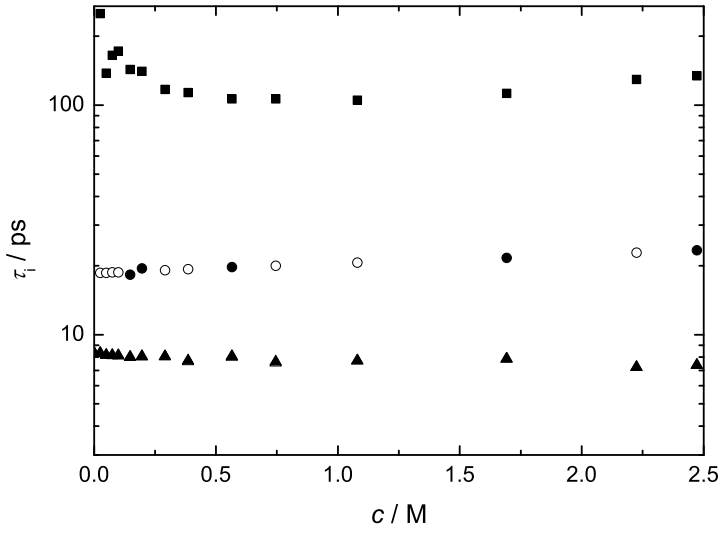

Figure 4.25: Concentration dependence of the solute relaxation time, τ_1 (■); the slow-water relaxation time, τ_s (●); and the bulk-water relaxation time, τ_b (▲) for NaOBz(aq) at 25 °C. Open symbols represent the τ_s values which were held constant during the fitting procedure.

The average relaxation time, τ_s(NaOBz) ≈ 20 ps,[‡] and the spectral position of the intermediate ($j = 2$) process, centered at ∼8 GHz is similar to the "slow-water" relaxation already observed for aqueous solutions of short-chain alkylcarboxylates[106] (Section 4.1) and other salts studied with DRS.[112–114] This intermediate-frequency mode can therefore be assigned to the slow-water relaxation. Similar to that of NaOPr(aq) and NaOBu(aq) (Section 4.1), τ_s for NaOBz(aq) increases slightly with increasing c (Figure 4.25). This increase of τ_s is consistent with the DRS[181] study on aqueous solutions of the amphiphilic TMU.

[‡]Note that the τ_s values for some of the concentrations of NaOBz(aq) were held constant during the fitting procedure to reduce the scatter of the corresponding amplitude.

The slowest ($j = 1$) process centered at ~1 GHz for NaOBz(aq) is similar to that observed for aqueous solutions of NaOPe(aq). The relaxation time τ_1 of this slowest process decreases sharply up to $c \approx 0.5$ M for NaOBz(aq) and then goes through a shallow minimum (Figure 4.25). This behaviour is similar to τ_1(NaPe(aq)). Since OBz^- has a permanent dipole moment, $\mu_- = 9.7$ D (MOPAC), the relaxation at ~1 GHz can reasonably be assigned to the diffusional reorientation of benzoate ions. At $c \lesssim 0.5$ M some contribution from ion-cloud and/or ion-pair relaxations may be present.
Similar to the alkylcarboxylates (Sections 3.1, 3.2, & 4.1) the fast water mode centred at ~400 GHz[110], which is sometimes[112,113] but not always[106,115] detected in aqueous electrolyte solutions, could not be resolved for the present samples although the obtained values of $\varepsilon_\infty \approx 5$ - 6.5 (Table 4.6) suggest its presence.

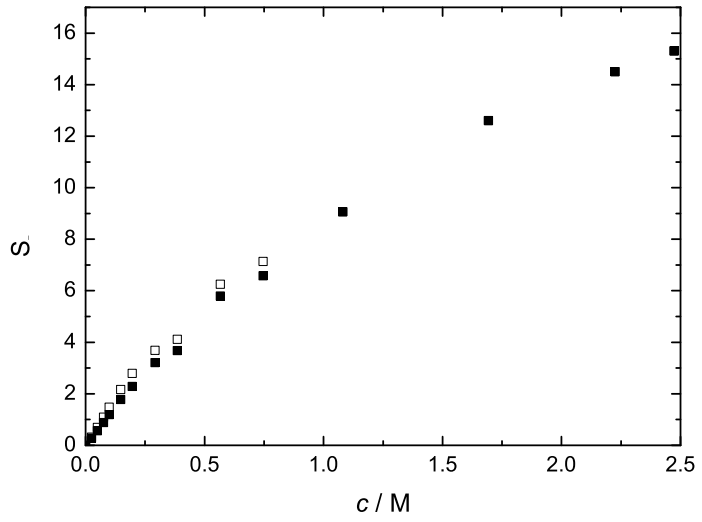

Figure 4.26: Concentration dependence of the solute-relaxation amplitude, S_1, for NaOBz(aq) at 25 °C. Open symbols represent the S_1 values obtained using the fit parameters of restricted 3D fit model.

4.2.3 Solute relaxation amplitude

The solute relaxation amplitude, $S_1 \approx S_-$, for NaOBz(aq) increases linearly with increasing c at $c < 0.5$ M but deviates from linearity at higher concentrations (Figure 4.26). If the ion-cloud and ion-pair relaxations are negligible, this deviation suggests aggregation of the OBz^-. This is confirmed by analysis of S_1 with Eq. 1.71. The effective dipole moment, $\mu_{\mathrm{eff},-}$, so obtained strongly decreases with increasing c (Figure 4.27a). As already described in Section 4.1.3, $\mu_{\mathrm{eff},-}$ is related to the apparent dipole moment of the anion, $\mu_{\mathrm{ap},-}$, via Eq. 4.2. Extrapolation of $\mu_{\mathrm{eff},-}$ to $c \to 0$ yields an apparent dipole moment of the anion of

$\mu_{\mathrm{ap},-} = 11.8\,\mathrm{D}$ (Figure 4.27a), which is somewhat smaller than the solvent phase (apparent) dipole moment value of 14.1 D for OBz^-(aq) obtained from MOPAC. However, the value of $\mu_{\mathrm{ap},-} = 13.8\,\mathrm{D}$ (Figure 4.27a) derived using S_- obtained from the relaxation parameters of restricted 3D model is in excellent agreement with the MOPAC value. This suggests that the restricted 3D model is slightly better than the free three Debye fit model. The good agreement of the experimentally obtained $\mu_{\mathrm{ap},-} = 11.8\,\mathrm{D}$ (from the free three Debye fit model) and $\mu_{\mathrm{ap},-} = 13.8\,\mathrm{D}$ (from the restricted 3D model fit model)(Figure 4.27a) with the MOPAC-calculated value confirms that OBz^- is the dominant contributing species to the slowest-relaxation mode in NaOBz(aq) and our assignment of this mode to OBz^- reorientation is plausible (Section 4.2.2).

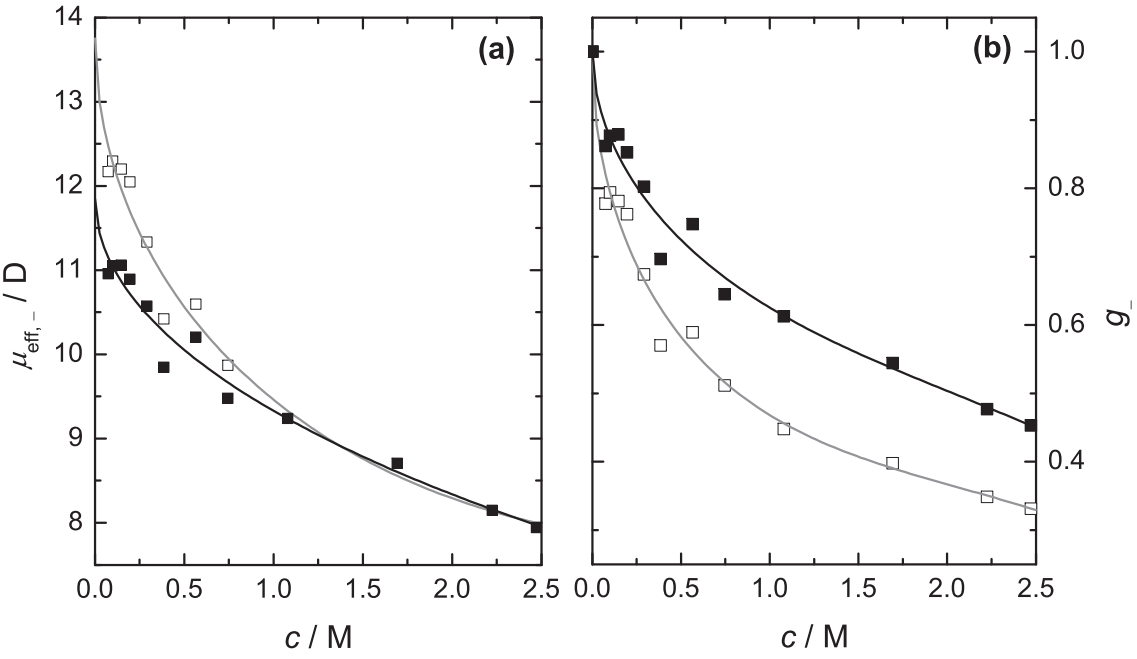

Figure 4.27: Concentration dependence in aqueous solution of NaOBz(aq) at 25 °C of: (**a**) the effective dipole moment of OBz^-(aq), $\mu_{\mathrm{eff},-}$, calculated using the relaxation amplitude, S_1; and (**b**) the correlation factor, g_-, of OBz^-(aq). Open symbols represent the $\mu_{\mathrm{eff},-}$ and g_- values calculated using the fit parameters of restricted 3D fit model. Lines are included as a visual guide only.

The apparent dipole moment for OBz^-, $\mu_{\mathrm{ap},-}$, can be used to estimate the orientational correlation factor, g_-, using Eq. 4.2. The correlation factor so obtained for OBz^-(aq) using both sets of fitting parameters (Tables 4.6 & 4.7) is given in Figure 4.27b. The value of g_- drops remarkably with increasing c for both sets, ultimately reaching the values of ∼0.45 and ∼0.33 at the highest concentration studied, $c = 2.47\,\mathrm{M}$. This suggests that aggregation of amphiphilic dipolar OBz^- in aqueous media increases with increasing solute concentration and that aggregation starts at low c. It also indicates that the alignment of OBz^- ions in aqueous media is antiparallel. This seems realistic since the charged ($-COO^-$) centres would be expected to repel while the alignment of the benzene rings should

be favourable.

4.2.4 Water relaxations and ion hydration

As discussed above, the intermediate ($j = 2$) mode centered at ∼8 GHz and the highest frequency ($j = 3$) mode at ∼20 GHz are assigned to slow water and bulk water, respectively. The amplitude of the slow-water relaxation, $S_s = \varepsilon_2(c) - \varepsilon_3(c)$ increases rapidly with increasing c at $c \lesssim 0.5$ M whereas at $c \gtrsim 0.5$ M, it increases more graduall (Figure 4.28a). However the amplitude of bulk-water relaxation, $S_b = \varepsilon_3(c) - \varepsilon_\infty$, decreases with increasing c (Figure 4.28b). The S_s and S_b values for NaOBz(aq) were used to estimate c_s^{ap} and c_b^{ap}, respectively, via the Cavell equation (Eq. 1.71), as described in Section 3.1.2.

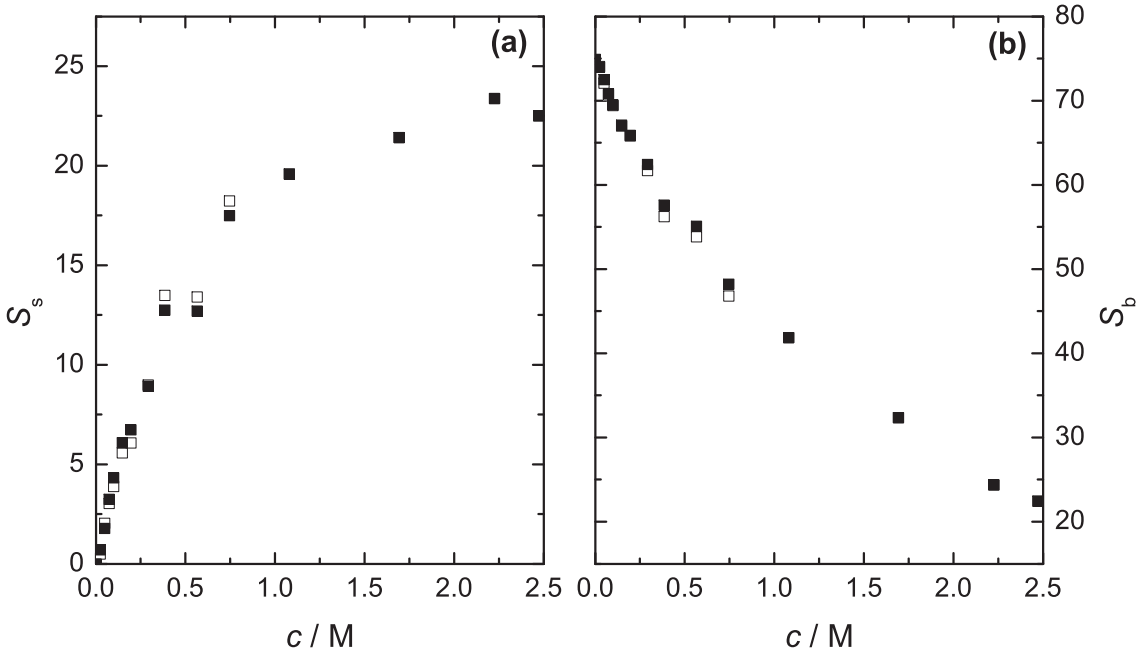

Figure 4.28: Concentration dependence for NaOBz(aq) at 25 °C of (**a**) the slow-water relaxation amplitude, S_s, and (**b**) the bulk-water relaxation amplitude, S_b, . Open symbols represent the relaxation amplitude values obtained using the fit parameters of restricted 3D fit model.

Similar to the alkylcarboxylates (Sections 3.1, 3.2, & 4.1), for NaOBz(aq) the sum of the DRS-detected water ($c_s^{ap} + c_b^{ap}$) is less than the analytical total water concentration, c_w. Water missing from the DR spectrum can be ascribed to the presence of ib water molecules and an effective hydration number, Z_{ib}, can then be determined via Eq. 3.6. The values of $c_s^{ap}(c)$, obtained from S_s via Eq. 1.71, can also be used directly to calculate the effective number of *slow* water molecules, Z_s, via Eq. 3.7.

The Z_{ib} values calculated in this way for NaOBz(aq) at 25 °C (Figure 4.29) were mostly smaller than or, at higher c, equal to $Z_{ib}(Na^+)$,[169] indicating that $Z_{ib} \approx 0$ for OBz^-(aq). The lower values of Z_{ib}(NaOBz), Similar to Z_{ib}(NaOPr) and Z_{ib}(NaOBu) (Section 4.1),

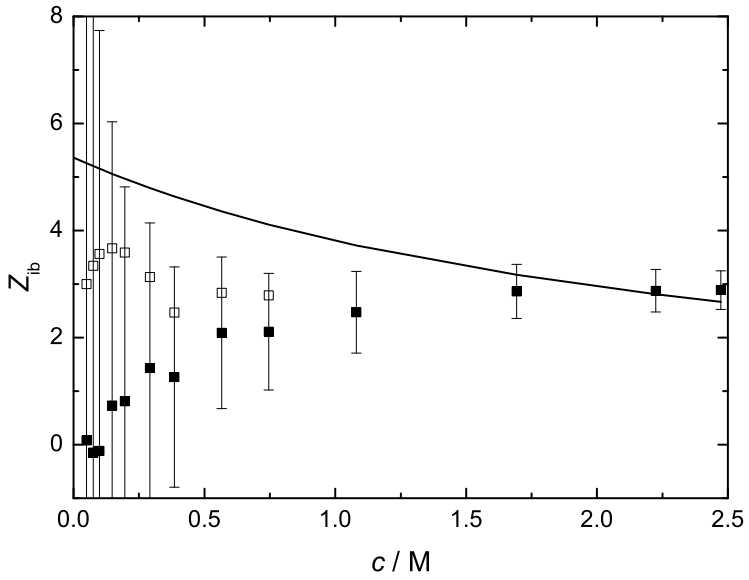

Figure 4.29: Concentration dependence of irrotationally bound water molecules, Z_{ib}, for NaOBz(aq) at 25 °C.[132] Solid line represents $Z_{\mathrm{ib}}(\mathrm{Na}^+)$.[169] Open symbols represent the Z_{ib} values calculated using the relaxation parameters obtained from restricted 3D fit model.

may indicate improper estimation of S_{b} for aqueous solutions of both salts due to overlapping ion-cloud, ion-pair and anion relaxations. As can be seen in Figure 4.29, the $Z_{\mathrm{ib}}(\mathrm{OBz}^-)$ values at $c < 1\,\mathrm{M}$, calculated by using the relaxation parameters obtained by fixing the τ_1 to the values obtained by linear extrapolation of τ_1 values at $c > 1\,\mathrm{M}$, has been improved considerably. This may reflect that the relatively low values for $Z_{\mathrm{ib}}(\mathrm{NaOBz})$ are due to the effects coming from overlapping relaxation modes at lower frequencies.

The effective number of *slow* water molecules, Z_{s}, calculated for NaOBz(aq) with Eq. 3.7 are shown in Figure 4.30. Since aqueous solutions of typical inorganic salts containing sodium ions do not show any slow water process[45,131,133] it is reasonable to assign Z_{s} entirely to OBz^-(aq). At infinite dilution ∼32 water molecules are weakly bound by OBz^-. It is interesting to compare this result with that of the simplest aliphatic alkyl-hydrotrope (NaOPe(aq)). At infinite dilution, $Z_{\mathrm{s}}(\mathrm{OPe}^-) \approx 43$ is larger than corresponding $Z_{\mathrm{s}}(\mathrm{OBz}^-)$ ≈ 32. One of the reasons for this relatively larger $Z_{\mathrm{s}}(\mathrm{OPe}^-)$ may be the larger surface area of OPe^- cf. OBz^-, with MOPAC-calculated values of 144.2 and 138.5 Å^2 respectively.

Figure 4.30 shows that Z_{s} for both OBz^- and OPe^- decreases with increasing c. At $c \lesssim 0.5\,\mathrm{M}$ the decrease of $Z_{\mathrm{s}}(\mathrm{OPe}^-(\mathrm{aq}))$ is more rapid as compared to $Z_{\mathrm{s}}(\mathrm{OBz}^-(\mathrm{aq}))$ however at $c \gtrsim 0.5\,\mathrm{M}$ the the decreasing pattern of Z_{s} for both anions is similar with $Z_{\mathrm{s}}(\mathrm{OPe}^-(\mathrm{aq}))$ slightly larger than $Z_{\mathrm{s}}(\mathrm{OBz}^-(\mathrm{aq}))$. At highest $c \approx 2.5\,\mathrm{M}$ the Z_{s} for both OBz^- and OPe^- tends to approach the $Z_{\mathrm{s}}(-\mathrm{COO}^-) = 5\text{-}6$[106] (Figure 4.30). This indicates that the $-\mathrm{COO}^-$

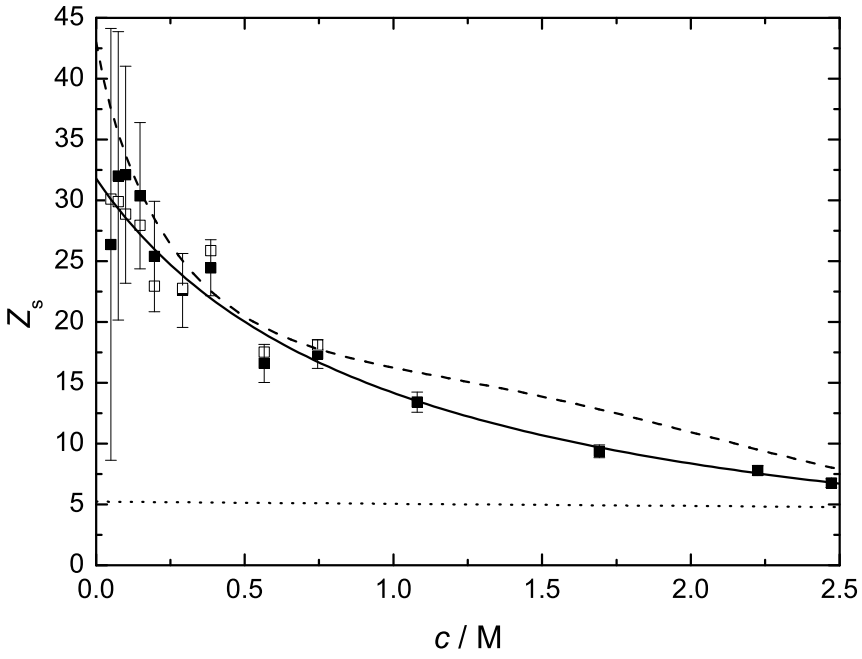

Figure 4.30: Concentration dependence of the slow-water hydration number, Z_s, for OBz^-(aq) in aqueous solution of NaOBz(aq) at 25 °C.[132] The dashed line represents $Z_s(OPe^-)$(aq) and the dotted line represents $Z_t(OFm^-)$(aq). Open symbols represent the Z_s values calculated using the relaxation parameters obtained from restricted 3D fit model.

moiety of the simplest aromatic carboxylate (OBz^-) also retains its hydration shell intact similar to that in the aliphatic alkylcarboxylates (Sections 3.1, 3.2, & 4.1).
As 5-6 *slow* water molecules are bound by the $-COO^-$ (Section 3.1.4),[106] the remaining slow water, $Z_s(-Ph) = Z_s - Z_s(-COO^-)$, is reasonably assigned to water molecules close to hydrophobic moiety (–Ph) of the OBz^-.[106,112,139–141] The "hydrophobic" hydration number for –Ph at $c \to 0$, $Z_s(–Ph) \approx 27$. As can be seen in Figure 4.30, Z_s for benzoate and hence $Z_s(–Ph)$, decreases rapidly with increasing c. However at $c \lesssim 0.5$ M, $Z_s(–Ph)$ in OBz^-(aq) is less rapid than $Z_s(–C_4H_9)$ in OPe^-(aq). This may suggest that aggregation of the hydrophobic $–C_4H_9$ group in OPe^-(aq) is more pronounced as compared to –Ph group in OBz^-(aq).

Chapter 5

Methylsulfate and Methanesulfonate

Long chain alkylsulfates and alkylsulfonates are most commonly used in detergent and soap industry as surface active agents.[15] Organosulfates and sulfonates are also important anionic headgroups in biomolecules[14] where hydrophilic sulfate and sulfonate parts are attached to the hydrophobic organic moiety. Keeping in mind the applications of these potentially important classes of organic compounds, a detailed DRS study of the aqueous solutions of sodium methylsulfate (CH_3OSO_3Na, NaMS) and sodium methanesulfonate (CH_3SO_3Na, NaMSn) is presented in this section. Methylsulfate ($CH_3OSO_3^-$, MS^-) and methanesulfonate ($CH_3SO_3^-$, MSn^-), are the simplest anions of their respective functional groups having both hydrophobic and hydrophilic moieties. Furthermore, a detailed DRS study of Na_2SO_4(aq) is already available in literature,[45] a comparison of hydration and ion-binding of inorganic salt (Na_2SO_4(aq)) with organic salts (NaMS(aq) and NaMSn(aq)) may be interesting.
Aqueous solutions of both salts were investigated up to ∼2.7 M each over the frequency range $0.2 \lesssim \nu/\text{GHz} \leq 89$ at 25 °C. DR spectra over the frequency range $0.2 \lesssim \nu/\text{GHz} \leq 50$ were measured using Agilent E8364B VNA combined with the high temperature probe ($0.2 \lesssim \nu/\text{GHz} \leq 20$) and a waveguide-transmission cell ($27 \lesssim \nu/\text{GHz} \leq 40$); high frequency data were obtained using the E-band interferometer (Section 2.2). To the best of our knowledge this is the first systematic application of DRS to investigate ion-binding and hydration of NaMS(aq)) and NaMSn(aq)).

5.1 Choice of fit model and assignment of relaxation modes

Typical DR spectra obtained for NaMS(aq) and NaMSn(aq) at 25 °C as a function of solute concentration are given in Figures 5.1 and 5.2. As is already observed for the aqueous solutions of amphiphiles (Sections 3.1-4.2), the $\varepsilon''(\nu)$ curves for NaMS(aq) and NaMSn(aq) (Figures 5.1 & 5.2) also show a great decrease in the dominant peak centered at ∼ 18 GHz with increasing solute c. Furthermore, the broadness of that peak increases with increasing solute c.
The combined $\hat{\varepsilon}(\nu)$ data were analyzed using Equation (1.65) according to the procedure

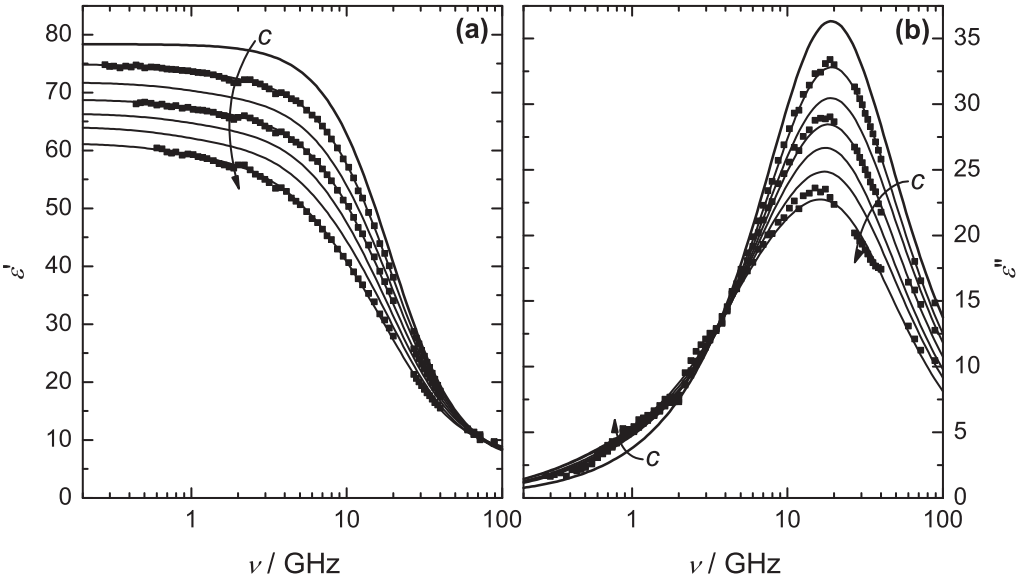

Figure 5.1: Dielectric permittivity (**a**) and loss (**b**) spectra for NaMS(aq) at 25 °C. Arrows indicate increasing concentrations: c / M = 0, 0.5117, 0.9466, 1.352, 1.747, 2.166, and 2.668. Symbols are experimental data (partly omitted for visual clarity); lines represent the D+D+D fit.

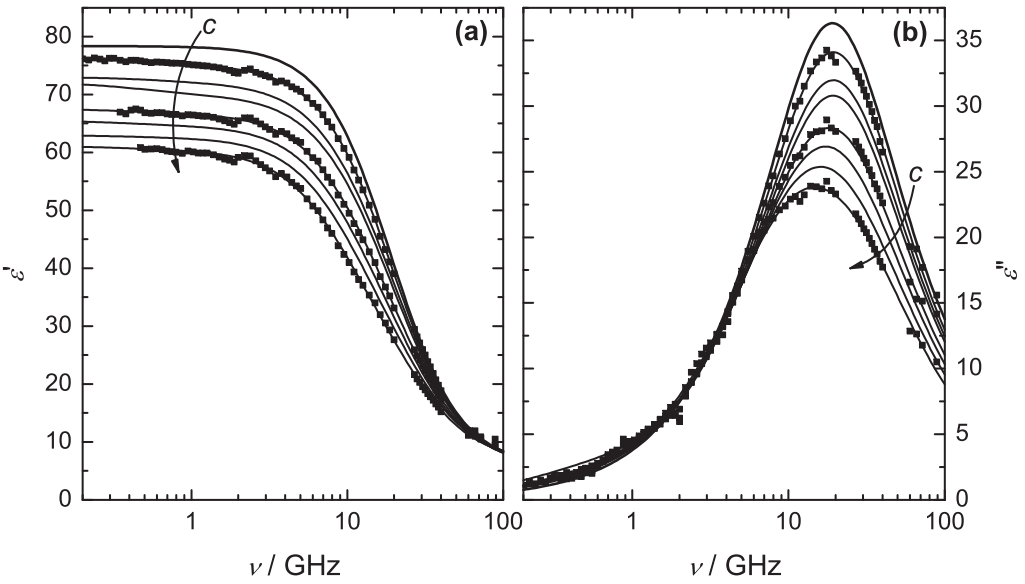

Figure 5.2: Dielectric permittivity (**a**) and loss (**b**) spectra for NaMSn(aq) at 25 °C. Arrows indicate increasing concentrations: c / M = 0, 0.2955, 0.6803, 0.9450, 1.442, 1.815, 2.228, and 2.717. Symbols are experimental data (partly omitted for visual clarity); lines represent the D+D+D fit.

described in detail in Section 2.2.3. The spectra of NaMS(aq) and NaMSn(aq) were best described by a model consisting of three Debye processes. Typical fits obtained with these D+D+D models for NaMS(aq) and NaMSn(aq) are shown in Figures 5.1 - 5.4. All fitting parameters obtained from the present spectra are summarized in Tables 5.1 and 5.2.

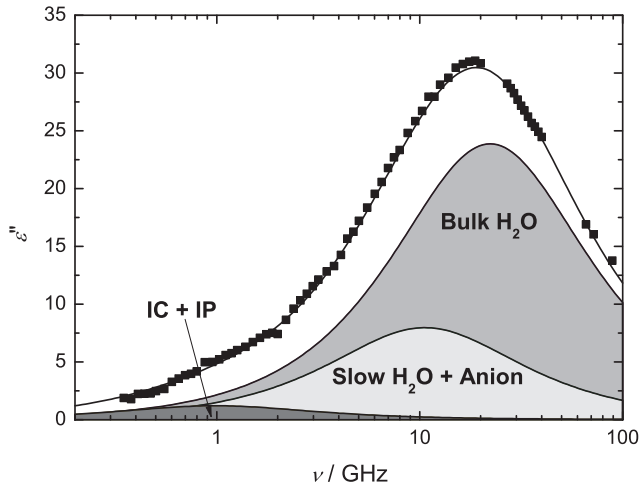

Figure 5.3: Dielectric loss curve of 0.9466 M NaMS(aq) at 25 °C, showing contributions of the three Debye processes. Symbols represent experimental data, lines through the experimental data represent the D+D+D fit, and shaded areas indicate the contributions of the various relaxation modes.

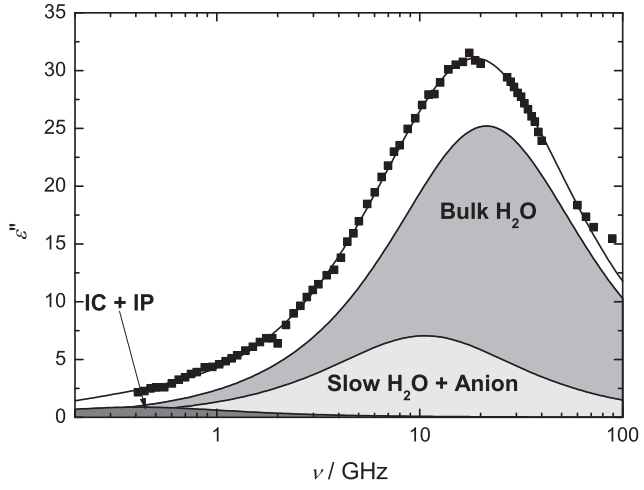

Figure 5.4: Dielectric loss curve of 0.8600 M NaMSn(aq) at 25 °C, showing contributions of the three Debye processes. Symbols represent experimental data, lines through the experimental data represent the D+D+D fit, and shaded areas indicate the contributions of the various relaxation modes.

Table 5.1: Densities, ρ; Electrical Conductivities, κ; Limiting Permittivities, ε_j; Relaxation Times, τ_j; and Reduced Error Function Values, χ^2_r, for NaMS(aq) at Concentrations, c; and 25 °C [a]

c	ρ	κ	ε	τ_1	ε_2	τ_2 [b]	ε_3	τ_3 [b]	ε_∞	χ^2_r
0[c]			78.37					8.32	3.48	0.048
0.04577	1.0006	0.445	78.04	244	77.41	15.0F	75.58	8.11	5.64	0.028
0.05598	1.0013	0.542	77.99	234	77.30	14.7	74.40	8.00F	5.54	0.049
0.07720	1.0030	0.726	77.85	208	76.99	15.0F	74.87	8.08	5.68	0.049
0.09949	1.0047	0.910	77.77	217	76.76	15.0F	73.08	7.94	5.47	0.042
0.1495	1.0085	1.30	77.51	197	76.17	15.0F	71.98	7.90	5.55	0.053
0.1967	1.0121	1.66	77.39	190	75.62	15.0F	71.15	7.90F	5.56	0.052
0.2475	1.0159	2.03	76.85	167	75.11	15.0F	70.21	7.90F	5.68	0.059
0.5117	1.0359	3.77	74.92	148	72.69	15.0F	63.93	7.68	5.80	0.073
0.7137	1.0510	4.95	73.42	154	71.05	15.0F	59.34	7.52	5.93	0.092
0.9466	1.0682	6.08	71.80	166	69.46	16.0F	55.74	7.29	5.81	0.106
1.352	1.0980	7.63	68.83	167	66.52	17.0F	51.52	7.35	6.37	0.125
1.747	1.1263	8.92	66.40	174	63.86	18.7	48.94	7.54	6.88	0.164
2.166	1.1568	9.89	64.10	192	61.35	21.0	45.42	7.42	6.78	0.186
2.529	1.1820	10.3	61.61	190	59.54	23.8	43.82	7.65	7.27	0.179
2.668	1.1917	10.4	61.28	201	58.67	24.2	42.27	7.58	7.34	0.181

[a] Units: c in M; ρ in kg L^{-1}; κ in Ω^{-1} m^{-1}; τ_j in 10^{-12} s. [b] Parameter values followed by the letter F were held constant during the fitting procedure. [c] Reference 84.

DR spectra of aqueous solutions of both salts were further analyzed according to the bias-free fitting procedure published by Zasetzky and Buchner.[91] Typical results of that analysis are shown in Figures 5.5 and 5.6. Presence of three relaxation modes centered approximately at 1, 8, and 20 GHz (Figures 5.3 & 5.4) for both systems was confirmed by that analysis. However, an additional relaxation mode at very high frequencies (Figure 5.5), which was not resolved through our standard fitting procedure, was further resolved for NaMS(aq). This small relaxation mode with relaxation time of 0.813 ps resolved only for NaMS(aq) (Figure 5.5) with bias-free analysis can be attributed to the very fast water process (centred at ~400 GHz[110] for pure water) which is sometimes[112,113] but not always[106,115] detected in aqueous electrolyte solutions. This relaxation mode could not be resolved for aqueous solutions of both NaMS(aq) and NaMSn(aq) using our routine fitting procedure (Section 2.2.3). Nevertheless, similar to the R-COONa(aq) (Sections 3.1, 3.2, 4.1, & 4.2), the fitted values of $\varepsilon_\infty \approx 5.5$-7 (Tables 5.1 & 5.2) are considerably larger than the $\varepsilon_\infty = 3.48$ obtained for pure water for spectra extending to the terahertz region,[84,110] which suggests that the fast water process is still making a minor, if unresolvable, contribution to the present spectra.

Table 5.2: Densities, ρ; Electrical Conductivities, κ; Limiting Permittivities, ε_j; Relaxation Times, τ_j; and Reduced Error Function Values, χ^2_r, for NaMSn(aq) at Concentrations, c; and 25 °C [a]

c	ρ	κ	ε	τ_1	ε_2	τ_2 [b]	ε_3	τ_3 [b]	ε_∞	χ^2_r
0[c]			78.37					8.32	3.48	0.048
0.05243	1.0006	0.450	78.94	462	77.29	15.0F	75.42	8.29	6.32	0.198
0.1015	1.0036	0.781	78.74	407	76.76	15.0F	73.66	8.25	6.49	0.322
0.1966	1.0095	1.42	77.74	299	75.73	15.0F	72.54	8.17	5.84	0.198
0.2955	1.0163	2.04[d]	76.34	275	75.06	15.0F	68.02	7.80	5.70	0.069
0.3894[e]	1.0220	2.59	76.12	254	73.93	15.0F	66.67	7.77F	5.77	0.295
0.4769	1.0271	3.07[d]	74.83	260	73.56	15.0F	64.01	7.70	5.93	0.111
0.5762[e]	1.0330	3.58	74.66	250	72.42	15.0F	62.62	7.54F	5.52	0.377
0.6803	1.0401	4.09[d]	73.00	254	72.03	15.0F	58.12	7.26	5.56	0.126
0.7631[e]	1.0456	4.48	73.20	261	71.05	15.0F	58.80	7.34F	5.76	0.472
0.8600	1.0515	4.91[d]	72.32	387	70.58	15.0F	56.49	7.46	6.10	0.149
0.9450[e]	1.0579	5.26	72.05	334	69.90	15.0F	54.89	7.16F	5.60	0.566
1.442	1.0861	7.05	67.53	392	66.73	14.9	44.08	6.66F	5.85	0.185
1.815	1.1087	8.04[d]	65.49	396	64.63	15.0F	38.78	6.45	6.06	0.156
2.228	1.1332	8.84	62.99	405	62.57	15.4	33.97	6.20F	6.47	0.184
2.717	1.1620	9.46	61.16	449	60.44	17.0	31.55	6.10	6.55	0.169

[a] Units: c in M; ρ in kg L^{-1}; κ in Ω^{-1} m^{-1}; τ_j in 10^{-12} s. [b] Parameter values followed by the letter F were held constant during the fitting procedure. [c] Reference 84. [d] Interpolated using measured data. [e] VNA (0.2-20 GHz) and E-band (60-89 GHz) data only.

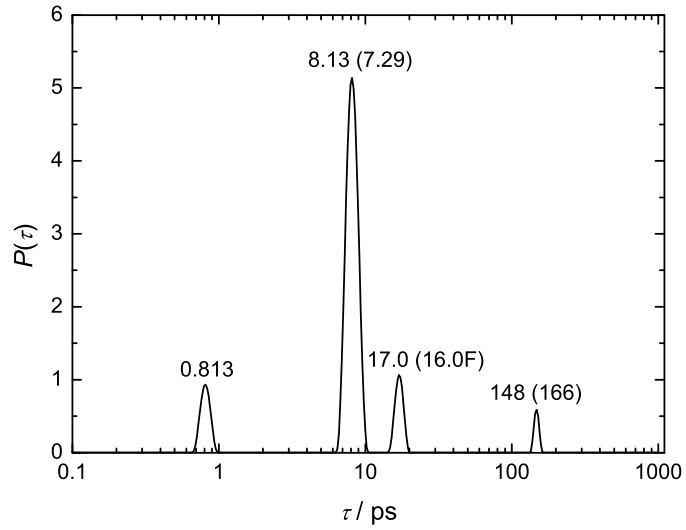

Figure 5.5: Relaxation time distribution function, $P(\tau)$, of 0.9466 M NaMS(aq) at 25 °C obtained with the bias-free fitting procedure of Zasetzky and Buchner.[91] Relaxation times for the resolved modes are indicated together with the corresponding values from Table 5.1 (in brackets; F = fixed).

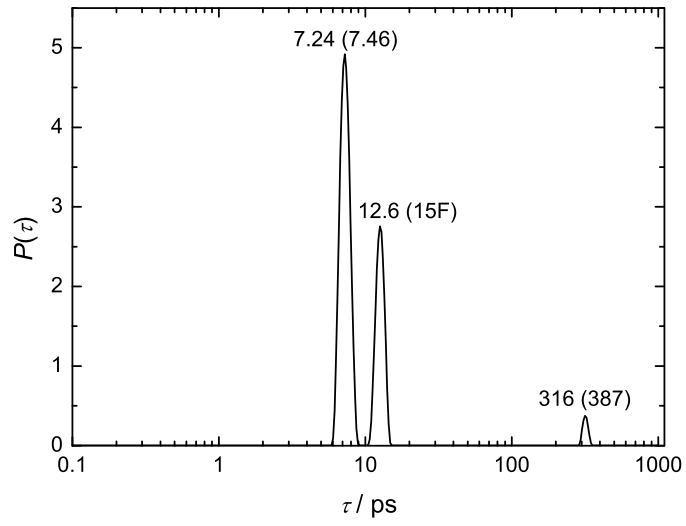

Figure 5.6: Relaxation time distribution function, $P(\tau)$, of 0.8600 M NaMSn(aq) at 25 °C obtained with the bias-free fitting procedure of Zasetzky and Buchner.[91] Relaxation times for the resolved modes are indicated together with the corresponding values from Table 5.2 (in brackets; F = fixed).

The assignment of the highest frequency mode centered at ∼20 GHz (Figures 5.3 & 5.4) in DR spectra of NaMS(aq) and NaMSn(aq) to cooperative relaxation of H-bond network of bulk water is straight forward. The relaxation time, $\tau_3(c) = \tau_b$[195] of this highest frequency mode for NaMS(aq) and NaMSn(aq) decreases with increasing solute c (Figures 5.7 & 5.8). However, the decrease of τ_b with increasing c for NaMSn(aq) is more pronounced as compared to that of NaMS(aq) *e.g.* at highest studied $c \approx 2.7$ M of aqueous solutions of both salts, the decrease of τ_b(NaMSn(aq) is ∼27 % whereas the decrease of τ_b(NaMS(aq) is only ∼9 % as compared to $\tau_b = 8.32$ ps[84] for pure water. This indicates that NaMSn(aq) influences the dynamics of bulk water more than that of NaMS(aq).

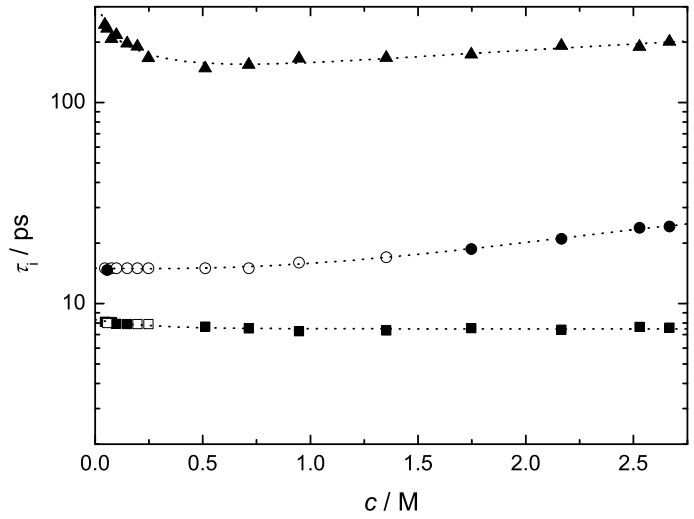

Figure 5.7: Concentration dependence of the solute relaxation time, τ_1 (▲), the composite-mode relaxation time, τ_{comp} (●), and the bulk-water relaxation time, τ_b (■), for NaMS(aq) at 25 °C. Open symbols represent the τ_i values fixed during the fitting procedure.

The average relaxation time[195] of the intermediate ($j = 2$) process, $\tau_2 = \tau_{comp} \approx 16$ ps (Figures 5.3 & 5.4) and the spectral position of this relaxation mode is similar to the "slow-water" relaxation already observed for number of salts studied with DRS.[106,112–114] However, for aqueous Na_2SO_4, an intermediate relaxation process with almost similar relaxation time (25 ps) has been assigned reasonably to the ion pairs.[45] Also, it must be remembered that both MS^- and MSn^- have dipole moments (the gas phase values of μ_- are 3.91 D and 4.65 D respectively).[100] Since DRS is sensitive to all dipolar species,[11] both ions will also contribute to the spectra. As no other separate relaxation process was observed for either anion so it is likely that the relaxation associated with their reorientation, which would be expected to occur at ∼5-10 GHz, is making its presence in the intermediate mode. However, the considerably larger amplitude of the intermediate relaxation mode (cf. estimated relaxation amplitude of both anions via Eq. 1.71, see later) hinders the possibility of assigning this relaxation mode entirely to the anion-reorientation. In light of the above

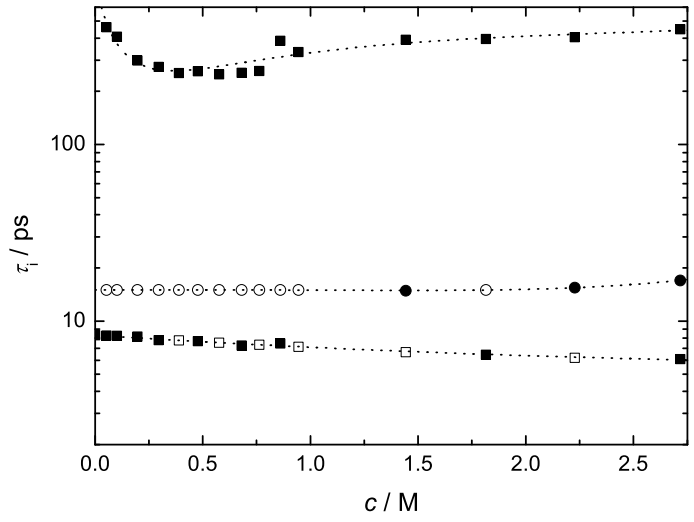

Figure 5.8: Concentration dependence of the solute relaxation time, τ_1 (▲), the composite-mode relaxation time, τ_{comp} (●), and the bulk-water relaxation time, τ_{b} (■), for NaMSn(aq) at 25 °C. Open symbols represent the τ_{i} values fixed during the fitting procedure.

discussion, the intermediate mode can be considered as a composite mode either due to anion-reorientation and slow-water (as for NaOFm(aq), NaOAc(aq) and $NaOAcF_3$(aq), Sections 3.1 & 3.2) or anion-reorientation and ion-pair relaxation. Another possible assumption may be the overlapping of the anion, slow-water and ion-pair relaxations. All the above described possibilities were considered and finally the assumption of overlapping anion and slow-water was found more reasonable, as other assumptions produced unrealistic results *e.g* very high association constants (see later) between sodium and MS^-(aq) and MSn^-(aq) and very large Z_{ib} values (see later) for both anions. Also, it should be kept in mind that the value of $\tau_{\text{comp}} \approx 15 - 24$ ps is considerably smaller than the ion-pair relaxation times (> 80 ps) usually found for aqueous solutions of ion pairs including ions of the size of MS^-(aq) and MSn^-(aq) (see Section 5.3, Table 5.4).

The magnitude of τ_1 (Figures 5.7 & 5.8) of the slowest ($j = 1$) process centered at ∼1 GHz for NaMS(aq) and NaMSn(aq) (Figures 5.3 & 5.4) is in the range typically found for solute relaxation processes. A rapid decrease of τ_1 at $c \lesssim 0.5$ M points at the contribution of ion-cloud relaxation[169,171] which is a generic feature of **all** electrolyte systems. Recent DRS investigations[106,169,196] (Sections 4.1 & 4.2) have also shown that the contribution of ion-cloud relaxation to the low-frequency modes observed in DR spectra of weakly associating electrolytes can not be neglected. However, ion-cloud relaxation cannot be the sole origin of the solute mode as its relaxation time should decrease strongly and monotonically with increasing concentration.[169,171] This is neither the case for NaMS(aq) (Figure 5.7, Table 5.1) nor for NaMSn(aq) (Figure 5.8, Table 5.2). Thus, ion pairs must also contribute to the observed solute relaxation as their relaxation time is expected to be roughly constant

or slightly increasing.[11] In accordance with the above discussion, a rapid decrease of τ_1 at low $c \lesssim 0.5\,\mathrm{M}$ and then a slight increase at $c \gtrsim 0.5\,\mathrm{M}$ (Figures 5.7 & 5.8)indicates that the slowest mode is also a composite mode due to the ion-cloud and ion-pair relaxations.

5.2 Water relaxations and ion hydration

As already described in previous sections, the bulk and fast relaxations for water (at ~20 GHz and ~400 GHz respectively) can be treated collectively by assuming: $S_\mathrm{b} = \varepsilon_3(c) - \varepsilon_\infty$, where S_b is the amplitude of bulk-water relaxation. The value of $\varepsilon_\infty = 3.48$[84] was used for these calculations for the reasons already described previously (Section 3.1.2). As can be seen the magnitude of S_b for NaMS(aq) and NaMSn(aq) exhibits a considerable decrease with increasing c (Figures 5.9 & 5.10). This effect is typical for all electrolyte solutions and its magnitude is specific to the electrolyte/solvent combination. Along with the dilution of solvent dipole density and appearance of the slow-water mode (overlapping with the anion reorientation), the other reason for this significant decrease of the magnitude of S_b for both electrolytes may be the presence of strong ion-solvent interactions resulting in the "freezing" of solvent molecules.[11,45] The S_b values derived from the experimental DR data were further used to estimate the apparent bulk water concentration, c_b^ap, with Cavell equation (Eq. 1.71), as described in Section 3.1.2.

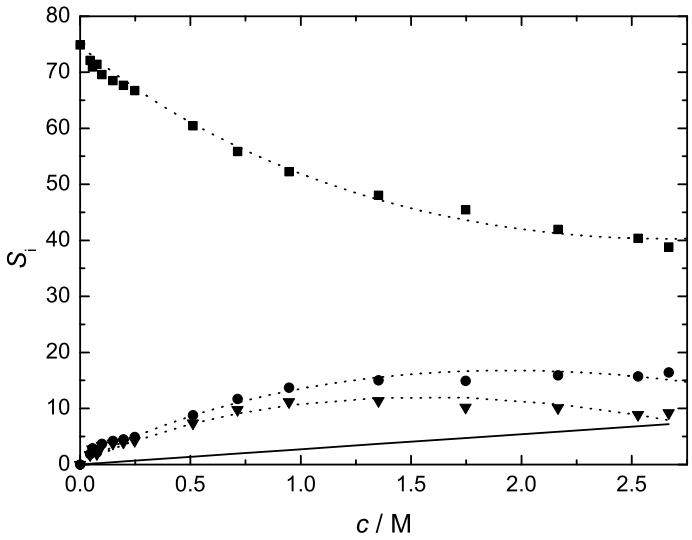

Figure 5.9: Concentration dependence of the relaxation amplitudes of bulk water, S_b (■), the composite mode, $S_\mathrm{s} + S_-$ (●), and slow water, S_s (▼) for NaMS(aq) at 25 °C. The solid line represents S_-, calculated via Eq. 1.71; the dotted lines are included only as a visual guide.

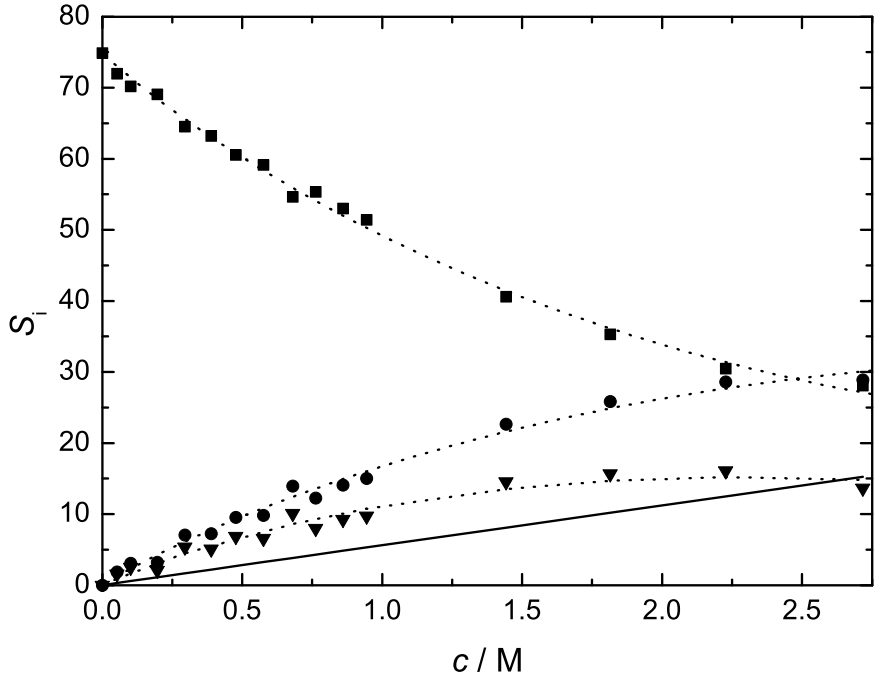

Figure 5.10: Concentration dependence of the relaxation amplitudes of bulk water, S_b (■), the composite mode, $S_\mathrm{s} + S_-$ (●), and slow water, S_s (▼) for NaMSn(aq) at 25 °C. The solid line represents S_-, calculated via Eq. 1.71; the dotted lines are included only as a visual guide.

As discussed above, the intermediate ($j = 2$) relaxation of both (NaMS(aq) and NaMSn(aq)) is a composite mode due to dipolar anions and slow water. The amplitude of composite mode for NaMS(aq) and NaMSn(aq), $S_\mathrm{comp} = S_2 = \varepsilon_2(c) - \varepsilon_3(c)$, initially increases strongly with increasing c but then starts to level off at $c \gtrsim 1\,\mathrm{M}$ (Figures 5.9 & 5.10). Figures 5.9 and 5.10 further reveal that the magnitude of S_comp for NaMSn(aq) is lager than that of S_comp(NaMS(aq)) at all c. One of the reasons for this is the greater anion contribution from MSn^-(aq) to S_comp(NaMSn(aq)), which has a larger dipole moment as compared to MS^-(aq) (see below). Similar to that of NaOFm(aq), NaOAc(aq), and $\mathrm{NaOAcF_3}$(aq) (Sections 3.1 & 3.2), the amplitude S_comp for NaMS(aq) and NaMSn(aq) can be split into its constituent relaxation amplitudes (Eq. 3.4). Since ion pairing is weak for the present systems, the magnitude of S_- for both anions can be obtained from Eq. 1.71 with the effective anion dipole moment, $\mu_-^\mathrm{eff} = \mu_-/(1 - f_-\alpha_-)$, of 5.87 D and 8.47 D for MS^-(aq) and MSn^-(aq) respectively, from MOPAC calculations.[100] This yields the amplitude of slow-water, S_s, via Eq. 3.4 and subsequently the apparent concentration of slow water, $c_\mathrm{s}^\mathrm{ap}(c)$, via Eq. 1.71.

According to the procedure described in detail in previous sections, DRS-detected c_b^ap can

be used to calculate the effective hydration number, Z_{ib}, of ib (frozen on DRS time scale) water molecules via Eq. 3.6. Whereas the values of $c_{\mathrm{s}}^{\mathrm{ap}}(c)$, obtained from S_{s} with Eq. 1.71, can be used directly to calculate the effective number of *slow* water molecules, Z_{s}, via Eq. 3.7.

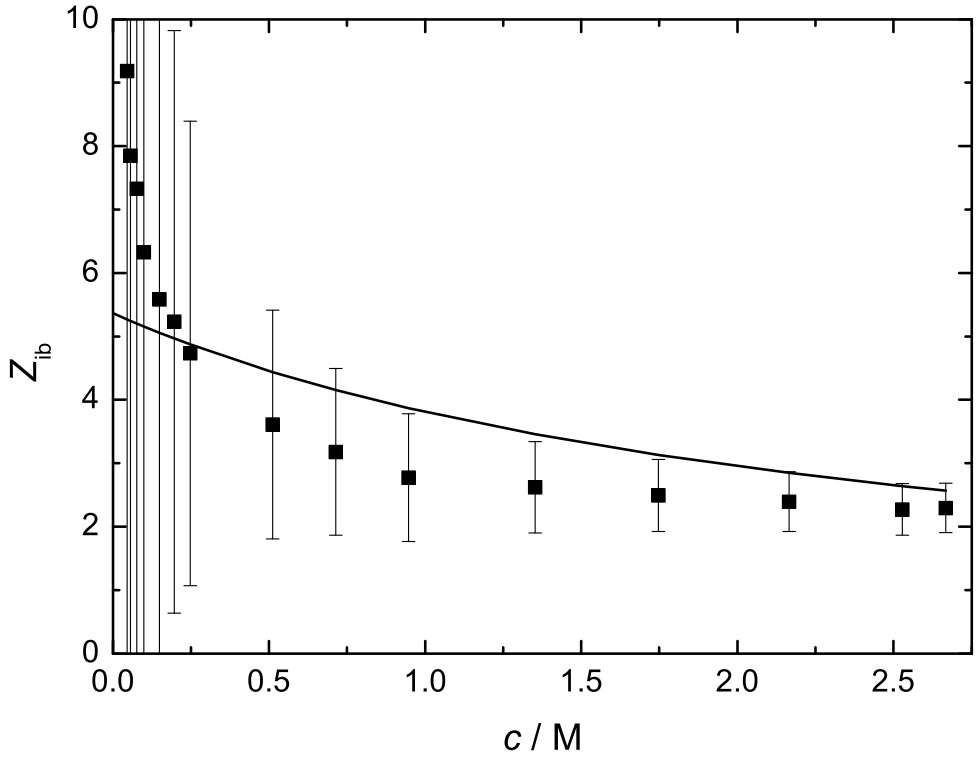

Figure 5.11: Concentration dependence of effective hydration number, Z_{ib}, for NaMS(aq) (■) at 25 °C;[132] the solid line represents $Z_{\mathrm{ib}}(\mathrm{Na}^+)$.[169]

The Z_{ib} values calculated in this way for NaMS(aq) and NaMSn(aq) at 25 °C are shown in Figures 5.11 & 5.12. Figure 5.11 indicates that the Z_{ib} values obtained for NaMS(aq) are either larger (at $c \lesssim 0.2\,\mathrm{M}$) or slightly smaller (at $c \gtrsim 0.5\,\mathrm{M}$) than $Z_{\mathrm{ib}}(\mathrm{Na}^+)$.[169] At low concentrations ($c \lesssim 0.2\,\mathrm{M}$), larger Z_{ib}(NaMS(aq)) values may be due to slight under estimation of S_{b} and consequently over estimation of S_{comp} (Figure 5.9) at those concentrations. Whereas, slightly smaller Z_{ib}(NaMS(aq)) at $c \gtrsim 0.5\,\mathrm{M}$ may represent that the value of μ_-^{eff} of MS^- theoretically calculated via MOPAC is small resulting in the slight over estimation of S_{s}, as a result Z_{ib} is under estimated according to Eq. 3.6. Considering the experimental and analytical limitations, it is reasonable to conclude $Z_{\mathrm{ib}}(\mathrm{MS}^-) \approx 0$. This contradicts clearly with $Z_{\mathrm{ib}}(\mathrm{SO}_4^{2-}) = 10$[45] but is in line with the DRS results of sodium dodecylsulfate (SDS)[197] and more recent choline dodecylsulfate (ChDS),[198] which suggest

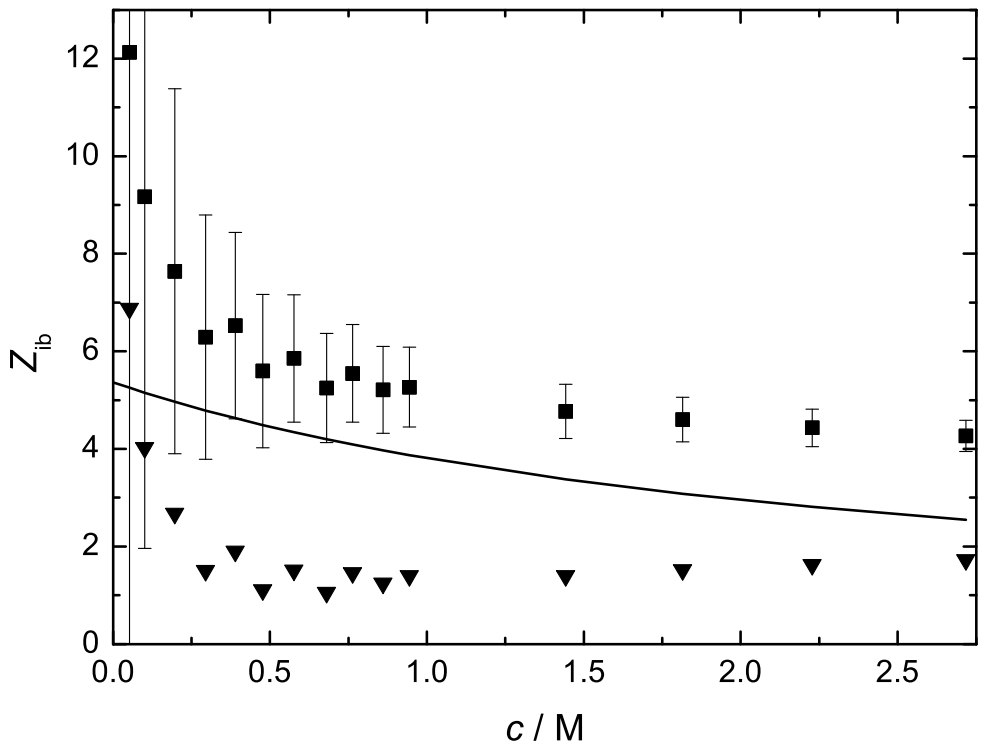

Figure 5.12: Concentration dependence of effective hydration numbers, Z_{ib}, for NaMSn(aq) (■), and MSn^-(aq) (▼) at 25 °C;[132] the solid line represents $Z_{\mathrm{ib}}(Na^+)$.[169]

$Z_{\mathrm{ib}} = 0$ for dodecylsulfate (DS) in aqueous solution. The obtained Z_{ib}(NaMSn(aq)) were also corrected for $Z_{\mathrm{ib}}(Na^+)$[169] to yield the effective number of H_2O molecules "frozen" by the MSn^-(aq), which are also shown in Figure 5.12. Within the investigated concentration range, MSn^-(aq) binds ∼1-2 water molecules strongly. This number is also considerably smaller than $Z_{\mathrm{ib}}(SO_4^{-2}) = 10$ but in line with the reduced charge of MSn^-(aq) and similar to what was found for the carboxylate group (Sections 3.1 & 3.2). Figure 5.13 indicates that the headgroup oxygens of MS^-(aq) are less negative cf. that of MSn^-(aq), which may explain $Z_{\mathrm{ib}}(MS^-(aq)) \approx 0$ cf. $Z_{\mathrm{ib}}(MSn^-(aq)) \approx 1-2$.
The effective number of *slow* water molecules, Z_{s}, calculated for NaMS(aq) and NaMSn(aq) with Eq. 3.7 are shown in Figure 5.14. The noisy and large Z_{s} values at $c \lesssim 0.2$ M are due to, as already described earlier, over estimation of S_{comp} (and consequently S_{s}) at those concentrations. Since aqueous solutions of typical inorganic salts containing sodium ions do not show any slow water process[45,131,133] it is reasonable to assign Z_{s} for NaMS(aq) and NaMSn(aq) entirely to MS^-(aq) and MSn^-(aq). At infinite dilution, the Z_{s} values for MS^-(aq) and MSn^-(aq) are ∼14.4 and ∼10.5, respectively. These Z_{s} values are somewhat

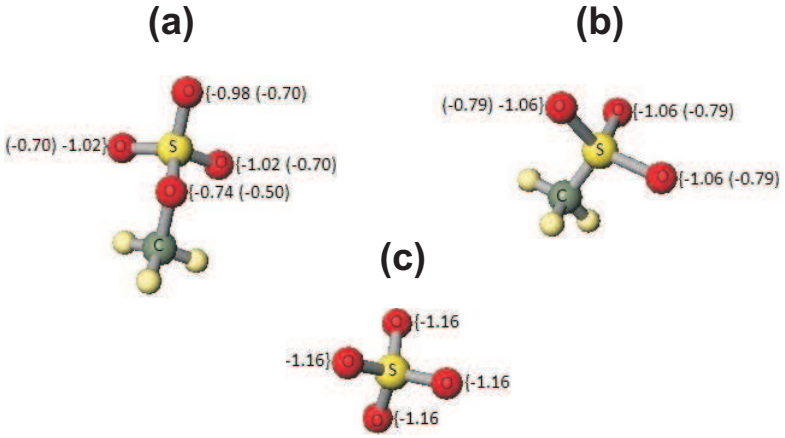

Figure 5.13: Distribution of net-atomic charges on oxygens of (**a**) MS^- (**b**) MSn^- and (**c**) SO_4^{2-} calculated through MOPAC. Values shown in brackets are the calculated CHELPG[199] atomic charges taken from Reference 199.

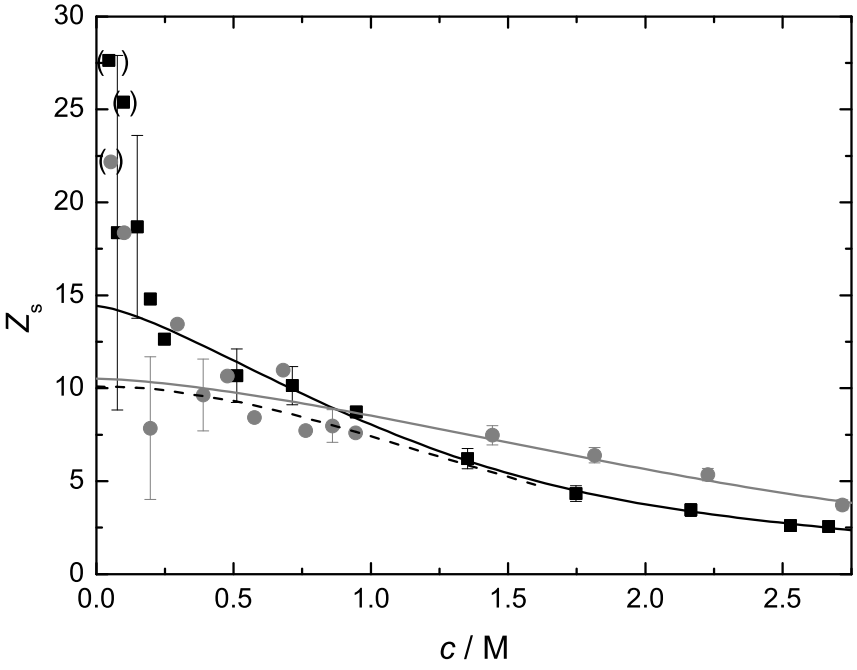

Figure 5.14: Concentration dependence of the slow-water hydration number, Z_s, for MS^-(aq) (■) and MSn^-(aq) (●) in aqueous solutions of their corresponding sodium salts at 25 °C.[132] Dashed line represents $Z_{ib}(SO_4^{2-})$(aq) taken from Reference 45 for comparison. Outliers are bracketed.

smaller than $Z_s(\mathrm{SDS}) = 20$.[197] This can be understood on the basis of larger hydrophobic alkylchain of dodecylsulfate and also larger polar surface area due to SDS micelles. Furthermore, $Z_s(\mathrm{SDS}) = 20$ includes possible contribution from sodium ions bound to the surface of micelles.[197] The Z_s for both MS^-(aq) and MSn^-(aq) decreases with increasing solute c due to hydration shell(s) overlap.

It is interesting to observe that organic anions MS^-(aq) and MSn^-(aq) essentially slow down water molecules in their hydration spheres ($Z_{ib}(MS^-) = 0$, $Z_s(MS^-) = 14.4$ and $Z_{ib}(MSn^-) =$1-2, $Z_s(MSn^-) = 10.5$) in contrast to inorganic SO_4^{2-}(aq) which binds water molecules irrotationally ($Z_{ib}(SO_4^{2-}) = 10$, $Z_s(SO_4^{2-}) = 0$) in its hydration sphere. This remarkable difference of hydration pattern between inorganic (SO_4^{2-}(aq)) and organic (MS^-(aq) and MSn^-(aq)) anions can be explained in terms of reduction of charge on anions (from -2 for SO_4^{2-}(aq) to -1 for MS^- and MSn^-) and difference of charge distribution on oxygens of the anions. Figure 5.13 clearly indicates that presence of $-CH_3$ reduces the charge on headgroup oxygens of MS^-(aq) and MSn^-(aq) as compared to that on SO_4^{2-}(aq) oxygens. As a result of reduced charge the interactions between H_2O molecules and the organic-anions headgroups are not strong enough to irrotationally bind H_2O molecules, as in case of SO_4^{2-}(aq), but are stronger than H_2O-H_2O interactions, resulting in the slow dynamics of water molecules in vicinity of anions.

Figure 5.14 reveals that at $c \lesssim 1$ M, $Z_s(MS^-)$ is larger than $Z_{ib}(SO_4^{2-})$, this may indicate the contribution coming from $-CH_3$ as a result of its hydrophobic hydration, as recently observed through DRS study of OAc^-(aq).[106] With increasing solute c the difference of hydration number between MS^-(aq) and SO_4^{2-}(aq) decreases and at $c \gtrsim 1$ M both anions have same hydration number. This may indicate that hydration of $-CH_3$ is fragile *i.e* decreases rapidly with increasing solute c, again similar to that has been observed for $-CH_3$ moiety of OAc^-(aq).[106] At infinite dilution total hydration number, $Z_t = Z_{ib} + Z_s$, of MS^-(aq) and MSn^-(aq) is ∼14.4 and ∼12.5, respectively. The corresponding Z_t of "slow" water molecules decreases with increasing solute c for both anions. At infinite dilution, $Z_s(-CH_3) \approx 6$[106] is observed for OAc^-(aq). Assuming, same number of water molecules are slowed down by the $-CH_3$ moiety attached to the sulfate and sulfonate headgroups, ∼8.4 and ∼6.5 slow water molecules hydrophilically bind to each headgroup, respectively, can be estimated. However, in order to confirm the contribution of hydrophobic hydration of $-CH_3$ in MS^-(aq) and to estimate its magnitude, DRS study of aqueous sodium hydrogensulfate is highly recommended.

At infinite dilution, $Z_s(MSn^-(aq)) < Z_s(MS^-(aq))$, this is consistent with the relatively larger size and more number of charge centers of MS^-(aq) as compared to MSn^-(aq). Furthermore, it is interesting to observe that hydration of MSn^-(aq) is slightly less fragile as compared to that of MS^-(aq) and SO_4^{2-}(aq) (Figure 5.14).

5.3 Ion association

As already described in Section 5.1, the lowest-frequency process centered at ∼1 GHz, for NaMS(aq) and NaMSn(aq) (Figures 5.3 & 5.4) is a composite mode due to ion-cloud and ion-pair relaxations. The amplitude, S_1, of that relaxation process increases very rapidly at $c \lesssim 0.5$ M for aqueous solutions of both salts (Figure 5.15). However, at $c \gtrsim 0.5$ M, S_1 for NaMs(aq) is essentially constant in contrast to S_1(NaMSn(aq)), which decreases with increasing c (Figure 5.15). This may indicate that at $c \gtrsim 0.5$ M the ion-pair species formed in NaMS(aq) remain stable whereas in NaMSn(aq) these species redissociate.

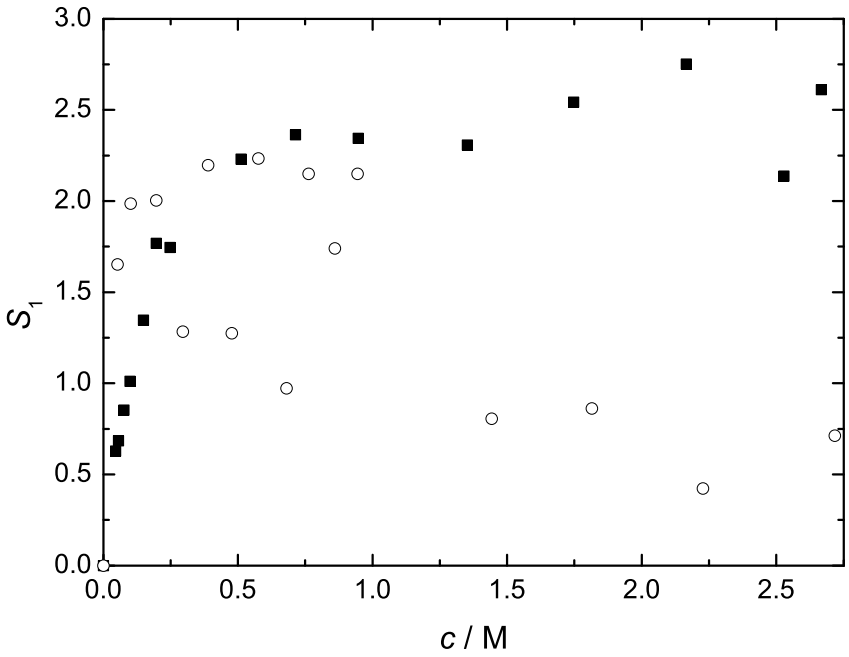

Figure 5.15: Concentration dependence of solute relaxation amplitudes, S_1, for NaMS(aq) (■) and NaMSn(aq) (◯), at 25 °C.

In order to calculate the ion-pair concentrations, c_{IP}, using Eq. 1.71, it is important to separate the contribution of ion-cloud relaxation from S_1. However, independent estimation of the magnitude of ion-cloud relaxation is not possible. Hence, the subsequent analysis of $S_1 \approx S_{\mathrm{IP}} \approx \varepsilon(c) - \varepsilon_2(c)$ was performed under the assumption of negligible ion-cloud relaxation. Thus the associated standard-state association constants, K_{A}°, derived using S_1 according to the standard procedure described previously are an **upper limit** for the degree of ion pairing in NaMS(aq) and NaMSn(aq).
Unfortunately, no independent information on the nature of the ion pairs is available. Thus, S_1 was evaluated assuming that the solute relaxation arises either from CIPs, SIPs, or 2SIPs. The polarizabilities of the different IP types required as input for Eq. 1.71 were

calculated according to the procedure described in Section 3.1.3, using polarizabilities of individual ions and water as: $\alpha/(4\pi\varepsilon_0\,\text{Å}^3) = 0.211$ (Na^+),[66] 4.70 (MS^-),[100] 4.20 (MSn^-),[100] and 1.444 (H_2O).[66] The dipole moments of the various ion-pair types, μ_{IP}, calculated with MOPAC[100] are listed in Table 5.3. From the calculated ion-pair concentrations for the CIP, SIP and 2SIP assumptions, the standard state association constants, K_A°, of Table 5.3 were derived with Eq. 1.91, together with the corresponding B_K and C_K values. Figure 5.16 shows the $K_A(I)$ values obtained with the 2SIP evaluation for NaMS(aq) and NaMSn(aq), as well as the corresponding Guggenheim fits.

Table 5.3: Ion association constants, log K_A°, and related parameters for NaMS(aq) and NaMSn(aq) at 25 °C[a]

Model	μ_{IP}	log K_A°	B_K	C_K
NaMS(aq)				
CIP	10.79	3.11±0.26	-5.53±0.81	2.54±0.47
SIP	25.24	0.99±0.08	-3.31±0.31	1.47±0.19
2SIP	37.29	0.55±0.07	-3.11±0.28	1.37±0.17
NaMSn(aq)				
CIP	5.62	3.10±1.17	-4.02±2.41	1.55±1.26
SIP	18.14	1.16±0.20	-3.24±0.57	1.29±0.33
2SIP	30.02	0.52±0.17	-2.85±0.48	1.10±0.28

[a] Ion-Pair Dipole Moments, μ_{IP}; and resulting parameters B_K and C_K of Eq 1.91. Units: μ_{IP} in Debye (1 D = 3.3356×10^{-30} C·m), B_K in L·mol^{-1}, C_K in L$^{3/2}$·mol$^{-3/2}$.

No experimental K_A° value is available for association between Na^+ and both anions (MS^-(aq) and MS^-(aq)) in aqueous media. However, a combined MD and *ab initio* study[25] has revealed that Na^+ prefers OAc^-(aq) over MS^-(aq) and MSn^-(aq) for ion-binding. These findings were also consistent with the "law of matching water affinities" proposed by Collins.[23,24] As recent DRS results which are supported by other experimental and simulation methods (for details see Section 3.1) have shown that the association between Na^+(aq) and OAc^-(aq) is very weak, this predicts very weak association between Na^+(aq) and MS^-(aq) and MS^-(aq) also. The formation of CIPs can be neglected in accordance with the above made discussion as calculation assuming CIP model has produced very high K_A° values (Table 5.3) for NaMS(aq) and NaMSn(aq). To help to establish which IP types are present in aqueous solution of NaMS and NaMSn, it was useful to compare the experimental τ'_{IP} with estimated τ', calculated according to the procedure described in detail in Section 3.1.3 for NaOAc(aq). Present DRS data also definitely rule out CIPs for NaMS(aq) and NaMSn(aq) because the estimated rotational correlation time, τ', is far too short compared to the experimental value, τ'_{IP} (Table 5.4).
According to the data of Table 5.4 the 2SIP is the most probable type of ion pair present

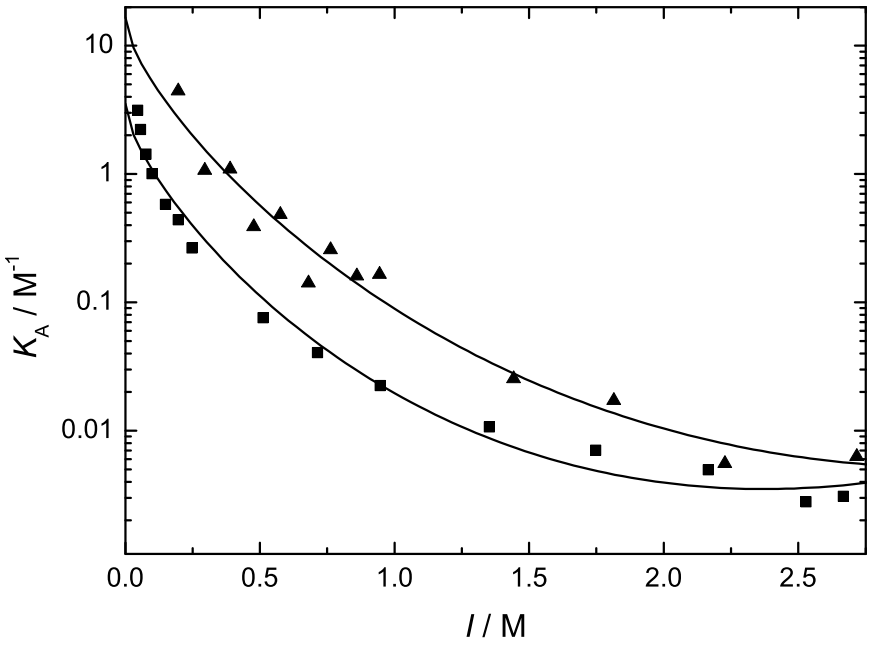

Figure 5.16: Ion association constants, K_A, for NaMS(aq) (■) and NaMSn(aq) (▲) as a function of nominal ionic strength, I, at 25 °C. The K_A values were calculated from the solute relaxation amplitude, S_1, under the assumption that 2SIPs predominate. Also included (lines) are the fits of K_A with Eq. 1.91. For clarity values of K_A for NaMSn(aq) are multiplied by 5.

Table 5.4: Comparison of Experimental, τ'_{IP},[a] and Calculated, τ'_{slip} and τ'_{stick},[b] Rotational Correlation Times for *Stick* and *Slip* Boundary Conditions for Ion-Pair Reorientation in Aqueous Solutions of NaMS(aq) and NaMSn(aq) at 25 °C.[c]

electrolyte	τ'_{IP}	IP	τ'_{slip}	τ'_{stick}
NaMS	130	CIP	26.7	99.3
		SIP	74.8	161
		2SIP	144	242
NaMSn	232	CIP	15.4	78.1
		SIP	47.7	121
		2SIP	103	188

[a] Obtained via Powles-Glarum relation (Eq. 1.85). [b] Averaged values obtained from SED relation (Eq. 1.80). [c] Unit: τ_i in ps.

in NaMS(aq) and NaMSn(aq). This assignment is supported by the strong hydration of Na^+ and of sulfate and sulfonate groups, see Section 5.2. Accordingly, keeping in mind the likely contribution of ion-cloud relaxation to the solute amplitude, we can give upper limit of $K^\circ_{\mathrm{A}}(\mathrm{NaMS(aq)}) \approx 3.5\,\mathrm{M}^{-1}$ and $K^\circ_{\mathrm{A}}(\mathrm{NaMSn(aq)}) \approx 3.3\,\mathrm{M}^{-1}$ for the association constant of aqueous sodium methylsulfate and methanesulfonate and postulate 2SIPs as the dominating ion-pair species at all c.

Summary and conclusions

The present thesis deals with the first systematic broadband DRS study into the hydration of organic anions and provides very useful information relevant for the understanding of water-biomolecule interactions. Carboxylate, sulfate and sulfonate groups were studied as representatives of hydrophilic headgroups of biomolecules. Hydrophobic hydration was studied by systematically varying the alkyl moiety of $RCOO^-$. Effect of different hydrophobic entities attached to the biomolecules was investigated by studying fluorinated and aromatic carboxylates.

Small Alkylcarboxylates

The DR spectra at $0.2 \lesssim \nu/\mathrm{GHz} \leq 89$ have shown that OFm^-, OAc^- and $OAcF_3^-$ are moderately well hydrated in aqueous solution. However, unlike simple inorganic ions such as CO_3^{2-}, which "freeze" (irrotationally bind) water molecules, these carboxylate ions essentially just slow down the dynamics of the water molecules in their first hydration shell, with only 1 or 2 water molecules becoming completely immobilized on the DRS timescale. The much larger number of 'slow' water molecules around each anion arises from two sources: **hydrophilic** interaction with the $-COO^-$ moiety and **hydrophobic** hydration of the $-CH_3$ and $-CF_3$ group. The corresponding hydration number, Z_s, of slow water molecules can be split into a contribution arising from the hydrophilic hydration of the carboxylate moiety, $Z_\mathrm{s}(-COO^-) \approx 4-5$, and a remainder, $Z_\mathrm{s}(-R)$, associated with the hydration of the hydrophobic moiety. The latter scales with the size of –R ($Z_\mathrm{s}(-H) \approx 0$,[106] $Z_\mathrm{s}(-CH_3) \approx 6$ & $Z_\mathrm{s}(-CF_3) \approx 15$ at $c \to 0$). The total hydration number of the carboxylate group, $Z_\mathrm{t}(-COO^-) = Z_\mathrm{s}(-COO^-) + Z_\mathrm{ib}(-COO^-) \approx 5-6$, appears to be rather independent of salt concentration and of the attached substituent, –R (at least within the series NaOFm, NaOAc, $NaOAcF_3$). On the other hand the hydration shell around the hydrophobic moiety is rather fragile, *i.e.*, strongly decreases with increasing c.
For NaOAc(aq) the activation enthalpy and entropy of the bulk-water relaxation suggested major changes in structure and dynamics. Possibly, this is due to the formation of isolated bulk water pools with restricted H-bonding confined to the interstices remaining between the hydrated ions at high solute concentrations.
The association between Na^+ and $-COO^-$ (OFm^-, OAc^- and $OAcF_3^-$) in aqueous media is very weak. The observed solute relaxation is almost certainly a composite mode of ion-pair reorientation and ion-cloud relaxation. Analysis of the data revealed that the water-mediated interaction between Na^+ and $-COO^-$ favors the formation of 2SIPs for NaOAc(aq) and $NaOAcF_3$(aq). Accurate determination of association constant was not

possible because of the unknown magnitude of ion-cloud relaxation[169] but an upper limit of $K_A^\circ(\mathrm{NaOAc(aq)}) \lesssim 1.5\,\mathrm{M}^{-1}$ and $K_A^\circ(\mathrm{NaOAcF_3(aq)}) \lesssim 1.7\,\mathrm{M}^{-1}$ could be obtained.

Amphiphilic Carboxylates

The DR spectra at $0.2 \lesssim \nu/\mathrm{GHz} \leq 89$ have revealed that OPr^-, OBu^-, OPe^- and OBz^- ions slow down the dynamics of surrounding water molecules in their aqueous solutions. The dynamics of water molecules in the hydration shell(s) of these anions was ∼2-3 times slower cf. bulk water. The number of 'slow' water molecules was found to increase with increasing size of the hydrophobic entity (–R). Similar to that for OAc^- and OAcF_3^-, the number of slow water molecules around each anion arises from both hydrophilic interaction with the $–\mathrm{COO}^-$ group and hydrophobic hydration of the –R moiety. The total hydration number of $–\mathrm{COO}^-$, $Z_t(-\mathrm{COO}^-) \approx 5-6$, remained largely unaffected by solute concentration while the –R moiety dehydrated markedly with increasing c. At infinite dilution approximately 6-10 slow water molecules are hydrophobically bound by each $–\mathrm{CH}_3$ or $–\mathrm{CH}_2–$ group in alkylcarboxylates. In case of OBz^- at $c \to 0$, ∼27 slow water molecules are bound by the –R (= –Ph) group.

Amplitudes related to the slow-water relaxation process, and the corresponding $Z_s(c)$ values calculated from them for OPr^-(aq) and OBu^-(aq) hint at some aggregation of these anions at higher c. Aggregation of OPe^-(aq) and OBz^-(aq) is much more pronounced and starts at much lower concentrations as indicated by $Z_s(c)$ of these anions. Aggregation of OPe^-(aq) and OBz^-(aq) is further confirmed by the strong decrease in the dipole-dipole correlation factor, g, of these anions with increasing c.

For NaOPr(aq) and NaOBu(aq) at $c \lesssim 1\,\mathrm{M}$ the observed solute relaxation mode is a composite of anion and ion-pair reorientation and ion-cloud relaxation. For NaOPe(aq) and NaOBz(aq), however, the observed solute relaxation is mostly due to anion reorientation. Because of the unknown magnitude of ion-cloud relaxation[169], similar to that of OAc^- and OAcF_3^-, an upper limit of $K_A^\circ(\mathrm{NaOPr}) < 30\,\mathrm{M}^{-1}$ and $K_A^\circ(\mathrm{NaOBu}) < 32\,\mathrm{M}^{-1}$ assuming the formation of 2SIP has been estimated. Somewhat larger values of K_A° in aqueous solution for both salts as compared to $K_A^\circ(\mathrm{NaOAc}) \lesssim 1.5\,\mathrm{M}^{-1}$ (Section 3.1.3) and $K_A^\circ(\mathrm{NaOAcF_3}) \lesssim 1.7\,\mathrm{M}^{-1}$ (Section 3.2.3) may indicate a relatively higher contribution from ion-cloud relaxation for these salt solutions.

Methylsulfate and Methanesulfonate

The present DR study has shown that MS^-(aq) and MSn^-(aq) are considerably hydrated in aqueous solution. However, the hydration of both organic anions (MS^-(aq) and MSn^-(aq)) is different from that of inorganic SO_4^{2-}(aq), which "freezes" (irrotationally binds) water molecules in its hydration shell(s). Methylsulfate and methanesulfonate essentially slow down the dynamics of water molecules in their hydration shell(s), with only 1 or 2 water molecules becoming completely immobilized on the DRS timescale in case of MSn^-(aq) and non for MS^-(aq). The reduction of charge on anion (from -2 for SO_4^{2-}(aq) to -1 for MS^- and MSn^-) is probably the reason for this different hydration behaviour of organic anions cf. inorganic SO_4^{2-}(aq). At infinite dilution total hydration number, Z_t, of MS^-(aq)

and MSn^-(aq) is ∼14.4 and ∼12.5, respectively. The corresponding Z_t for both anions decreases with increasing solute c. At infinite dilution, $Z_s(-CH_3) \approx 6$ [106] is observed for OAc^-(aq). Assuming same number of water molecules are slowed down by $-CH_3$ moiety attached to sulfate and sulfonate headgroups, ∼8.4 and ∼6.5 slow water molecules can be estimated around each headgroup, respectively.

The observed solute relaxation at ∼1 GHz is a composite mode of ion-pair reorientation and ion-cloud relaxation. Analysis of the data revealed that the water-mediated interaction between Na^+ and the charged headgroups of both anions favors the formation of 2SIPs for NaMS(aq) and NaMSn(aq). The upper limit of $K_A^\circ(\mathrm{NaMS(aq)}) \lesssim 3.5\,M^{-1}$ and $K_A^\circ(\mathrm{NaMSn(aq)}) \lesssim 3.3\,M^{-1}$, assuming no ion-cloud relaxation [169] indicates that the association between Na^+ and MS^- and MSn^- in aqueous solution is very weak.

Appendix

A.1 Dielectric data of aqueous sodium chloride

Since suitable data for $Z_{\mathrm{ib}}(\mathrm{Na}^+)$ at 15 °C were not available, the DR spectra of NaCl(aq) were recorded at this temperature in the frequency range $0.2 \leq \nu/\mathrm{GHz} \leq 50$ and analysed with Eq. 1.71. Also, the existing literature DR data for NaCl(aq)[123] at 25 °C and 35 °C were reanalysed with Eq. 1.71 to get $Z_{\mathrm{ib}}(\mathrm{Na}^+)$ at these temperatures.
Following pages provide the recorded DR spectra of NaCl(aq) at 15 °C along with the fit parameters and $Z_{\mathrm{ib}}(\mathrm{Na}^+)$ from reanalysed data at 25 °C and 35 °C.

Table A.1: Electrical Conductivities, κ; Limiting Permittivities, ε_j; Relaxation Time, τ; and Reduced Error Function Values, χ^2_r, for NaCl(aq) at Concentrations, c; and 15 °C[a]

c	κ[b]	ε	τ	α	ε_∞	χ^2_r
0[c]		82.03	10.8		3.66	0.056
0.06975	0.610	80.86	10.9	0	6.11	0.032
0.1139	0.973	80.20	10.8	0	6.08	0.048
0.2722	2.21	77.93	10.7	0	6.54	0.092
0.5226	4.03	74.81	10.4	0	6.91	0.141
0.7567	5.62	72.03	10.4	0	7.24	0.155
0.9999	7.16	69.50	10.3	0	7.84	0.150
1.894	12.1	60.99	9.52	0.042	6.28	0.171
2.819	16.0	53.71	8.98	0.057	6.07	0.275
3.263	17.5	50.48	8.92	0.062	6.62	0.312
3.681	18.8	47.49	8.73	0.074	6.87	0.265
4.121	19.9	45.13	8.70	0.084	7.03	0.271

[a] Units: c in M, κ in $\Omega^{-1}\,m^{-1}$; τ in 10^{-12} s.
[b] κ interpolated from literature data[123] at different temperatures. [c] Reference 84.

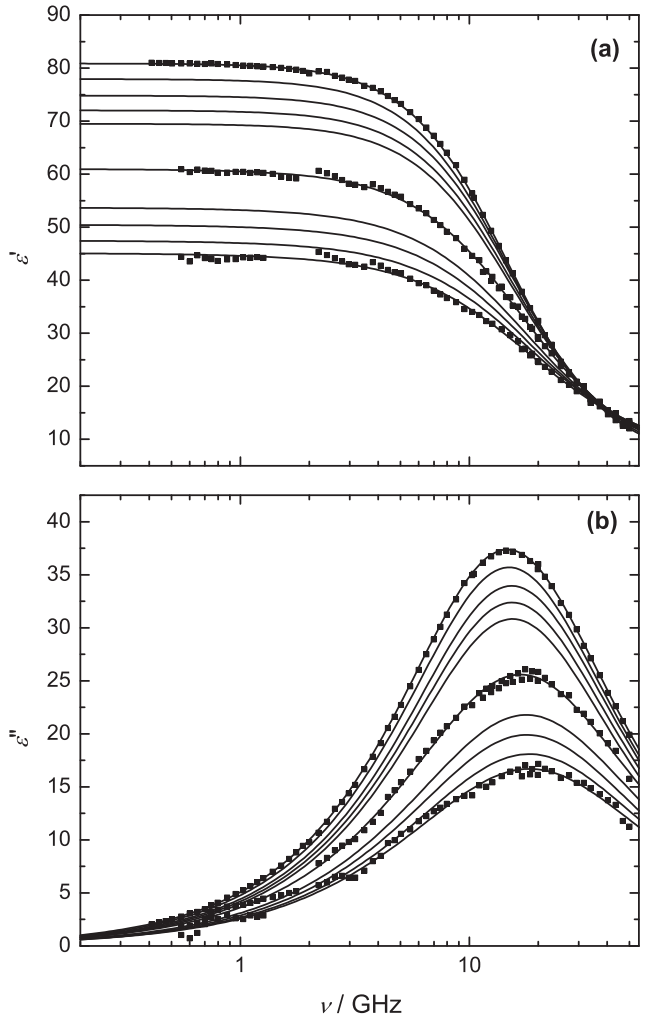

Figure A.1: Permittivity, $\varepsilon'(\nu)$ (**a**), and dielectric loss, $\varepsilon''(\nu)$ (**b**), spectra for NaCl(aq) at 15 °C and concentrations c/M = 0.06975, 0.2722, 0.5226, 0.7567, 0.9999, 1.894, 2.819, 3.263, 3.681, and 4.121 (top to bottom). Symbols show experimental data (others are omitted for visual clarity); lines represent either the D or CC fits.

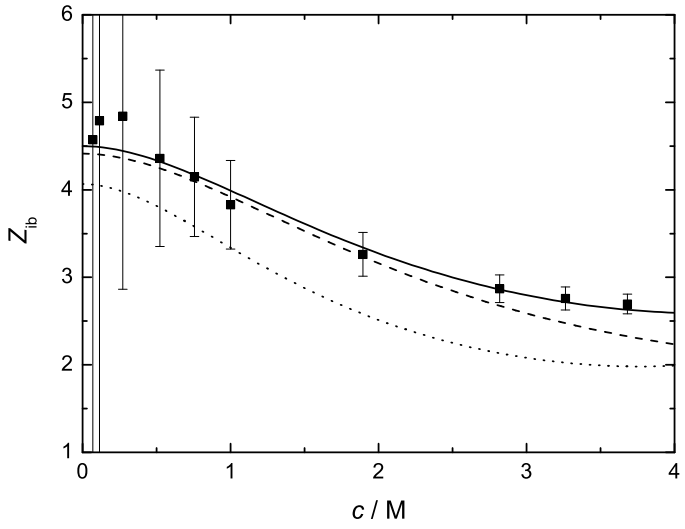

Figure A.2: Concentration dependence of the effective hydration number, Z_{ib}, of NaCl(aq) [$= Z_{\mathrm{ib}}(\mathrm{Na}^+)$] at 15 °C (solid line, ■), 25 °C (dashed line), and 35 °C (dotted line).

The effective cation hydration numbers in Figure A.2 can be expressed as $Z_{\mathrm{ib}}(\mathrm{Na}^+) = 1/(a_0 + a_1 c^2 + a_2 c^{5/2})$ with empirical parameters given in Table A.2.

Table A.2: Empirical Parameters, a_j, and fit standard error, $\mathrm{r}^2_{\mathrm{fit}}$, for $Z_{\mathrm{ib}}(\mathrm{Na}^+)$ at temperatures, t [a]

t	a_0	a_1	a_2	$\mathrm{r}^2_{\mathrm{fit}}$
15	0.2223±0.0054	0.0465±0.0060	-0.0181±0.0030	0.9773
25	0.2266±0.0064	0.0433±0.0064	-0.0148±0.0031	0.9500
35	0.2460±0.0089	0.0910±0.0141	-0.0375±0.0077	0.9318

[a] Units: t in °C; a_1 in $\mathrm{L}^2\ \mathrm{mol}^{-2}$; a_2 in $\mathrm{L}^{5/2}\ \mathrm{mol}^{-5/2}$.

A.2 DRS of aqueous solutions of rubidium fluoride

The following pages give a reprint of the paper

Fedotova, M. V; Kruchinin, S. E; Rahman, H. M. A; Buchner, R. *'Features of Ion Hydration and Association in Aqueous Rubidium Fluoride Solutions at Ambient Conditions.' J. Mol. Liq.* **2011**, *159*, 9.

This work was done in collaboration with M. V. Fedotova and S. E. Kruchinin during the time period of present PhD thesis as a side project. I was mainly involved in recording the DR spectra of aqueous solutions of rubidium fluoride at $0.2 \lesssim \nu/\mathrm{GHz} \leq 89$. DRS results of that study were presented (as poster) at "8$^{\mathrm{th}}$ International and 20$^{\mathrm{th}}$ National Chemistry conference" held in Islamabad/Pakistan on 15$^{\mathrm{th}}$-17$^{\mathrm{th}}$ February, 2010.

Journal of Molecular Liquids 159 (2011) 9–17

Contents lists available at ScienceDirect

Journal of Molecular Liquids

journal homepage: www.elsevier.com/locate/molliq

Features of ion hydration and association in aqueous rubidium fluoride solutions at ambient conditions

M.V. Fedotova [a,b,*], S.E. Kruchinin [a], H.M.A. Rahman [c], R. Buchner [c,*]

[a] Institute of Solution Chemistry, Russian Academy of Sciences, Academicheskaya st., 1, Ivanovo, Russia
[b] Ivanovo State University, Ermak st., 39, Ivanovo, Russia
[c] Institut für Physikalische und Theoretische Chemie, Universität Regensburg, D-93040 Regensburg, Germany

ARTICLE INFO

Available online 24 April 2010

Keywords:
Electrolytes
Ion hydration
Ion association
Dielectric relaxation spectroscopy
Integral equation method

ABSTRACT

Aqueous RbF solutions have been investigated at ambient conditions by dielectric relaxation spectroscopy (DRS) over the concentration range of $0 \le c/M \le 5$ and by statistical mechanics (RISM integral equation theory) in the concentration range of 2.15–9.18 M. The behavior of the dielectric spectra and their characteristic parameters (dispersion amplitudes and relaxation times) is discussed, as well as the pair correlation functions and partial coordination numbers derived from statistical mechanics. The paper focuses on the influence of salt concentration on the features of ion hydration and association. The observed changes in the dielectric properties indicate a decrease of the effective hydration number from ~15–18 at infinite dilution to ~3.5 at 5 M and possibly weak association involving stable ion pairs at $c \le 0.5$ M. A major finding is that both ions, Rb^+ and F^-, slow down surrounding water molecules, leading to the emergence of a separate "slow water" relaxation in the spectra. According to the analysis of RISM equilibrium properties, an average number of ~6 water molecules coordinates both Rb^+ and F^- at $c = 2.15$ M. This number decreases by ~19% for the cation and by ~10% for the anion as c growths up to 9.18 M. The RISM-data indicate a significant increase in the number of contact and solvent-separated ion pairs with increasing c. The possibility of ion clustering is discussed for concentrated RbF(aq) solutions.

1. Introduction

The properties of aqueous electrolyte solutions are strongly influenced by ion type and concentration and knowledge of the properties of the hydration shells surrounding the ions provides essential information needed to understand the origin of their rich and varied behavior. However, even for solutions of simple electrolytes, like alkali halides, information on their structural features is still limited. This especially concerns solutions of rubidium salts. For instance, structural data for RbF(aq) – the subject of the present study – are absent so far. One likely reason for the lack of information on rubidium salt solutions is the common assumption that the properties of Rb^+ should be rather similar to Cs^+ so that it suffices to study the latter. However, also the instability of the structures formed by Rb^+ ions and a number of experimental complications, with X-ray diffraction studies in particular [1], hamper the investigation of rubidium salt solutions.

Available literature data reveal a significant spread in the characteristics of the hydration-shell structure around the rubidium ion (see reviews [1–5]). According to various studies at ambient conditions, the coordination number (CN) of this cation varies from 3.5, obtained with NMR [6], up to 7–8, determined by X-ray and neutron diffraction [7] and anomalous X-ray diffraction [8]. Reported average Rb–O distances vary from 0.288 nm (EXAFS [9]) to 0.320 nm (neutron diffraction [10]). The situation is similarly unsatisfactory for the fluoride ion. According to various literature sources, this anion can hydrate from 4 (X-ray diffraction [11]) to 6.8 (MD simulation [12]) water molecules in the first hydration shell, with average F–O distances from 0.254 nm (neutron diffraction [13]) to 0.292 nm (X-ray diffraction [14]). This means that at present no adequate models for the hydration-shell structures of rubidium and fluoride ions are available. Note also that these models will depend on salt concentration as the coordination of the ions in concentrated solutions should differ from that in dilute solutions.

The rubidium ion has a large radius, $r_+ = 0.149$ nm [15], thus a low surface charge density and a rather high first-shell coordination number. The inference from many studies at ambient conditions clearly characterizes Rb^+ as a "structure-breaking" ion, *i.e.* as an ion which would distort the hydrogen bonded network of neighbouring water molecules by breaking some of their H-bonds [5,16–18]. This contrasts the F^- anion, which has a somewhat smaller radius, $r_- = 0.133$ nm [15], thus a higher surface charge density, and which additionally forms strong hydrogen bonds with H_2O. F^- is

* Corresponding authors. Fedotova is to be contacted at Institute of Solution Chemistry, Russian Academy of Sciences, Academicheskaya st., 1, Ivanovo, Russia.
E-mail addresses: mvf@isuct.ru (M.V. Fedotova), Richard.Buchner@chemie.uni-regensburg.de (R. Buchner).

0167-7322/$ – see front matter © 2010 Elsevier B.V. All rights reserved.
doi:10.1016/j.molliq.2010.04.009

considered to be a “structure maker” [13,16] or a "borderline ion" [5]. Since cations and anions are simultaneously present in solution and each of them influences the surrounding water structure according to their individual properties, the net impact on water structure in this combination of “structure-making” and “structure-breaking” ions for RbF will depend on the relative strength of H_2O–H_2O, Rb^+–H_2O and F^-–H_2O interactions. Obviously, the total effect will grow with salt concentration and change its quality as the hydration shells of cations and anions overlap and ion–ion interactions become important. Correspondingly, the physical and chemical properties of the solutions will change.

In this paper we use dielectric relaxation spectroscopy (DRS) and statistical mechanics, namely the integral equation method in the RISM-approach, to study at 25 °C how some of the dynamic and equilibrium properties of RbF(aq) change as the ion concentration increases. Varying the salt concentration in the range of $0 \le c/\mathrm{M} \le 5$ for DRS (limited by excessive conductivity) and up to 9.18 M in the RISM calculations helps to spot trends in terms of structural changes arising from the increasing solute to solvent ratio. We will focus our discussion on features of ion hydration and ion association as these processes play an important role in various natural phenomena and technologies.

Dielectric relaxation spectroscopy monitors fluctuations of the macroscopic dipole moment of the sample in terms of the complex permittivity spectrum, $\varepsilon^*(\nu) = \varepsilon'(\nu) - i\varepsilon''(\nu)$, with $\varepsilon'(\nu)$ being the relative permittivity and $\varepsilon''(\nu)$ is the associated dielectric loss at frequency ν [19]. DRS has proven to be a valuable tool in the investigation of electrolyte solutions as it allows to monitor the dynamics of the H-bond network of water, to determine effective hydration numbers indicative for the balance of ion–solvent *vs.* water–water interactions, and to detect ion pairs provided their lifetime is at least in the order of their rotational correlation time [20]. A weakness of DRS is, however, that only effects of the salt can be determined but not directly the contributions from the individual ions.

The advantage of statistical mechanics within the framework of RISM theory is that the obtained intermolecular correlations can be split into individual components via atom–atom pair correlation functions. This allows to evaluate the contributions from individual interparticle interactions to the structural changes in the system [21], yielding thus information on ion hydration and ion association phenomena at a molecular level. This is illustrated for the present system by recent publications where RISM theory has been successfully used to calculate the hydration free energies of Rb^+ and F^- [22,23].

2. Experimental and data analysis

Solutions were prepared by weight without buoyancy corrections from deionized water (Millipore™) and RbF (Alfa Aesar, 99.7%) dried for 4 days under vacuum at ~100 °C. Densities of the solutions, required to calculate their molar concentration, c, were determined with a vibrating-tube densimeter (DMA 60 and DMA 601 HT) at (298.15 ± 0.02) K. The instrument was calibrated with degassed water and purified nitrogen at atmospheric pressure assuming densities from standard sources [24].

Dielectric spectra were recorded at $\nu_{\min} \le \nu \le 89$ GHz using a waveguide interferometer for 60–89 GHz [25] and two reflection probe heads, covering 0.2–20 GHz and 1–50 GHz, in conjunction with an Agilent E8364B vector network analyzer (VNA) and a corresponding ECal module. Calibration of the VNA-based spectrometer followed the method described in Ref. [26]. Depending on the dc conductivity, κ, $\nu_{\min}$ varied between 0.2 GHz for dilute solutions and ~2 GHz at the highest concentration. All dielectric measurements were performed at (298.15 ± 0.05) K. The dc conductivity required to correct the experimentally accessible total loss of the sample, $\eta''(\nu) = \varepsilon''(\nu) + \kappa/(2\pi\nu\varepsilon_0)$ (ε_0 is the permittivity of vacuum), was obtained from the plateau value reached for $2\pi\nu\varepsilon_0\eta''(\nu)$ at low frequencies. Typical spectra for $\varepsilon^*(\nu)$ are shown in Fig. 1.

For their formal description the spectra were fitted to many conceivable relaxation models based on sums of n distinct relaxation processes, testing various band-shape functions for the individual modes j [20]. It was found that the spectra for $c > 0.8$ M were best described by a sum of $n = 2$ Debye-type relaxations (the 2D model),

$$\varepsilon^*(\nu) = \varepsilon_\infty + \sum_{j=1}^{n} \frac{\varepsilon_j - \varepsilon_{j+1}}{1 + i2\pi\nu\tau_j}, \quad (1)$$

whereas for lower concentrations the assumption of an additional low-frequency Debye mode ($n = 3$, the 3D model) yielded slightly better fits as indicated by the value for the normalized error function, χ^2. In Eq. (1) $\varepsilon_\infty = \varepsilon_{n+1}$ is the high-frequency limiting permittivity, $S_j = \varepsilon_j - \varepsilon_{j+1}$ is the amplitude (relaxation strength) of mode j with relaxation time τ_j. The values obtained for the fit parameters, together with χ^2, are summarized in Table 1; typical fits are shown in Fig. 2.

3. Calculation methods

For the theoretical study of the features of ion hydration and ion association in solutions with high salt concentration we used the integral equation method within the framework of the Reference Interaction Site Model with hypernetted chain closure (extended RISM or XRISM) [27,28]. Here we present only a brief outline of RISM theory because its basic concepts were explained in detail in Refs. [29–31]. The central idea, originally formulated by Chandler and Andersen [32], is the inclusion of intramolecular correlation functions in the

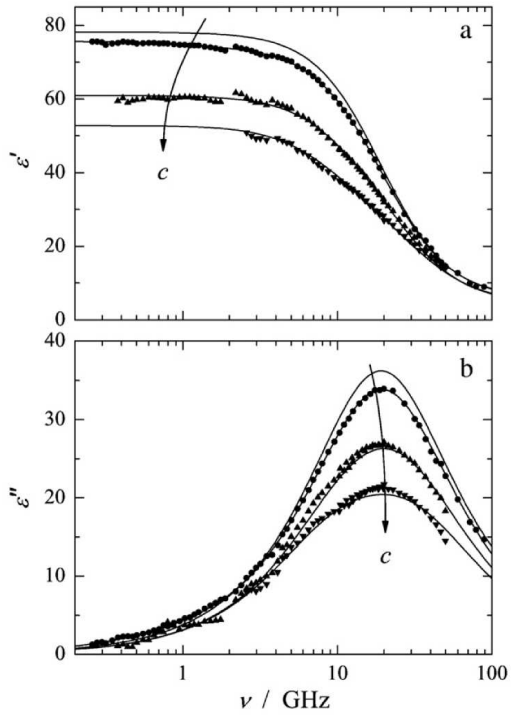

Fig. 1. Spectra of (a) the relative permittivity, $\varepsilon'(\nu)$, and (b) the associated dielectric loss, $\varepsilon''(\nu)$, of aqueous RbF solutions at 25 °C and salt concentrations of $c = 0$, 0.40 M, 2.12 M, and 4.93 M increasing in arrow direction. Symbols indicate experimental data, the lines were calculated with Eq. (1) from the parameters of Table 1.

Table 1
Limiting permittivities, ε_j, relaxation times, τ_j, and associated values for the reduced error function, χ^2, for aqueous RbF solutions of molar concentration, c, at 25 °C. Parameter values followed by the letter "F" were not adjusted during the fitting procedure.

c/M	ε_1	τ_1/ps	ε_2	τ_2/ps	ε_3	τ_3/ps	ε_∞	χ^2
0.1014	77.73	246	76.89	13.5F	75.31	8.22	5.98	0.042
0.1999	76.98	224	76.07	13.5F	71.83	8.05	4.87	0.177
0.3022	76.33	181	75.09	13.5F	69.26	7.92	5.94	0.054
0.4002	75.73	182	74.27	12.1	65.22	7.8F	5.94	0.069
0.4914	74.43	237	73.62	13.5F	62.98	7.58	4.77	0.186
0.5952	74.09	184	72.96	14.2	62.64	7.59	6.08	0.140
0.7332	73.06	179	71.93	12.2	57.29	7.5F	6.05	0.138
0.9754	69.86		69.86	13.5F	52.31	6.92	4.65	0.228
1.5496	66.67		66.67	13.1	46.18	6.77	6.26	0.252
2.1226	60.94		60.94	13.5F	39.79	6.11	4.53	0.48
2.9090	56.37		56.37	13.5F	34.96	5.88	5.61	0.59
4.9347	52.81		52.81	16.6	31.12	5.04	4.61	0.43

Ornstein–Zernike equation for multicomponent systems. For convenience, a multicomponent multiatomic system is divided into groups of atoms (sites) rigidly bound with each other. RISM then calculates site–site pair correlation functions (PCF) via the site–site Ornstein–Zernike (SSOZ) integral equation using interaction potentials which are the sum of spherically symmetric site–site potentials. This model provides a description of molecular and ion-molecular liquids in terms of statistically averaged site–site PCFs. These PCFs are an effective tool to study the molecular behavior of fluids as they relate the microscopic structure of the fluid to its macroscopic thermodynamic properties. A detailed introduction into the concepts and examples for the application of this theory to various chemical and biological systems can be found in a recent textbook by Hirata [31].

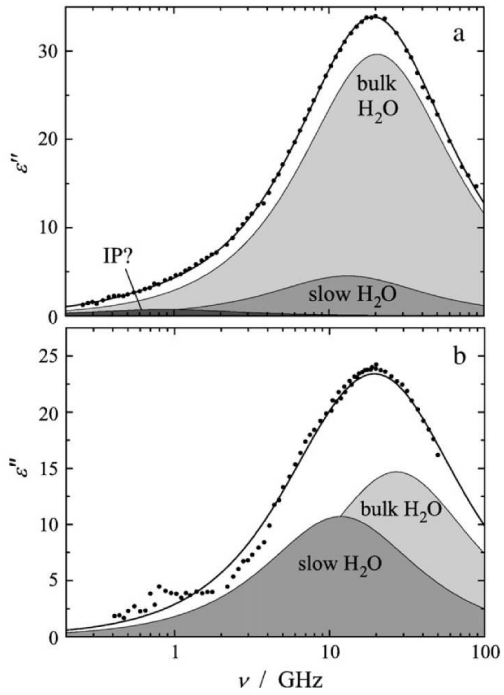

Fig. 2. Spectra of the dielectric loss, $\varepsilon''(\nu)$, of (a) 0.40 M and (b) 2.91 M aqueous RbF solutions at 25 °C (symbols) together with their fit curves calculated with Eq. (1) from the parameters of Table 1. The shaded areas indicate the contributions of the resolved modes.

The SSOZ integral equation is [32]

$$\hat{h}(k) = \hat{s}(k)*\hat{c}(k)*\hat{s}(k) + \hat{s}(k)*\hat{c}(k)\,\hat{h}(k), \tag{2}$$

where the symbol (*) denotes a matrix multiplication (further on omitted in formulas (2)–(4) for brevity); a caret (^) denotes the Fourier transform of a function. In formula (2) $\hat{h}(k)$, $\hat{c}(k)$ and $\hat{s}(k)$ are matrices with elements:

$$\hat{h}^{xy}_{\alpha\beta}(k) = \frac{4\pi}{k}\sqrt{\rho_x\rho_y}\int_0^\infty r\,dr\,h^{xy}_{\alpha\beta}(r)\sin(kr),$$

$$\hat{c}^{xy}_{\alpha\beta}(k) = \frac{4\pi}{k}\sqrt{\rho_x\rho_y}\int_0^\infty r\,dr\,c^{xy}_{\alpha\beta}(r)\sin(kr),$$

$$\hat{s}^{xy}_{\alpha\beta}(k) = \delta_{xy}\left[\delta_{\alpha\beta} + \left(1-\delta_{\alpha\beta}\right)\frac{\sin\left(kl^x_{\alpha\beta}\right)}{kl^x_{\alpha\beta}}\right],$$

where x and y are the species of the particles, α and β are the labels for their molecular sites, $h^{xy}_{\alpha\beta}(r)$ and $c^{xy}_{\alpha\beta}(r)$ are the total and direct site–site correlation functions of sites α and β belonging to the molecules x and y, ρ_x is the number density of molecules of type x, $l^x_{\alpha\beta}$ is the intramolecular distance between sites α and β on the same molecule x, $\delta_{\alpha\beta}$ is the Kronecker delta, δ_{xy} is the Dirac delta function.

For the case of ion-molecular systems Eq. (2) is separated into three equations for $\hat{h}_{ww}(k)$, $\hat{h}_{iw}(k)$ and $\hat{h}_{ii}(k)$, the solvent–solvent, solvent–solute and solute–solute correlations function matrices, respectively:

$$\rho_w\hat{h}_{ww}(k) = \hat{s}_w(k)\hat{c}_{ww}(k)\hat{s}_w(k) + \rho_w\hat{s}_w(k)\hat{c}_{ww}(k)\hat{h}_{ww}(k) + \rho_i\hat{s}_w(k)\hat{c}_{wi}(k)\hat{h}_{iw}(k), \tag{3}$$

$$\hat{h}_{iw}(k) = \hat{c}_{iw}(k)\hat{s}_w(k) + \rho_w\hat{c}_{iw}(k)\hat{h}_{ww}(k) + \rho_i\hat{c}_{ii}(k)\hat{h}_{iw}(k), \tag{4}$$

$$\hat{h}_{ii}(k) = \hat{c}_{ii}(k) + \rho_w\hat{c}_{iw}(k)\hat{h}_{wi}(k) + \rho_i\hat{c}_{ii}(k)\hat{h}_{ii}(k), \tag{5}$$

where ρ_w and $\hat{s}_w(k)$ refer only to the solvent (for $\rho_i \to 0$ the set of coupled integral equations for an infinitely diluted solution is obtained). Since each site may carry a charge, it is most convenient to represent these equations in renormalized form and then use a closure which takes advantage of this renormalization. The details for this procedure used by us previously can be found in Refs. [32–34].

The closure used for Eqs. (3)–(5) was the hypernetted chain (HNC) closure:

$$h^{xy}_{\alpha\beta}(r) + 1 \equiv g^{xy}_{\alpha\beta}(r) = \exp\left\{-\beta U^{xy}_{\alpha\beta}(r) + h^{xy}_{\alpha\beta}(r) - c^{xy}_{\alpha\beta}(r)\right\}. \tag{6}$$

Here $\beta = 1/k_BT$ (k_B is Boltzmann's constant, T is the absolute temperature), $g^{xy}_{\alpha\beta}(r)$ is the PCF, $U^{xy}_{\alpha\beta}(r)$ is the potential of interaction defined by

$$U^{xy}_{\alpha\beta}(r) = \varphi^{xy}_{\alpha\beta}(r) + \Phi^{xy}_{\alpha\beta}(r), \tag{7}$$

where $\varphi^{xy}_{\alpha\beta}(r)$ and $\Phi^{xy}_{\alpha\beta}(r)$ are short- and long-range parts of site–site interactions, respectively.

We sequentially solved Eqs. (3)–(5) with the closure relation (6) following the numerical procedure given in Ref. [35]. However, for some electrolyte concentrations the simple Picard iteration seems to work better than the combination of Newton–Raphson method with direct iterations proposed in Ref. [35]. The method of Ng [36] for long-range interactions was applied to avoid divergence when numerically solving the SSOZ integral equation.

The SPC (Simple Point Charge) model for water [37] in the modified version of Ref. [38] was used to account for water–water interparticle interactions. Ion–water interactions were described by sum of Coulomb and Lennard-Jones terms. The parameters for the latter were taken from Refs. [39,40]. The interionic potential was represented by the Huggins–Mayer form

$$U_{ij}(r) = \frac{q_i q_j}{r} + B_{ij} e^{-r/\rho_{ij}} - \frac{C_{ij}}{r6}, \quad (8)$$

where q_i is the charge of ion i; the parameters B, C, and ρ are those of Fumi and Tosi [41]. The densities of the studied RbF(aq) solutions, required as input for the calculations, were taken from Ref. [42].

In addition to pair correlation functions, solution structure is also expressed in partial coordination numbers (CN), $n_{\alpha\beta}$, which were calculated from the corresponding PCFs as

$$n_{\alpha\beta} = 4\pi\rho_\beta \int_0^{r_{m_i}} g_{\alpha\beta}(r) r^2 dr, \quad (9)$$

where the position of i-th minimum of $g_{\alpha\beta}(r)$, r_{m_i}, defines the radius of the i-th coordination shell around the reference site α; ρ_β is the number density of β sites. Thus, the partial CN is the average number of sites/particles of β-type in a sphere of radius r_{m_i} around an α-type site/particle. Values for the first-shell and the second-shell coordination number were determined, together with their relative changes

$$\Delta n_{\alpha\beta} = \left(n^2_{\alpha\beta} - n^1_{\alpha\beta}\right) / n^1_{\alpha\beta} \cdot 100\%, \quad (10)$$

when going from concentration 1 (with $n^1_{\alpha\beta}$) to concentration 2 (with $n^2_{\alpha\beta}$). The calculations for RbF(aq) were performed for four compositions ($c = 2.15$ M, molar ratio RbF:$H_2O = 1{:}25$; 2.95 M, 1:18; 5.08 M, 1:10; 9.18 M, 1:5) at 25.00 °C.

For the purposes of the present study we will analyze the PCFs $g_{IW}(r)$ (I: Rb^+ or F^-; W: water) and their partial CNs, n_{IW}, which characterize ion hydration, as well as the PCFs $g_{II}(r)$ and their partial CNs, n_{II}, defining ion association.

4. Results and discussion

4.1. Dielectric spectroscopy

Compared to the dielectric spectrum of pure water, RbF addition induces new features at the low-frequency side of the water relaxation centered at ~18 GHz (Fig. 1), which cannot be accounted for by simply assuming a broadening of the water relaxation. However, these contributions are not very pronounced, making a numerical decomposition of $\varepsilon^*(\nu)$ into individual modes difficult. All conceivable relaxation models combining up to $n = 4$ individual modes of various band shapes were tested along the lines described in detail in Ref. [43]. Two rather close modes at ~12 GHz and at ~20–30 GHz could always be resolved. However, free-running fits showed considerable scatter of the amplitudes, S_j, and relaxation times, τ_j. Thus, a 2D model was adopted, where the relaxation time of the lower-frequency mode was fixed at its average value of 13.5 ps if the value of the free-running fit was outside the interval $12 \le \tau_2/\text{ps} \le 17$. This procedure consistently yielded minimum χ^2 for $c > 0.73$ M and limiting permittivities, ε_j, and relaxation times, τ_j, smoothly changing with RbF concentration (Table 1, Figs. 3 and 4). Only for low concentrations, $c \le 0.73$ M, assumption of a further relaxation at ~0.8 GHz, *i.e.* a 3D model, slightly improved the fit (Table 1, Fig. 2).

The relaxation time, τ_3, of the high-frequency mode smoothly extrapolates to the value of pure water, $\tau_3(0) = 8.32$ ps [44] (Fig. 4), as does ε_3 (Fig. 3). Thus, at least for low RbF concentrations this mode can be unequivocally assigned to the relaxation of bulk water, *i.e.* H_2O molecules beyond the hydration spheres of the ions. Similar to the bulk-water relaxation times of aqueous solutions of other inorganic electrolytes [45] τ_3 decreases significantly with increasing concentration, following to the relation

$$\tau_3(c) = a \times \exp(-b \times c) + (\tau_3(0) - a). \quad (11)$$

For the magnitude parameter $a = (3.78 \pm 0.24)$ ps was found whereas the sensitivity parameter is $b = (0.39 \pm 0.04)$ L mol^{-1}. Compared to the sodium salts studied by Wachter et al. [45] a is much larger whereas b is significantly smaller. Probably, this is partly a reflection of the much wider concentration range studied here. Nevertheless, the data clearly indicate that Rb^+ and/or F^- significantly affect the structure of water outside their hydration shells and

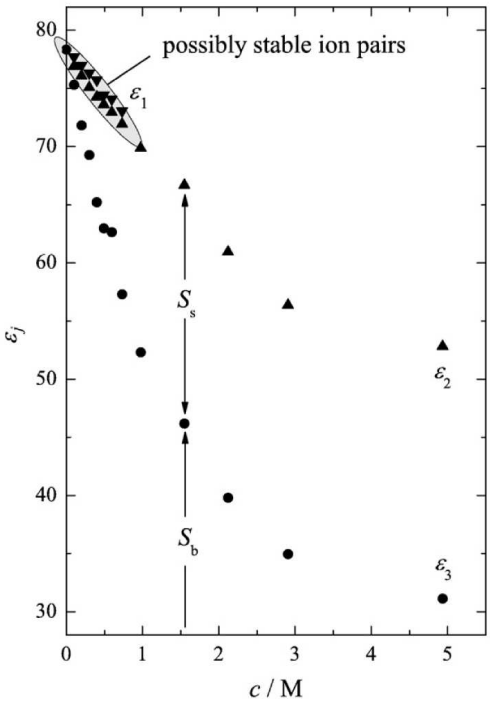

Fig. 3. Limiting permittivities ε_1, ε_2, and ε_3, as a function of RbF concentration, c.

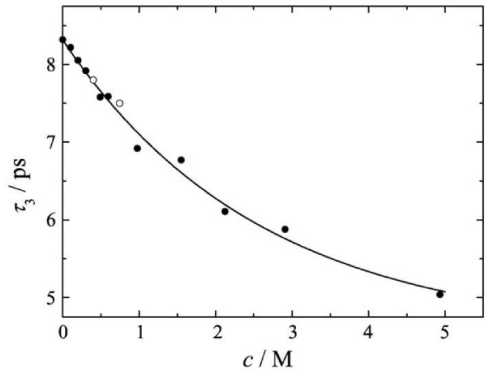

Fig. 4. Relaxation times of bulk water, τ_3 (symbols), for aqueous RbF solutions at 25 °C. The line represents the fit with Eq. (11) where fixed values for τ_3 (○, see Table 1) were not considered.

considerably speed up its dynamics. Since (bulk) water relaxation is commonly associated with the cooperative relaxation of its hydrogen-bond network catalyzed by the presence of 'defects' [46], a view supported by recent computer simulations [47], the smoothly accelerating dynamics with increasing concentration hints at a gradual breakdown of the H-bond network, accompanied by an increasing number of 'defects', *i.e.* free H-bond donor and acceptor sites.

The relaxation time of the intermediate-frequency process, $\tau_2 \approx 13.5$ ps, is similar to the relaxation time observed for "slow" water molecules hydrating either hydrophobic solutes [48] or carboxylate ions [49], *i.e.* anions forming strong hydrogen bonds. Since the radius of Rb^+ is rather large, thus the surface charge density of this cation rather small, we may tentatively assume that Rb^+ acts as a hydrophobic solute and is therefore surrounded by "slow" water molecules optimizing the number of H-bonds formed among themselves and with the bulk, reducing thus the number of 'defects' required to trigger relaxation [46]. Alternatively, one might assume that the interactions of Rb^+ with H_2O are just strong enough to slow down the hydrating water molecules but, in contrast to Na^+ [45], are too weak to "freeze" them [46]. On the other hand, F^- is known to form rather strong hydrogen bonds to H_2O which affects the dynamics of the hydration shell [50]. Thus, water molecules hydrating fluoride are likely to be slowed down in a similar way as those around carboxylate groups. We thus tentatively assign the τ_2 mode to H_2O hydrating Rb^+ and/or F^-.

The relaxation time of the low-frequency mode, $\tau_1 \approx 200$ ps, is of a magnitude expected for the reorientation of solvent-shared ion pairs [20]. According to common knowledge ion association of aqueous alkali fluorides, including RbF(aq), is very weak [51–54]. The small amplitude, $S_1 < 1.5$, of the observed low-frequency relaxation appears thus to be compatible with an assignment of the (S_1, τ_1) mode to ion-pair relaxation, as would be the maximum of S_1 at ~0.35 M indicating redissociation of ion pairs due to increasing charge crowding [55]. Unfortunately, S_1, which is at the resolution limits of the instrumentation, scatters too much to allow a meaningful estimation of an association constant for RbF(aq). Note here that the failure of dielectric spectroscopy to detect ion pairs at high RbF concentrations *does not contradict* the presence of direct or solvent-mediated anion–cation contacts which are clearly evidenced by the present HNC calculations (see below) and which obviously must be formed for steric reasons at $c \geq 5$ M. For the detection of ion pairs DRS requires the lifetime of this species to be at least comparable to its rotational correlation (here estimated to ~150–200 ps) [56]. Ion crowding and thus the increasing ion–ion interactions decrease the lifetime of the ion pairs below this threshold [20].

For relaxation processes arising from the orientation fluctuations of effective molecular dipole moments, $\mu_{j,\mathrm{eff}}$, their dispersion amplitudes, S_j, are connected to the concentration of the relaxing species, c_j, via

$$c_j = \frac{2\varepsilon + 1}{\varepsilon} \times \frac{k_B T \varepsilon_0}{N_A} \times \frac{S_j}{\mu^2_{j,\mathrm{eff}}}. \quad (12)$$

In Eq. (12) ε ($=\varepsilon_1$ of Table 1 for the 3D and $=\varepsilon_2$ for the 2D model) is the static permittivity of the solution and T is the Kelvin temperature; k_B, ε_0 and N_A have their usual meaning. The effective dipole moment, $\mu_{j,\mathrm{eff}}$, incorporates polarizability effects which can be estimated from the polarizability and the reaction field factor of the dipole [20]. However, when solvent-related dispersion amplitudes are analyzed, as done in the following, it is convenient to eliminate $\mu_{j,\mathrm{eff}}$ by normalizing Eq. (12) to the pure solvent [20].

The present investigation yielded well defined amplitudes for the cooperative relaxation of bulk water, S_3, and for the mode at ~13 ps tentatively assigned to "slow" water, S_2 (Figs. 3 and 5a). Whilst the latter can be directly evaluated with Eq. (12), yielding the concentration of "slow" water, $c_s = c_2$, and thus an effective hydration number

$$Z_s = c_s / c \quad (13)$$

of "slow" water molecules per equivalent of RbF, analysis of S_3 has to take into account the small-amplitude (~3–4% of the total dispersion $S_b = \varepsilon - \varepsilon_\infty$) fast water mode at ~300 GHz [44] that could not be resolved in the present study due to the limited frequency range. The origin of this very high-frequency contribution to the water spectrum is not yet fully understood [44] but it appears to be a consecutive process to the 18 GHz mode, so that the sum of their amplitudes should be evaluated with Eq. (12) [57]. It can be reasonably assumed that the small amplitude of the ~300 GHz relaxation depends only weakly on salt concentration. Thus, we use the limiting permittivity of pure water, $\varepsilon_\infty(0) = 3.48$, determined with a 2D model from $\varepsilon^*(\nu)$ including THz data [58], to obtain the corrected amplitude of bulk-water relaxation, $S_b(c) = \varepsilon_3(c) - \varepsilon_\infty(0)$, for the investigated RbF solutions.

The bulk-water amplitude, $S_b(c)$, shows a non-linear decrease with increasing concentration (Fig. 3) that seems to level at $c > 5$ M. On the other hand, the amplitude assigned to "slow" water strongly increases at low c but then levels at $S_s(c) = 21.6$ for $c \geq 1.4$ M (Fig. 5a). Interestingly, this threshold roughly coincides with the concentration, $c_{\mathrm{cont}} = 1.34$ M, where the average distance between the ions, $d_{\mathrm{cont}}/\mathrm{nm} = 0.94 \times [c/\mathrm{M}]^{-1/3}$, equals the contact distance of the hydrated ions, *i.e.* $d_{\mathrm{cont}} = r_+ + r_- + 4r_w = 0.852$ nm [5].

From $S_s(c)$ the concentration of "slow" water, $c_s(c)$, and thus the effective hydration numbers, $Z_s(c)$, are obtained with Eqs. (12) and

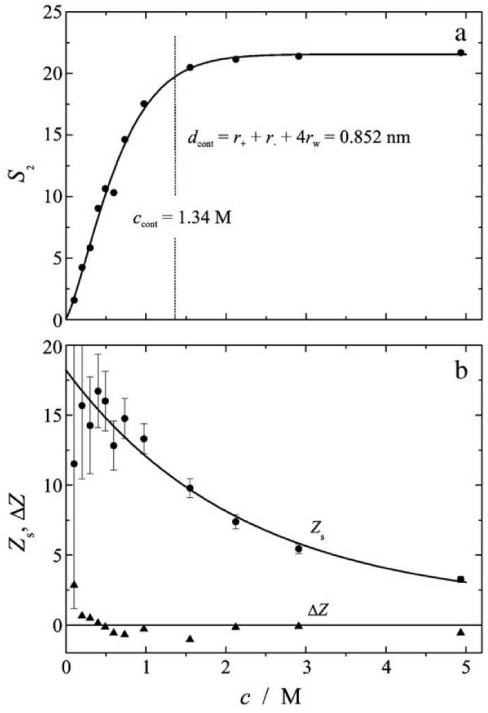

Fig. 5. (a) Amplitude of the slow water relaxation, S_s (●), and (b) associated effective hydration number, Z_s (●), according to Eqs. (12) and (13). Also indicated in (b) is the residual hydration number, $\Delta Z = Z - Z_s$ (▲), derived from the amplitude S_b of the bulk-water relaxation (see text).

(13). As can be seen from Fig. 5b, $Z_s(c)$ decreases from ~15–18 at $c \to 0$ to ~3 for 5 M RbF. Due to the small values of $S_s(c)$ for $c < 0.5$ M and aggravated by the need to separate also the small ion-pair relaxation, $Z_s(c)$ is rather noisy at low salt concentrations (error bars in Fig. 5b represent amplitude uncertainties of $2\sigma(S_s) = 1.4$) so that it cannot be decided if $Z_s(c)$ monotonically decreases, as suggested by the fit curve included in Fig. 5b, or – more likely – starts with a low-c plateau associated with isolated anions and cations surrounded by largely unperturbed hydration shells, as was observed for large tetraalkylammonium ions [57]. In any case, $Z_s(c)$ significantly decreases for $c \geq c_{cont}$. This may be either due to "melting" of the hydration shells on overlap as a result of competing ion–solvent interactions or to ion clustering, as suggested by the RISM calculations (Figs. 8 and 11), releasing water molecules to a highly disturbed "bulk" characterized by a small τ_3 (Fig. 3). Very likely, both effects are operative. In any case, these results, in conjunction with the only moderate slowing down of the involved H_2O molecules, $\tau_2 \approx 1.6\tau_3(0)$, indicate that the interactions of the "slow" water molecules with the ions are somewhat but not very much stronger than H_2O–H_2O interactions.

The above analysis of $S_s(c)$ focuses on "slow" water only. An evaluation of the bulk-water amplitude, $S_b(c)$, corrected for kinetic depolarization [20], with Eq. (12) yields the apparent concentration of bulk water, $c_b(c)$, which can be compared with the analytical water concentration, c_w. This allows calculation of the total effective solvation number

$$Z = (c_w - c_b)/c \tag{14}$$

It turns out that correction of $S_b(c)$ for kinetic depolarization under the assumption of *stick* boundary conditions for the translational motion of the ions yields $Z = Z_s$ within error limits for the entire concentration range (Fig. 5b). On the other hand, if *slip* boundary conditions or negligible kinetic depolarization are assumed Z is significantly larger than Z_s. This would mean that, in addition to the rather large effective hydration number of $Z_s(0) \approx 15$–18 at $c \to 0$, a further number $\Delta Z(0) = Z(0) - Z_s(0) \approx 8$–10 water molecules should be strongly bound ("frozen") by the ions [46]. Although the effective hydration numbers determined with dielectric spectroscopy are not necessarily restricted to the first hydration shell as they depend on the relative magnitude of ion–solvent *vs.* solvent–solvent interactions [20], the large values obtained for Z under the assumption of negligible or *slip* kinetic depolarization would be clearly incompatible with the present RISM calculations (see below) and the available literature data for Rb^+ and F^- coordination numbers in water [7,8,12]. On the other hand, the result for *stick* boundary conditions, $Z(0) = Z_s(0) \approx 15$–18 is reasonable, as is the concentration dependence of Z_s.

Fluoride hydration occurs via essentially linear F^-…H–O hydrogen bonds [59], leaving thus the dipole vectors of the hydrating water molecules rotating freely in a cone around the H-bonds, simultaneously tumbling with the entire $[F(H_2O)_n]^-$ complex [46]. To our knowledge the rotational correlation time of the hydrated fluoride ion was not yet determined but Kropman et al. [59] found values in the range of 8–12 ps for the other halide ions, which is very similar to the present "slow"-water relaxation time of $\tau_2 \approx 13.5$ ps. Also, with computer simulations Chowdhuri and Chandra [50] found a ratio of 2:1 for the orientational correlation times of H_2O dipoles hydrating F^- and in pure water, which is close the present $\tau_2/\tau_3(0)$. Thus, the observed dynamics of "slow" water is compatible with H_2O hydrating the anion.

However, the effective hydration number, $Z_s(0)$, is too large to be only due to F^-. Not only is $CN(F^-) \approx 6$ but also dielectric data for NaF and KF suggest $Z(F^-) \approx 5$–7 [51]. This indicates that also the water molecules hydrating the Rb^+ cation have to contribute to Z_s. Recent dielectric studies have shown that, in contrast to Na^+ which effectively "freezes" ~4.5 H_2O dipoles with its CN = 6 [60], K^+ and Cs^+ are unable to strongly bind water [45,61]. No "slow"-water relaxation similar to the present τ_2 mode could be resolved for the studied cesium and potassium salts but this might be a reflection of the limited accuracy of those studies. As stated in Ref. [45], there are indications that the chosen fit model was not fully appropriate. Nevertheless, with the current information we can only say that Rb^+ is most probably surrounded by water molecules with reduced dynamics and it appears that the relaxation time of these H_2O dipoles is similar to those surrounding F^-.

4.2. Statistical mechanics

4.2.1. Ion–water correlations

Graphs of the obtained pair correlation functions are shown in Figs. 6 and 7. The first peaks of the PCFs $g_{RbW}(r)$ and $g_{FW}(r)$, where W stands for O or H, are defined by the interactions of the cation, respectively anion, with the water molecules in its close environment. The height of these peaks increases for $g_{RbW}(r)$ (W = O and H) and $g_{FH}(r)$ but decreases for $g_{FO}(r)$ as c grows to 9.18 M (Table 2). At the same time the positions of the first peaks do not change, except for $g_{RbH}(r)$ (Table 2).

Calculation of partial CNs by Eq. (8) is straightforward for F^- as the PCFs $g_{FW}(r)$ have well resolved peaks for all salt concentrations. It was found that for 2.15 M RbF(aq) an average number of 5.9 water molecules coordinates F^- with an average F^-–O distance of 0.278 nm (Table 2). As c grows to 9.18 M this CN decreases by ~10% (Fig. 8). This is in line with recent RISM studies of concentrated KF(aq) solutions, which yielded $CN(F^-) \approx 6$ at the same F^-–O distance [62].

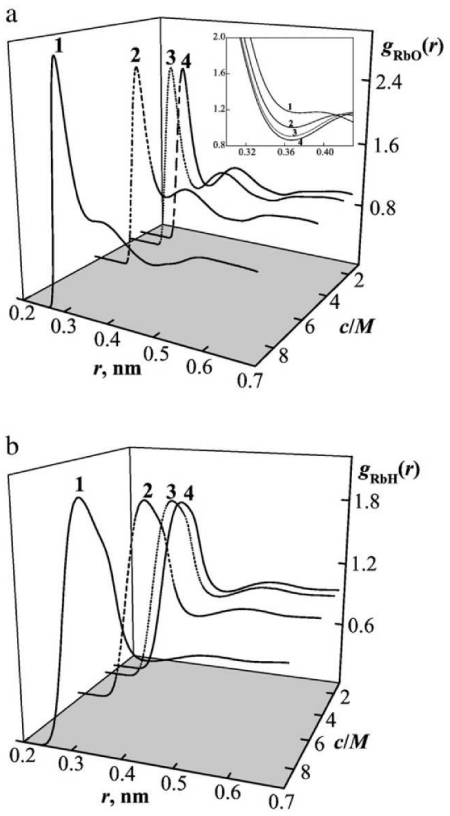

Fig. 6. Pair correlation functions $g_{RbO}(r)$ (a) and $g_{RbH}(r)$ (b) of aqueous RbF solutions at ambient conditions: 1 — 9.18 M, 2 — 5.08 M, 3 — 2.95 M, 4 — 2.15 M.

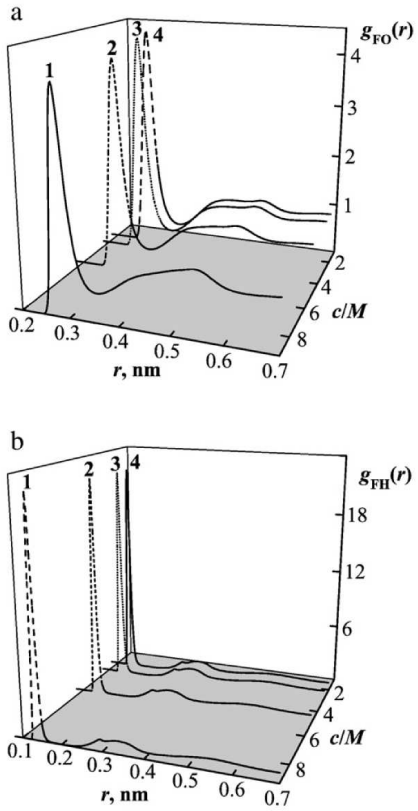

Fig. 7. Pair correlation functions $g_{FO}(r)$ (a) and $g_{FH}(r)$ (b) of aqueous RbF solutions at ambient conditions: 1 – 9.18 M, 2 – 5.08 M, 3 – 2.95 M, 4 – 2.15 M.

Unfortunately, for all investigated solutions the first peaks of the PCFs $g_{RbO}(r)$ are not well resolved because of partly overlapping first and second hydration shells (Fig. 6a). Since in this case straightforward application of Eq. (8) will give incorrect cation CNs, we decomposed $g_{RbO}(r)$ in the region from 0 to 0.7 nm into Gaussians $g_{\alpha\beta}(r) = \sum_i \tilde{A}_i(r)$ with a least-squares fitting procedure. This approach allows extraction of the component corresponding to the first hydration shell. Seven Gaussians were assumed for the decomposition where four of them approximate the first peak of $g_{RbO}(r)$ and the others represent the second peak and some background contributed by further water layers. Fig. 9 shows this approximation for 9.18 M RbF(aq) as an example. Since the used procedure cannot give a unique solution the aim was not only to achieve best fit but also to provide reasonably smooth and consistent concentration trends for all the parameters of the deconvolution (positions, widths and amplitudes of the Gaussian components) over the entire concentration range studied for RbF(aq). As a result of this approach, an average number of 6.24 water molecules was found to coordinate Rb^+ at the average Rb^+–O distance of 0.302 nm for 2.15 M RbF (aq) (Table 2). This CN decreases by ~18.5% as *c* growths to 9.18 M (Fig. 8).

Table 2
Characteristic parameters for the PCFs, $g_{\alpha\beta}(r)$, and for the partial CNs, $n_{\alpha\beta}$, of aqueous RbF solutions at ambient conditions.

	2.15 M	2.95 M	5.08 M	9.18 M
$g_{RbO}(r_{M1})$	2.404 (0.302)	2.453 (0.302)	2.574 (0.302)	2.901 (0.302)
$g_{RbO}(r_{m1})$	0.864 (0.366)	0.906 (0.366)	1.004 (0.368)	1.166 (0.376)
$g_{RbH}(r_{M1})$	1.740 (0.354)	1.787 (0.350)	1.879 (0.344)	2.064 (0.334)
$g_{RbH}(r_{m1})$	0.908 (0.454)	0.913 (0.454)	0.891 (0.452)	0.858 (0.452)
$g_{FO}(r_{M1})$	4.330 (0.278)	4.265 (0.278)	4.037 (0.278)	3.990 (0.280)
$g_{FO}(r_{m1})$	0.422 (0.354)	0.436 (0.355)	0.466 (0.356)	0.533 (0.358)
$g_{FH}(r_{M1})$	21.894 (0.136)	21.901 (0.136)	22.106 (0.136)	22.600 (0.136)
$g_{FH}(r_{m1})$	0.021 (0.196)	0.021 (0.194)	0.022 (0.194)	0.024 (0.194)
$g_{RbF}(r_{M1})$	39.935 (0.250)	30.420 (0.250)	18.990 (0.252)	13.850 (0.252)
$g_{RbF}(r_{m1})$	0.305 (0.350)	0.273 (0.348)	0.284 (0.346)	0.275 (0.346)
$g_{RbF}(r_{M2})$	1.746 (0.458)	1.622 (0.458)	1.574 (0.456)	1.329 (0.450)
$g_{RbF}(r_{m2})$	0.672 (0.608)	0.668 (0.606)	0.831 (0.544)	0.806 (0.536)
n_{RbO}	6.24[a]	5.98[a]	5.78[a]	5.08[a]
n_{FO}	5.88	5.83	5.53	5.30
n_{CIP}	1.43	1.52	1.74	2.37
n_{SSIP}	0.95	1.20	1.62	2.43

$g(r_{Mi})$ and (in brackets r_{Mi}) are the heights and (positions in nm) of peak *i*, respectively; $g(r_{mi})$ and (r_{mi}) are depth and (position in nm) of minimum *i*, respectively.
[a] Values obtained by approximating $g_{RbO}(r)$ as a sum of four Gaussians (see text).

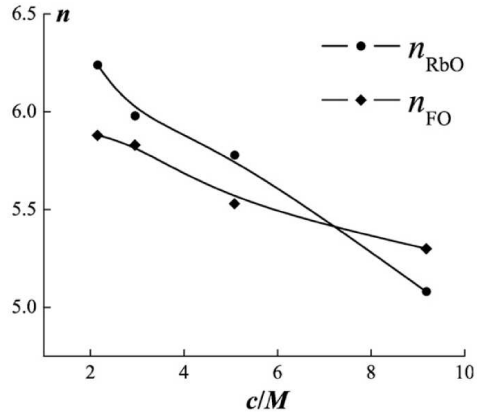

Fig. 8. Partial coordination numbers n_{RbO} and n_{FO} as a function of RbF concentration, *c*.

4.2.2. Cation–anion correlations

Not surprising for the high concentrations studied with statistical mechanics, the cation–anion PCFs, $g_{RbF}(r)$, of all studied concentrations have a well resolved first peak, indicating the presence of direct cation–anion contacts (for simplicity called contact ion pairs, CIP). Additionally, and in marked contrast to aqueous rubidium chloride solution [63], also a second peak is found which arises from configurations where anions and cations are separated by a single water molecule (solvent-separated ion pairs, SSIP) (Fig. 10). This is an

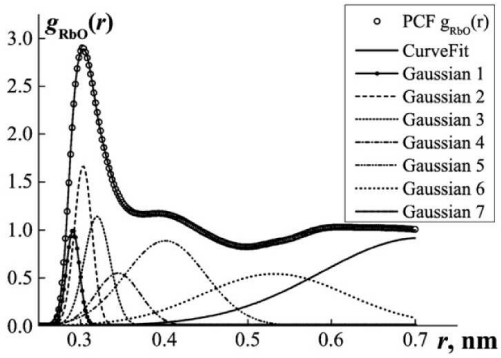

Fig. 9. Decomposition of the pair correlation function $g_{RbO}(r)$ into Gaussians for 9.18 M RbF(aq) as an example. The first peak was approximated by 4 Gaussians.

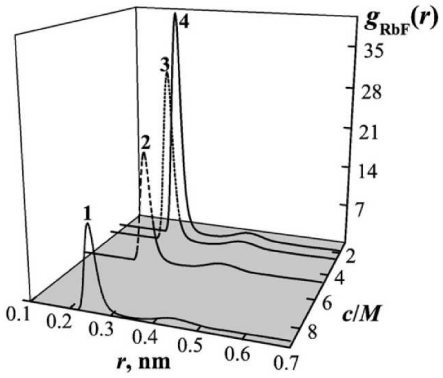

Fig. 10. Pair correlation functions $g_{RbF}(r)$ of aqueous RbF solutions at ambient conditions: 1 — 9.18 M, 2 — 5.08 M, 3 — 2.95 M, 4 — 2.15 M.

immediate reflection of (compared to Cl^-) the stronger interactions of fluoride with water leading to a more stable hydration for this anion. For 2.15 M RbF(aq) the number of CIPs, n_{CIP}, is about 1.43 and the number of SSIPs, ^{n}SSIP, is about 0.95 (Table 2). Note, that the average value of $n_{CIP}>1$ suggests the formation of ion aggregates with more complex configurations than true contact ion pairs involving a single anion and a single cation. Almost certainly, this includes ion triples but possibly even larger ionic clusters.

The peaks of $g_{RbF}(r)$ decrease sharply in height and broaden when the salt concentration increases (Fig. 10). As a result, a significant growth in the number of direct (CIPs) and solvent-mediated anion–cation contacts (SSIPs) is observed with increasing c (Fig. 11). Thus, for 9.18 M RbF(aq) $n_{CIP}=2.37$ and $n_{SSIP}=2.43$. The average distance of 0.250 nm between Rb^+ and F^- in the CIP does not change with increasing c, but the Rb^+–OH_2–F^- distance in the SSIP decreases from ~0.458 nm to 0.450 nm (Table 2). The latter means a reduction of the Rb^+–OH_2–F^- angle from 134° to 129°.

5. Concluding remarks

The present RISM calculations clearly show that for concentrations $c>2$ M water molecules in the first hydration shells of Rb^+ and F^- are more and more replaced by direct cation–anion contacts. Interestingly, and in contrast to RbCl [63], also the number of water-bridged pairs strongly increases (Fig. 11). In part, this is a necessary consequence of the decreasing H_2O:RbF ratio where at ~3–3.5 M – depending on the exact coordination numbers of the ions, see above and Refs. [7,8,12] – the threshold for the formation of complete hydration shells around Rb^+ and F^- is passed. However, according to the RISM calculations ion clustering starts already well below that limit. On the other hand, even at the highest concentration a significant amount of SSIP configurations remain for RbF(aq) as a result of the strong hydration of fluoride. The formed clusters – more accurately: the contact ion pairs among them – must have a limited lifetime, less than ~100 ps, because no such species could be detected with dielectric spectroscopy. If *long-lived* ion pairs are really formed – and the present results are at the detection limit – then as solvent-shared species at $c<0.7$ M and, in agreement with published association constants [52–54], only to a very small amount.

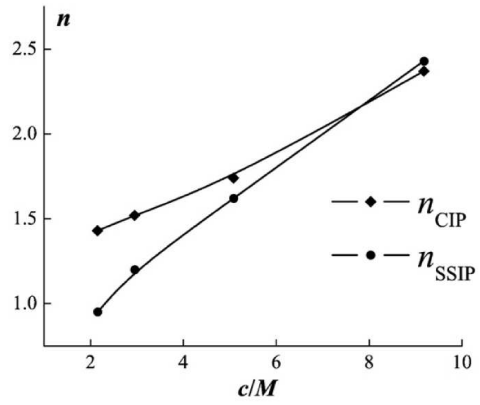

Fig. 11. Average numbers of CIP, n_{CIP}, and SSIP configurations, n_{SSIP}, as a function of RbF concentration, c.

The dynamics of RbF(aq) is interesting as a pronounced "slow" water relaxation is observed. Such a mode has not been observed for KCl and CsCl [61]. The large effective hydration number of $Z_s(0)\approx 15$–18 at $c\to 0$, which is roughly the sum of the coordination numbers of Rb^+ and F^-, suggests that in dilute solutions anions *and* cations are surrounded by a shell of water molecules with moderately reduced mobility (as compared to the dynamics of pure water and in contrast to Cs^+ and Cl^- [45]). Probably already at lower concentration but certainly for $c\geq c_{cont}$, where the primary hydration shells of the ions start to overlap, $Z_s(c)$ decreases significantly, dropping to ~3.5 *per pair of RbF ions* at 5 M, a number far too small to hydrate even a contact pair of Rb^+ and F^-. Parallel to the drop of $Z_s(c)$ the relaxation time of "bulk"-like water, τ_3, decreases markedly (Fig. 3), indicating the breakdown of the extended three-dimensional H-bond network present in pure water and dilute solutions. Obviously, the structure of "bulk"-like water is heavily perturbed and a large amount of these H_2O molecules is in direct contact with the ions (compare the CNs from RISM, Fig. 8, with $Z_s(c)$, Fig. 5b). Unfortunately, the present results do not permit locating the remaining "slow" water molecules at high c but one may speculate that at least some of them bridge Rb^+ and F^- in the ion clusters.

Acknowledgements

H.M.A.R thanks the Higher Education Commission of Pakistan for a PhD grant enabling this research and DAAD for support. R.B. gratefully acknowledges travel support from DFG for visiting Ivanovo at early stages of this research.

References

[1] H. Ohtaki, T. Radnai, Chem. Rev. 93 (1993) 1157.
[2] M. Magini, G. Lichieri, G. Paschina, G. Piccaluga, G. Pinna, X-ray Diffraction of Ions in Aqueous Solutions, CRC Press, Florida, 1988.
[3] H. Ohtaki, Monatsh. Chem. 132 (2001) 1237.
[4] E.V. Vinogradov, P.R. Smirnov, V.N. Trostin, Russ. Chem. Bull. 52 (2003) 1253.
[5] Y. Marcus, Chem. Rev. 109 (2009) 1346.
[6] B.F.J. Vorgin, P.S. Knapp, W.L. Flint, A. Anton, G. Highberger, E.R.J. Malinovski, J. Chem. Phys. 54 (1971) 178.
[7] I. Harsányi, P. Jóvári, G. Mészáros, L. Pusztai, Ph.A. Bopp, J. Mol. Liq. 131–132 (2007) 60.
[8] S. Ramos, A.C. Barnes, G.W. Neilson, M. Capitan, J. Chem. Phys. 171 (2000) 258.
[9] H. Bertagnolli, T.S. Ertel, M. Hoffmann, R. Frahm, Ber. Bunsenges. Phys. Chem. 95 (1991) 704.
[10] S. Cummings, J.E. Enderby, G.W. Neilson, J.R. Newsome, R.A. Howe, W.S. Howells, A.K. Soper, Nature 287 (1980) 714.
[11] E.L. Nikologorskaya, V.V. Kuznetsov, O.V. Grechin, V.N. Trostin, Russ. J. Inorg. Chem. 45 (2000) 1904.
[12] Gy.J. Szasz, K. Heinzinger, Z. Naturforsch. 38a (1983) 214.
[13] A.K. Soper, K. Weckström, Biophys. Chem. 124 (2006) 180.
[14] H. Bertagnolli, J.-U. Weidner, H.W. Zimmermann, Ber. Bunsenges. Phys. Chem. 78 (1974) 2.
[15] Y. Marcus, Ion Properties, Dekker, New York, 1997.
[16] G.A. Krestov, Thermodynamics of Solvation, Ellis Horwood, NewYork, 1991.
[17] I. Harsányi, L. Pusztai, J.-C. Soetens, Ph.A. Bopp, J. Mol. Liq. 129 (2006) 80.
[18] I. Harsányi, L. Pusztai, J. Phys. Condens. Matter 19 (2007) 335208 (12 pp.).
[19] F. Kremer, A. Schönhals (Eds.), Broadband Dielectric Spectroscopy, Springer, Berlin, 2003.

[20] R. Buchner, G. Hefter, Phys. Chem. Chem. Phys. 11 (2009) 8984.
[21] M.V. Fedotova, M.F. Holovko, The Integral Equation Method in Equilibrium Statistical Theory of Liquids (Monograph in Russian), URSS, Moscow (in press).
[22] M.V. Fedorov, A.A. Kornyshev, Mol. Phys. 105 (2007) 1.
[23] G.N. Chuev, M.V. Fedorov, S. Chiodo, N. Russo, E. Sicilia, J. Comput. Chem. 29 (2008) 2406.
[24] D.R. Lide, CRC Handbook of Chemistry and Physics, CRC Press, Boca Raton, 2004.
[25] J. Barthel, K. Bachhuber, R. Buchner, H. Hetzenauer, M. Kleebauer, Ber. Bunsenges. Phys. Chem. 95 (1991) 853.
[26] R. Buchner, G.T. Hefter, P.M. May, J. Phys. Chem. A 103 (1999) 1.
[27] F. Hirata, P.J. Rossky, Chem. Phys. Lett. 83 (1981) 329.
[28] F. Hirata, P.J. Rossky, B.M. Pettitt, J. Chem. Phys. 78 (1983) 4133.
[29] D. Chandler, H.C. Andersen, J. Chem. Phys. 57 (1972) 1930.
[30] P.A. Monson, G.P. Morris, in: I. Prigogine, S.A. Rice (Eds.), Advances, Chem. Phys., 77, Wiley, New York, 1990, p. 451.
[31] F. Hirata, Molecular Theory of Solvation, Kluwer Academic, Dordrecht, 2003.
[32] M.F. Holovko, 1984, Preprint, Inst. Theor. Phys. No 187P, Kiev.
[33] M.F. Holovko, Yu.V. Kalyuznyi, Mol. Phys. 68 (1989) 1239.
[34] Yu.V. Kalyuznyi, M.V. Fedotova, M.F. Holovko, V.N. Trostin, 1994, Preprint, Inst. Condens. Matt. Phys. No 27P, Lviv.
[35] S. Labik, A. Malievsky, P. Voňka, Mol. Phys. 56 (1985) 709.
[36] K.-C. Ng, J. Chem. Phys. 61 (1974) 2680.
[37] H.J.C. Berendsen, J.P.M. Postma, W.F. van Gunsteren, W.F. Hermans, in: B. Pullman (Ed.), Intermolecular Forces, Reidel, Dordrecht, 1981, p. 331.
[38] B.M. Pettitt, P.J. Rossky, J. Chem. Phys. 77 (1982) 1451.
[39] L.X. Dang, J. Am. Chem. Soc. 117 (1995) 6954.
[40] B.M. Pettitt, P.J. Rossky, J. Chem. Phys. 84 (1986) 5836.
[41] F.G. Fumi, M.P. Tosi, J. Phys. Chem. Solids 25 (1964) 45.
[42] J. Tamas, Acta Chim. Acad. Sci. Hung. 40 (1964) 117.
[43] J. Hunger, A. Stoppa, R. Buchner, G. Hefter, J. Phys. Chem. B 113 (2009) 9527.
[44] T. Fukasawa, T. Sato, J. Watanabe, Y. Hama, W. Kunz, R. Buchner, Phys. Rev. Lett. 95 (2005) 197802.
[45] W. Wachter, W. Kunz, R. Buchner, G. Hefter, J. Phys. Chem. A 109 (2005) 8675.
[46] R. Buchner, Pure Appl. Chem. 80 (2008) 1239.
[47] D. Laage, J.T. Hynes, J. Phys. Chem. B 112 (2008) 14230.
[48] W. Wachter, R. Buchner, G. Hefter, J. Phys. Chem. B 110 (2006) 5147.
[49] A. Tromans, P.M. May, G. Hefter, T. Sato, R. Buchner, J. Phys. Chem. B 108 (2004) 13789.
[50] S. Chowdhuri, A. Chandra, J. Phys. Chem. B 110 (2006) 9674.
[51] R. Buchner, G.T. Hefter, J. Barthel, J. Chem. Soc., Faraday Trans. 90 (1994) 2475.
[52] A.D. Pethybridge, D.J. Spiers, J. Chem. Soc., Faraday Trans. I 73 (1977) 768.
[53] C.B. Chan, N.H. Tioh, G.T. Hefter, Polyhedron 3 (1984) 845.
[54] C.J. Fennel, A. Bizjak, V. Vlachy, K.A. Dill, J. Phys. Chem. B 113 (2009) 6782.
[55] W. Wachter, Š. Fernandez, R. Buchner, G. Hefter, J. Phys. Chem. B 111 (2007) 9010.
[56] R. Buchner, J. Barthel, J. Mol. Liq. 63 (1995) 55.
[57] R. Buchner, C. Hölzl, J. Stauber, J. Barthel, Phys. Chem. Chem. Phys. 4 (2002) 2169.
[58] S. Schrödle, Effects of non-ionic surfactants and related compounds on the cooperative and molecular dynamics of their aqueous solutions, PhD Thesis, Regensburg, Germany, 2005.
[59] M.F. Kropman, H.-K. Nienhuys, H.J. Bakker, Phys. Rev. Lett. 88 (2002) 077601.
[60] R. Buchner, S.G. Capewell, G.T. Hefter, P.M. May, J. Phys. Chem. B 103 (1999) 1185.
[61] T. Chen, G. Hefter, R. Buchner, J. Phys. Chem. A 107 (2003) 4025.
[62] M.V. Fedotova, E.L. Gavrilova, Russ. J. Gen. Chem. 79 (2009) 7.
[63] R.D. Oparin, M.V. Fedotova, V.N. Trostin, Russ. J. Gen. Chem. 74 (2004) 17.

A.3 DRS of non-aqueous electrolyte solutions

The following pages give a reprint of the paper

Płaczek, A.; Hefter, G.; Rahman, H. M. A.; Buchner, R. *'Dielectric Relaxation Study of the Ion Solvation and Association of $NaCF_3SO_3$, $Mg(CF_3SO_3)_2$, $Ba(ClO_4)_2$ in N,N-Dimethylformamide.'* *J. Phys. Chem. B* **2011**, *115*, 2234.

This work was done in collaboration with A. Płaczek and G. Hefter during the time period of present PhD thesis as a side project. I was mainly involved in recording the DR spectra of some selected concentrations of the studied salts in DMF at $0.2 \lesssim \nu/\mathrm{GHz} \leq 50$. Furthermore, I analysed selected spectra according to the bias-free fitting procedure of Zasetzky and Buchner[91] and have done the MOPAC-calculations to estimate the dipole moments of ion pairs.

THE JOURNAL OF PHYSICAL CHEMISTRY B

ARTICLE

pubs.acs.org/JPCB

Dielectric Relaxation Study of the Ion Solvation and Association of $NaCF_3SO_3$, $Mg(CF_3SO_3)_2$, and $Ba(ClO_4)_2$ in *N*,*N*-Dimethylformamide

Anna Płaczek,[†,‡] Glenn Hefter,[*,†] Hafiz M. A. Rahman,[‡] and Richard Buchner[*,‡]

[†]Chemistry Department, Murdoch University, Murdoch, WA 6150, Australia

[‡]Institut für Physikalische und Theoretische Chemie, Universität Regensburg, D-93040, Regensburg, Germany

Supporting Information

ABSTRACT: Solutions of sodium trifluoromethanesulfonate, magnesium trifluoromethanesulfonate, and barium perchlorate in *N*,*N*-dimethylformamide (DMF) have been investigated using broadband dielectric relaxation spectroscopy at 25 °C. All spectra were dominated by a solvent relaxation process centered at ~15 GHz but also exhibited one (for $NaCF_3SO_3$) or two (for the 2:1 salts) low-amplitude processes, centered at frequencies below 2 GHz, that could be attributed to the presence of ion pairs. Effective solvation numbers calculated from the solvent relaxation amplitudes indicated strong solvation of all three cations, with evidence for the formation of a second solvation sheath for Mg^{2+} and possibly Ba^{2+}. Detailed analysis of the solute-related processes showed that solvent-shared ion pairs (SIPs) were formed in $NaCF_3SO_3$ solutions in DMF. The data for $Mg(CF_3SO_3)_2$ and $Ba(ClO_4)_2$ solutions were not definitive but, consistent with the solvation evidence, favored the presence of double solvent-separated ion pairs and SIPs. Overall association constants, K_A, were small for all three salts in DMF and increased in the order: $NaCF_3SO_3 < Ba(ClO_4)_2 < Mg(CF_3SO_3)_2$.

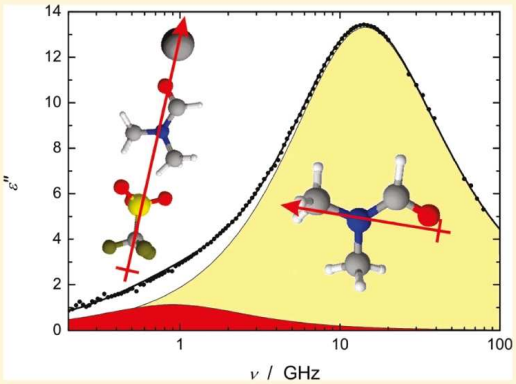

1. INTRODUCTION

Dielectric relaxation spectroscopy (DRS) is a widely applicable but relatively under-utilized technique for the study of electrolyte solutions.[1−3] In principle, it can provide detailed and quantitative information about both the dynamics and thermodynamics of such solutions and, in favorable cases, even structural insights. While most published DRS studies have been of aqueous systems, the technique is readily applicable to nonaqueous solutions. Molecular-solvent solutions investigated to date have included: propylene carbonate,[4,5] acetonitrile,[6,7] methanol,[8] formamide,[9,10] *N*-methylformamide,[9,10] and *N*,*N*-dimethylacetamide,[11] although such studies have in general been limited to a narrow range of monovalent (1:1) electrolytes.

Liquid *N*,*N*-dimethylformamide (DMF) is a versatile solvent for organic and inorganic substances and has been employed extensively as a solvent for polymers and paints and as a reaction medium.[12] It has a reasonably high dielectric constant (ε = 36.71 at 25 °C)[13] and a sizable dipole moment (μ = 3.86 D).[13] With a Gutmann donor number of 26.6,[13] DMF is a strong electron-density donor and thus a powerful solvator of cations. On the other hand, it is a rather poor solvator of anions, with a Gutmann acceptor number of just 16.0 (similar to acetonitrile and propylene carbonate).[13]

As might be expected from these generally favorable characteristics, the physicochemical properties of electrolyte solutions in DMF have been widely investigated. Such studies have included determinations of Gibbs energies,[14] enthalpies and entropies,[15] and viscosities,[16] although again most were restricted to relatively small numbers of 1:1 electrolytes. Recently, a comprehensive report of the molar volumes and heat capacities of a wide range of electrolytes, including non-1:1 charge types, has appeared.[17]

An ongoing problem for such studies is the reliable extrapolation to infinite dilution of experimental data measured at finite electrolyte concentrations to obtain the desired standard state properties. Because the extrapolation functions used for this purpose (such as the Redlich−Meyer and Pitzer equations)[18] assume that electrolytes are fully dissociated, this can lead to significant errors in the standard state values.[19] This difficulty is usually more pertinent to electrolyte solutions in nonaqueous solvents (because such solutions typically exhibit higher levels of ion association than their aqueous counterparts)[20,21] and becomes acute when dealing with salts containing higher-charged ions. While theoretical treatments have been developed that make allowance for ion association,[22] the required equilibrium constants are almost invariably lacking for nonaqueous solutions, and the available methods for estimating such quantities[21] are too

Received: December 7, 2010
Revised: January 11, 2011
Published: February 22, 2011

The Journal of Physical Chemistry B ARTICLE

crude to be reliable. To minimize such errors most researchers have employed electrolytes containing weakly complexing counterions, such as perchlorate (ClO_4^-) for cations or tetraalkylammonium (R_4N^+) ions for anions, and then *assumed* complete dissociation. While this approach has produced many useful and self-consistent results it clearly has limitations. The justification for such a choice requires a better understanding of the competing processes of ion solvation and ion association of electrolytes in nonaqueous solvents.[3]

As already noted, DRS can provide useful insights into both ion solvation and ion association processes.[3] Solvation information can be obtained in a straightforward manner from DR spectra, which have produced a coherent picture of the solvation characteristics of a range of (mostly monovalent) ions in a variety of solvents.[6,7,9−11] The study of ion association by DRS is especially fruitful as this technique is very sensitive to the formation of weak complexes and has a unique ability to detect and quantify solvent-separated and contact ion pairs in solution.[1] Unlike many popular techniques for determining ion-association constants, DRS is equally applicable to aqueous and nonaqueous solutions and to symmetrical and nonsymmetrical electrolytes.[1,21]

The present study employs broadband DRS to investigate solutions of sodium trifluoromethanesulfonate (sodium "triflate", $NaCF_3SO_3$), magnesium triflate ($Mg(CF_3SO_3)_2$), and barium perchlorate ($Ba(ClO_4)_2$) in DMF at 25 °C. These salts were chosen to represent the range of electrolytes used in comprehensive thermodynamic investigations.[17] All three salts are readily soluble in DMF and, because of the low charge density of their anions, they are expected to be relatively weakly associated; i.e., they are nominally strong electrolytes in DMF. Except for a preliminary study[9] on $NaClO_4$, to the best of our knowledge the only previous DRS investigation of electrolyte solutions in DMF is that of Wurm et al.[11] who reported spectra for lithium, sodium, and tetra-*n*-butylammonium perchlorates at 25 °C over a frequency range similar to that employed here. The present paper is the first to provide information on nonsymmetrical electrolytes.

2. EXPERIMENTAL SECTION

2.1. Reagents. Sodium and magnesium triflates were prepared by neutralization of suspensions of Na_2CO_3 and MgO, respectively, in methanol (analytical reagent grade) with trifluoromethanesulfonic ("triflic") acid (3M, AR grade), as described elsewhere.[17] The products were recrystallized from AR ethanol and dried under vacuum at 50 °C for several days. Hydrated barium perchlorate was prepared by neutralization of an aqueous suspension of BaO with perchloric acid (UNIVAR, AR grade, 72% w/w). The $Ba(ClO_4)_2$ hydrate so obtained was recrystallized twice from water and then dehydrated and dried under vacuum at 150 °C for 4 days. Solvent *N*,*N*-dimethylformamide (Merck, AR grade, 99.5%) was dried and stored over freshly activated 3 Å molecular sieves and had a typical water content of <200 ppm (coulometric Karl Fischer titration). Solvent for solution preparation was taken from an undisturbed storage vessel by syringe immediately prior to use. Solutions were prepared by weight in a drybox, without buoyancy corrections.

2.2. Instrumentation and Measurements. Dielectric measurements at frequencies $0.2 \lesssim \nu/\mathrm{GHz} \leq 20$ were performed at Murdoch University using a Hewlett-Packard model HP 85070 M Dielectric Probe System, consisting of an HP 8720D vector network analyzer (VNA) and an HP 85070 dielectric probe kit. Additional coaxial-line reflection measurements were carried out in Regensburg with an Agilent E8364B VNA combined with Agilent 85070E-020 (0.2−20 GHz) and 85070E-050 (0.5−50 GHz) probes. Both VNAs were calibrated using air, mercury, and *N*,*N*-dimethylacetamide (Fluka, > 99.8%, stored over activated 4 Å molecular sieves) as standards. Each solution was measured at least twice using independent calibrations, with relative permittivity, $\varepsilon'(\nu)$, and total loss, $\eta''(\nu)$, recorded at 101 frequencies equidistant on a logarithmic scale. Most solutions were also measured at higher frequencies ($27 \leq \nu/\mathrm{GHz} \leq 89$) at Regensburg University using two waveguide interferometers. Detailed descriptions of these instruments and the measurement principles have been published previously.[23,24] All DRS measurements (VNAs and interferometers) were made at 25 ± 0.02 °C, with a NIST-traceable accuracy of ±0.05 °C. The probable maximum errors in ε' and η'' are 2% of the static permittivity of the sample.

Solution densities, ρ, were determined at 25 ± 0.01 °C at Regensburg using a vibrating-tube densimeter (Paar DMA 60/601HT) calibrated with nitrogen (ρ = 1.1456 mg·cm^{-3})[25] and water (ρ = 0.997043 g·cm^{-3}).[25] Electrical conductivities, κ, were measured at 25 ± 0.005 °C, over the frequency range $0.1 \leq \nu/\mathrm{kHz} \leq 10$ with an accuracy of ±0.5%, using an AC bridge and capillary cells as described elsewhere.[26−28] Infinite-frequency resistances, $R_\infty = \lim_{\nu\to\infty} R(\nu)$, were obtained by extrapolation using the empirical function $R(\nu) = R_\infty + A/\nu^a$, where A is specific to the cell and $a \approx 0.5$.[28,29]

2.3. Calculations. DRS involves measurement of the complex relative dielectric permittivity $\hat{\varepsilon}(\nu)$ of a sample as a function of the frequency ν of an applied electromagnetic field

$$\hat{\varepsilon}(\nu) = \varepsilon'(\nu) - i\varepsilon''(\nu) \quad (1)$$

where $\varepsilon'(\nu)$ is the relative permittivity and $\varepsilon''(\nu)$ is the dielectric loss.[30,31] The latter is obtained from the measurable total loss

$$\eta''(\nu) = \varepsilon''(\nu) + \kappa/(2\pi\nu\varepsilon_o) \quad (2)$$

where ε_o is the permittivity of free space. A typical spectrum for $\eta''(\nu)$ and the corresponding $\varepsilon''(\nu)$ is shown in Figure S1 of the Supporting Information. The conductivity contribution $(\kappa/2\pi\nu\varepsilon_o)$ ultimately swamps the signal of interest $(\varepsilon''(\nu))$ at low frequencies and thus determines the minimum frequency for meaningful DR measurements.[32] In principle, κ is accessible from separate (low-frequency conductivity) measurements, but in practice, for reasons discussed at length elsewhere,[32] it is usually treated as an adjustable parameter in the data-fitting procedure. Nevertheless, experimental κ values were taken as the starting approximation in the fitting process at each concentration, and the fit and experimental results always agreed to better than 5%.

Conductivity-corrected experimental spectra were fitted with plausible models based on n individual relaxation processes

$$\hat{\varepsilon}(\nu) = \sum_{j=1}^{n} \frac{S_j}{(1 + (i2\pi\nu\tau_j)^{1-\alpha_j})^{\beta_j}} + \varepsilon_\infty \quad (3)$$

with each dispersion step j of amplitude S_j and relaxation time τ_j being modeled using either a Havriliak−Negami (HN) equation, with relaxation-time distribution parameters $0 \leq \alpha_j < 1$ and $0 < \beta_j \leq 1$, or any of its simplified variants: the Debye (D; $\alpha_j = 0, \beta_j = 1$), Cole−Cole (CC; $\beta_j = 1$), or Cole−Davidson (CD; $\alpha_j = 0$) models. The static (relative) permittivity of the sample is defined as $\varepsilon = \Sigma S_j + \varepsilon_\infty$ where $\varepsilon_\infty = \lim_{\nu\to\infty} \varepsilon'(\nu)$ is the so-called infinite-frequency permittivity. The preferred model was that which gave the lowest value of the reduced error function (χ^2)[33] *and*

dx.doi.org/10.1021/jp1116307 |J. Phys. Chem. B 2011, 115, 2234–2242

The Journal of Physical Chemistry B ARTICLE

relaxation amplitudes and times that were physically realistic and varied smoothly with solute concentration. Additionally, selected spectra were analyzed with a recently published procedure[34] that allows an unbiased determination of the number of relaxation processes required for the formal description of $\hat{\varepsilon}(\nu)$. Typical results from these analyses are given in the Supporting Information, Figures S4−S6.

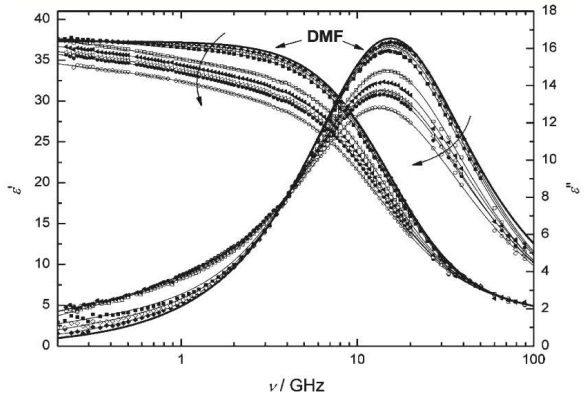

Figure 1. Permittivity, $\varepsilon'(\nu)$, and dielectric loss, $\varepsilon''(\nu)$, spectra of neat DMF and solutions containing various concentrations of $Ba(ClO_4)_2$ in DMF at 25 °C. The curved arrows indicate increasing solute concentration (as listed in Table 1). Lines are fits using the D + D + CD model; heavy lines denote the neat solvent spectra.

3. RESULTS AND DISCUSSION

3.1. Process Assignment. A typical set of experimental spectra (for $Ba(ClO_4)_2$) obtained for the present electrolyte solutions in DMF is shown in Figure 1. Equivalent data for $NaCF_3SO_3$ and $Mg(CF_3SO_3)_2$ solutions are given in the Supporting Information (Figures S2 and S3). Values of the parameters obtained by application of eq 3 to the experimental spectra are summarized in Table 1, which also includes densities, experimental conductivities, and χ^2 values. A full discussion of the various quantities in Table 1 is given below.

The DR spectra of all of the present electrolyte solutions in DMF are dominated by a large-amplitude process centered at ca. 15 GHz (Figure 1 and Supporting Information Figures S2 and S3). This process is readily assigned, by comparison with the spectrum for neat DMF[35] (Figure 1), to the rotational diffusion of solvent molecules. A detailed study[35] of the temperature

Table 1. Densities, Conductivities, and Fitting Parameters (Using D + CD or D + D + CD Models) of the DR Spectra for DMF Solutions of $NaCF_3SO_3$, $Mg(CF_3SO_3)_2$, and $Ba(ClO_4)_2$ at 25 °C[a]

c	ρ	κ	ε	S_{IP1}	τ_{IP1}	S_{IP2}	τ_{IP2}	S_S	τ_S	β	ε_∞	$10^3\,\chi^2$
						$NaCF_3SO_3$						
0.0	0.943838[b]	0.0	37.31						10.4		3.02	
0.0478			37.19	0.48	360			32.74	10.6	0.970	3.98	18.3
0.1024			37.23	1.10	374			32.20	10.9	0.957	3.92	8.7
0.1832	0.962874	0.761	35.89	1.81	228			29.54	10.7	0.999	4.54	11.9
0.2858	0.973380	1.063	34.72	2.14	180		n/a	28.17	11.0	0.981	4.42	15.5
0.3303	0.977963	1.251	34.25	2.25	175			28.03	11.5	0.941	3.97	10.5
0.3647	0.981400	1.334	33.89	2.27	177			28.13	12.2	0.885	3.50	7.6
0.4183	0.986753	1.454	33.08	2.41	165			27.39	12.8	0.850	3.29	13.0
						$Mg(CF_3SO_3)_2$						
0.0137			37.82	0.71	640	0.16	200[c]	33.16	10.6	0.965	3.79	8.4
0.0280			37.89	0.87	542	0.37	199	32.73	10.7	0.963	3.92	5.5
0.0466			37.87	1.09	450	0.51	168	32.29	10.9	0.960	3.98	11.5
0.1100	0.967286	0.823	37.40	1.26	419	2.13	159	30.46	11.6	0.908	3.55	4.2
0.1607	0.977882	1.080	36.40	1.35	363	2.35	129	29.12	12.0	0.895	3.58	3.9
0.1858	0.983110	1.189	35.84	1.41	314	2.30	120	28.61	12.3	0.880	3.52	4.5
0.1940	0.984790	1.221	35.68	1.45	313	2.35	114	27.95	12.0	0.913	3.93	13.9
0.2359	0.993617	1.376	34.88	1.49	288	2.35	106	27.46	12.9	0.863	3.57	9.6
0.2866	1.004146	1.523	34.20	1.46	363	2.79	99	26.17	13.2	0.866	3.78	11.4
						$Ba(ClO_4)_2$						
0.0141			37.49	0.56	330	0.00	-	33.00	10.5	0.974	3.93	4.6
0.0273			37.79	0.85	471	0.34	194	32.58	10.6	0.976	4.02	6.7
0.0465			38.19	1.21	630	0.81	183	32.10	10.8	0.971	4.07	13.2
0.1000	0.971526	0.870	38.00	1.90	492	2.21	141	29.85	11.1	0.952	4.03	8.0
0.1463	0.984269	1.169	37.68	1.97	714	2.85	139	29.24	12.0	0.897	3.62	6.1
0.1771	0.992814	1.334	37.02	1.99	723	3.01	128	28.37	12.2	0.888	3.64	5.2
0.1929	0.997180	1.416	36.78	2.01	788	3.09	129	28.29	12.7	0.859	3.39	5.7
0.2460	1.011665	1.649	35.63	2.03	773	3.17	119	27.03	13.3	0.835	3.39	4.6

[a] Units: c in mol L^{-1}; ρ in g cm^{-3}; κ in S m^{-1}; τ_j in ps; ε, ε_∞, S_j, and β are dimensionless. [b] Neat DMF densities varied slightly between runs and were 0.943 910 for $Mg(CF_3SO_3)_2$ and 0.943 816 for $Ba(ClO_4)_2$ solutions. [c] Fixed value.

dx.doi.org/10.1021/jp1116307 |J. Phys. Chem. B 2011, 115, 2234–2242

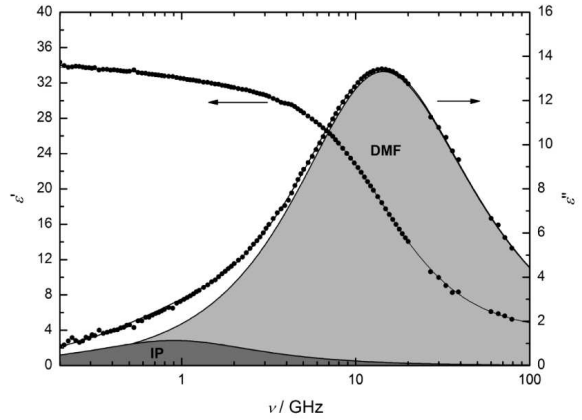

Figure 2. Permittivity, $\varepsilon'(\nu)$, and dielectric loss, $\varepsilon''(\nu)$, spectra of 0.3647 mol L^{-1} $NaCF_3SO_3$ in DMF at 25 °C. The shaded areas show the contributions of the ion-pair (IP) and of the solvent relaxation process (DMF) to $\varepsilon''(\nu)$.

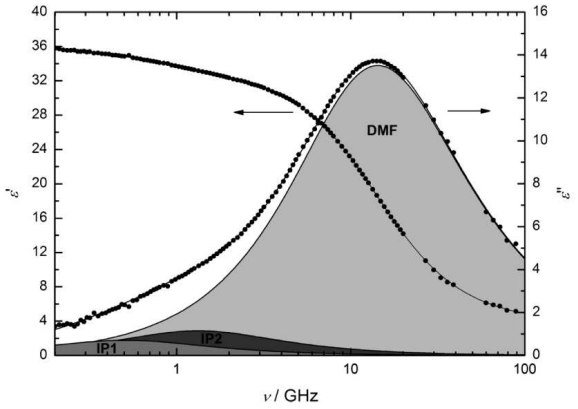

Figure 3. Permittivity, $\varepsilon'(\nu)$, and dielectric loss, $\varepsilon''(\nu)$, spectra of 0.1858 mol L^{-1} $Mg(CF_3SO_3)_2$ in DMF at 25 °C. The shaded areas show the contributions of two ion-pairs (IP1 and IP2) and of the solvent relaxation process (DMF) to $\varepsilon''(\nu)$.

dependence of the DR spectrum of neat DMF revealed additional small but systematic effects at high frequencies, probably arising from low-energy librational modes and molecular inertia. For fitting purposes, these effects were formally described with a small-amplitude Debye process centered at ca. 150 GHz.[35] However, in the present study these small deviations were accounted for by fitting the DMF spectrum with an asymmetrically broadened (Cole−Davidson) model. This approach has the advantage of requiring one less fitting parameter than a two-D model,[35] which aids the overall fitting of the DR spectra of the salt solutions.

In addition to the dominant solvent relaxation, the present DR spectra for all three sets of salt solutions in DMF showed either one ($NaCF_3SO_3$) or two ($Mg(CF_3SO_3)_2$ and $Ba(ClO_4)_2$) low-frequency Debye processes centered at $\nu < 2$ GHz. The presence of these low-frequency modes was essential for an accurate fit of the observed spectra at low frequencies and was confirmed by the recently developed method for bias-free determination of the number of relaxation processes required for the formal fit of a given spectrum[34] (Supporting Information, Figures S4−S6). From their location in the spectrum and the concentration dependence of their amplitudes, all of these low-frequency processes can be assigned with confidence to the rotational diffusion of ion pairs in solution. The triflate anion also has a dipole moment that must therefore contribute to the observed spectra. However, because it is fairly small and has a relatively low dipole moment ($\mu_- \approx 3.6$ D from quantum mechanical calculations),[36] the contribution from the triflate ion is small over the investigated concentration ranges and probably occurs at relatively high frequencies. It is therefore reasonable to assume that the triflate mode is subsumed by the much more intense solvent relaxation without significantly affecting the quantitative interpretation of the latter.

Overall fits of the spectra were achieved, therefore, with either a two-process (D + CD; for $NaCF_3SO_3$) or a three-process (D + D + CD; for $Mg(CF_3SO_3)_2$ and $Ba(ClO_4)_2$) model. The quality of the fits obtained and the contributions of the individual processes to the observed spectra are summarized in Table 1 and illustrated for $NaCF_3SO_3$ and $Mg(CF_3SO_3)_2$ in Figures 2 and 3, respectively. Fits for $Ba(ClO_4)_2$ in DMF were similar to the latter (Supporting Information, Figure S7). A quantitative analysis of the spectra is given below.

3.2. Solvent Relaxation and Ion Solvation. A representative plot, for $Mg(CF_3SO_3)_2$, of the dispersion amplitude (relaxation strength, S_s) of the major solvent process at 15 GHz, observed in all of the present solutions in DMF, is included (uppermost curve) in Figure 4(a). The corresponding relaxation times, τ_s, are plotted (lowermost curve) in Figure 4(b). Similar data were obtained for the other two sets of salt solutions (Supporting Information, Figures S8 and S9). For all of the present salt solutions, the magnitude of S_s decreases steadily with solute concentration, c, which is indicative of strong ion solvation.

The extent of ion−solvent interactions can be quantified using the generalized Cavell equation[37]

$$c_j = \frac{3(\varepsilon + (1-\varepsilon)A_j)}{\varepsilon} \cdot \frac{k_B T \varepsilon_o}{N_A} \cdot \frac{(1-\alpha_j f_j)^2}{g_j \mu_j^2} \cdot S_j \qquad (4)$$

normalized with respect to the pure solvent. In eq 4, S_j is the amplitude, c_j the concentration, μ_j the dipole moment, α_j the polarizability of the relaxing species, ε (= $\lim_{\nu \to 0} \varepsilon'(\nu)$) the static permittivity of the solution, and T the thermodynamic temperature in Kelvin, and k_B and N_A are, respectively, the Boltzmann and Avogadro constants. The reaction-field and cavity-field factors, f_j and A_j, are defined by the size and shape of the rotating dipole,[30] while the static (Kirkwood) dipole−dipole correlation factor, g_j, accounts for orientational correlation of neighboring species of the same kind. For the present reasonably dilute solutions it was assumed that the correlation factor of the solvent is independent of the salt concentration and thus cancels out in the normalization of eq 4. This is reasonable as the value of g_j is close to unity in neat DMF,[35] consistent with the absence of significant long-range dipole−dipole correlations of the solvent molecules.

Effective solvation numbers for the solute were obtained from the solvent dispersion amplitudes as described previously.[24,38] Briefly, this involves correction of the observed solvent dispersion amplitude for kinetic depolarization (kd), which is related to the movement of the solvated ions in the applied field. The kd was calculated using the Hubbard−Onsager continuum model.[39,40] The apparent concentration of rotationally free solvent molecules,

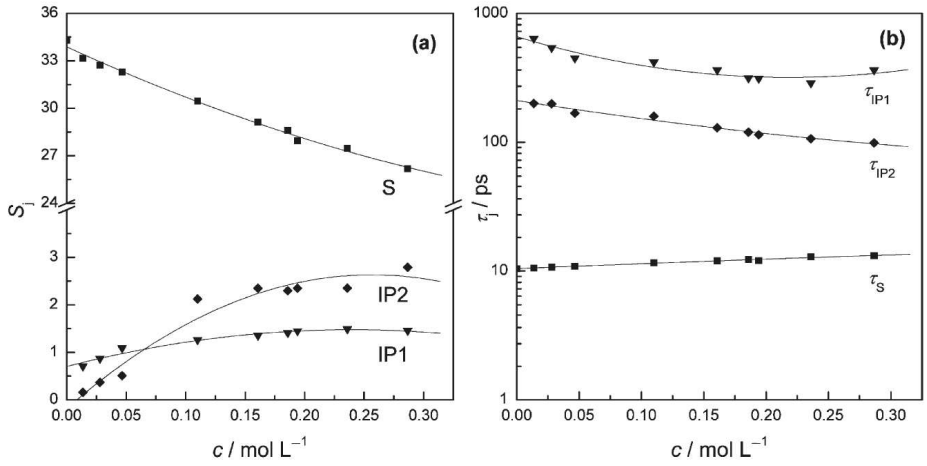

Figure 4. (a) Dispersion amplitudes, S_j, and (b) relaxation times, τ_j, as functions of solute concentration for DMF solutions of $Mg(CF_3SO_3)_2$ at 25 °C (lines included only as a visual guide).

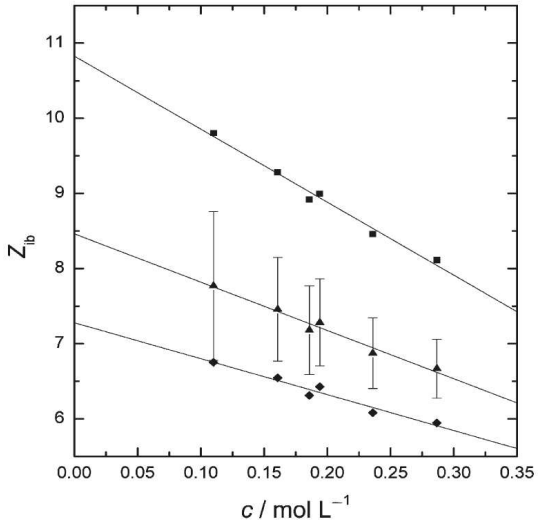

Figure 5. Effective solvation numbers, Z_{ib}, for $Mg(CF_3SO_3)_2$ in DMF at 25 °C as a function of solute concentration under various transport boundary conditions: ■ no kd, ▲ slip kd, ♦ stick kd. Error bars correspond to the standard deviation of a fit of the equation $S_S(c) = S_S(0)$ [=34.29] $+ a_1c + a_2c^{3/2}$ to the experimental solvent amplitudes.

c_s^{ap}, was then determined for three limiting cases: negligible kd and kd with ion transport under *slip* or *stick* boundary conditions. Subtraction of c_s^{ap} from the analytical (total) solvent concentration, c_s, then allows determination of the effective solvation number, Z_{ib}, the number of irrotationally bound (ib) solvent molecules per "particle" of solute

$$Z_{ib} = (c_s - c_s^{ap})/c \qquad (5)$$

where c is the (total) electrolyte concentration in the solution. As defined, Z_{ib} can be thought of as the average number of solvent molecules per solute particle "frozen" on the DR time scale and thus not contributing to the solvent relaxation process.[38]

Typical results obtained for $Z_{ib}(c)$ in $Mg(CF_3SO_3)_2$ solutions in DMF are shown in Figure 5. Similar values were determined for the other two sets of salt solutions (Supporting Information, Figures S10 and S11). Note that the increase in the uncertainty in $Z_{ib}(c)$ as $c \rightarrow 0$ is normal. This is because, while the uncertainty of S_s (estimated as one standard deviation of the fit of the empirical equation $S_s(c) = S_s(0)$ [=34.29] $+ a_1c + a_2c^{3/2}$ to the experimental solvent amplitudes) and thus of c_s^{ap} is constant, the uncertainty in $Z_{ib}(c)$ rises as both $(c_s - c_s^{ap})$ and $c \rightarrow 0$. Within these uncertainty limits, Z_{ib} was found to vary smoothly with c for all three systems and ion-transport boundary conditions. The infinite dilution values, $Z_{ib}(0)$, obtained by linear extrapolation of $Z_{ib}(c)$ are collected in Table 2. As would be expected, they vary in the order *stick* < *slip* < no kd for each electrolyte; *slip* conditions are generally considered to be the most realistic for the dielectric relaxation of solvated ions.[3]

Table 2. Effective Solvation Numbers at Infinite Dilution, $Z_{ib}(0)$, for $NaCF_3SO_3$, $Mg(CF_3SO_3)_2$, and $Ba(ClO_4)_2$ in DMF Solutions at 25 °C Obtained with Various Ion-Transport Boundary Conditions[a]

electrolyte	$Z_{ib}(0)$ (no kd)	$Z_{ib}(0)$ (*slip*)	$Z_{ib}(0)$ (*stick*)
$NaCF_3SO_3$	6.2(3)	5.0(3)	4.4(3)
$Mg(CF_3SO_3)_2$	10.8(2)	8.5(2)	7.3(2)
$Ba(ClO_4)_2$	13.4(6)	10.6(6)	9.3(6)

[a] Numbers in parentheses are standard deviations in the last digit, derived from linear least-squares fits.

Literature data show that neither $CF_3SO_3^-$ nor ClO_4^- is well solvated in DMF,[11,41−44] consistent with the low charge density of both ions and the poor acceptor properties of DMF.[13,20] This suggests that it is reasonable to assume that $Z_{ib}(CF_3SO_3^-) \approx Z_{ib}(ClO_4^-) \approx 0$ in DMF and thus, following Wurm et al.,[11] that the Z_{ib} values given in Table 2 can be assigned fully to the cations. The present results therefore indicate that at infinite dilution in DMF the cation Na^+ has an effective solvation number on the DRS time scale of ~5, which is essentially the same as the value of $Z_{ib}(0) = 4.9 \pm 0.3$ derived for Na^+ by Wurm et al. from DRS measurements on $NaClO_4$ in DMF assuming *slip* conditions.[11] The Z_{ib} values for both Mg^{2+} and Ba^{2+} (Table 2) suggest at least partial formation of a second solvation sheath. This is undoubtedly true for Mg^{2+}, which is certainly too small ($r_+ = 72$ pm)[45] to

The Journal of Physical Chemistry B ARTICLE

accommodate the likely number of immobilized solvent molecules (~9) in its first coordination shell.

The present $Z_{ib}(0)$ values for the cations in DMF (Table 2) can be compared with those obtained from DRS measurements in water, ~4.5 and ~14 for Na^+ and Mg^{2+}, respectively, under *slip* boundary conditions (Ba^{2+} does not appear to have been studied by DRS in aqueous solution).[3] The similarity of $Z_{ib}(Na^+)$ in DMF and H_2O is a little surprising at first glance, given the much greater molecular size of DMF, but the present results are broadly compatible with the solvation numbers reported for Na^+ in DMF of ~3 (from transference measurements)[46] and ~6 (from NMR data).[47] Also, it has to be kept in mind that Z_{ib} is mainly determined by the strength of ion−solvent interactions, whereas coordination numbers are more sensitive to packing requirements. For Mg^{2+} the present value of $Z_{ib} \approx 9$ in DMF is considerably smaller than that observed in H_2O, which is a reflection of the highly developed second hydration shell of $Mg^{2+}(aq)$ associated, at least in part, with extensive H-bonding. On the other hand the present value in DMF is rather larger than the (solid state) coordination number of six DMF molecules obtained from single-crystal X-ray diffraction studies[48,49] and the (solution) solvation number, also ~6, estimated by Raman spectroscopy in DMF solutions.[50] These differences reflect the greater role of packing effects in determining coordination numbers, as well as the sensitivity of Raman to nearest-neighbor interactions. The present value of $Z_{ib}(Ba^{2+})_{DMF} \approx 10.6$ (Table 2) is slightly larger than the value of 8.4 obtained from Raman data[50] and again implies at least the partial existence of a second solvation shell.

3.3. Solute Relaxations and Ion Association. Ion association in electrolyte solutions is usually best described by the well-known Eigen−Tamm model[51]

$$M^{n+} + L^- \overset{K_1}{\leftrightarrow} \underset{2SIP}{[MS_2L]^{(n-1)+}} \overset{K_2}{\leftrightarrow} \underset{SIP}{[MSL]^{(n-1)+}} \overset{K_3}{\leftrightarrow} \underset{CIP}{[ML]^{(n-1)+}} \quad (6)$$

in which solvated ions initially combine with their solvation sheaths essentially intact, to form double solvent separated ion pairs (2SIPs). The 2SIPs may then lose their intervening oriented solvent molecules (S) to form successively solvent-shared (SIPs) and contact (CIPs) ion pairs. While the Eigen−Tamm mechanism (eq 6) is thought to be generally applicable, this does not mean that all species will be present (or at least detectable) in any given electrolyte/solvent mixture.

The DMF solutions of all three investigated electrolytes exhibit a low-amplitude but well-defined solute-related relaxation process centered at $\nu < 1.0$ GHz (Figures 2 and 3 and Supporting Information Figure S7). In addition, both $Mg(CF_3SO_3)_2$ and $Ba(ClO_4)_2$ show an additional process centered at ~2 GHz. From their location in the spectra and the concentration dependence of their amplitudes, these low-frequency processes can be attributed to the presence of ion pairs in solution. To help to establish which ion-pair types are present, it is useful to compare the observed ion-pair relaxation times with calculated values.

Ion-Pair Relaxation Times. The observable macroscopic relaxation time τ_{obs} for a Debye process is a collective property that can be related to the corresponding molecular rotational correlation time τ'_{obs} via the Powles−Glarum equation[52,53]

$$\tau_{obs} = \frac{3\varepsilon}{2\varepsilon + \varepsilon_\infty} \cdot \tau'_{obs} \quad (7)$$

Table 3. Comparison of Experimental, τ'_{obs},[a] and Calculated Rotational Correlation Times for *Stick* and *Slip* Boundary Conditions, τ'_{stick} and τ'_{slip},[b] for Ion-Pair Reorientation in Salt Solutions in DMF at 25 °C[c]

electrolyte	τ'_{obs}	IP	τ'_{slip}	τ'_{stick}
$NaCF_3SO_3$	122	CIP	7	105
		SIP	102	310
		2SIP	348	697
$Mg(CF_3SO_3)_2$	104 (τ_2)	CIP	4	94
		SIP	88	284
	299 (τ_1)	2SIP	318	653
$Ba(ClO_4)_2$	103 (τ_2)	CIP	8	65
		SIP	96	228
	478 (τ_1)	2SIP	323	551

[a] Obtained via the Powles−Glarum relation (eq 7). [b] Obtained from the SED relation (eq 8). [c] Unit: τ_j in ps.

The τ'_{obs} values can be compared with the theoretical values of the rotational correlation time, τ', calculated from the molecular volume of rotation, V_r, and the bulk solution viscosity, η, via the Stokes−Einstein−Debye equation[54,55]

$$\tau' = \frac{3V_r}{k_B} \cdot \frac{\eta}{T} \quad (8)$$

Solution viscosities were assumed, in the absence of experimental data, to be the same as neat DMF (0.802 mPa s).[13] The value of V_r is obtained via the relationship $V_r = V_m f_\perp C$, where V_m is the (geometric) molecular volume of the rotating species; $f_\perp$ is a shape factor; and C is the hydrodynamic coupling constant between the rotating species and its environment ($C = 1$ for *stick* or $C = 1 - f_\perp^{-2/3}$ for *slip* boundary conditions). For convenience, the ion pairs were approximated as prolate ellipsoids when calculating $f_\perp$ using the approach of Dote and Kivelson.[54]

Microscopic relaxation times obtained using eq 8 for all plausible ion-pair types rotating under *slip* and *stick* hydrodynamic boundary conditions are collected in Table 3 along with the observed molecular rotational correlation times. Unfortunately, comparisons of the observed results (calculated via eq 7) with those calculated using the SED model (eq 8) do not unequivocally identify the relaxing species in the present solutions. Considering the simplest system ($NaCF_3SO_3$) first, the τ'_{obs} value of 122 ps is consistent with either a SIP rotating under *slip* conditions or a CIP under *stick* conditions (Table 3). As *slip* conditions are generally considered more likely for dissolved molecular-level species,[55] this implies (but does not prove) the presence of SIPs rather than CIPs, which is also consistent with the strong solvation of Na^+ by DMF and the weak solvation of $CF_3SO_3^-$ (Section 3.2).

For solutions of $Mg(CF_3SO_3)_2$ and $Ba(ClO_4)_2$ in DMF, the situation is also not clear-cut. The observed relaxation times for the two solute-related processes centered at $\nu < 2$ GHz appear to be consistent with either a combination of SIPs and 2SIPs rotating under *slip* boundary conditions or a CIP + SIP combination rotating under *stick* conditions (Table 3). The former would appear to be more likely, consistent with the preference of *slip* conditions for molecular rotation[55] and the evidence from the Z_{ib} values for the existence of at least a partial second solvation shell around the doubly charged cations (Section 3.2). Nevertheless, it must be recognized that, while the SED equation (originally derived for

macroscopic bodies rotating in a continuous medium) works surprisingly well for molecular-level entities,[54,55] significant approximations must be made in calculating the relaxation times.[54] For example, a more sophisticated analysis of the solvated ion-pair geometry, e.g., by making allowance for the specific orientation of the intervening solvent molecule(s),[8] might be necessary to produce more realistic values of IP rotational correlation times.

Ion-Pair Concentrations. The observed solute-related amplitudes (collectively labeled S_{IP}) can be used to estimate the corresponding ion-pair concentrations (c_{IP}) via the Cavell equation. As the types of ion pairs present are not known a priori, the required input parameters for eq 4, α_j, g_j, f_j, A_j, and μ_j were calculated for all plausible ion-pair structures. Polarizabilities of the ion pairs were estimated assuming: $\alpha_{IP} = \alpha_+ + \alpha_- + n\alpha_{DMF}$, with $\alpha/4\pi\varepsilon_o$Å^3 = 0.211 (Na^+),[56] 0.111 (Mg^{2+}),[57] 1.50 (Ba^{2+}),[58] 6.84 ($CF_3SO_3^-$),[59] 5.45 (ClO_4^-),[58] 7.88 (DMF),[35] and n = 0, 1, or 2. Because the ion-pair concentrations are low, interactions between them should be negligible, and so g_{IP} values were assumed to be unity throughout. The field factors f_j and A_j were calculated by standard procedures.[37] Evaluation of the ion-pair dipole moments μ_j, which represent the major uncertainty in calculating ion-pair concentrations via eq 4, is discussed in the following section.

Estimation of Ion-Pair Dipole Moments. The dipole moment of an ion pair in solution, μ_{IP}, is given by

$$\mu_{IP} = \mu^o_{IP} - \mu_{ind} - n\mu_s - \mu_- \qquad (9)$$

which involves adjustment of μ^o_{IP}, the gas-phase dipole moment, for the presence of n (= 0, 1, or 2) oriented solvent molecules of dipole moment μ_s between the ions, for the induced dipole moment, μ_{ind}, due to the polarizabilities of the ions,[60] and for the dipole moments of the ions themselves.[37] For the salts studied here, only the triflate ion has a dipole moment (μ_- = 3.60 D).[36]

The values of μ^o_{IP} for the monovalent electrolyte $NaCF_3SO_3$ ($z_+ = |z_-| = 1$) were calculated as[37]

$$\mu^o_{IP} = ze_o d \qquad (10)$$

where e_o is the elementary charge and d the distance between the charges ($d = r_+ + r_- + 2nr_s$, where n = 0, 1, or 2 for CIPs, SIPs, and 2SIPs, respectively). Calculation of μ^o_{IP} for the charged ion pairs, $MgCF_3SO_3^+$ and $BaClO_4^+$, formed in solutions of the two asymmetric electrolytes, is less straightforward because the reference point is no longer uniquely defined. A natural choice of reference point is the pivot of the charged dipole.[37] For a spherocone with $C_{n\infty}$ symmetry, the pivot is located on the symmetry axis at a point o_B defined by the positions of the cation and anion centers (o_+ and o_-), yielding[37]

$$\mu^o_{IP} = e_o|z_+(o_+ - o_B) + z_-(o_- - o_B)| \qquad (11)$$

The center of hydrodynamic stress was taken as the pivot, o_B, as it is more appropriate for dipole rotation in a viscous medium than the center of mass.[37] The radii assumed for the calculation of the ion-pair dipole moments were:[45] r_+/pm = 102 (Na^+), 72 (Mg^{2+}), 136 (Ba^{2+}); r_-/pm = 307 ($CF_3SO_3^-$, taken as an ellipsoid)[61] and 240 (ClO_4^-), and r_s/pm = r_{DMF} = 330.[35] Induced dipole moments were calculated as

$$\mu_{ind} = \frac{d^4(z_-\alpha_+ + z_+\alpha_-) + 2(z_+ + z_-)d\alpha_+\alpha_-}{d^6 - 4\alpha_+\alpha_-} \cdot e_o \qquad (12)$$

The μ_{IP} values obtained from these calculations are summarized in Table 4. Dipole moments for the CIPs[62] were also calculated with MOPAC[36] to crosscheck the above approach, although such calculations for ion pairs are not without their problems.[63] For $NaCF_3SO_3^0$ (μ_{IP} = 13.0 D) and $BaClO_4^+$ (16.0 D), the MOPAC-calculated moments agree very well with the corresponding values listed in Table 4 (14.0 and 17.4 D, respectively). For $MgCF_3SO_3^+$, the difference (21.7 vs 27.1 D) is larger, which can be attributed in part to the different reference points of the two calculations (MOPAC uses the center of mass). Nevertheless, the comparison lends credence to the calculation procedure (eqs 9−12) which at present is the only route to μ_{IP} values for SIPs and 2SIPs.

Table 4. Estimated Ion-Pair Dipole Moments, μ_{IP}, and Standard Overall Association Constants, K^o_A, for DMF Solutions of $NaCF_3SO_3$, $Mg(CF_3SO_3)_2$, and $Ba(ClO_4)_2$ at 25 °C[a]

	$NaCF_3SO_3$		$Mg(CF_3SO_3)_2$			$Ba(ClO_4)_2$	
	μ_{IP}	K^o_A	μ_{IP}	K^o_A		μ_{IP}	K^o_A
CIP	14.0	68 ± 16	27.1			17.4	
SIP	43.6	**5 ± 2**	51.3	**84 ± 7**[b]	224 ± 11[c]	38.2	**21 ± 6**[b] 48 ± 1500[c,d]
2SIP	71.7	2.2 ± 0.7	71.9			55.3	

[a] Units: μ_{IP} in D; K^o_A in L mol^{-1}. Preferred K^o_A values (see text) in bold underline. [b] Combined 2SIP + SIP model. [c] Combined SIP + CIP model. [d] The large uncertainty is an artifact of the fitting process.

Ion-Pair Formation. Assuming only species of 1:1 stoichiometry are formed, the overall ion association constant for an electrolyte, K_A, can be expressed as

$$K_A = \frac{c_{IP}}{c_+c_-} \qquad (13)$$

where here c_{IP} is the *total* ion pair concentration (i.e., the sum of all IP types present) and c_+ and c_- are the *free* ion concentrations. Combination of c_{IP} determined from eq 4 and the usual mass balance relationships gives K_A at each value of the electrolyte concentration, c. The standard state (infinite dilution) constant K^o_A can then be obtained from $K_A(c)$ using, for example, a Guggenheim-type equation[11]

$$\log K_A = \log K^o_A - \frac{2A_{DH}|z_+z_-|\sqrt{I}}{1 + a_K\sqrt{I}} + b_K I + c_K I^{3/2} \qquad (14)$$

where A_{DH} (= 1.5554 L$^{1/2}$ mol$^{-1/2}$)[64] is the Debye−Hückel constant for DMF; y_K ($y = a, b, c$) are empirical parameters; and I is the stoichiometric ionic strength ($I = (1/2)\sum_i c_i z_i^2$).[11]

The overall association constants, $K_A(c)$, for $NaCF_3SO_3$ in DMF obtained via eqs 4 and 13 assuming only SIPs were formed are plotted against I in Figure 6. Extrapolation to infinite dilution with eq 14 gave a standard value of $K^o_A = (5 \pm 2)$ L mol^{-1}, which is comparable with the value of 4.2 L mol^{-1} reported for SIPs for $NaClO_4$ in DMF, also obtained by DRS.[11] As expected, quite different values of K^o_A are obtained if different types of ion pairs are assumed to be present (Table 4). However, as noted above, the DRS data for $NaCF_3SO_3$ appear to be most consistent with the presence of SIPs alone, which suggests that the degree of association of this salt in DMF is very small. This finding vindicates the assumption of complete dissociation for this salt in previous thermodynamic studies.[17] It would be useful to compare the present K^o_A value with, e.g., conductivity measurements; however, to the best of our knowledge, no such data are available in the literature, and it should be noted that the quantification of such a weak association using conventional techniques such as conductometry is not a trivial task.[21]

Interpretation of the ion association data for both $Mg(CF_3SO_3)_2$ and $Ba(ClO_4)_2$ is complicated by the presence in the DR spectra of

the two strongly overlapping but weak ion-pair modes. This produces parameter coupling in the fit, which in turn affects the accuracy with which the ion-pair amplitudes can be determined (Figure 4 and Supporting Information, Figure S9). Even so, bias-free fitting[34] clearly shows there are two low-frequency modes in the DR spectra of both 2:1 salts (Supporting Information, Figures S5 and S6). As usual, the overall level of ion association is strongly dependent on the nature of the IPs taken to be present (Table 4). Consistent with the Z_{ib} values and the assumption of *slip* boundary conditions (see above), assignment of the two low-frequency processes (Figures 3 and S6) to the rotational diffusion of 2SIPs (centered at $\nu \approx 0.2$ GHz) and SIPs (centered at $\nu \approx 1.5$ GHz) seems most plausible. The K_i values obtained on the basis of this model are plotted in Figure 7 for both $Mg(CF_3SO_3)_2$ and $Ba(ClO_4)_2$ solutions in DMF. As would be expected from the reaction scheme summarized in eq 6, the values of $K_2(c)$, which correspond to an equilibrium that involves only a change in solvation, are virtually independent of I (the decreases in $K_2(c)$ at $I \lesssim 0.3$ mol L^{-1} are almost certainly a reflection of errors), while K_1 and therefore K_A ($= K_1 + K_1K_2$), which involve charged species, show the expected increase as $I \rightarrow 0$.

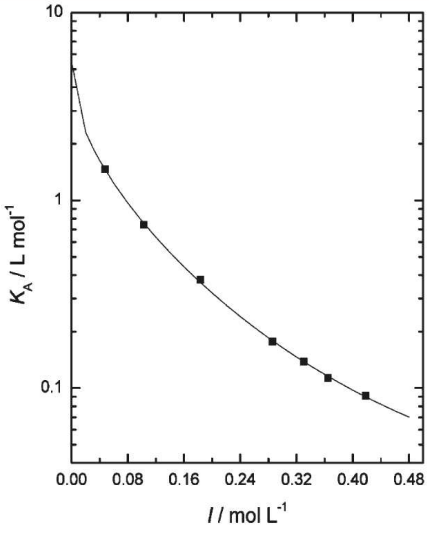

Figure 6. Overall association constant, K_A, for $NaCF_3SO_3$ in DMF at 25 °C as a function of ionic strength, I, assuming only SIPs are present. The curve represents the fit obtained using eq 14 with the y_K values listed in the Supporting Information (Table S1).

On the basis of the 2SIP + SIP model, it appears that both $Mg(CF_3SO_3)_2$ and $Ba(ClO_4)_2$ are only moderately associated in DMF at 25 °C, with K_A° values of just 84 and 21 L mol^{-1}, respectively (Table 4). As for $NaCF_3SO_3$, there are no data available in the literature that are directly comparable with the present values. Nevertheless, a K_A° of 182 L mol^{-1} has been reported[7] for $Mg(ClO_4)_2$ in acetonitrile using a combination of DR and infrared spectroscopies. While acetonitrile has a dielectric constant and acceptor number that are similar to those of DMF, it is a much weaker cation solvator (electron-density donor),[20] which implies a higher level of ion association than in DMF. The results for both of the present 2:1 electrolytes suggest that ion association will have only relatively minor effects on the determination of their thermodynamic properties in DMF,[17] especially when it is remembered that the association constants of higher-charged electrolytes decrease quickly with increasing concentration (Figure 7).

4. CONCLUDING REMARKS

The present DR spectra have shown that all three cations, Na^+, Mg^{2+}, and Ba^{2+}, are strongly solvated in DMF with indications of a well-developed second solvation shell for Mg^{2+} and to a lesser extent for Ba^{2+}. Detailed analysis of the spectra have indicated the presence of only SIPs in DMF solutions of $NaCF_3SO_3$ and two types of ion pairs (most likely SIPs and 2SIPs) in $Mg(CF_3SO_3)_2$ and $Ba(ClO_4)_2$ solutions. The overall level of association for all three salts was low, with standard association constants (K_A°) increasing in the order: $NaCF_3SO_3$ < $Ba(ClO_4)_2$ < $Mg(CF_3SO_3)_2$. These results support, to some extent, the widespread assumption of complete dissociation of these and related electrolytes in thermodynamic studies.

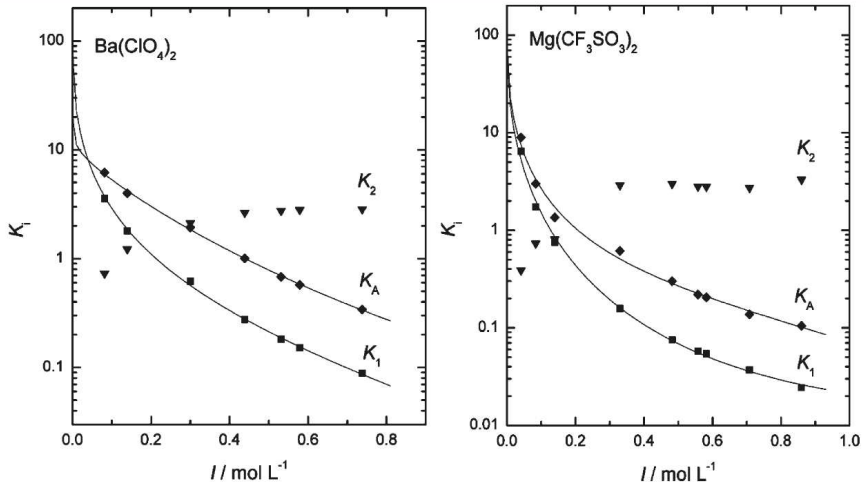

Figure 7. Overall association constants, K_A, and stepwise formation constants K_1 and K_2 as functions of ionic strength, I, assuming a 2SIP + SIP model for DMF solutions of $Ba(ClO_4)_2$ and $Mg(CF_3SO_3)_2$ at 25 °C. Curves for K_A and K_1 were obtained using eq 14 with the y_K values for K_A listed in the Supporting Information, Table S1.

The Journal of Physical Chemistry B ARTICLE

■ ASSOCIATED CONTENT

Supporting Information. Figures showing the conductivity contribution, the relaxation-time distribution functions obtained with the method of ref 34, and figures analogous to Figures 1, 3, 4, and 5 for the other electrolytes. This material is available free of charge via the Internet at http://pubs.acs.org.

■ AUTHOR INFORMATION

Corresponding Author

*E-mail: g.hefter@murdoch.edu.au; richard.buchner@chemie.uni-regensburg.de.

■ ACKNOWLEDGMENT

Murdoch University and the German Academic Exchange Service (DAAD) are gratefully acknowledged for funding AP's stays in Australia and Germany, respectively. HMAR thanks the Higher Education Commission of Pakistan for financial support. AP thanks Prof. Wacław Grzybkowski for his ongoing encouragement.

■ REFERENCES

(1) Buchner, R. Dielectric Spectroscopy of Solutions. In *Novel Approaches to the Structure and Dynamics of Liquids: Experiments, Theories and Simulations*; Samios, J., Durov, V. A., Eds.; Kluwer: Dordrecht, Netherlands, 2004.
(2) Buchner, R. *Pure Appl. Chem.* **2008**, *80*, 1239.
(3) Buchner, R.; Hefter, G. *Phys. Chem. Chem. Phys.* **2009**, *11*, 8984.
(4) Barthel, J.; Feuerlein, F. *J. Solution Chem.* **1984**, *13*, 393.
(5) Barthel, J.; Feuerlein, F. *Z. Phys. Chem.* **1986**, *148*, 157.
(6) Barthel, J.; Kleebauer, M.; Buchner, R. *J. Solution Chem.* **1995**, *24*, 1.
(7) Eberspächer, P.; Wismeth, E.; Buchner, R.; Barthel, J. *J. Mol. Liq.* **2006**, *129*, 3.
(8) Buchner, R.; Hefter, G. *J. Solution Chem.* **2002**, *31*, 521.
(9) Barthel, J.; Bachhuber, K.; Buchner, R. *Z. Naturforsch., A: Phys. Sci.* **1995**, *50*, 65.
(10) Wurm, B.; Baar, C.; Buchner, R.; Barthel, J. *J. Mol. Liq.* **2006**, *127*, 14.
(11) Wurm, B.; Münsterer, M.; Richardi, J.; Buchner, R.; Barthel, J. *J. Mol. Liq.* **2005**, *119*, 97.
(12) Chadwick, S. S. *Encyclopedia of Industrial Chemistry*; Wiley-VCH: Weinheim, 2006.
(13) Marcus, Y. *The Properties of Solvents*; John Wiley: London, 1998.
(14) Kalidas, C.; Hefter, G.; Marcus, Y. *Chem. Rev.* **2000**, *100*, 819.
(15) Hefter, G.; Marcus, Y.; Waghorne, W. E. *Chem. Rev.* **2002**, *102*, 2773.
(16) Jenkins, H. D. B.; Marcus, Y. *Chem. Rev.* **1995**, *95*, 2695.
(17) Płaczek, A.; Grzybkowski, W.; Hefter, G. *J. Phys. Chem. B* **2008**, *112*, 12366.
(18) Pitzer, K. S. *Activity Coefficients in Electrolyte Solutions*, 2nd ed.; CRC Press: Boca Raton, USA, 1991.
(19) Marcus, Y.; Hefter, G. *Chem. Rev.* **2004**, *104*, 3405.
(20) Marcus, Y. *Ion Solvation*; Wiley: New York, 1985.
(21) Marcus, Y.; Hefter, G. *Chem. Rev.* **2006**, *106*, 4585.
(22) Côté, J.-F.; Desnoyers, J. *J. Solution Chem.* **1999**, *28*, 396.
(23) Barthel, J.; Bachhuber, K.; Buchner, R.; Hetzenauer, H.; Kleebauer, M. *Ber. Bunsen-Ges. Phys. Chem.* **1991**, *95*, 853.
(24) Barthel, J.; Buchner, R.; Eberspächer, P.-N.; Münsterer, M.; Stauber, J.; Wurm, B. *J. Mol. Liq.* **1998**, *78*, 83.
(25) Lide, D. R. *CRC Handbook of Chemistry and Physics*, 77th ed.; CRC Press: Boca Raton, USA, 1996.
(26) Barthel, J.; Wachter, R.; Gores, H.-J. In *Modern Aspects of Electrochemistry*; Conway, B. E., Bockris, J. O'M., Eds.; Plenum: New York, 1979; Vol. 13.
(27) Barthel, J.; Feuerlein, F.; Neueder, R.; Wachter, R. *J. Solution Chem.* **1980**, *9*, 209.
(28) Stoppa, A.; Hunger, J.; Buchner, R. *J. Chem. Eng. Data* **2009**, *54*, 472.
(29) Hoover, T. B. *J. Phys. Chem.* **1964**, *68*, 876.
(30) Böttcher, C. F. J. *Theory of Electric Polarization*, 2nd ed.; Elsevier: Amsterdam, 1973; Vol. 1.
(31) Böttcher, C. F. J.; Bordewijk, P. *Theory of Electric Polarization*, 2nd ed.; Elsevier: Amsterdam, 1978; Vol. 2.
(32) Hunger, J.; Stoppa, A.; Schrödle, S.; Hefter, G.; Buchner, R. *ChemPhysChem* **2009**, *10*, 723.
(33) Buchner, R.; Chen, T.; Hefter, G. *J. Phys. Chem. B* **2004**, *108*, 2365.
(34) Zasetsky, A. Y.; Buchner, R. *J. Phys.: Condens. Matter* **2011**, *23*, 025903.
(35) Barthel, J.; Buchner, R.; Wurm, B. *J. Mol. Liq.* **2002**, *98*−*99*, 51.
(36) Stewart, J. J. P. *MOPAC2009*, version 9.097W ed.; Stewart Computational Chemistry, 2009.
(37) Barthel, J.; Hetzenauer, H.; Buchner, R. *Ber. Bunsen-Ges. Phys. Chem.* **1992**, *96*, 1424.
(38) Buchner, R.; Hefter, G. T.; May, P. M. *J. Phys. Chem. A* **1999**, *103*, 1.
(39) Hubbard, J.; Onsager, L. *J. Chem. Phys.* **1977**, *67*, 4850.
(40) Hubbard, J. B. *J. Chem. Phys.* **1978**, *68*, 1649.
(41) Szymańska-Cybulska, J.; Kamieńska-Piotrowicz, E. *J. Solution Chem.* **2006**, *35*, 1631.
(42) Kamieńska-Piotrowicz, E.; Stangret, J.; Szymańska-Cybulska, J. *Spectrochim. Acta, Part A* **2007**, *66*, 1.
(43) James, D. W.; Mayes, R. E. *J. Phys. Chem.* **1984**, *88*, 637.
(44) Krumgalz, B. S.; Barthel, J. *Z. Phys. Chem.* **1983**, *142*, 161.
(45) Marcus, Y. *Ion Properties*; Marcel Dekker: New York, 1997.
(46) Ohtaki, H. *Pure Appl. Chem.* **1987**, *59*, 1143.
(47) Sacco, A.; Piccinni, M. C.; Holz, M. *J. Solution Chem.* **1992**, *21*, 109.
(48) Ruben, M.; Walther, D.; Knake, R.; Görls, H.; Beckert, R. *Eur. J. Inorg. Chem.* **2000**, 1055.
(49) Rao, C. P.; Rao, A. M.; Rao, C. N. R. *Inorg. Chem.* **1984**, *23*, 2080.
(50) Asada, M.; Fujimori, T.; Fujii, K.; Kanzaki, R.; Umebayashi, Y.; Ishiguro, S.-i. *J. Raman Spectrosc.* **2007**, *38*, 417.
(51) Eigen, M.; Tamm, K. *Z. Elektrochem.* **1962**, *66*, 107.
(52) Powles, J. G. *J. Chem. Phys.* **1953**, *21*, 633.
(53) Glarum, S. H. *J. Chem. Phys.* **1960**, *33*, 639.
(54) Dote, J. L.; Kivelson, D. *J. Phys. Chem.* **1983**, *87*, 3889.
(55) Alavi, D. S.; Hartman, R. S.; Waldeck, D. H. *J. Chem. Phys.* **1991**, *94*, 4509.
(56) Böttcher, C. F. J. *Recl. Trav. Chim. Pays-Bas* **1946**, *65*, 19.
(57) Fajans, K.; Joos, G. *Z. Phys. A* **1924**, *23*, 1.
(58) Pyper, N. C.; Pike, C. G.; Edwards, P. P. *Mol. Phys.* **1992**, *76*, 353.
(59) Płaczek, A. *Determination of polarizability of the triflate anion in N,N-dimethylformamide by refractive index measurements*. Unpublished results, 2008.
(60) Rittner, E. S. *J. Chem. Phys.* **1951**, *19*, 1030.
(61) Okan, S. E.; Champeney, D. C. *J. Solution Chem.* **1997**, *26*, 405.
(62) For SIPs and 2SIPs such calculations were not possible with MOPAC.
(63) Hunger, J.; Stoppa, A.; Buchner, R.; Hefter, G. *J. Phys. Chem. B* **2009**, *113*, 9527.
(64) Bockris, J. O. M.; Reddy, A. K. N. *Modern Electrochemistry: 1. Ionics*, 2nd ed.; Plenum: New York, 1998.

Bibliography

[1] *Hydration Processes in Biology*; Bellisent-Funel, M.-C., Ed.; IOS Press: Dordrecht, 1998.

[2] Sasisanker, P.; Weingärtner, H. *ChemPhysChem* **2008**, *9*, 2802.

[3] Halle, V. P., B.; Denisov *Methods Enzymol.* **2001**, *338*, 178.

[4] Oleinikova, A.; Sasisanker, P.; Weingärtner, H. *J. Phys. Chem. B* **2004**, *108*, 8467.

[5] Modig, K.; Liepinsh, E.; Otting, G.; Halle, B. *J. Am. Chem. Soc.* **2004**, *126*, 102.

[6] Xu, B. J., H.; Berne *J. Phys. Chem. B* **2001**, *105*, 11929.

[7] Liang, T.; Walsh, T. R. *Phys. Chem. Chem. Phys.* **2006**, *8*, 4410.

[8] Kameda, Y.; Sugawara, K.; Usuki, T.; Uemura, O. *Bull. Soc. Chem. Jpn.* **2003**, *76*, 935.

[9] McLain, S. E.; Soper, A. K.; Terry, A. E.; Watts, A. *J. Phys. Chem. B* **2007**, *111*, 4568.

[10] Buchner, R. *Pure Appl. Chem.* **2008**, *80*, 1239.

[11] Buchner, R.; Hefter, G. *Phys. Chem. Chem. Phys.* **2009**, *11*, 8954.

[12] Wyttenbach, T.; Bowers, M. G. *Chem. Phys. Lett.* **2009**, *480*, 1.

[13] Beveridge, A.; Heywood, G. *Biochemistry* **1993**, *32*, 3325.

[14] Bentolila, A.; Vlodavsky, I.; Haloun, C.; Domb, A. J. *Polym. Adv. Technol.* **2000**, *11*, 377.

[15] *Industrial Applications of Surfactants IV*; Karsa, D. R., Ed.; Royal Society of Chemistry: Cambridge, UK, 1999.

[16] *Molecular Cell Biology*; Darnell, J., Lodish, H., Baltimore, D., Eds.; Scientific American Books: New York, 1990.

[17] *Applied Biophysics*; Waigh, T. A., Ed.; Wiley & Sons: Chichester, 2007.

[18] *Ion Solvation*; Marcus, Y., Ed.; Wiley: Chichester, U.K., 1985.

[19] Vrbka, L.; Vondrasek, J.; Jagoda-Cwiklik, B.; Vacha, R.; Jungwirth, P. *Proc. Natl. Acad. Sci.* **2006**, *103*, 15440.

[20] Jagoda-Cwiklik, B.; Vácha, R.; Lund, M.; Srebro, M.; Jungwirth, P. *J. Phys. Chem. B* **2007**, *111*, 14077.

[21] Emad, F. A.; Ottosson, N.; Eisebitt, S.; Eberhardt, W.; Jagoda-Cwiklik, B.; Vácha, R.; Jungwirth, P.; Winter, B. *J. Phys. Chem. B* **2008**, *112*, 12567.

[22] Hess, B.; Van der Vegt, N. F. A. *Proc. Natl. Acad. Sci.* **2009**, *106*, 13296.

[23] Collins, K. D. *Methods* **2004**, *34*, 300.

[24] Collins, K. D.; Neilson, G. W.; Enderby, J. E. *Biophysical Chemistry* **2007**, *128*, 95.

[25] Vlachy, N.; Jagoda-Cwiklik, B.; Vácha, R.; Touraud, D.; Jungwirth, P.; Kunz, W. *Adv. colloid Interface Sci.* **2009**, *146*, 42.

[26] Uejio, J. S.; Schwarz, C. P.; Duffin, A. M.; Drisdell, W. S.; Cohen, R. C.; Saykally, R. J. *Proc. Natl. Acad. Sci.* **2008**, *105*, 6809.

[27] Ottosson, N.; Eisebitt, S.; Eberhardt,; Jagoda-Cwiklik, B.; Vacha, R.; Jungwirth, P.; Winter, B. *J. Phys. Chem. B* **2008**, *112*, 12567.

[28] Meng, E. C.; Kollman, P. *J. Phys. Chem.* **1996**, *100*, 11460.

[29] Alagona, G.; Ghio, C.; Kollman, P. *J. Am. Chem. Soc.* **1986**, *108*, 185.

[30] Jorgensen, W. L.; Gao, J. *J. Phys. Chem.* **1986**, *90*, 2174.

[31] Kuntz, I. D. *J. Am. Chem. Soc.* **1971**, *93*, 514.

[32] Kameda, Y.; Mori, T.; Nishiyama, T.; Usuki, T.; Uemura, O. *Bull. Soc. Chem. Jpn.* **1996**, *69*, 1495.

[33] Kameda, Y.; Fukahara, K.; Mochiduki, K.; Naganuma, H.; Usuki, T.; Uemura, O. *J. Non-Cryst. Solids* **2002**, *312-314*, 433.

[34] Kameda, Y.; Ebata, H.; Usuki, T.; Uemura, O.; Misawa, M. *Bull. Soc. Chem. Jpn.* **1994**, *67*, 3159.

[35] Naganuma, H.; Kameda, Y.; Usuki, T.; Uemura, O. *J. Phys. Soc. Jpn. Suppl. A* **2001**, *70*, 356.

[36] Leung, K.; Rempe, S. B. *J. Am. Chem. Soc.* **2004**, *126*, 344.

[37] Max, J. J.; Chapados, C. *J. Phys. Chem. A* **2004**, *108*, 3324.

[38] *Ion Properties*; Marcus, Y., Ed.; Marcel Dekker: New York, 1997.

[39] Gojlo, E.; Gampe, T.; Krakowiak, J.; Stangret, J. *J. Phys. Chem. A* **2007**, *111*, 1827.

[40] Gojlo, E.; Śmiechowski, M.; Stangret, J. *J. Mol. Struct.* **2005**, *744-747*, 809.

[41] Panuszko, A.; Gojlo, E.; Zielkiewicz, J.; Śmiechowski, M.; Krakowiak, J.; Stangret, J. *J. Phys. Chem. B* **2008**, *112*, 2483.

[42] Stangret, J.; Gampe, T. *J. Phys. Chem. B* **1999**, *103*, 3778.

[43] Pieniążek, P. A.; Stangret, J. *Vibr. Spectrosc.* **2005**, *39*, 81.

[44] Stangret, J.; Gampe, T. *J. Phys. Chem. A* **2002**, *106*, 5393.

[45] Buchner, R.; Capewell, S. G.; Hefter, G.; May, P. M. *J. Phys. Chem. B* **1999**, *103*, 1185.

[46] Maxwell, J. C. *A Treatise on Electricity and Magnetism*; Claredon Press: Oxford, 1881.

[47] Greschner, G. S. *Maxwellgleichungen*; Hüthig: Basel, 1981.

[48] Böttcher, C. F. J.; Bordewijk, P. *Theory of Electric Polarization*; Elsevier: Amsterdam, 1978; Vol. 1 and 2.

[49] Falkenhagen, H. *Theorie der Elektrolyte*; Hirzel: Leipzig, 1971.

[50] Ghowsi, K.; Gale, R. J. *J. Electrochem. Soc.* **1989**, *136*, 2806.

[51] Barthel, J.; Buchner, R. *Chem. Soc. Rev.* **1992**, *21*, 263.

[52] Barthel, J.; Buchner, R.; Steger, H. *Wiss. Zeitschr. THLM* **1989**, *31*, 409.

[53] Debye, P. *Polar Molecules*; Dover Publ.: New York, 1930.

[54] Pellat, H. *Ann. Chim. Phys.* **1899**, *18*, 150.

[55] Cole, K. S.; Cole, R. H. *J. Chem. Phys.* **1941**, *9*, 341.

[56] Cole, K. S.; Cole, R. H. *J. Chem. Phys.* **1942**, *10*, 98.

[57] Davidson, D. W.; Cole, R. H. *J. Chem. Phys.* **1950**, *18*, 1417.

[58] Davidson, D. W.; Cole, R. H. *J. Chem. Phys.* **1951**, *19*, 1484.

[59] Havriliak, S.; Negami, S. *J. Polym. Sci., Part C* **1966**, *14*, 99.

[60] Chalmers, J. M.; Griffiths, P. R. *Handbook of Vibrational Spectroscopy*; Wiley–VCH: Weinheim, 2001.

[61] Onsager, L. *J. Am. Chem. Soc.* **1936**, *58*, 1486.

[62] Kirkwood, J. G. *J. Chem. Phys.* **1939**, *7*, 911.

[63] Fröhlich, H. *Theory of Dielectrics*, 2nd ed.; Oxford University Press: Oxford, 1965.

[64] Cavell, E. A. S.; Knight, P. C.; Sheikh, M. A. *Trans. Faraday Soc.* **1971**, *67*, 2225.

[65] Scholte, T. G. *Physica* **1949**, *15*, 437.

[66] Barthel, J.; Hetzenauer, H.; Buchner, R. *Ber. Bunsen–Ges. Phys. Chem.* **1992**, *96*, 1424.

[67] Kivelson, D.; Madden, P. *Annu. Rev. Phys. Chem.* **1980**, *31*, 523.

[68] Dote, J. C.; Kivelson, D.; Schwartz, R. N. *J. Phys. Chem.* **1981**, *85*, 2169.

[69] Barthel, J.; Kleebauer, M.; Buchner, R. *J. Solution Chem.* **1995**, *24*, 1.

[70] Dote, J. C.; Kivelson, D. *J. Phys. Chem.* **1983**, *87*, 3889.

[71] Powles, J. G. *J. Chem. Phys.* **1953**, *21*, 633.

[72] Glarum, S. H. *J. Chem. Phys.* **1960**, *33*, 639.

[73] Madden, P.; Kivelson, D. *Adv. Chem. Phys.* **1984**, *56*, 467.

[74] Eigen, M.; Tamm, K. *Z. Electrochem.* **1962**, *66*, 93 & 107.

[75] Buchner, R. *Pure Appl. Chem.* **2008**, *80*, 1239.

[76] Marcus, Y.; Hefter, G. *Chem. Rev.* **2006**, *106*, 4585.

[77] Robinson, R. A.; Stokes, R. H. *Electrolyte Solutions*, 2nd ed.; Butterworths: London, 1970.

[78] Moore, W. J.; Hummel, D. O. *Physikalische Chemie*; de Gruyter: Berlin, 1986.

[79] Glasstone, S.; Laidler, K. J.; Eyring, H. *The Theory of Rate Processes*; McGraw Hill: New York, 1977.

[80] Hunger, J. Ph.D. thesis, Regensburg, 2010.

[81] Levine, H.; Papas, C. H. *J. Appl. Phys.* **1951**, *22*, 29.

[82] Blackham, D. V.; Pollard, R. D. *IEEE Trans. Instr. Meas.* **1997**, *46*, 1093.

[83] Wölbl, J. Ph.D. thesis, Regensburg, 1982.

[84] Schrödle, S. Ph.D. thesis, Regensburg, 2005.

[85] Schrödle, S.; Hefter, G.; Kunz, W.; Buchner, R. *Langmuir* **2006**, *22*, 924.

[86] Barthel, J.; Bachhuber, K.; Buchner, R.; Hetzenauer, H.; Kleebauer, M. *Ber. Bunsen–Ges. Phys. Chem.* **1991**, *95*, 853.

[87] Hunger, J.; Stoppa, A.; Hefter, G.; Buchner, R. *J. Phys. Chem. B* **2008**, *112*, 12913.

[88] Gregory, A. P.; Clarke, R. N. *Meas. Sci. Technol.* **2007**, *18*, 1372.

[89] Bevington, P. R. *Data Reduction and Error Analysis for the Physical Sciencies*; McGraw–Hill: New York, 1969.

[90] Steger, H. Ph.D. thesis, Regensburg, 1988.

[91] Zasetsky, A. Y.; Buchner, R. *J. Phys.: Condens. Matter* **2001**, *23*, 025903.

[92] Tikhonov, A. *Dokl. Acad. Nauk SSSR* **1963**, *151*, 501.

[93] Kratky, O.; Leopold, H.; Stabinger, H. *Z. Angew. Phys.* **1969**, *27*, 273.

[94] *CRC Handbook of Chemistry and Physics*, 85th ed.; Lide, D. R., Ed.; CRC Press: Boca Raton, USA, 2004.

[95] Barthel, J.; Wachter, R.; Gores, H. J. Temperature dependence of conductance of electrolytes in nonaqueous solutions. In *Modern Aspects of Electrochemistry*; Conway, B. E., Bockris, J. O., Eds.; Plenum: New York, 1979; Vol. 13, pp 1–79.

[96] Barthel, J.; Graml, H.; Neueder, R.; Turq, P.; Bernard, O. *Curr. Top. Solution Chem.* **1994**, *1*, 223.

[97] Stoppa, A.; Hunger, J.; Buchner, R. *J. Chem. Eng. Data* **2009**, *54*, 472.

[98] Barthel, J.; Feuerlein, F.; Neueder, R.; Wachter, R. *J. Solution Chem.* **1980**, *9*, 209.

[99] Hoover, T. B. *J. Phys. Chem.* **1964**, *68*, 876.

[100] Stewart, J. J. P. MOPAC2009, Stewart Computational Chemistry, Colorado Springs, CO, USA.

[101] Stewart, J. J. P. *J. Mol. Modeling* **2007**, *13*, 1173.

[102] Baker, J. *J. Com. Chem.* **1986**, *7*, 385.

[103] Klamt, A.; Schüürmann, G. *J. Chem. Soc. Perkin Trans.* **1993**, *2*, 799.

[104] Bondi, A. *J. Phys. Chem.* **1964**, *68*, 441.

[105] Senda, N. Winmostar, version 3.78f. http://winmostar.com.

[106] Rahman, H. M. A.; Hefter, G.; Buchner, R. *J. Phys. Chem. B* **2012**, *116*, 314.

[107] Lileev, A. S.; Balakaeva, I. V.; Lyashchenko, A. K. *J. Mol. Liq.* **2000**, *87*, 11.

[108] Longinova, D. V.; Lileev, A. S.; Lyashchenko, A. K.; Khar'kin, V. S. *Russ. J. Inorg. Chem.* **2003**, *48*, 278.

[109] Longinova, D. V.; Lileev, A. S.; Lyashchenko, A. K.; Aladko, L. *J. Non-Cryst. Solids* **2005**, *351*, 2882.

[110] Fukasawa, T.; Sato, T.; Watanabe, J.; Hama, Y.; Kunz, W.; Buchner, R. *Phys. Rev. Lett.* **2005**, *95*, 197802.

[111] Note that at low c, τ_1 for NaOFm(aq) and τ_2 for NaOAc(aq) were fixed to their average values to reduce the scatter of the corresponding amplitudes.

[112] Buchner, R.; Hölzl, C.; Stauber, J.; Barthel, J. *Phys. Chem. Chem. Phys.* **2002**, *4*, 2169.

[113] Wachter, W.; Buchner, R.; Hefter, G. *J. Phys. Chem. B* **2006**, *110*, 5147.

[114] Tromans, A.; May, P. M.; Hefter, G.; Sato, T.; Buchner, R. *J. Phys. Chem. B* **2004**, *108*, 13789.

[115] Fedotova, M. V.; Kruchinin, S. E.; Rahman, H. M. A.; Buchner, R. *J. Mol. Liq.* **2011**, *159*, 9.

[116] Wachter, W.; Buchner, R.; Hefter, G. *In preparation*.

[117] Serr, A.; Netz, R. R. *Int. J. Quantum Chem.* **2006**, *106*, 2960.

[118] Bončina, M.; Apelblat, A.; Bešter-Rogač, M. *J. Chem. Eng. Data* **2010**, *55*, 1951.

[119] Buchner, R.; Chen, T.; Hefter, G. *J. Phys. Chem. B* **2004**, *108*, 2365.

[120] Hubbard, J. B.; Onsasager, L. *J. Chem. Phys.* **1977**, *67*, 4850.

[121] Hubbard, J. B. *J. Chem. Phys.* **1978**, *68*, 1649.

[122] Hubbard, J. B.; Colonomos, P.; Wolynes, P. G. *J. Chem. Phys.* **1979**, *71*, 2652.

[123] Buchner, R.; Hefter, G. T.; May, P. M. *J. Phys. Chem. A* **1999**, *103*, 1.

[124] Daniele, P. G.; Robertis, A. D.; Stefano, C. D.; Sammartano, S.; Rigano, C. *J. Chem. Soc. Dalton Trans.* **1985**, 2353.

[125] Hefter, G. T. *J. Solution Chem.* **1984**, *13*, 179.

[126] Partanen, J. I. *Acta Chem. Scand.* **1998**, *52*, 985.

[127] Alavi, D. S.; Hartman, R. S.; WaldeckYamaguchi, D. H. *J. Chem. Phys.* **1991**, *94*, 4509.

[128] Korson, L.; Drost-Hansen, W.; Millero, F. J. *J. Phys. Chem.* **1969**, *73*, 34.

[129] As Figure 3.12b shows that S_b and S_{comp} from additional set of measurements for NaOAc(aq) are fitting very well with the first set of data, the separate quantitative analysis from that set of data to obtain the hydration numbers of ions is not included in this Section, to make it compatible with the published paper[106].

[130] Strictly, additivity is applicable only at infinite dilution but, given the approximate nature of these calculations and consistent with previous experience,[10,11,123] it continues to hold reasonably well at finite concentrations.

[131] Wachter, W.; Kunz, W.; Buchner, R.; Hefter, G. *J. Phys. Chem. A* **2005**, *109*, 8675.

[132] Error bars for Z_{ib} were calculated for each temperature from the standard deviations of fits of the polynomial $S_b(c) = S_b(0) - a_1c + a_2c^{3/2}$ to S_b with $S_b(0)$ fixed to the corresponding pure-water value of ref. 84. Those for Z_s were obtained from the standard deviations of $S_s(c) = a_1c + a_2c^{3/2}$.

[133] Capewell, S. G.; Buchner, R.; Hefter, G.; May, P. M. *Phys. Chem. Chem. Phys.* **1999**, *1*, 1933.

[134] Payaka, A.; Tongraar, A.; Rode, B. M. *J. Phys. Chem. A* **2009**, *113*, 3291.

[135] Sterpone, F.; Stirnemann, G.; Hynes, J. T.; Laage, D. *J. Phys. Chem. B* **2010**, *114*, 2083.

[136] Fedotova, M. V.; Kruchinin, S. E. personal communication.

[137] Buchner, R.; Samani, F.; May, P. M.; Sturm, P.; Hefter, G. *Chem. Phys. Chem.* **2003**, *4*, 373.

[138] Backlund, S.; Eriksson, F.; Friman, R.; Rundt, K.; Sjöblom, J. *Acta Chem. Scand. A* **1980**, *34*, 381.

[139] Luzar, A. *Faraday Discuss. Chem. Soc.* **1996**, *103*, 29.

[140] Laage, D.; Hynes, J. T. *J. Phys. Chem. B* **2008**, *112*, 14230.

[141] Laage, D.; Stirnemann, G.; Hynes, J. T. *J. Phys. Chem. B* **2009**, *113*, 2428.

[142] Payaka, A.; Tongraar, A.; Rode, B. M. *J. Phys. Chem. A* **2010**, *114*, 10443.

[143] No, K. T.; Grant, A.; Jhon, M. S.; Scheraga, H. A. *J. Phys. Chem.* **1990**, *94*, 4740.

[144] Bakker, H. J. *Chem. Rev.* **2008**, *108*, 1456.

[145] Mancinelli, R.; Botti, A.; Bruni, F.; Ricci, M. A.; Soper, A. K. *Phys. Chem. Chem. Phys.* **2007**, *9*, 2959.

[146] Marcus, Y. *J. Solution Chem.* **2009**, *38*, 513.

[147] Turton, D. A.; Hunger, J.; Hefter, G.; Buchner, R.; Wynne, K. *J. Chem. Phys.* **2008**, *128*, 161102.

[148] Buchner, R.; Barthel, J.; Stauber, J. *Chem. Phys. Lett.* **1999**, *306*, 57.

[149] Walrafen, G. E.; Fisher, M. R.; Hokmabadi, M. S.; Yang, W. H. *J. Chem. Phys.* **1986**, *85*, 6970.

[150] The value for pure water, $\bar{n}_{\mathrm{HB}} = 2.48$,[148] is supported by a number of data from other methods.[200–202].

[151] Cornish-Bowden, A. *J. Biosci.* **2002**, *27*, 121.

[152] Kurhe, D. N.; Dagade, D. H.; Jadhav, J. P.; Govindwar, S. P.; Patil, K. J. *J. Phys. Chem. B* **2009**, *113*, 16612.

[153] Petruska, J.; Goodman, M. F. *J. Biol. Chem.* **1995**, *270*, 746.

[154] Chen, C.; Russu, I. M. *Biophys. J.* **2004**, *87*, 2545.

[155] Starikov, E. B.; Nordén, B. *J. Phys. Chem. B* **2009**, *113*, 4698.

[156] Hefter, G.; Marcus, Y.; Waghorne, W. E. *Chem. Rev.* **2002**, *102*, 2773, and references cited therein.

[157] Lumry, R.; Rajender, S. *Biopolymers* **1970**, *9*, 1125.

[158] Danil de Namor, A. F.; Jafou, O. *J. Phys. Chem. B* **2001**, *105*, 8018.

[159] Degrado, W.; Summa, C.; Pavone, V.; Nastri, F.; Lombardi, A. *Annu. Rev. Biochem.* **1999**, *68*, 779.

[160] Giver, L.; Gershenson, A.; Freskgard, P.; Arnold, F. *Proc. Natl. Acad. Sci.* **1995**, *95*, 12809.

[161] Osipov, S.; Burger, K. *Tetrahedron Lett.* **2000**, *41*, 5659.

[162] *Fluorinated Surfactants: Synthsis, Properties, Applications*; Kiss, E., Ed.; Marcel Decker: New York, 1994.

[163] Riess, J. G. *Colloids Surf. A* **1994**, *84*, 33.

[164] Kraft, M. P.; Riess, J. G. *Biochimie* **1998**, *80*, 489.

[165] Yoder, N. C.; Kumar, K. *Chem. Soc. Rev.* **2002**, *31*, 335.

[166] Lee, H. Y.; Lee, K. H.; Al-Hashimi, H. M.; Marsh, E. N. G. *J. Am. Chem. Soc.* **2006**, *128*, 337.

[167] Bilgicer, B.; Kumar, K. *Proc. Natl. Acad. Sci.* **2004**, *101*, 15324.

[168] Note that at low c, relaxation times for $NaOAcF_3$(aq) were fixed to their average values to reduce the scatter of the corresponding amplitudes.

[169] Eiberweiser, A.; Buchner, R. *J. Mol. Liq.* **2012**, doi:10.1016/j.molliq.2012.03.025.

[170] Bondi, A. *J. Phys. Chem.* **1964**, *68*, 441.

[171] Yamaguchi, T.; Matsuoka, T.; Koda, S. *J. Chem. Phys.* **2009**, *130*, 094506.

[172] Hunger, J.; Stoppa, A.; Schrödle, S.; Hefter, G. T.; Buchner, R. *Phys. Chem. Chem. Phys.* **2009**, *10*, 723.

[173] Note that the τ_b and τ_s values for some of the concentrations of NaOPr(aq), NaOBu(aq), and NaOPen(aq) were fixed during the fitting procedure to reduce the scatter of the corresponding amplitudes.

[174] Okouchi, S.; Moto, T.; Ishihara, Y.; Numajiri, H.; Uedaira, H. *J. Chem. Soc., Faraday Trans.* **1996**, *92*, 1853.

[175] Ishihara, Y.; Okouchi, S.; Uedaira, H. *J. Chem. Soc., Faraday Trans.* **1997**, *93*, 3337.

[176] Fumino, K.; Yukiyasu, K.; Shimizu, A.; Taniguchi, Y. *J. Mol. Liq.* **1998**, *75*, 1.

[177] Shimizu, A.; Fumino, K.; Yukiyasu, K.; ; Taniguchi, Y. *J. Mol. Liq.* **2000**, *85*, 269.

[178] Rezus, Y. L. A.; Bakker, H. J. *Phys. Rev. Lett.* **2007**, *99*, 148301.

[179] Rezus, Y. L. A.; Bakker, H. J. *J. Phys. Chem. A* **2008**, *112*, 2355.

[180] Petersen, C.; Tielrooij, K. J.; Bakker, H. J. *J. Chem. Phys.* **2009**, *130*, 214511.

[181] Tielrooij, K. J.; Hunger, J.; Buchner, R.; Bonn, M.; Bakker, H. J. *J. Am. Chem. Soc.* **2010**, *132*, 15671.

[182] Hunger, J.; Stoppa, A.; Buchner, R.; Hefter, G. *J. Phys. Chem. B* **2009**, *113*, 9527.

[183] Gross, K. U. *Environ. Sci. Technol.* **2008**, *42*, 456.

[184] Lee, I. J.; Jung, G. S.; Kim, K. *J. Solution Chem.* **1994**, *23*, 1283.

[185] Henne, A. L.; Fox, C. J. *J. Am. Chem. Soc.* **1951**, *73*, 2323.

[186] Danielsson, I.; Stenius, P. *J. Colloid Interface Sci.* **1971**, *37*, 264.

[187] Kropman, M. F.; Bakker, H. J. *Science* **2001**, *291*, 2118.

[188] Ohmine, I.; Tanaka, H. *Chem. Rev.* **1993**, *93*, 2545.

[189] Kaatze, U.; Behrends, R.; Pottel, R. *J. Non-Cryst. Solids* **2002**, *305*, 19.

[190] Sato, T.; Buchner, R. *J. Chem. Phys.* **2003**, *119*, 10789.

[191] Stanley, H. E.; Teixeira, J. *J. Chem. Phys.* **1980**, *73*, 3404.

[192] Laage, D.; Stirnemann, G.; Hynes, J. T. *Sci China Phys Mech Astron* **2010**, *53*, 1068.

[193] Laage, D.; Stirnemann, G.; Hynes, J. T. *Acc. Chem. Res.* **2011**, doi:10.1021/ar200075u.

[194] Friberg, S. E.; Lochhead, R. V.; Blute, I.; Waernheim, T. *J. Dipersion Sci. Technol.* **2004**, *25*, 243.

[195] Note that the τ_b and τ_s values for some of the concentrations of NaMS(aq) and NaMSn(aq) were held constant during the fitting procedure to reduce the scatter of the corresponding amplitudes.

[196] Rahman, H. M. A.; Buchner, R. *J. Mol. Liq.* **2012**, doi:10.1016/j.molliq.2012.05.017.

[197] Fernandez, P.; Schrödle, S.; Buchner, R.; Kunz, W. *ChemPhysChem* **2003**, *4*, 1065.

[198] Shaukat, S.; Buchner, R. Unpublished results.

[199] Ficke, L. E.; Brennecke, J. F. *J. Phys. Chem. B* **2010**, *114*, 10496.

[200] Hawlicka, E.; Dlugoborski, T. *Chem. Phys. Lett.* **1997**, *268*, 325.

[201] Bertolini, D.; Cassettari, M.; Ferrario, M.; Grigolini, P.; Salvetti, G. *Adv. Chem. Phys.* **1985**, *62*, 277.

[202] Wernet, P.; Nordlund, D.; Bergmann, U.; Cavalleri, M.; Odelius, M.; Ogasawara, L. A., H.; Näslund; Hirsch, T. K.; Ojamäe, L.; Glatzel, P.; Pettersson, L. G. M.; Nilsson, A. *Science* **2004**, *304*, 995.

Regensburg, den 20.06.2012

Hafiz M. Abd ur Rahman